



D4.1 Product Validation & Intercomparison Report (PVIR-SIT)

Doc Ref: SICCI-PVIR-SIT

Version: 1.1

Date: 23 July 2018



Consortium Members



Change Record

Issue	Date	Reason for Change	Author
PVIR_P2 1.0.D	10 January 2017	First draft of PVIR_P2_v1.0	Stefan Kern
	January 26 2017	Added SIC0 results	Stefan Kern
	February 06 2017	Added SIC1 results	Stefan Kern
	February 08 2017	Completed scientific content; added input from Henriette	Stefan Kern, Henriette Skourup
PVIR-SIT v1.1 version01	January 10 2018	Cut PVIR_P2 into two parts. This document is the SIT part	Stefan Kern
PVIR-SIT v1.1 version01 shared with CGI	January 30 2018	Included all results from NERSC/NIERSC and ICDC; results from DTU have been provided via PPT slides on January 29 and are NOT YET included. Missing as well is a summary and – like for the PVIR-SIC - the reference list needs to be revised.	Stefan Kern, Kirill Khvorostovsky
PVIR-SIT v1.1 version 02	February 13 2018	Reference list revised Summary & Outlook included	Stefan Kern, Kirill Khvorostovsky
PVIR-SIT v1.1 version 03	July 8 2018	Intercomparison with OIB sea-ice freeboard included Comparison with UCL-CPOM and NSIDC CryoSat-2 SIT data included Results updated to v2.0 of the SIT data set for consistency analysis, comparison to ULS (except BGEP), comparison to ASPeCt/Assist/ Ice-Watch	Stefan Kern, Henriette Skourup
PVIR-SIT v1.1	July 23 2018	Issued for Milestone #6 (KO+42)	Stefan Kern, Henriette Skourup

Authorship

Role	Name	Signature
Written by:	Stefan Kern, Kirill Khvorostovsky, Henriette Skourup	
Checked by:	Gary Timms	
Approved by:	Stein Sandven	
Authorised by:	Pascal Lecomte	

Distribution

Organisation	Names	Contact Details
ESA	Pascal Lecomte, Anna Maria	Pascal.Lecomte@esa.int ; Anna.Maria.Trofaier@esa.int
NERSC	Stein Sandven, Kirill Khvorostovsky	Stein.Sandven@nersc.no ; kirill.khvorostovsky@nersc.no
CGI	Gary Timms, Sabrina Mbajon, Clive Farquhar	gary.timms@cgi.com ; sabrina.mbajon.njiche@cgi.com ; clive.farquhar@cgi.com
MET Norway	Thomas Lavergne, Atle Sørensen	t.lavergne@met.no ; atlems@met.no
DMI	Rasmus Tonboe	rtt@dm.dk
DTU	Roberto Saldo, Henriette Skourup, Leif Toudal Pedersen	rs@space.dtu.dk ; hsk@space.dtu.dk ; lt@space.dtu.dk
FMI	Marko Mäkynen, Eero Rinne	marko.makynen@fmi.fi ; eero.rinne@fmi.fi ;
University of Hamburg	Stefan Kern, Lars Kaleschke, Xiangshan Tian-Kunze	stefan.kern@zmaw.de ; lars.kaleschke@uni-hamburg.de ; xiangshan.tian-kunze@uni-hamburg.de
University of Bremen	Georg Heygster	heygster@uni-bremen.de
MPI-M	Dirk Notz, Louisa Bell	dirk.notz@mpimet.mpg.de ; louisa.bell@mpimet.mpg.de
Ifremer	Fanny Arduin	Fanny.Arduin@ifremer.fr
AWI	Marcel Nicolaus, Stefan Hendricks, Thomas Hollands	marcel.nicolaus@awi.de ; stefan.hendricks@awi.de ; thomas.hollands@awi.de

Table of Contents

1	Introduction	18
1.1	Purpose and Scope	18
1.2	Document Structure	18
1.3	Document Status	18
1.4	Applicable Documents	18
1.5	Reference Documents.....	18
1.6	Acronyms and Abbreviations	23
2	Preface	26
3	Sea Ice Thickness Evaluation	27
3.1	Evaluation of the SICCI 2 sea-ice freeboard (SIF) product	68
3.2	Evaluation / Inter-comparison with in situ measurements from North-Pole (NP) drifting stations.....	74
3.3	SIT evaluation with other in-situ measurements.....	84
3.4	SIT evaluation with EM observations.....	86
3.5	SIT validation with moored ULS	92
3.6	SICCI-2 SIT evaluation with ICESat SIT data	106
3.7	Comparison against ship-based sea-ice thickness estimates	143
3.8	SICCI-2 SIT evaluation with CryoSat-2 SIT data.....	149
4	Summary	190
5	Open issues / Outlook	193

List of Figures

- Figure 3-1: Sample freeboard map (March 2003) for the Northern Hemisphere with the seven locations marked by black diamonds. Going from left to right these are "Southern Beaufort Sea" (SBS), "North of Bering Strait" (NofBS), "BGEP mooring area" (BGEP), "Canadian Arctic Archipelago" (CAA), "Central Arctic" (CENARC), "Laptev Sea" (LS), and "Fram Strait" (FS). Note that the size and orientation of the symbols do not represent the actual grid cell box used. 28
- Figure 3-2: Sample freeboard map (September 2002) for the Southern Hemisphere with the six locations marked by black diamonds. Going clockwise around the continent starting at the Antarctic Peninsula these are "Central Southern Weddell Sea" (CSWS), "North of Neumayer Station" (NofNS), "North of Syowa Station" (NofSS), "North of Amery Ice Shelf" (NofAIS), "Ross Sea" (RS), and "Amundsen Sea" (AS). Note that the size and orientation of the symbols do not represent the actual grid cell box used. 29
- Figure 3-3: Time series of the hemispheric average freeboard difference CS2 minus Envisat for the Northern Hemisphere for the overlap period of CS2 and Envisat. Note that only months October through April are used. 29
- Figure 3-4: As Figure 3-3 but showing the standard deviation of the freeboard difference CS2 minus Envisat for the Northern Hemisphere. 30
- Figure 3-5: Time series of the hemispheric average freeboard difference CS2 minus Envisat for the Southern Hemisphere for the full length of the overlap period of CS2 and Envisat. 30
- Figure 3-6: As Figure 3-5 but showing the standard deviation of the freeboard difference CS2 minus Envisat for the Southern Hemisphere. 31
- Figure 3-7: Time series of the regional mean radar (blue) and sea-ice (black) freeboard for Envisat (diamonds) and CS-2 (crosses) for Northern Hemisphere regions Fram Strait, Canadian Arctic Archipelago, and Central Arctic (see Figure 3-1). Vertical bars denote plus/minus one standard deviation computed from a minimum of 3 and a maximum of 11x11 grid cells. Black and blue symbols have been separated a bit along the time axis for better visibility. Note the different scales of the y-axis. 32
- Figure 3-8: Time series of the regional mean radar (blue) and sea-ice (black) freeboard for Envisat (diamonds) and CS-2 (crosses) for Southern Hemisphere regions Central Southern Weddell Sea, North of Neumayer Station, and North of Syowa Station (see Figure 3-2). Vertical bars denote plus/minus one standard deviation computed from a minimum of 3 and a maximum of 5x5 grid cells. Black and blue symbols have been separated a bit along the time axis for better visibility. Note the different scales of the y-axis. 35
- Figure 3-9: Time series of the hemispheric average freeboard uncertainty difference CS2 minus Envisat for the Northern Hemisphere for the overlap period of CS-2 and Envisat. Only months October through April are used. 38
- Figure 3-10: As Figure 3-9 but showing the freeboard uncertainty difference standard deviation. 38
- Figure 3-11: Time series of the hemispheric average freeboard uncertainty difference CS2 minus Envisat for the Southern Hemisphere for the full overlap period of CS-2 and Envisat. 39

Figure 3-12: As Figure 3-11 but showing the freeboard uncertainty difference standard deviation.....	39
Figure 3-13: Time series of the regional mean freeboard uncertainty for Envisat (diamonds) and CS-2 (crosses) for Northern Hemisphere regions Fram Strait, Canadian Arctic Archipelago, and Central Arctic. Vertical bars denote plus/minus one standard deviation computed from a minimum of 3 and a maximum of 11x11 grid cells.....	40
Figure 3-14: Time series of the regional mean freeboard uncertainty for Envisat (diamonds) and CS-2 (crosses) for Southern Hemisphere regions Central Southern Weddell Sea, North of Neumayer Station, and North of Syowa Station (see Figure 3-2). Vertical bars denote plus/minus one standard deviation computed from a minimum of 3 and a maximum of 5x5 grid cells.....	44
Figure 3-15: Time series of the hemispheric average sea-ice thickness difference CS2 minus Envisat for the Northern Hemisphere for the overlap period of CS-2 and Envisat. Only months October through April are used.	46
Figure 3-16: As Figure 3-15 but showing the sea-ice thickness difference standard deviation.....	46
Figure 3-17: Time series of the hemispheric average sea-ice thickness difference CS2 minus Envisat for the Southern Hemisphere for the full overlap period of CS-2 and Envisat.	47
Figure 3-18: As Figure 3-17 but showing the sea-ice thickness difference standard deviation.....	47
Figure 3-19: Time series of the regional mean sea-ice thickness for Envisat (diamonds) and CS-2 (crosses) for Northern Hemisphere regions Fram Strait, Canadian Arctic Archipelago, and Central Arctic (see Figure 3-1). Vertical bars denote plus/minus one standard deviation computed from a minimum of 3 and a maximum of 11x11 grid cells. Note the different scales of the y-axis.	48
Figure 3-20: Time series of the regional mean sea-ice thickness for Envisat (diamonds) and CS-2 (crosses) for Southern Hemisphere regions Central Southern Weddell Sea, North of Neumayer Station, and North of Syowa Station (see Figure 3-2). Vertical bars denote plus/minus one standard deviation computed from a minimum of 3 and a maximum of 5x5 grid cells. Note the different scales of the y-axis.	52
Figure 3-21: Time series of the hemispheric average sea-ice thickness uncertainty difference CS2 minus Envisat for the Northern Hemisphere for the overlap period of CS-2 and Envisat. Only months October through April are used.	55
Figure 3-22: As Figure 3-21 but showing the sea-ice thickness uncertainty difference standard deviation.....	56
Figure 3-23: Time series of the hemispheric average sea-ice thickness uncertainty difference CS2 minus Envisat for the Southern Hemisphere for the full overlap period of CS-2 and Envisat.	56
Figure 3-24: As Figure 3-23 but showing the sea-ice thickness difference standard deviation.....	56
Figure 3-25: Time series of the regional mean sea-ice thickness uncertainty for Envisat (diamonds) and CS-2 (crosses) for Northern Hemisphere regions Fram Strait,	

Canadian Arctic Archipelago, and Central Arctic. Vertical bars denote plus/minus one standard deviation computed from a minimum of 3 and a maximum of 11x11 grid cells.....	57
Figure 3-26: Time series of the regional mean sea-ice thickness uncertainty for Envisat (diamonds) and CS-2 (crosses) for Southern Hemisphere regions Central Southern Weddell Sea, North of Neumayer Station, and North of Syowa Station (see Figure 3-2). Vertical bars denote plus/minus one standard deviation computed from a minimum of 3 and a maximum of 5x5 grid cells.....	60
Figure 3-27: Time series of the correlation between valid freeboard values for the Envisat – CS-2 overlap period for the Northern.....	62
Figure 3-28: As Figure 3-27 but showing results for the Southern Hemisphere.....	63
Figure 3-29: Time series of the correlation between valid freeboard uncertainty values for the Envisat – CS-2 overlap period for the Northern Hemisphere.	63
Figure 3-30: As Figure 3-29 but showing results for the Southern Hemisphere.....	64
Figure 3-31: Time series of the correlation between valid sea-ice thickness values for the Envisat – CS-2 overlap period for the Northern Hemisphere.	64
Figure 3-32: As Figure 3-31 but showing results for the Southern Hemisphere.....	65
Figure 3-33: Time series of the correlation between valid sea-ice thickness uncertainty values for the Envisat – CS-2 overlap period for the Northern Hemisphere.....	65
Figure 3-34: As Figure 3-33 but showing results for the Southern Hemisphere.....	66
Figure 3-35: Example of along-track intercomparison of collocated SIF from OIB (green), Envisat (blue) and CS-2 (red) from March 16, 2011.....	68
Figure 3-36: Location of all OIB tracks used in the comparison for the overlap period between Envisat and CS-2 shown in Figure 3-37.....	69
Figure 3-37: Comparison of the data pairs from location shown in Figure 3-36; a) histogram of collocated SIF from OIB (green), Envisat (blue) and CS-2 (red); b) scatterplot of CS-2 vs Envisat SIF in the overlap period (i.e. from the red and blue parts of the histogram in a)) with, from top to bottom, the linear regression line equation, the linear correlation coefficient R, the root mean squared error (RMSE), and the count of valid data #.....	69
Figure 3-38: Location of all OIB tracks from 2009-2012 used in the comparison for the overlap period with Envisat shown in Figure 3-39.....	70
Figure 3-39: As Figure 3-37 but using only the official level 4 OIB data overlapping with Envisat, i.e. 2009-2012, which locations are given in Figure 3-38. Colors in b) denote the SICCI-2 SIF standard deviation in meters.	70
Figure 3-40: Location of all OIB tracks from 2011-2013 used in the comparison for the overlap period with CS-2 shown in Figure 3-41.....	71
Figure 3-41: As Figure 3-37 but using only the official level 4 OIB data overlapping with CS-2, i.e. 2011-2013, which locations are given in Figure 3-40. Colors in b) denote the SICCI-2 SIF standard deviation in meters.....	71

- Figure 3-42: Location of all OIB tracks from 2011-2016 used in the comparison for the overlap period with CS-2 shown in Figure 3-43..... 72
- Figure 3-43: As Figure 3-37 but using the official level 4 and the quicklook OIB data overlapping with CS-2, i.e. 2011-2016, which locations are given in Figure 3-42. Colors in b) denote the SICCI-2 SIF standard deviation in meters..... 72
- Figure 3-44: Comparison of different freeboard variation parameters for the OIB – Envisat overlap (2009-2012, left column) and the OIB – CS-2 overlap (2011-2016, right column): a) & b) colors denote the SICCI-2 SIF standard deviation in meters; c) & d) colors denote roughness from the OIB product; e) & f) colors denote the SIF retrieval uncertainty from the SICCI-2 SIF product. Note the different y-axis scales..... 73
- Figure 3-45: Location of the drifting stations NP-37, NP-38 and NP-39 collocated with Envisat and Cryosat-2 measurements (large circles – October to April, small circles – May to Sep)..... 75
- Figure 3-46: Measurement points along the polygon of the North Pole drifting stations NP-37, NP-38 and NP-39. Filled circles indicate locations of the measurements sampled every 10 days. Unfilled circles are locations of the measurements sampled every month for the NP-37 or with few gaps for the NP-39. 76
- Figure 3-47: Freeboard measurements from the NP-37 collocated with sea-ice freeboard from SICCI-2 gridded Envisat product. Top x-axis represents the grid cells (named by numbers) of SICCI-2 SIT product where the NP station was located. 77
- Figure 3-48: Freeboard measurements from the NP-37 collocated with individual along-track sea-ice freeboard from SICCI-2 Envisat product..... 77
- Figure 3-49: Collocated snow depth as used in the SICCI-2 SIT product from climatological values ([RD-08]) and in-situ measurements scaled for sea-ice type and in situ measurements from NP-37. See Figure 3-47 for top x-axis explanation. 78
- Figure 3-50: Collocated freeboard measurements from SICCI-2 Cryosat-2 gridded product and in-situ measurements from NP-39. Top x-axis represents the grid cells (named by numbers) of SICCI-2 SIT product where the NP station was located... 79
- Figure 3-51: Freeboard measurements from the NP-39 collocated with individual along-track sea-ice freeboard from SICCI-2 Envisat product..... 79
- Figure 3-52: Collocated snow depth as used in the SICCI SIT prototype from climatological values ([RD-08]) and in-situ measurements from NP-39. Top x-axis represents the grid cells (named by numbers) of SICCI-2 SIT product where the NP station was located..... 80
- Figure 3-53: Collocated snow depth as used in the gridded SICCI SIT prototype from climatological values ([RD-08]) scaled for sea ice type and in-situ measurements from NP-38. Spatial scale on the top represents the grid cells (named by numbers) of SICCI SIT product where drifting station was located. 80
- Figure 3-54: Collocated sea ice thickness from in-situ measurements on the drifting station NP-37 and SICCI SIT Envisat gridded product. Spatial scale on the top represents the grid cells (named by numbers) of SICCI SIT product where drifting station was located..... 81
- Figure 3-55: Figure 3-54 but for NP-38 and the Envisat and CryoSat-2 SIT products... 81

Figure 3-56: As Figure 3-54 but for NP-39 and the CryoSat-2 SIT product.....	82
Figure 3-57: Sea-ice density estimated with the equation given above using measurements of sea-ice freeboard, thickness and snow depth on the North Pole drifting station NP-37.....	83
Figure 3-58: As Figure 3-57 but using data from NP-39.	83
Figure 3-59: Locations of in situ SIT observations from drillings taken from the ASPeCt-BIO data set. Symbols are color-coded according to the year in the observation was made	84
Figure 3-60: Comparison between ASPeCt-BIO [RD-09] in situ SIT (x-axis) and SICCI-2 SIT (y-axis) using data from 2002-2007, i.e. from the Envisat period of the SICCI-2 SIT product. Filled circles denote the 0.5 m – wide bin averages over data from both expeditions. Through these a linear regression is computed (solid line). The dashed line is the line of 1-to-1 agreement.	85
Figure 3-61: Locations of AEM measurements used for the SICCI-2 SIT product evaluation in the Northern Hemisphere. Symbols are color-coded according to the year in which the AEM data were acquired.	87
Figure 3-62: Comparison between Envisat (red symbols) and CS-2 (blue symbols) SICCI-2 SIT and AEM TSIT. Crosses denote single co-located data pairs. Filled circles denote 0.5 m – bin wide averages of SIT and TSIT of the respective satellite data set. For bars see the text. Dashed black line denotes the 1-to-1 agreement. The colored solid lines denote the linear regressions for the respective data sets; the black solid line denotes the regression over all. <i>Southern Hemisphere</i>	88
Figure 3-63: Locations of AEM observations during ISPOL (Nov 13 2004 through Jan 4 2005) and WWOS (Sep/Oct 2006).	89
Figure 3-64: Comparison between AEM total SIT (x-axis) and SICCI-2 SIT (y-axis) for WWOS and ISPOL, i.e. for the Envisat data period of the SICCI-2 SIT product. Stars and open circles denote the co-located observations. Filled circles denote the 0.5 m – wide bin averages over data from both expeditions. Through these a linear regression is computed (solid line). The dashed line is the line of 1-to-1 agreement.	89
Figure 3-65: Location of AEM observations during ANTXXIX/6 and ANTXXIX/7.	90
Figure 3-66: Comparison between AEM total SIT (x-axis) and SICCI-2 SIT (y-axis) for ANTXXIX/6 and 7, i.e. from the CS-2 data period of the SICCI-2 SIT product. Stars and open circles denote the co-located observations for ANTXXIX/6 and ANTXXIX/7, respectively. Filled circles denote the 0.5 m – wide bin averages over data from both expeditions. Through these a linear regression is computed (solid line). The dashed line is the line of 1-to-1 agreement.	91
Figure 3-67: Location of ULS moorings from the Beaufort Gyre Exploration Project (BGEP).	92
Figure 3-68: Location of the moored ULS in the Fram Strait between Svalbard and Greenland owned by the Norwegian Polar Institute (NPI) (taken from [RD-23], see also [RD-24]).	92

Figure 3-69: Monthly mean sea-ice draft measurements from the BGEP ULS moorings and sea-ice draft estimates from collocated grid cells from the SICCI-2 SIT product for ULS at mooring location 'a'.	93
Figure 3-70: As Figure 3-69 but for ULS at mooring location 'b'.	94
Figure 3-71: As Figure 3-69 but for ULS at mooring location 'c'.	94
Figure 3-72: As Figure 3-69 but for ULS at mooring location 'd'.	94
Figure 3-73: Mean sea-ice draft of four BGEP ULS moorings and a mean sea-ice draft estimated from the grid cells of SICCI-2 SIT product covering sector of moorings' location (70° to 82° N by 130° to 160° W).	95
Figure 3-74: Difference monthly mean SICCI-2 sea-ice draft minus BGEP ULS sea-ice draft for ULS at mooring location 'a' (see Figure 3-69).	95
Figure 3-75: As Figure 3-74 but for ULS at mooring location 'b'.	96
Figure 3-76: As Figure 3-74 but for ULS at mooring location 'c'.	96
Figure 3-77: As Figure 3-74 but for ULS at mooring location 'd'.	96
Figure 3-78: As Figure 3-74 but using the average of all four moorings and the sector of moorings' location (70° to 82° N by 130° to 160° W) (compare Figure 3-73).	96
Figure 3-79: Location of the moorings from which we used ULS data from the NPI mooring location in the Fram Strait. The background is the SICCI-2 SIT from Envisat from February 2003.	97
Figure 3-80: Time series of the SICCI-2 SIT derived from Envisat (top, diamonds) and CS-2 (bottom, stars) and the co-located NPI ULS based monthly SIT estimates; mean and modal SIT values are given by triangles and squares, respectively. Error bars given denote the SICCI-2 SIT retrieval uncertainty.	98
Figure 3-81: Combined time-series of SICCI-2 SIT (Envisat: diamonds, CS-2: crosses) and NPI ULS SIT (mean and modal SIT given by triangles and squares, respectively) (top). Scatterplots between mean (left) and modal (right) ULS SIT and mean SICCI-2 SIT for Envisat data (diamonds) and CS-2 data (stars) together with the lines (solid for Envisat, dashed for CS-2) and equations of a linear regression and the RMSD values (bottom).	99
Figure 3-82: AWI mooring locations in the Weddell Sea. Moorings in the western Weddell Sea are, from left to right, AWI-206, AWI-207, and AWI-208; moorings in the eastern Weddell Sea along the Greenwich meridian are, from north to south, AWI-229, AWI-231, AWI-232, and AWI-233. The background is given by sea-ice draft (right, September 2002).	100
Figure 3-83: Time series of the monthly grid-cell mean sea-ice draft obtained from SICCI-2 SIT data (diamonds) and estimated from AWI ULS data (triangles) for the three AWI ULS in the western Weddell Sea. Error bars denote the sea-ice draft retrieval uncertainty computed as the root mean squared sum of the retrieval uncertainties of SIT and sea-ice freeboard; the uncertainty in sea-ice concentration is not taken into account.	101
Figure 3-84: As Figure 3-83 but for the four AWI ULS locations in the eastern Weddell Sea along the Greenwich meridian (see Figure 3-82).	103

- Figure 3-85: Scatterplot between mean ULS sea-ice draft and mean SICCI-2 sea-ice draft based on Envisat data only. Different AWI ULS sites are denote by different symbols, those in the western Weddell Sea (dominated by perennial sea ice) are given in green; those in the eastern Weddell Sea (seasonal sea ice) are given in black. Superposed are lines of the linear regression between the sea-ice draft data sets separately for seasonal sea ice (black) and perennial sea ice (green) AWI ULS sites. Sea-ice draft values < 0.2 m have been excluded from the regression analysis. 103
- Figure 3-86: Inter-comparison of NSIDC ICESat versus SICCI-2 Envisat sea-ice thickness (SIT) for ICESat measurement period ON03 (see Table 3-11). a) ICESat SIT, note that SIT values are interpolated over the polar data gap; b) Envisat SIT, the white circular disk denotes the polar data gap; d) Difference Envisat minus ICESat SIT; c) histograms of the SIT from both sensors for coinciding grid cells together with the count of data pairs "N", the root mean squared difference "RMSD" as well as the mean difference and its standard deviation; e) scatterplot of all co-located SIT values (black crosses) superposed by the mean Envisat SIT per 0.2 m ICESat SIT bin. The error bars denote plus/minus one standard deviation. The red dashed line is the 1-to-1 fit line. 108
- Figure 3-87: As Figure 3-86 but for ICESat measurement period FM04 (see Table 3-11).109
- Figure 3-88: Histograms of the NSIDC ICESat SIT and the SICCI-2 Envisat SIT for the Arctic Ocean for late fall (ON periods, left column) and winter (FM periods, right column) for winters 2003/04 through 2005/06. In each image the number of valid data pairs, the mean difference Envisat minus ICESat SIT and its standard deviation and the RMSD is given (see also Table 3-13). 110
- Figure 3-89: Scatterplot of individual data pairs SICCI-2 Envisat versus NSIDC ICESat SIT (black crosses) and mean Envisat SIT values derived for 0.2 m wide ICESat SIT bins starting with 0.0 m to 0.2 m (red diamonds). Error bars denote one standard deviation; the dashed red line denotes a 1-to-1 fit line. Like in Figure 3-88, the left (right) column is for ON (FM) periods for winters 2003/04 through 2005/06. 112
- Figure 3-90: Distribution of the difference SICCI-2 Envisat minus NSIDC ICESat SIT for ON periods (left) and FM periods (right) for winters 2003/04 through 2005/06 (from top to bottom). 114
- Figure 3-91: Comparison of SICCI-2 Envisat SIT and NSIDC ICESat SIT for grid cells with FYI concentration > 85% (left column) and MYI concentration > 85% (right column) for ON03. Difference SICCI-2 Envisat SIT minus NSIDC ICESat SIT for a) > 85% FYI and b) > 85% MYI; histograms (c,d) and scatterplots (e,f) of the respective sub-sets of the data sets (compare Figure 3-88 and Figure 3-89). 116
- Figure 3-92: As Figure 3-91 but for FM04. 117
- Figure 3-93: As Figure 3-93 but for > 85% FYI concentration. 118
- Figure 3-94: As Figure 3-89 but for > 85% MYI concentration. 120
- Figure 3-95: Top: NSIDC ICESat SIT for periods ON04 and ON07; middle: SICCI-2 Envisat SIT for these periods; bottom: SICCI-2 Envisat SIT for grid cells with > 85% MYI concentration. See text for black circles and red arrows. 123
- Figure 3-96: Inter-comparison of JPL ICESat versus SICCI-2 Envisat sea-ice thickness (SIT) for ICESat measurement period ON03 (see Table 3-11). a) ICESat SIT, note

that SIT values are interpolated over the polar data gap; b) Envisat SIT, the white circular disk denotes the polar data gap; d) Difference Envisat minus ICESat SIT; c) histograms of the SIT from both sensors for coinciding grid cells together with the count of data pairs "N", the root mean squared difference "RMSD" as well as the mean difference and its standard deviation; e) scatterplot of all co-located SIT values (black crosses) superposed by the mean Envisat SIT per 0.2 m ICESat SIT bin. The error bars denote plus/minus one standard deviation. The red dashed line is the 1-to-1 fit line. Note the increase in range of the SIT difference from -2.4 m ... 2.4 m (Figure 3-86) to -4.0 m ... 4.0 m here. 125

Figure 3-97: As Figure 3-96 but for ICESat measurement period FM04. 126

Figure 3-98: Maps of the SIT difference Envisat minus ICESat using the JPL product (left) and the NSIDC product (right) for periods ON03, ON04, and ON05. 127

Figure 3-99: As Figure 3-98 but for periods FM04, FM05, and FM06..... 128

Figure 3-100: Histograms of JPL ICESat SIT and SICCI-2 Envisat SIT for the Arctic Ocean (compare Figure 3-88) for ON-periods (left column) and FM-periods (right column) for winters 2003/04 through 2005/06. In each image the count of valid data pairs "N", the mean difference Envisat minus ICESat SIT and its standard deviation and the root mean squared difference "RMSD" is given. 130

Figure 3-101: Scatterplot of individual data pairs SICCI-2 Envisat versus JPL ICESat SIT (black crosses) and mean Envisat SIT values derived for 0.2 m wide ICESat SIT bins starting with 0.0 m to 0.2 m (red diamonds). Error bars denote one standard deviation; the dashed red line denotes a 1-to-1 fit line. Like in Figure 3-89, the left (right) column is for ON (FM) periods for winters 2003/04 through 2005/06. 132

Figure 3-102: Distribution of the difference SICCI-2 Envisat minus JPL ICESat SIT for ON-periods (left) and FM-periods (right) for winters 2003/04 through 2005/06. 134

Figure 3-103: As Figure 3-101 but using only grid cells with > 85% FYI concentration. 137

Figure 3-104: As Figure 3-103 but for > 85% MYI concentration..... 139

Figure 3-105: Monthly mean SICCI-2 SIT (also named "SAT") versus the monthly mean SIT based on ship-based observations (also named "ASPeCt") for the Northern Hemisphere. Error bars denote ± 1 standard deviation of the monthly mean. Size of the symbols denotes the number of valid co-located data pairs for the respective monthly mean value. Thick solid line is the linear regression line (not forced through zero). Given in the lower right corner is the mean difference and its standard deviation (in parenthesis), the equation of the linear regression, the root mean square difference (RMSD), the number of monthly data pairs N and the squared linear correlation coefficient R^2 . The diagonal dashed line denotes the line of 1-to-1 agreement. 144

Figure 3-106: As Figure 3-105 but showing results for the Southern Hemisphere, winter months. 145

Figure 3-107: As Figure 3-105 but showing results of the Southern Hemisphere, summer months..... 145

Figure 3-108: As Figure 3-105 but for the snow depth and with the statistical parameters grouped in the upper left instead of the bottom right corner. Note that N is smaller by one compared to Figure 3-105 because during one of the winter cruises no snow depth information was recorded. 146

Figure 3-109: As Figure 3-108 but for the Southern Hemisphere, winter.	147
Figure 3-110: As Figure 3-108 but for the Southern Hemisphere, summer.....	147
Figure 3-111: Inter-comparison of NSIDC versus SICCI-2 CS-2 sea-ice thickness (SIT) for fall 2011 (on11). a) NSIDC SIT, note that SIT values are interpolated over the polar data gap; b) SICCI-2 SIT, the white circular disk denotes the polar data gap; d) Difference SICCI-2 minus NSIDC SIT; c) histograms of the SIT from both data set for coinciding grid cells together with the count of data pairs "N", the root mean squared difference "RMSD" as well as the mean difference and its standard deviation; e) scatterplot of all co-located SIT values (black crosses) superposed by the mean SICCI-2 SIT value per 0.2 m NSIDC SIT bin. The error bars denote plus/minus one standard deviation. The red dashed line is the 1-to-1 fit line.....	150
Figure 3-112: As Figure 3-111 but for spring 2012 (ma12).	151
Figure 3-113: Histograms of NSIDC and SICCI-2 SIT for the Arctic Ocean for fall (ON periods, left column) and spring (MA periods, right column) for winters 2010/11 through 2012/13. In each image the number of valid data pairs, the mean difference SICCI-2 minus NSIDC SIT and its standard deviation and the RMSD is given (see also Table 3-19).	152
Figure 3-114: Scatterplot of individual data pairs SICCI-2 SIT versus NSIDC SIT (black crosses) and mean SICCI-2 SIT values derived for 0.2 m wide NSIDC SIT bins starting with 0.0 m to 0.2 m (red diamonds). Error bars denote one standard deviation; the dashed red line denotes a 1-to-1 fit line. Like in Figure 3-113, the left (right) column is for ON (MA) periods for winters 2010/11 through 2012/13.	155
Figure 3-115: Distribution of the difference SICCI-2 SIT minus NSIDC SIT for fall (left column) and spring (right column) for winters 2010/11 through 2012/13.	159
Figure 3-116: Comparison of SICCI-2 and NSIDC SIT for grid cells with FYI concentration > 85% (left column) and MYI concentration > 85% (right column) for fall 2011 (on11). Difference SICCI-2 SIT minus NSIDC SIT for a) > 85% FYI and b) > 85% MYI; histograms (c,d) and scatterplots (e,f) of the respective subsets of the data sets (compare Figure 3-111).	161
Figure 3-117: As Figure 3-116 but for spring 2012 (ma12).	162
Figure 3-118: Scatterplot of individual data pairs SICCI-2 SIT versus NSIDC SIT (black crosses) and mean SICCI-2 SIT values derived for 0.2 m wide NSIDC SIT bins starting with 0.0 m to 0.2 m (red diamonds) for > 85% FYI concentration. Error bars denote one standard deviation; the dashed red line denotes a 1-to-1 fit line. Like in Figure 3-114, the left (right) column is for ON (MA) periods for winters 2010/11 through 2012/13.	163
Figure 3-119: As Figure 3-118 but for > 85% MYI concentration.....	166
Figure 3-120: Inter-comparison of UCL versus SICCI-2 CS-2 sea-ice thickness (SIT) for fall 2011 (on11). a) UCL SIT, b) SICCI-2 SIT, the white circular disk denotes the polar data gap; d) Difference SICCI-2 minus UCL SIT; c) histograms of the SIT from both data set for coinciding grid cells together with the count of data pairs "N", the root mean squared difference "RMSD" as well as the mean difference and its standard deviation; e) scatterplot of all co-located SIT values (black crosses) superposed by the mean SICCI-2 SIT value per 0.2 m UCL SIT bin. The error bars denote plus/minus one standard deviation. The red dashed line is the 1-to-1 fit line.	170

Figure 3-121: As Figure 3-120 but for spring 2012 (ma12).	170
Figure 3-122: Histograms of UCL and SICCI-2 SIT for the Arctic Ocean for fall (ON periods, left column) and spring (MA periods, right column) for winters 2010/11 through 2012/13. In each image the number of valid data pairs, the mean difference SICCI-2 minus UCL SIT and its standard deviation and the RMSD is given (see also Table 3-22 and compare to Figure 3-113)	172
Figure 3-123: Scatterplot of individual data pairs SICCI-2 SIT versus UCL SIT (black crosses) and mean SICCI-2 SIT values derived for 0.2 m wide UCL SIT bins starting with 0.0 m to 0.2 m (red diamonds). Error bars denote one standard deviation; the dashed red line denotes a 1-to-1 fit line. Like in Figure 3-122, the left (right) column is for ON (MA) periods for winters 2010/11 through 2012/13 (compare Figure 3-114).	174
Figure 3-124: Distribution of the difference SICCI-2 SIT minus UCL SIT for fall (left column) and spring (right column) for winters 2010/11 through 2012/13.	177
Figure 3-125: Comparison of SICCI-2 and UCL SIT for grid cells with FYI concentration > 85% (left column) and MYI concentration > 85% (right column) for fall 2011 (on11). Difference SICCI-2 SIT minus UCL SIT for a) > 85% FYI and b) > 85% MYI; histograms (c,d) and scatterplots (e,f) of the respective sub-sets of the data sets (compare Figure 3-120).....	180
Figure 3-126: As Figure 3-125 but for spring 2012 (ma12).	181
Figure 3-127: Scatterplot of individual data pairs SICCI-2 SIT versus UCL SIT (black crosses) and mean SICCI-2 SIT values derived for 0.2 m wide UCL SIT bins starting with 0.0 m to 0.2 m (red diamonds) for > 85% FYI concentration. Error bars denote one standard deviation; the dashed red line denotes a 1-to-1 fit line. Like in Figure 3-123, the left (right) column is for ON (MA) periods for winters 2010/11 through 2012/13.	182
Figure 3-128: As Figure 3-127 but for > 85% MYI concentration.....	186

List of Tables

Table 1-1: Applicable Documents	18
Table 1-2: Reference Documents.....	23
Table 1-3: Acronyms	25
Table 3-1: Summary of the inter-comparison of the freeboard for the Northern Hemisphere for the seven regions shown in Figure 3-1: CAA: Canadian Arctic Archipelago, FS: Fram Strait, CeArc: Central Arctic, NofBS: North of Bering Strait, LS: Laptev Sea, SBS: Southern Beaufort Sea, BGEP: BGEP Mooring Area. Given is the average difference of the regional mean freeboard CS2 minus Envisat (FBDiff) and its standard deviation (SDEVofFBDiff), the difference CS2 minus Envisat of the regional freeboard standard deviation (FBSDEVDiff) and the number of months with valid data (maximum: 12).	34
Table 3-2: Summary of the inter-comparison of the freeboard for the Southern Hemisphere for the six regions shown in Figure 3-2: CSWS: Central Southern Weddell Sea, NofNS: North of Neumayer Station, NofSS: North of Syowa Station, NofAIS: North of Amery Ice Shelf, RS: Ross Sea, AS: Amundsen Sea. Given is the average difference of the regional mean freeboard CS2 minus Envisat (FBDiff) and its standard deviation (SDEVofFBDiff), the difference CS2 minus Envisat of the regional freeboard standard deviation (FBSDEVDiff) and the number of months with valid data (maximum: 17).	37
Table 3-3: Summary of the inter-comparison of the freeboard uncertainty for the Northern Hemisphere for regions: CAA: Canadian Arctic Archipelago, FS: Fram Strait, CeArc: Central Arctic, NofBS: North of Bering Strait, LS: Laptev Sea, SBS: Southern Beaufort Sea. BGEP: BGEP mooring area. Given is the average difference of the regional mean freeboard uncertainty CS2 minus Envisat (FBerrDiff) and its standard deviation (SDEVofFBerrDiff), the difference CS2 minus Envisat of the regional freeboard uncertainty standard deviation (FBerrSDEVDiff) and the number of months with valid data (maximum: 12).	42
Table 3-4: Summary of the inter-comparison of the freeboard uncertainty for the Southern Hemisphere for the six regions shown in Figure 3-2: CSWS: Central Southern Weddell Sea, NofNS: North of Neumayer Station, NofSS: North of Syowa Station, NofAIS: North of Amery Ice Shelf, RS: Ross Sea, AS: Amundsen Sea. Given is the average difference of the regional mean freeboard uncertainty CS2 minus Envisat (FBerrDiff) and its standard deviation (SDEVofFBerrDiff), the difference CS2 minus Envisat of the regional freeboard uncertainty standard deviation (FBerrSDEVDiff) and the number of months with valid data (maximum: 17).	43
Table 3-5: Summary of the inter-comparison of the sea-ice thickness for the Northern Hemisphere for the seven regions shown in Figure 3-1: CAA: Canadian Arctic Archipelago, FS: Fram Strait, CeArc: Central Arctic, NofBS: North of Bering Strait, LS: Laptev Sea, SBS: Southern Beaufort Sea, and BGEP. Given is the average difference of the regional mean sea-ice thickness CS2 minus Envisat (SITDiff) and its standard deviation (SDEVofSITDiff), the difference CS2 minus Envisat of the regional sea-ice thickness standard deviation (SITSDEVDiff) and the number of months with valid data (maximum: 12).	50
Table 3-6: Summary of the inter-comparison of the sea-ice thickness for the Southern Hemisphere for the six regions shown in Figure 3-2: CSWS: Central Southern Weddell Sea, NofNS: North of Neumayer Station, NofSS: North of Syowa Station,	

NofAIS: North of Amery Ice Shelf, RS: Ross Sea, AS: Amundsen Sea. Given is the average difference of the regional mean sea-ice thickness CS2 minus Envisat (SITDiff) and its standard deviation (SDEVofSITDiff), the difference CS2 minus Envisat of the regional sea-ice thickness standard deviation (SITSDEVDiff) and the number of months with valid data (maximum: 17).....	54
Table 3-7: Summary of the inter-comparison of the sea-ice thickness uncertainty for the Northern Hemisphere: CAA: Canadian Arctic Archipelago, FS: Fram Strait, CeArc: Central Arctic, NofBS: North of Bering Strait, LS: Laptev Sea, SBS: Southern Beaufort Sea, BGEP: BGEP mooring area. Given is the average difference of the regional mean sea-ice thickness uncertainty CS2 minus Envisat (SITerrDiff) and its standard deviation (SDEVofSITerrDiff), the difference CS2 minus Envisat of the regional sea-ice thickness uncertainty standard deviation (SITerrSDEVDiff) and the number of months with valid data (maximum: 12).....	59
Table 3-8: Summary of the inter-comparison of the sea-ice thickness uncertainty for the Southern Hemisphere for the six regions shown in Figure 3-2: CSWS: Central Southern Weddell Sea, NofNS: North of Neumayer Station, NofSS: North of Syowa Station, NofAIS: North of Amery Ice Shelf, RS: Ross Sea, AS: Amundsen Sea. Given is the average difference of the regional mean sea-ice thickness uncertainty CS2 minus Envisat (SITerrDiff) and its standard deviation (SDEVofSITerrDiff), the difference CS2 minus Envisat of the regional sea-ice thickness uncertainty standard deviation (SITerrSDEVDiff) and the number of months with valid data (maximum: 17).	62
Table 3-9: Statistics of the sea-ice freeboards presented in Figure 3-37, Figure 3-39, Figure 3-41, and Figure 3-43.	72
Table 3-10: Periods of collocation of the North Pole drifting stations NP-37, NP-38 and NP-39 with SICCI SIT prototype derived from Envisat and Cryosat-2 measurements. Parameters measured on the drifting stations are listed.....	75
Table 3-11: ICESat measurement periods. Acronyms ON, FM and MA refer to October/November, February/March and March/April, respectively, while 03, 04, ..., 08 refer to the year.	106
Table 3-12: ICESat measurement periods and periods from which Envisat data are used for the inter-comparison shown in this section (compare Table 3-11).....	107
Table 3-13: Per period mean SICCI-2 Envisat SIT, NSIDC ICESat SIT, the difference Envisat minus ICESat, the RMSD, the linear correlation, and the count N of collocated data pairs. Bold numbers at the end provide the averages over all ON, all FM, and all ON and FM values. Standard deviations 1σ given at the end are the averages of the respective values of the previous rows.	113
Table 3-14: Same as Table 3-13 but for > 85% FYI concentration.....	121
Table 3-15: Same as Table 3-13 but for > 85% MYI concentration.	122
Table 3-16: Per period mean SICCI-2 Envisat SIT, JPL ICESat SIT, the difference Envisat minus ICESat, the RMSD, the linear correlation, and the count N of collocated data pairs. Bold numbers at the end provide the averages over all ON, all FM, and all ON and FM values. Standard deviations 1σ given at the end are the averages of the respective values of the previous rows.	131
Table 3-17: Same as Table 3-16 but for > 85% FYI concentration.....	136

Table 3-18: Same as Table 3-16 but for > 85% MYI concentration.	138
Table 3-19: Per period (fall or spring) mean SICCI-2 SIT, NSIDC SIT, the difference SICCI-2 minus NSIDC, the RMSD, the linear correlation, and the count N of collocated data pairs. Bold numbers at the end provide the averages over all ON, all MA, and all ON and MA values. Standard deviations 1σ given at the end are the averages of the respective values of the previous rows.	154
Table 3-20: Per period (fall or spring) mean SICCI-2 SIT, NSIDC SIT, the difference SICCI-2 minus NSIDC, the RMSD, the linear correlation, and the count N of collocated data pairs for > 85% FYI concentration. Bold numbers at the end provide the averages over all ON, all MA, and all ON and MA values. Standard deviations 1σ given at the end are the averages of the respective values of the previous rows.	165
Table 3-21: Per period (fall or spring) mean SICCI-2 SIT, NSIDC SIT, the difference SICCI-2 minus NSIDC, the RMSD, the linear correlation, and the count N of collocated data pairs for > 85% MYI concentration. Bold numbers at the end provide the averages over all ON, all MA, and all ON and MA values. Standard deviations 1σ given at the end are the averages of the respective values of the previous rows.	168
Table 3-22: Per period (fall or spring) mean SICCI-2 SIT, UCL SIT, the difference SICCI-2 minus UCL, the RMSD, the linear correlation, and the count N of collocated data pairs. Bold numbers at the end provide the averages over all ON, all MA, and all ON and MA values. Standard deviations 1σ given at the end are the averages of the respective values of the previous rows.	176
Table 3-23: Per period (fall or spring) mean SICCI-2 SIT, UCL SIT, the difference SICCI-2 minus UCL, the RMSD, the linear correlation, and the count N of collocated data pairs for > 85% FYI concentration. Bold numbers at the end provide the averages over all ON, all MA, and all ON and MA values. Standard deviations 1σ given at the end are the averages of the respective values of the previous rows.	184
Table 3-24: Per period (fall or spring) mean SICCI-2 SIT, UCL SIT, the difference SICCI-2 minus UCL, the RMSD, the linear correlation, and the count N of collocated data pairs for > 85% MYI concentration. Bold numbers at the end provide the averages over all ON, all MA, and all ON and MA values. Standard deviations 1σ given at the end are the averages of the respective values of the previous rows.	187
Table 4-1: Overall difference (SIT DIFF) Envisat RA-2 minus ICESat SIT for the NSIDC and the JPL ICESat SIT products using all data (top), only FYI data (< 15% MYI concentration from SICCI2 product) (middle), and only MYI data (> 85% MYI concentration from SICCI2 product) (bottom) together with the root-mean squared difference (RMSD) and the linear correlation coefficient R. SIT DIFF and RMSD are given in meters. In bold we mark the "better" results	192
Table 4-2: Overall difference (SIT DIFF) SICCI-2 CS-2 minus CS-2 SIT for the NSIDC and the UCL products using all data (top), only FYI data (< 15% MYI concentration from SICCI2 product) (middle), and only MYI data (> 85% MYI concentration from SICCI2 product) (bottom) together with the root-mean squared difference (RMSD) and the linear correlation coefficient R. SIT DIFF and RMSD are given in meters. In bold we mark the "better" results	192

1 Introduction

1.1 Purpose and Scope

This document informs about the results of the validation and inter-comparison of the SICCI project Phase 2 sea ice thickness (SIT) data set.

1.2 Document Structure

After this introduction and the list of references, the document describes the Sea Ice Thickness validation and inter-comparison efforts.

1.3 Document Status

This is issue 1.1 released to ESA as part of the project's contractual deliverable set.

1.4 Applicable Documents

The following table lists the Applicable Documents that have a direct impact on the contents of this document.

Acronym	Title	Reference	Issue
AD-1	Sea Ice ECV Project Management Plan	ESA-CCI_SICCI_PMP_D6.1_v1.3	1.3

Table 1-1: Applicable Documents

1.5 Reference Documents

Acronym	Title	Reference	Issue
RD-01	Algorithm Theoretical Basis Document (ATBDv1)	Pedersen, L. T., et al.	v2.2, Sep. 2017
RD-02	Product Validation Plan (PVP)	Laxon, S., and L. T. Pedersen, SICCI-PVP-05-12	v1.1, Sep 2012
RD-03	Data Access Requirement Document (DARD)	Kern, S., SICCI-P2-DARD-08-15	v2.0, Sep 2015
RD-04	Round Robin Data Package for SICCI 2 SIT	Skourup, H., et al.,	June 2016
RD-05	Product Validation and Intercomparison Report for SICCI 1	Kern, S., et al., ESA-CCI-SICCI-PVIR	V1.1, Feb 2015

Acronym	Title	Reference	Issue
RD-06	CryoSat-2 estimates of Arctic sea ice thickness and volume	Laxon S.W., K. A. Giles, A. L. Ridout, D. J. Wingham, R. Willatt, R. Cullen, R. Kwok, A. Schweiger, J. Zhang, C. Haas, S. Hendricks, R. Krishfield, N. Kurtz, S. Farrell and M. Davidson (2013), Geophys. Res. Lett., 40, 732–737, doi:10.1002/grl.50193.	n.a.
RD-07	Variability of Arctic sea ice thickness and volume from CryoSat-2.	Kwok R, Cunningham GF. 2015, Phil. Trans. R. Soc. A 373: 20140157. http://dx.doi.org/10.1098/rsta.2014.0157	n.a.
RD-08	Snow depth on Arctic sea ice	Warren, S. G., I. G. Rigor, N. Untersteiner, V. F. Radionov, N. N. Bryazgin, Y. I. Aleksandrov, and R. Colony, Journal of Climate, 12, 1814-1829, 1999.	n.a.
RD-09	Chlorophyll-a in Antarctic sea ice from historical ice core data	Meiners, K. M. and 14 others, Geophysical Research Letters, 39, L21602, 2012	n.a.
RD-10	Helicopter-borne measurements of sea ice thickness, using a small and lightweight, digital EM system	Haas, C., Lobach, J., Hendricks, S., Rabenstein, L., Pfaffling, A., Journal of Applied Geophysics, 67(3), 234-241. 2009	n.a.

Acronym	Title	Reference	Issue
RD-11	Sea ice remote sensing, thickness profiling, and ice and snow analyses	Haas, C., J. Lieser, J. Lobach, T. Martin, A. Pfaffling, S. Willmes, V. Alexandrov, and S. Kern, In U. Schauer and G. Kattner with contributions of the participants (Eds.), The Expedition ARKTIS XIX/1 a, b and XIX/2 of the Research Vessel POLARSTERN in 2003, Rep. Pol. Mar. Res., 481, pp 13-46, ISSN 1618 – 3193, (2004)	n.a.
RD-12	The Sea Ice Experiment: Dynamic Nature of the Arctic	Jennifer K. Hutchings, The Sea Ice Experiment: Dynamic Nature of the Arctic (SEDNA) Applied Physics Laboratory Ice Station (APLIS) 2007, Field Report	n.a.
RD-13	Reduced ice thickness in Arctic Transpolar Drift favors rapid ice retreat	Haas, C., Pfaffling, A., Hendricks, S., Rabenstein, L., Etienne, J.-L., Rigor, I. Geophys. Res. Lett., 35, L17501, 2008	n.a.
RD-14	Russian-German Cooperation: The Transdrift I Expedition to the Laptev Sea	Please contact Thomas Krumpfen: thomas.krumpfen (at) awi.de, Funding Agency: BMBF (German Federal Ministry of Education and Research)	n.a.
RD-15	Synoptic airborne thickness surveys reveal state of Arctic sea ice cover // Seasonal Ice Zone Observing Network, Pan-Arctic Measurements and Arctic Regional climate model simulations)	Haas, C., S. Hendricks, H. Eicken, and A. Herber, Geophys. Res. Lett., 37, L09501, doi:10.1029/2010GL042652, 2010 // Netcare (AWI) PAM-ARCMIP report , Funding Agency (SIZONet): NSF	n.a.

Acronym	Title	Reference	Issue
RD-16	BREA – Beaufort Regional Environmental Assessment	http://www.beaufortrea.ca/publications/ , data provided by C. Haas	n.a.
RD-17	The Expeditions ANTARKTIS-XXII/1 and XXII/2 of the Research Vessel Polarstern in 2004/2005	El Naggar, S., G. Dieckmann, C. Haas, M. Schröder, and M. Spindler, Reports on Polar and Marine Research, 551, 268 pp, 2007, https://doi.org/10.2312/BzPM_0551_2007	n.a.
RD-18	The Expedition of the Research Vessel Polarstern to the Antarctic in 2006 (ANT-XXIII/7)	Lemke, P., Reports on Polar and Marine Research, 586, 147 pp, 2009, https://doi.org/10.2312/BzPM_0586_2009	n.a.
RD-19	The Expedition of the Research Vessel Polarstern to the Antarctic in 2013 (ANT-XXIX/6).	Lemke, P., Reports on Polar and Marine Research, 679, 154 pp, 2014, https://doi.org/10.2312/BzPM_0679_2014	n.a.
RD-20	The Expedition of the Research Vessel Polarstern to the Antarctic in 2013 (ANT-XXIX/7).	Meyer, B., and L. Auerswald, Reports on Polar and Marine Research, 674, 130 pp, 2014, https://doi.org/10.2312/BzPM_0674_2014	n.a.
RD-21	Upward Looking Sonar data at BGEP Moorings from 2003 through 2013	The data were collected and made available by the Beaufort Gyre Exploration Project based at the Woods Hole Oceanographic Institution (http://www.whoi.edu/beaufortgyre)	n.a.

Acronym	Title	Reference	Issue
RD-22	Deterioration of perennial sea ice in the Beaufort Gyre from 2003 to 2012 and its impact on the oceanic freshwater cycle	Krishfield, R. A., A. Proshutinsky, K. Tateyama, W. J. Williams, E. C. Carmack, F. A. McLaughlin, and M.-L. Timmermans, J. Geophys. Res. Oceans, 119, 1271-1305, doi:10.1002/2013JC008999, 2014	n.a.
RD-23	Thickness of sea ice measured in the Fram Strait. Environmental monitoring of Svalbard and Jan Mayen (MOSJ)	Norwegian Polar Institute (2018), URL: http://www.mosj.no/en/climate/ocean/sea-ice-thickness-arctic-ocean-fram-strait.html	n.a.
RD-24	Thinning of Arctic sea ice observed in Fram Strait: 1990-2011	Hansen, E., S. Gerland, M. A. Granskog, O. Pavlova, A. H. H. Renner, J. Haapala, T. B. Loynning, and M. Tschudi, Journal of Geophysical Research, 118, 5202-5221, doi:10.1002/jgrc.20393, 2013	n.a.
RD-25	Sea ice draft in the Weddell Sea, measured by upward looking sonars	Behrendt, A., W. Dierking, E. Fahrbach, and H. Witte, Earth System Science Data, 5, 209-226, doi: 10.5194/essd-5-209-2013, 2013	n.a.
RD-26	Sea ice thickness, freeboard, and snow depth products from Operation IceBridge airborne data	Kurtz, N. T., S. L. Farrell, M. Studinger, N. Galin, J. P. Harbeck, R. Lindsay, V. D. Onana, B. Panzer, and J. G. Sonntag, The Cryosphere, 7, 1035-1056, doi:10.5194/tc-7-1035-2013, 2013	n.a.

Acronym	Title	Reference	Issue
RD-27	<i>Arctic Sea Ice Freeboard and Thickness, Version 1</i>	Yi, D. and H. J. Zwally. 2009, updated 2014-04-15. [Arctic]. Boulder, Colorado USA. NSIDC: National Snow and Ice Data Center. doi: https://doi.org/10.5067/SXJVJ3A2XIZT . [2016].	2014-04-15
RD-28	ICESat over Arctic sea ice: Estimation of snow depth and ice thickness	Kwok, R., and G. F. Cunningham, Journal of Geophysical Research, 113, C08010, 2008	n.a.
RD-29	An improved CryoSat-2 sea ice freeboard retrieval algorithm through the use of waveform fitting	Kurtz, N. T., N. Galin, and M. Studinger. 2014. <i>The Cryosphere</i> , 8:1217-1237. doi:https://doi.org/10.5194/tc-8-1217-2014.	n.a.
RD-30	<i>CryoSat-2 Level-4 Sea Ice Elevation, Freeboard, and Thickness, Version 1</i>	Kurtz, N. and J. Harbeck. 2017. [Arctic]. Boulder, Colorado USA. NASA National Snow and Ice Data Center Distributed Active Archive Center. doi: https://doi.org/10.5067/96J00KIFDAS8 . [2018].	Version 1
RD-31	Estimating Arctic sea ice thickness and volume using CryoSat-2 radar altimeter data	Tilling, R. L., A. Ridout, and A. Shepherd, Advances in Space Research, 2017, https://doi.org/10.1016/j.asr.2017.10.051	n.a.
RD-32	Retrieval of multiyear ice (MYI) sea ice concentration (SIC) from satellite microwave brightness temperatures	Kern, S., Technical Report, ESA-SICCI-2	2.0, Sep. 2016

Table 1-2: Reference Documents**1.6 Acronyms and Abbreviations**

Acronym	Meaning
AMSR-E	Advanced Microwave Scanning Radiometer aboard EOS
AO	Announcement of Opportunity
ASCII	American Standard Code for Information Interchange

Acronym	Meaning
ASIRAS	Airborne Synthetic Aperture and Interferometric Radar Altimeter System
ATBD	Algorithm Theoretical Basis Document
CM-SAF	Climate Monitoring Satellite Application Facility
DMSP	Defence Meteorological Satellite Program
DWD	Deutscher Wetterdienst
EASE2	Equal-Area Scalable Earth Grid 2
ECV	Essential Climate Variable
Envisat	Environmental Satellite
ERS	European Remote Sensing satellite
ESA	European Space Agency
EUMETSAT	European Organisation for the Exploitation of Meteorological Satellites
FB	Freeboard
FCDR	Fundamental Climate Data Record
FOC	Free of Charge
FOV	Field-of-View
FTP	File Transfer Protocol
GB	GigaByte
GCOM	Global Change Observation Mission
H	Horizontal polarization
H+V	Horizontal and vertical polarization
L1B	Level 1b
MB	MegaByte
MODIS	Moderate Resolution Imaging Spectroradiometer
MSS	Mean Sea Surface
n.a.	Not applicable
NetCDF	Network Common Data Format
NSIDC	National Snow and Ice Data Center
OCOG	Offset Centre of Gravity
OIB	Operation Ice Bridge
OSI-SAF	Ocean and Sea Ice Satellite Application Facility
OW	Open Water
PI	Principal Investigator
PMW	Passive Microwave
POES	Polar Operational Environmental Satellite
PRF	Pulse Repetition Frequency
RA	Radar Altimeter
RADAR	Radio Detection and Ranging
SAR	Synthetic Aperture Radar
SGDR	Sensor Geophysical Data Record
SIC	Sea Ice Concentration

Acronym	Meaning
SIRAL	SAR/Interferometric Radar Altimeter
SIT	Sea Ice Thickness
SSM/I	Special Sensor Microwave / Imager
SSM/IS	Special Sensor Microwave / Imager+Sounder
TB	TeraByte
t.b.d.	To be determined
TM	Thematic Mapper
ULS	Upward Looking Sonar
URL	Uniform Resource Locator
V	Vertical polarization
WGS84	World Geodetic System revision -84

Table 1-3: Acronyms

2 Preface

The products are described in the netCDF file attributes and in the Product User guide (PUG). The algorithms used to obtain the products are described in the Algorithm Theoretical Basis Document (ATDB) [RD-01]. The Product Validation Plan (PVP) [RD-02] reveals the steps and strategies that ought to be used for the validation. The sources for the data to be used are compiled in the Data Access Requirement Document (DARD) [RD-03]. The data of the Round Robin Data Package for SICCI-2 were used for the evaluation of the sea-ice freeboard [RD-04].

The validation and inter-comparison steps presented in this report were mainly carried out using the v09 SIT product; v1.0 was issued mid January, which was too late to include this data into this report.

We note that passages of this report, where data input and methodologies did not change with respect to the SICCI phase 1 project are 1-to-1 copies of the respective report (PVIR) delivered in the context of the SICCI-1 project [RD-05].

3 Sea Ice Thickness Evaluation

Evaluation and consistency checks of the SICCI Phase 2 SIT product has been carried out. Sea-ice thickness (SIT) products are available for the Southern Hemisphere year-round for the time period 06/2002 through 04/2017, and for the Northern Hemisphere for winters 2002/03 through 2016/17 – based on Envisat RA-2 (until 03/2012) and CS-2) (since 11/2010) data. Winters comprise the months October to April.

Elements of the evaluation are:

- Evaluation of the SICCI 2 freeboard product using the data collection of the RRDP2
- Evaluation of the SICCI-2 along-track freeboard product against airborne observations
- Evaluation of the SICCI 2 sea-ice thickness product with:
 - In-situ observations
 - Airborne electromagnetic (EM) sounding
 - Moored upward looking sonar (ULS) data
- Inter-comparison with independent satellite observations: ICESat
- Inter-comparison with ship-based sea-ice thickness estimates
- Inter-comparison with independent satellite observations: CryoSat-2

We note that we skipped any evaluation / inter-comparison with data from submarine ULS. We recommend to keeping this evaluation source in mind for the case that also radar altimetry of ERS1/2 satellites will be used to compute sea-ice thickness because for that period the submarine ULS data are an invaluable evaluation data source because of the lack of other sources such as airborne EM sounding or OIB data.

We note further that we carried a consistency check of the data in the way that we compared data and/or time series for specific locations with focus on the overlap period between Envisat and CryoSat-2. This work could be considered an element of the long-term evolution. But since its results are important for the understanding of the limitations of the SICCI-2 SIT product and to get a feeling about SIT range, we present these results here, before we come to any evaluation. We will refer to figures and tables of this part with 3-X.

3.0 Consistency Investigation

This investigation targets i) the (sea-ice) freeboard, ii) the (sea-ice) freeboard uncertainty, iii) the sea-ice thickness, and iv) sea-ice thickness uncertainty.

We select 7 (Northern Hemisphere) and 6 (Southern Hemisphere) (see Figure 3-1 and Figure 3-2) to investigate the temporal development of parameters i) to iv) for the period 2002 through 2017 but also in particular

for the overlap period CryoSat-2 (CS2) – Envisat from November 2010 through March 2012. For each location freeboard values of a 11 x 11 grid cell box (Northern Hemisphere, = 275 km x 275 km) or a 5 x 5 grid cell box (Southern Hemisphere, = 250 km x 250 km) are averaged if a minimum of 3 valid freeboard values is present. The smaller number of grid cell boxes used in the Southern Hemisphere is explained with the larger grid cell size: 50 km compared to 25 km for the Northern Hemisphere.

For both hemispheres also the hemispheric averages of parameters i) to iv) are investigated for the overlap period.

We use only data where the status flag indicates nominal retrieval (= 0).

In addition to that it turned out that the sea-ice thickness uncertainty peaks at abnormally high values thanks to the extraordinary and unrealistically high or low snow density values. Therefore, for the investigation of the Northern Hemisphere hemispheric-wide sea-ice thickness and its uncertainty only grid cells with snow density values between 100 kg/m³ and 400 kg/m³ were allowed.

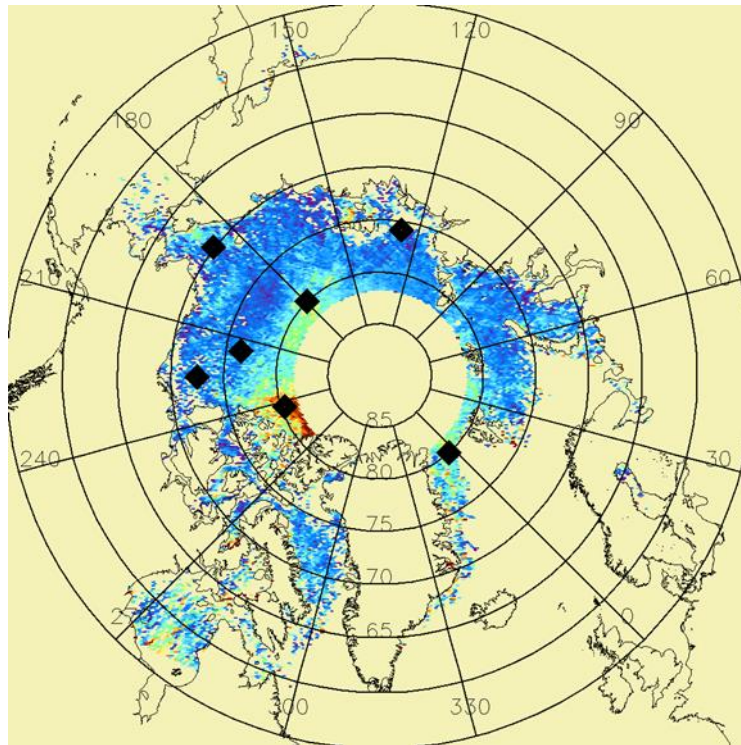


Figure 3-1: Sample freeboard map (March 2003) for the Northern Hemisphere with the seven locations marked by black diamonds. Going from left to right these are "Southern Beaufort Sea" (SBS), "North of Bering Strait" (NofBS), "BGEP mooring area" (BGEP), "Canadian Arctic Archipelago" (CAA), "Central Arctic" (CENARC), "Laptev Sea" (LS), and "Fram Strait" (FS). Note that the size and orientation of the symbols do not represent the actual grid cell box used.

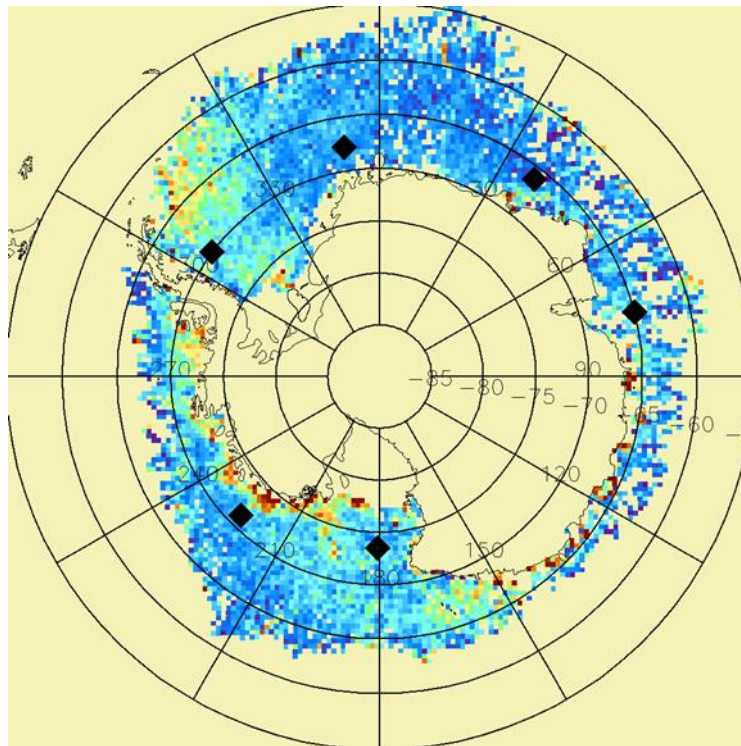


Figure 3-2: Sample freeboard map (September 2002) for the Southern Hemisphere with the six locations marked by black diamonds. Going clockwise around the continent starting at the Antarctic Peninsula these are “Central Southern Weddell Sea” (CSWS), “North of Neumayer Station” (NofNS), “North of Syowa Station” (NofSS), “North of Amery Ice Shelf” (NofAIS), “Ross Sea” (RS), and “Amundsen Sea” (AS). Note that the size and orientation of the symbols do not represent the actual grid cell box used.

Sea-ice freeboard

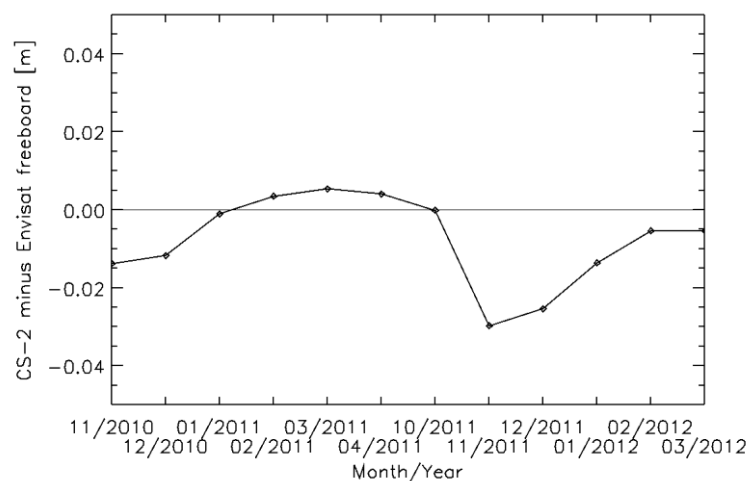


Figure 3-3: Time series of the hemispheric average freeboard difference CS2 minus Envisat for the Northern Hemisphere for the overlap period of CS2 and Envisat. Note that only months October through April are used.

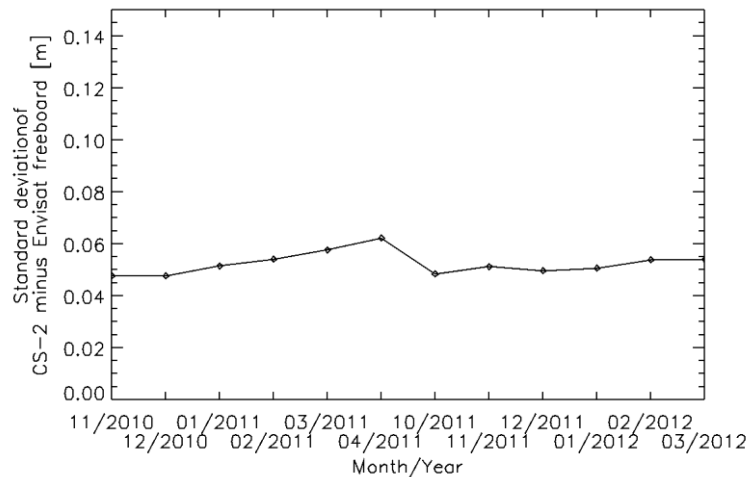


Figure 3-4: As Figure 3-3 but showing the standard deviation of the freeboard difference CS2 minus Envisat for the Northern Hemisphere.

Figure 3-3 shows that for the Northern Hemisphere, hemispheric freeboard retrieved from CS-2 and Envisat agree within 0.02 m except for Nov./Dec. 2011. Absolute differences tend to be larger during late fall than during winter and early spring. The standard deviation of the freeboard difference is around 0.05-0.06 m (Figure 3-4).

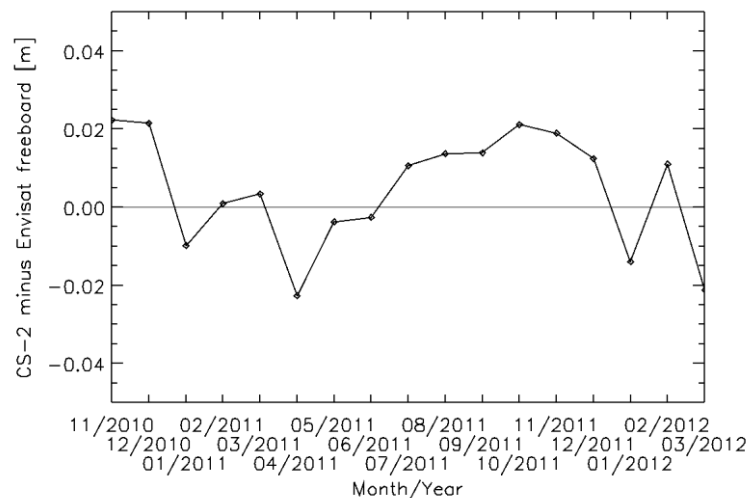


Figure 3-5: Time series of the hemispheric average freeboard difference CS2 minus Envisat for the Southern Hemisphere for the full length of the overlap period of CS2 and Envisat.

For the Southern Hemisphere, shown in Figure 3-5, CS-2 and Envisat freeboard also agree mostly within 0.02 m. The standard deviation of the freeboard difference is quite stable during winter months and into spring (November) around 0.09 m; it is larger than in the Northern Hemisphere (compare Figure 3-4). From late spring through late fall standard deviations are generally above 0.1 m (Figure 3-6).

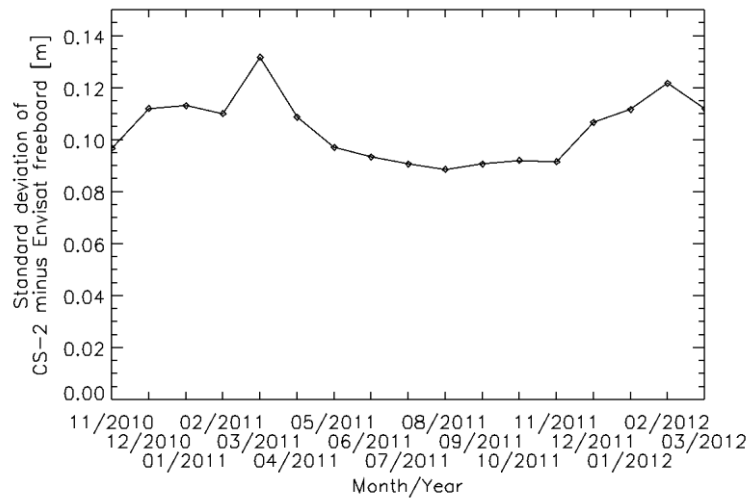


Figure 3-6: As Figure 3-5 but showing the standard deviation of the freeboard difference CS2 minus Envisat for the Southern Hemisphere.

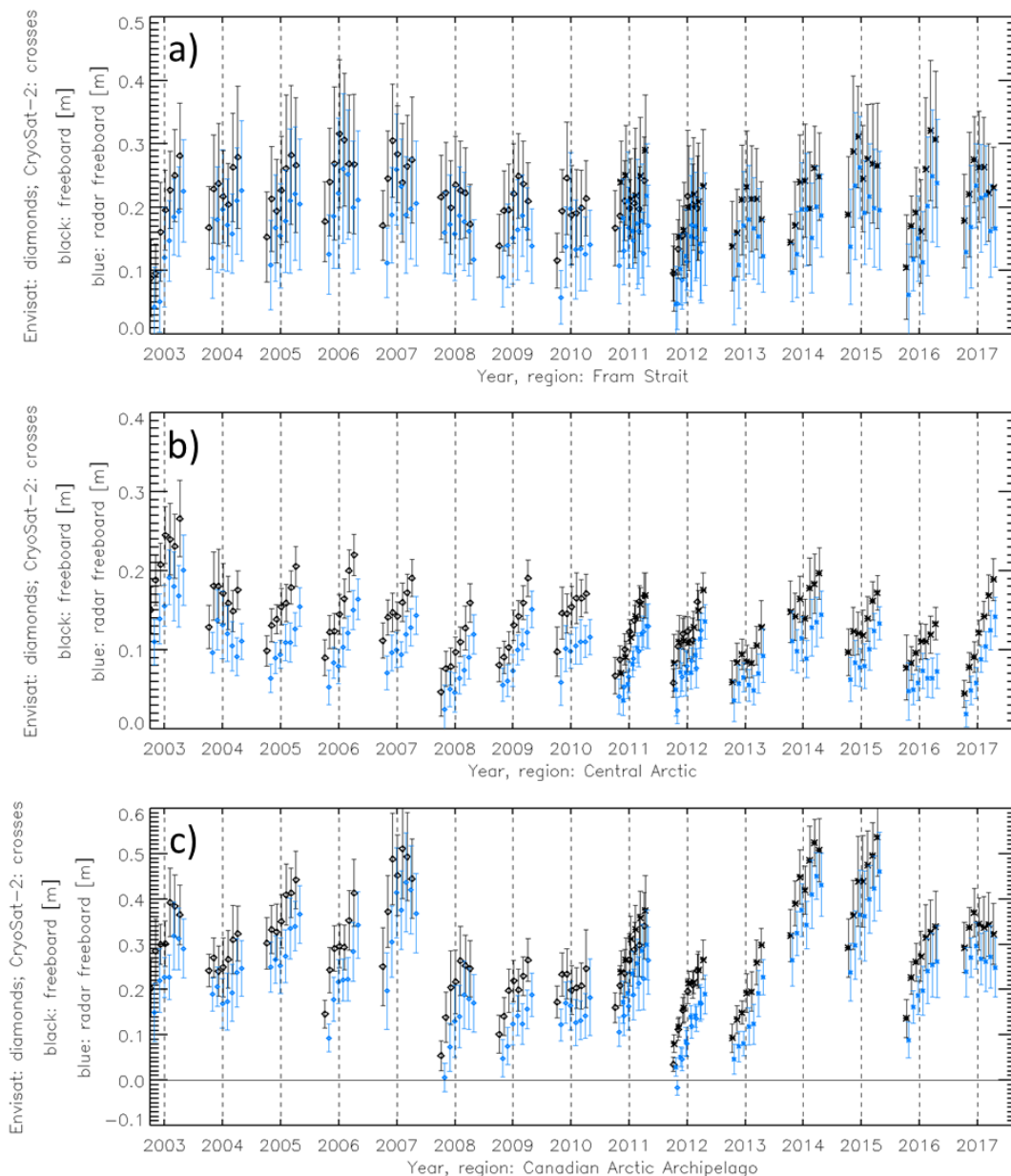


Figure 3-7: Time series of the regional mean radar (blue) and sea-ice (black) freeboard for Envisat (diamonds) and CS-2 (crosses) for Northern Hemisphere regions Fram Strait, Canadian Arctic Archipelago, and Central Arctic (see Figure 3-1). Vertical bars denote plus/minus one standard deviation computed from a minimum of 3 and a maximum of 11x11 grid cells. Black and blue symbols have been separated a bit along the time axis for better visibility. Note the different scales of the y-axis.

In Figure 3-7 we show the entire time series of the radar freeboard and the sea-ice freeboard for the seven regions in the Northern Hemisphere (compare Figure 3-1). There are almost no negative radar freeboard values. There are no negative sea-ice freeboard values. Month-to-month changes in freeboard seem to be reasonable with expected changes in the ice conditions. Note that different changes in ice conditions can cause different month-to-month changes in sea-ice freeboard. 1) Drift of thick ice, e.g.

multiyear ice (MYI) into or out of a region replacing first-year ice (FYI) or being replaced by FYI most likely causes a month-to-month increase or decrease of the sea-ice freeboard. 2) Thermodynamic sea-ice growth causes in increase in sea-ice freeboard. 3) Sustained snow fall without too much thermodynamic sea-ice growth can cause a decrease in sea-ice freeboard. These need to be kept in mind when interpreting the time series shown in Figure 3-7 (and also similar Figures of this kind after that).

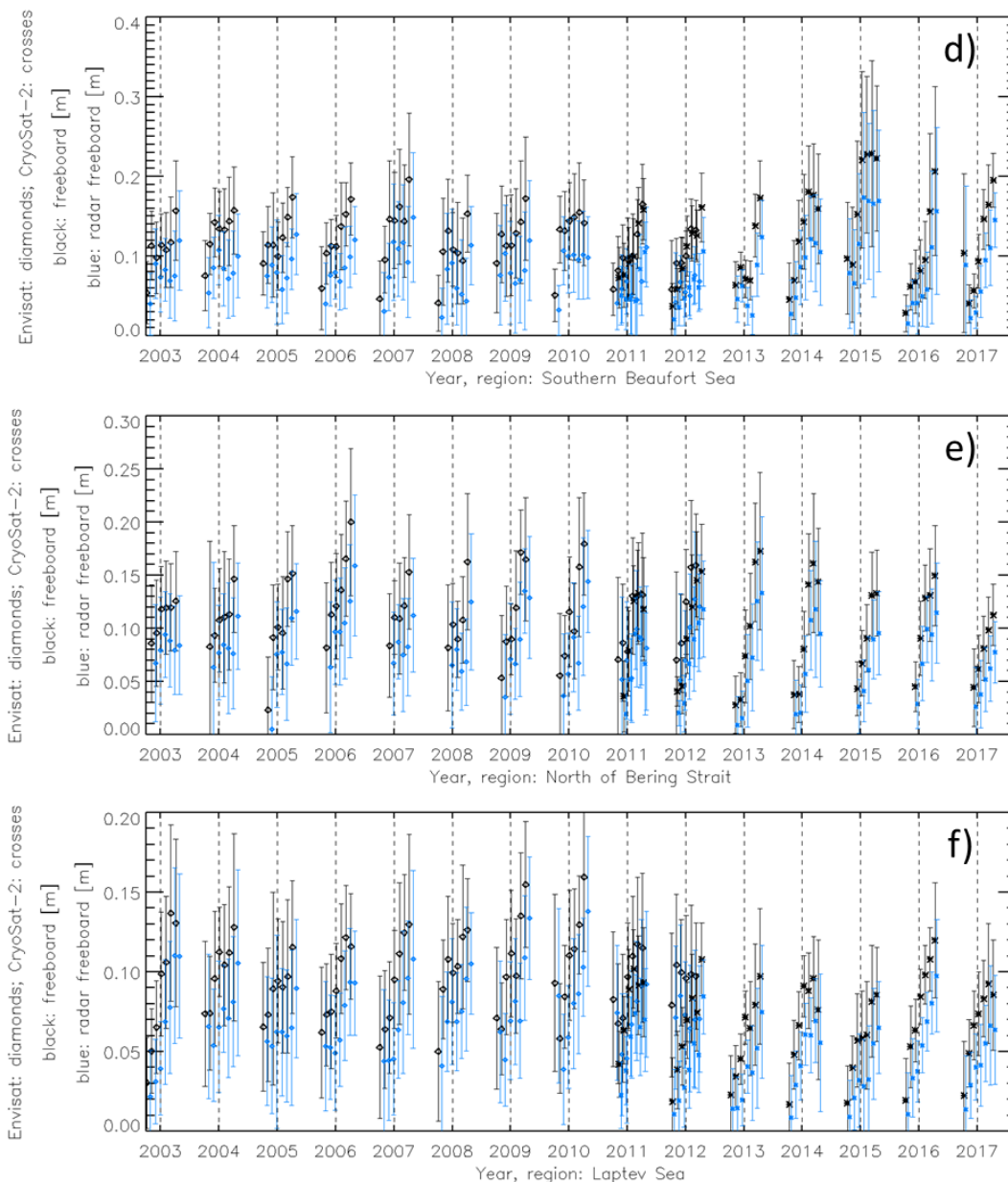


Figure 3-7 continued for Northern Hemisphere regions Southern Beaufort Sea, North of Bering Strait, and Laptev Sea (see Figure 3-1). Note the difference scales of the y-axis.

Differences in the monthly freeboard between CS-2 and Envisat seem small for the overlap period and tend not to exceed 0.05 m. The largest differences occur in regions North of Bering Strait (Figure 3-7 e)) and Laptev Sea (Figure 3-7 f)), both regions dominated by FYI. The average

differences between CS-2 and Envisat freeboard are of the order of a few centimeters at most as illustrated in Table 3-1.

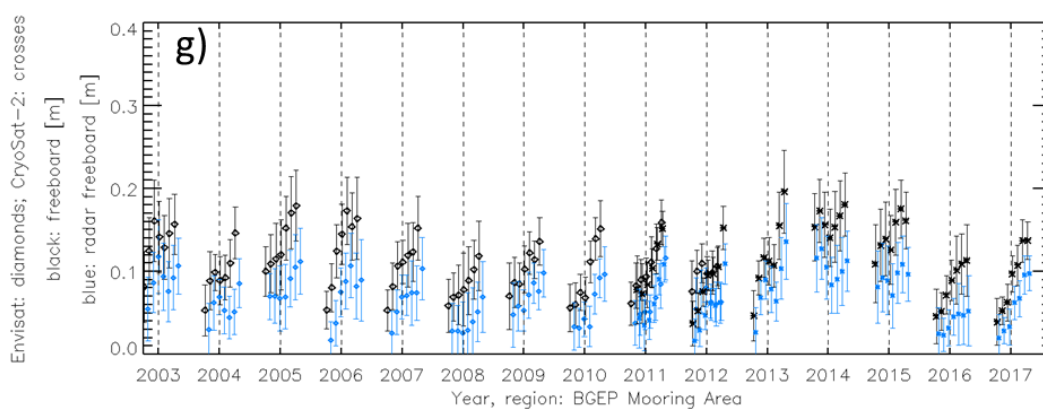


Figure 3-7 continued for Northern Hemisphere region BGEP mooring area (see Figure 3-1).

Table 3-1: Summary of the inter-comparison of the freeboard for the Northern Hemisphere for the seven regions shown in Figure 3-1: CAA: Canadian Arctic Archipelago, FS: Fram Strait, CeArc: Central Arctic, NofBS: North of Bering Strait, LS: Laptev Sea, SBS: Southern Beaufort Sea, BGEP: BGEP Mooring Area. Given is the average difference of the regional mean freeboard CS2 minus Envisat (FBDiff) and its standard deviation (SDEVofFBDiff), the difference CS2 minus Envisat of the regional freeboard standard deviation (FBSDEVDiff) and the number of months with valid data (maximum: 12).

Region	CAA	FS	CeArc	NofBS	LS	SBS	BGEP
FBDiff [m]	0.027	0.021	-0.002	-0.022	-0.028	-0.008	-0.014
SDEVofFBDiff [m]	0.020	0.022	0.013	0.019	0.020	0.013	0.017
FBSDEVDiff [m]	-0.001	0.016	0.004	-0.017	0.014	-0.005	-0.002
NofMONTHS	12	12	12	10	12	12	12

On average, CS-2 provides larger freeboard than Envisat for the regions dominated by MYI (CAA and FS) while the reverse applies for regions dominated by FYI (NofBS and LS) where CS-2 provides smaller freeboard than Envisat. The standard deviation of the freeboard difference is around 1 to 2 cm. There is a tendency that freeboard from CS-2 is more variable than freeboard from Envisat in region FS (positive FBSDEVDiff) while it is less variable than from Envisat within regions LS and NofBS.

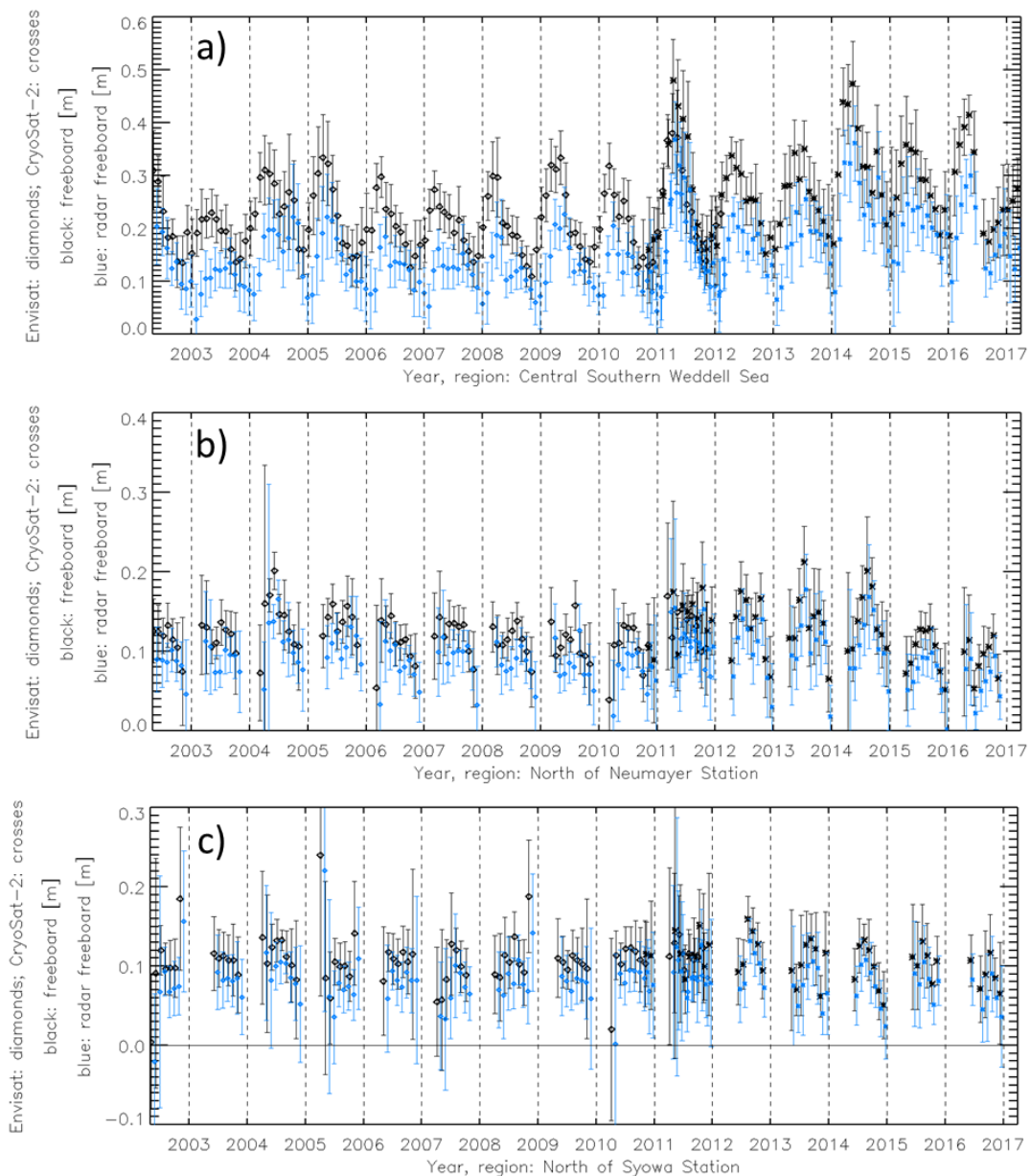


Figure 3-8: Time series of the regional mean radar (blue) and sea-ice (black) freeboard for Envisat (diamonds) and CS-2 (crosses) for Southern Hemisphere regions Central Southern Weddell Sea, North of Neumayer Station, and North of Syowa Station (see Figure 3-2). Vertical bars denote plus/minus one standard deviation computed from a minimum of 3 and a maximum of 5x5 grid cells. Black and blue symbols have been separated a bit along the time axis for better visibility. Note the different scales of the y-axis.

In Figure 3-8 we show the entire time series of the radar freeboard and the sea-ice freeboard for the six regions in the Southern Hemisphere (compare Figure 3-2). There are no negative values of the radar and the sea-ice freeboard. Month-to-month changes in freeboard seem to be reasonable with expected changes in the ice conditions which differ from those in the Northern Hemisphere in two aspects.

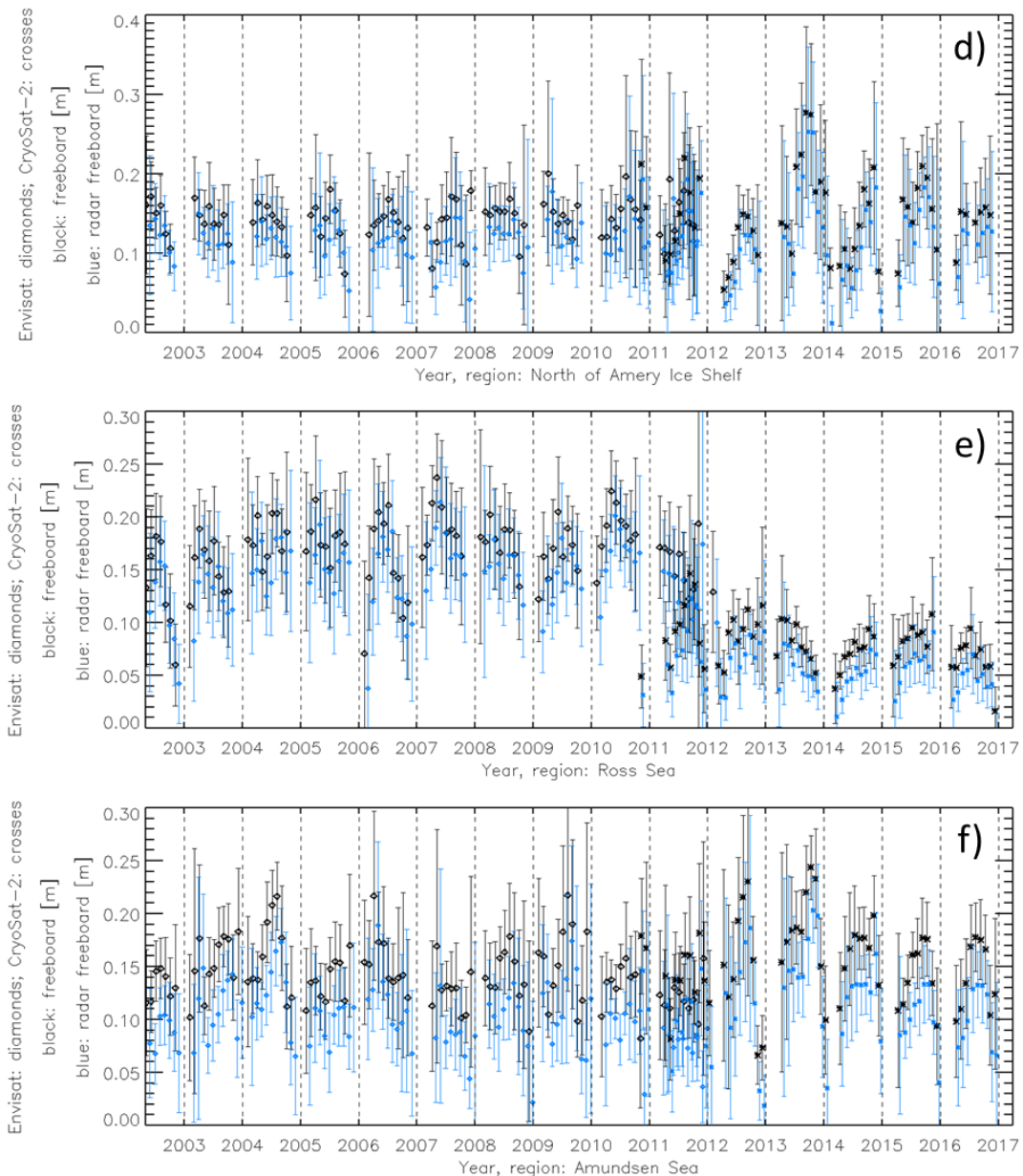


Figure 3-8 continued for Southern Hemisphere regions North of Amery Ice Shelf, Ross Sea, and Amundsen Sea (see Figure 3-2). Note the different scales of the y-axis.

First, MYI is basically confined to the region Central Southern Weddell Sea (CSWS); only region Amundsen Sea (AS) might also occasionally have some MYI. Therefore in bullet 1) of the explanation to Figure 3-7 MYI and FYI should better be replaced by thick and thin sea ice. Secondly, an additional bullet 4) applies to the Southern Hemisphere: Snow fall paired with flooding and subsequent snow-ice formation can cause a rather constant sea-ice freeboard. Characteristic for region CSWS (Figure 3-8 a)) is a peak in freeboard in early winter followed by a decrease throughout winter; this can be explained by bullet 1): thick ice being replaced by thin ice. In contrast to the Northern Hemisphere (compare Figure 3-7), most regions in the Southern Hemisphere do not reveal a general increase in freeboard during winter. Occasionally such an increase is observed, e.g. in years 2004, 2012,

and 2013 in the Amundsen Sea or in years 2007, 2012, and 2014 in region North of Amery Ice Shelf (NofAIS). Otherwise freeboard tends to vary around one value during winter. It needs to be noted that year-round but particularly from late spring to fall wet and layered snow on top of the sea ice can affect the freeboard retrieval from both Envisat and CS-2 because of a reduced penetration depth of the radar waves into the snow.

Differences in the monthly freeboard between CS-2 and Envisat seem small for most regions during winter of the overlap period and tend not to exceed 0.1 m. Differences can be substantially larger in the transition months from spring to fall, e.g. in region CSWS and Ross Sea (RS). Three different types of differences can be notified: A) CS-2 freeboard exceeds Envisat freeboard in most of the months, e.g. regions CSWS, AS, and NofAIS; B) Envisat freeboard exceeds CS-2 freeboard in most of the months, e.g. region RS; C) Month-to-month variations in the sign of the difference, e.g. region North of Syowa Station (NofSS) and North of Neumayer Station (NofNS). The average differences between CS-2 and Envisat freeboard can be up to several centimeters as illustrated in Table 3-2.

Table 3-2: Summary of the inter-comparison of the freeboard for the Southern Hemisphere for the six regions shown in Figure 3-2: CSWS: Central Southern Weddell Sea, NofNS: North of Neumayer Station, NofSS: North of Syowa Station, NofAIS: North of Amery Ice Shelf, RS: Ross Sea, AS: Amundsen Sea. Given is the average difference of the regional mean freeboard CS2 minus Envisat (FBDiff) and its standard deviation (SDEVofFBDiff), the difference CS2 minus Envisat of the regional freeboard standard deviation (FBSDEVDiff) and the number of months with valid data (maximum: 17).

Region	CSWS	NofNS	NofSS	NofAIS	RS	AS
FBDiff [m]	0.040	0.012	0.003	0.009	-0.068	0.025
SDEVofFBDiff [m]	0.038	0.023	0.028	0.043	0.050	0.036
FBSDEVDiff [m]	0.017	0.009	0.006	0.002	-0.028	0.006
NofMONTHS	17	11	10	10	11	12

On average, CS-2 provides larger freeboard than Envisat for two regions: CSWS: ~0.04 m and AS: ~0.02 m. In contrast, for the region RS, where MYI is practically absent and much less deformation occurs compared to the other five regions, CS-2 provides smaller freeboard than Envisat; the average difference is 0.07 m. The time series of the freeboard (Figure 3-8 e)) clearly indicates a jump in freeboard from higher values for the Envisat period and lower values for the CS-2 period. Because this region is located downstream of the Ross Ice Shelf polynya, the largest coastal polynya in the Southern Hemisphere, it can be expected that the sea ice at that location is quite thin. Therefore it can be stated that CS-2 freeboard estimates are more realistic here. The reason for the freeboard overestimation by Envisat in this region needs to be investigated. Hence, except for the region RS we observe a relatively smooth transition between the Envisat and the CS-2 period.

The standard deviation of the freeboard difference CS-2 minus Envisat is, on average, twice as large as in the Northern Hemisphere (compare Table 3-1) and takes values between ~ 0.02 m (NofNS) and ~ 0.04 m (RS, NofAIS, CSWS).

The difference between the freeboard standard deviations suggest a larger variability of the CS-2 freeboard within the 5x5 grid cell box used for regions CSWS, NofNS, and NofSS while the reverse applies to region RS where the variability of the Envisat freeboard exceeds that of the CS-2 freeboard. This is, however, not surprising in view of the notable larger freeboard obtained with Envisat than with CS-2 for this region (see again Figure 3-8 e)).

Sea-ice freeboard uncertainty

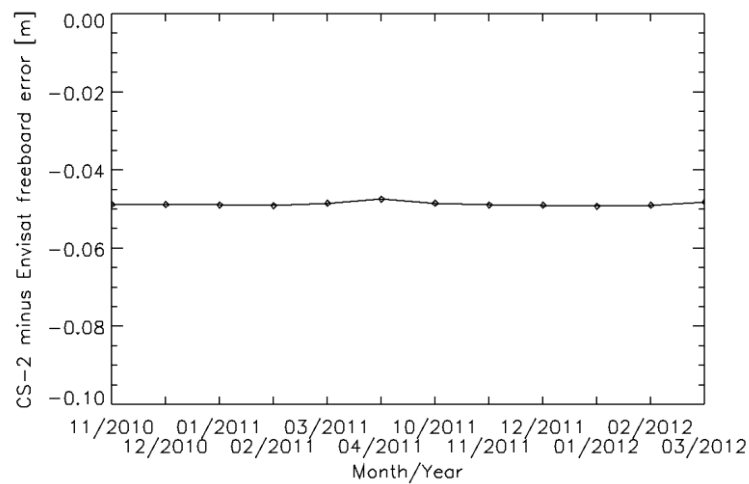


Figure 3-9: Time series of the hemispheric average freeboard uncertainty difference CS2 minus Envisat for the Northern Hemisphere for the overlap period of CS-2 and Envisat. Only months October through April are used.

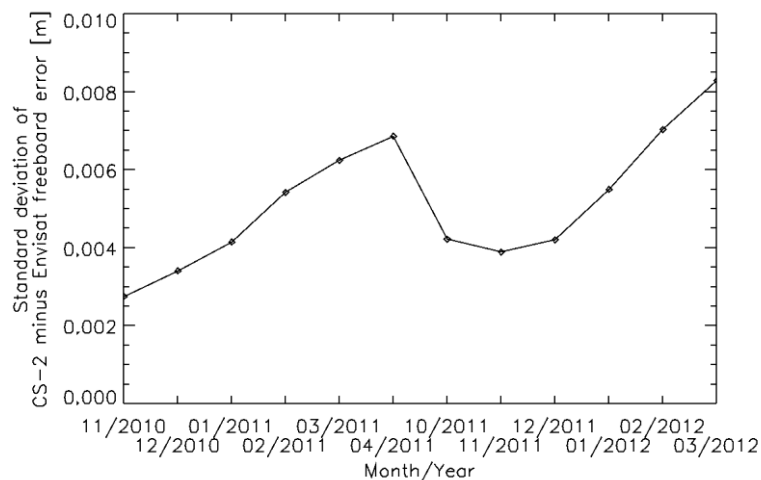


Figure 3-10: As Figure 3-9 but showing the freeboard uncertainty difference standard deviation.

Figure 3-9 illustrates that for the Northern Hemisphere the hemispheric average difference CS-2 minus Envisat freeboard uncertainty is negative throughout the overlap period and takes absolute values around 5 cm. The freeboard uncertainty for Envisat retrieval is hence considerably larger than for CS-2. The standard deviation of the difference increases from 3-4 mm during late fall to 7-8 mm during late winter / early spring (Figure 3-10). With that the difference in the freeboard uncertainty is one order of magnitude less variable than the difference in the freeboard itself (compare Figure 3-4).

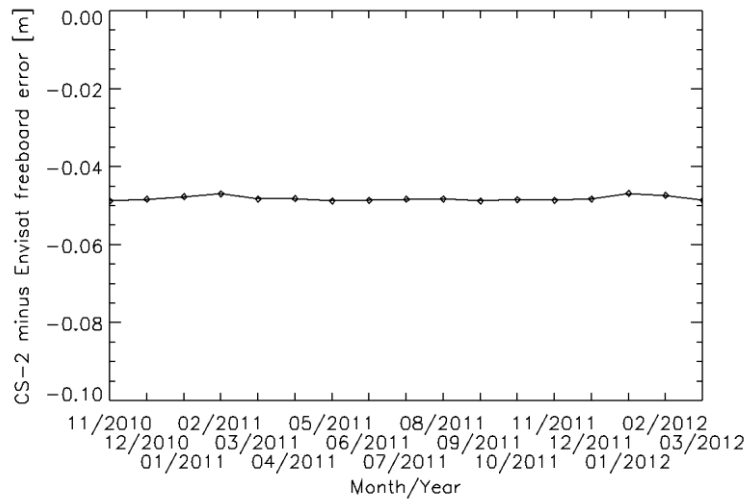


Figure 3-11: Time series of the hemispheric average freeboard uncertainty difference CS2 minus Envisat for the Southern Hemisphere for the full overlap period of CS-2 and Envisat.

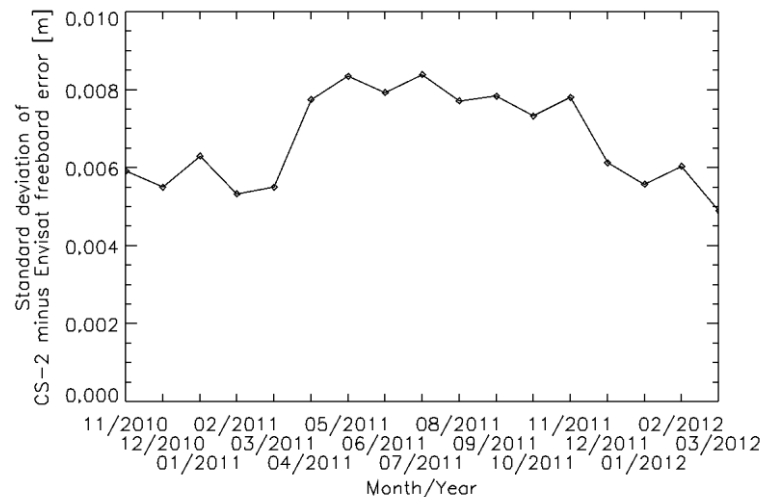


Figure 3-12: As Figure 3-11 but showing the freeboard uncertainty difference standard deviation.

Figure 3-11 shows the respective time series for the Southern Hemisphere. Like in the Northern Hemisphere the hemispheric average freeboard uncertainty difference CS-2 minus Envisat is negative and absolute values are about 5 cm – very similar to the Northern Hemisphere. That is, also in the Southern Hemisphere the Envisat freeboard uncertainty is considerably higher than for CS-2. The standard deviation of the freeboard uncertainty

difference is larger than in the Northern Hemisphere and mostly takes values around 8 mm during winter without too much variation (Figure 3-12). This temporal behavior is in line with the observations of the freeboard itself (see Figure 3-5 and Figure 3-6) as is the relationship between magnitudes of freeboard differences and freeboard uncertainty differences, which is similar to that observed for the Northern Hemisphere.

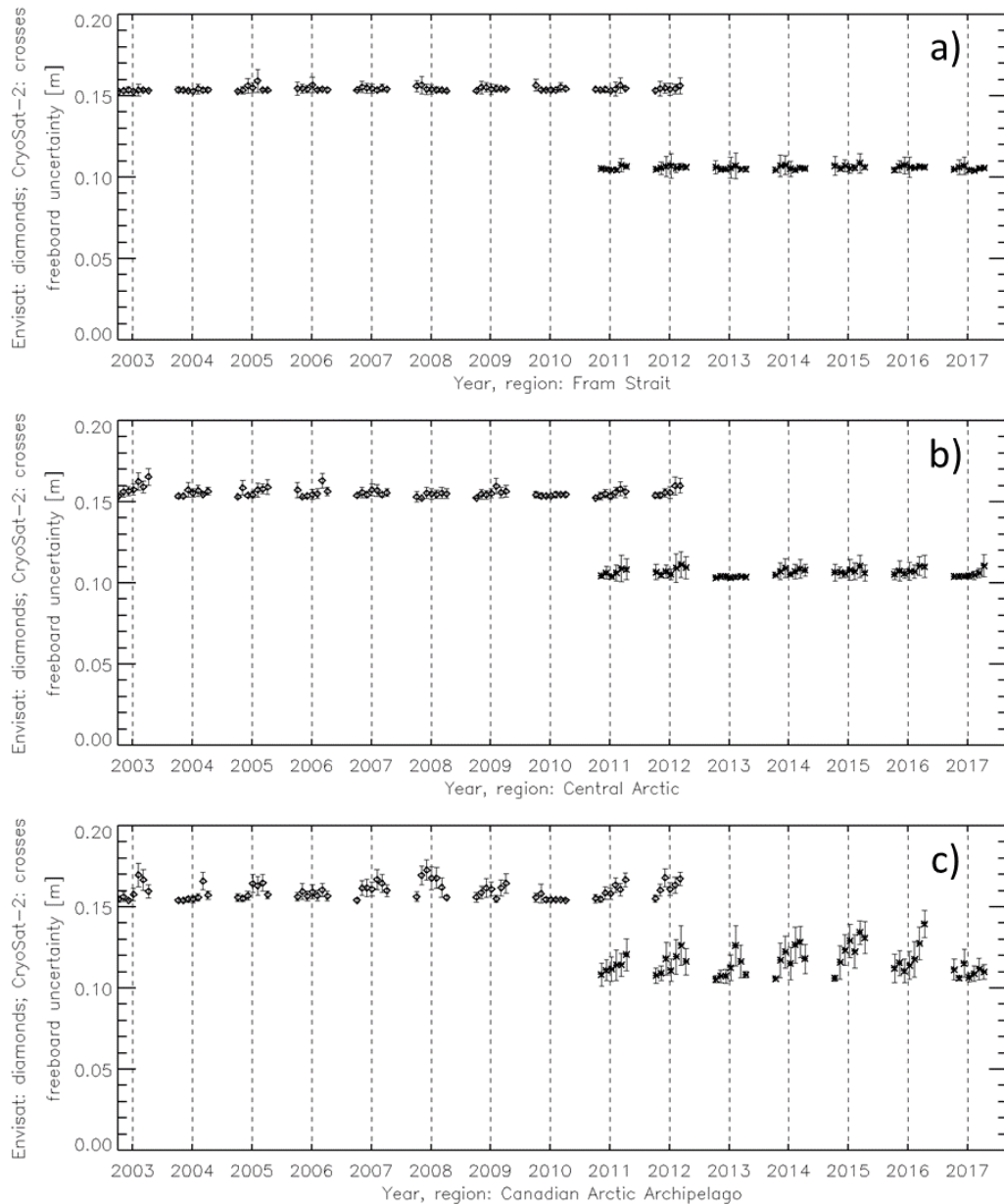


Figure 3-13: Time series of the regional mean freeboard uncertainty for Envisat (diamonds) and CS-2 (crosses) for Northern Hemisphere regions Fram Strait, Canadian Arctic Archipelago, and Central Arctic. Vertical bars denote plus/minus one standard deviation computed from a minimum of 3 and a maximum of 11x11 grid cells.

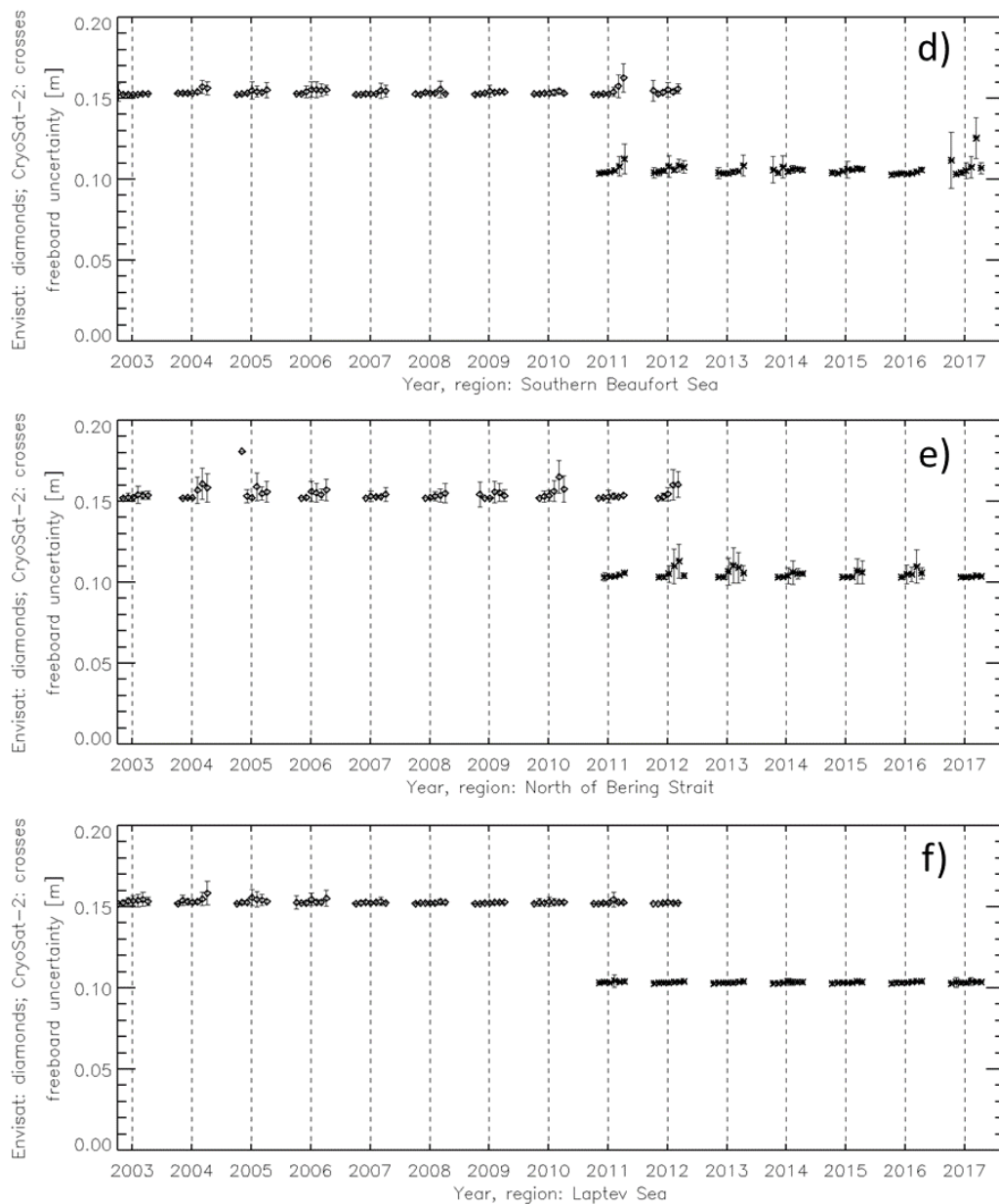


Figure 3-13 continued for Northern Hemisphere regions Southern Beaufort Sea, North of Bering Strait, and Laptev Sea.

Figure 3-13 illustrates that freeboard uncertainties for the seven regions of the Northern Hemisphere are quite constant throughout the entire time series of each sensor with little variation during the winter (as indicated already by Figure 3-9). There is a clear reduction (=improvement) in uncertainty between Envisat and CS-2. The largest variations in the freeboard uncertainty occur in regions Central Arctic (CeArc) and Canadian Arctic Archipelago (CAA). As summarized in Table 3-3, average differences in the freeboard uncertainties are negative and uniform at ~ 5 cm. The standard deviation of these differences is 4 mm for region CAA and less than that for the other six regions. There is almost no difference in the spatial variability of the freeboard uncertainty within the 11x11 grid cells.

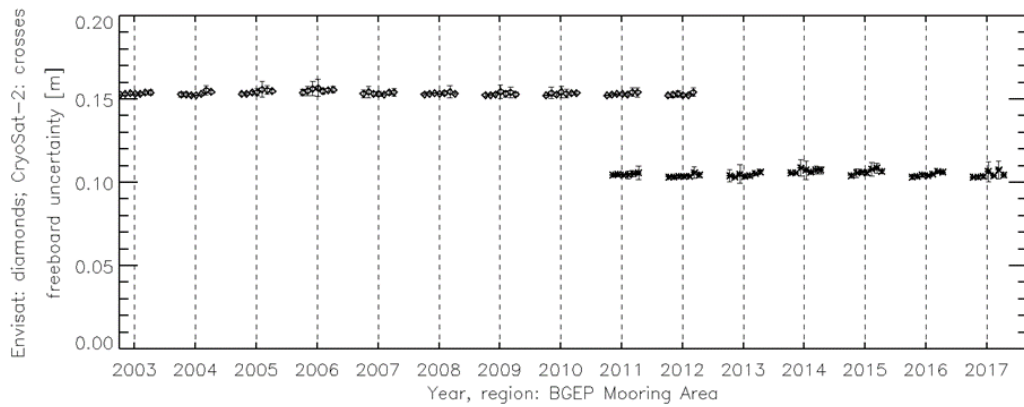


Figure 3-13 continued for Northern Hemisphere region BGEF mooring area (see Figure 3-1).

Table 3-3: Summary of the inter-comparison of the freeboard uncertainty for the Northern Hemisphere for regions: CAA: Canadian Arctic Archipelago, FS: Fram Strait, CeArc: Central Arctic, NofBS: North of Bering Strait, LS: Laptev Sea, SBS: Southern Beaufort Sea. BGEF: BGEF mooring area. Given is the average difference of the regional mean freeboard uncertainty CS2 minus Envisat (FBerrDiff) and its standard deviation (SDEVofFBerrDiff), the difference CS2 minus Envisat of the regional freeboard uncertainty standard deviation (FBerrSDEVDiff) and the number of months with valid data (maximum: 12).

Region	CAA	FS	CeArc	NofBS	LS	SBS	BGEF
FBerrDiff [m]	-0.047	-0.049	-0.049	-0.049	-0.049	-0.049	-0.049
SDEVofFBerrDiff [m]	0.003	0.001	0.001	0.001	<0.001	0.001	<0.001
FBerrSDEVDiff [m]	0.004	< 0.001	0.001	<0.001	< 0.001	< 0.001	<0.001
NofMONTHS	12	12	12	10	12	12	12

Figure 3-14 illustrates that freeboard uncertainties for the six regions of the Southern Hemisphere (see Figure 3-2) are also quite constant throughout the entire time series per sensor with little variation during the winter and with a considerable reduction in uncertainty between Envisat and CS-2 which is the same as in the Northern Hemisphere. The largest variations in the freeboard uncertainty occur in region Central Southern Weddell Sea (CSWS) where one can note kind of a seasonal cycle; the amplitude of this cycle is, however, smaller than 0.01 m. Isolated elevated freeboard uncertainty values are observed throughout the entire time series in all regions and can most likely be attributed to very few data points in combination to transition period retrieval conditions such as wet and layered snow.

Table 3-4: Summary of the inter-comparison of the freeboard uncertainty for the Southern Hemisphere for the six regions shown in Figure 3-2: CSWS: Central Southern Weddell Sea, NofNS: North of Neumayer Station, NofSS: North of Syowa Station, NofAIS: North of Amery Ice Shelf, RS: Ross Sea, AS: Amundsen Sea. Given is the average difference of the regional mean freeboard uncertainty CS2 minus Envisat (FBerrDiff) and its standard deviation (SDEVofFBerrDiff), the difference CS2 minus Envisat of the regional freeboard uncertainty standard deviation (FBerrSDEVDiff) and the number of months with valid data (maximum: 17).

Region	CSWS	NofNS	NofSS	NofAIS	RS	AS
FBerrDiff [m]	-0.048	-0.048	-0.048	-0.049	-0.049	-0.049
SDEVofFBerrDiff [m]	0.001	0.005	0.002	0.002	0.002	0.004
FBerrSDEVDiff [m]	-0.001	<0.001	0.002	0.001	<0.001	<0.001
NofMONTHS	17	11	10	10	11	12

As summarized in Table 3-4, average regional differences in the freeboard uncertainties in the Southern Hemisphere are uniform, amount ~5 cm and are hence very similar to the values found for the Northern Hemisphere. The standard deviation of these differences is 5 mm for region North of Neumayer Station (NofNS), only 1 mm for CSWS and 2-4 mm for the other four regions. There is almost no difference in the spatial variability of the freeboard uncertainty within the 5x5 grid cells.

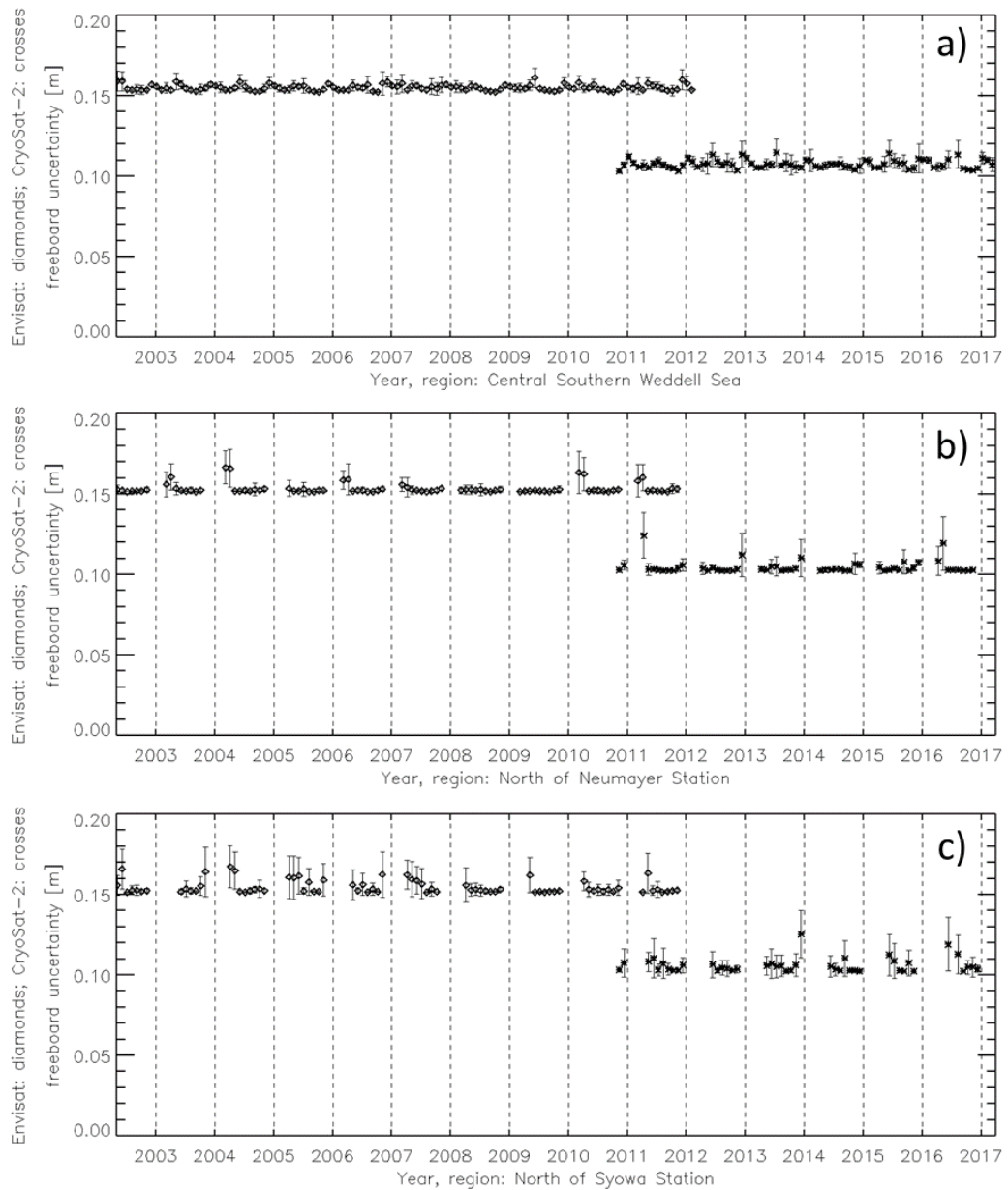


Figure 3-14: Time series of the regional mean freeboard uncertainty for Envisat (diamonds) and CS-2 (crosses) for Southern Hemisphere regions Central Southern Weddell Sea, North of Neumayer Station, and North of Syowa Station (see Figure 3-2). Vertical bars denote plus/minus one standard deviation computed from a minimum of 3 and a maximum of 5x5 grid cells.

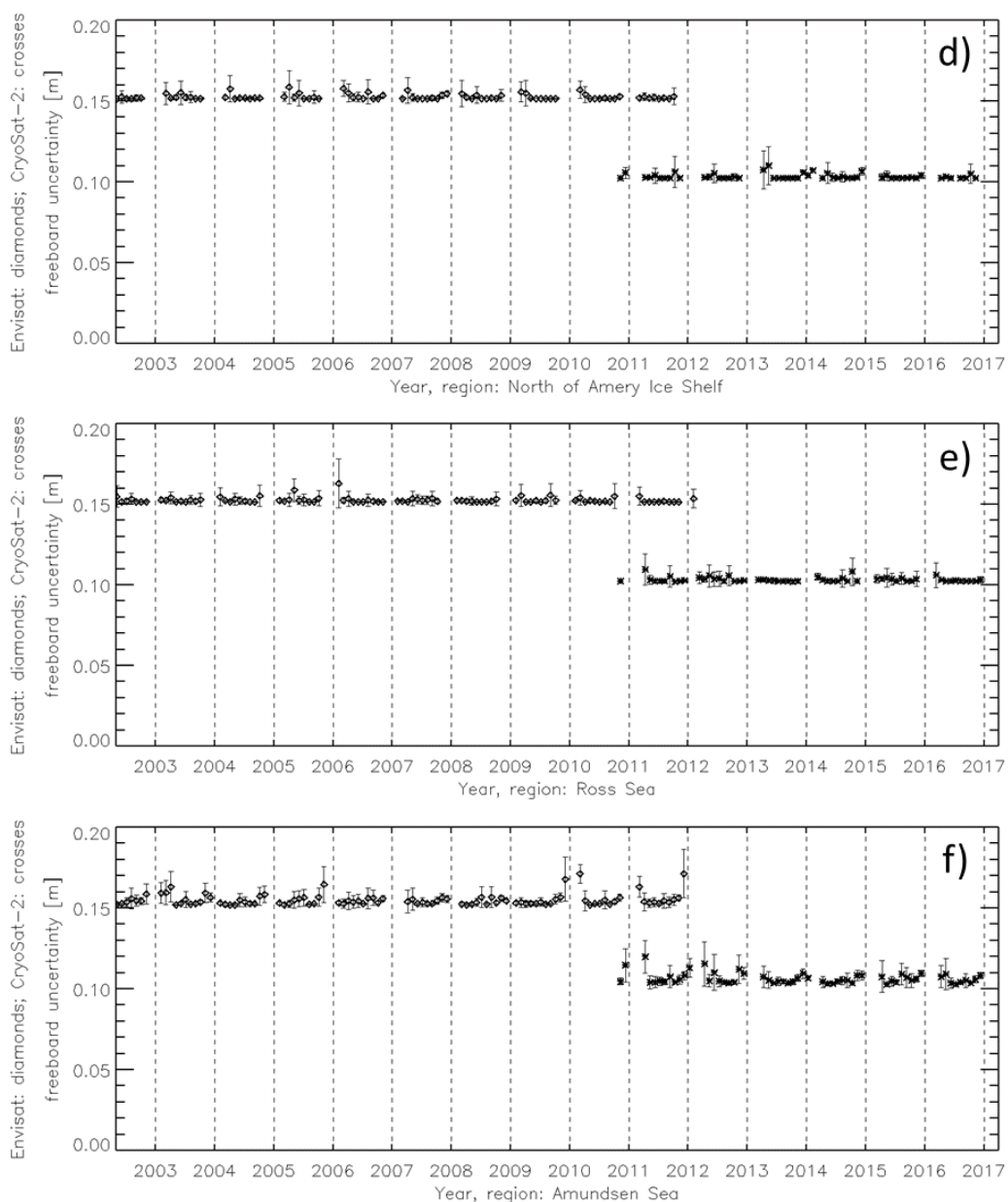


Figure 3-14 continued for Southern Hemisphere regions North of Amery Ice Shelf, Ross Sea, and Amundsen Sea (see Figure 3-2).

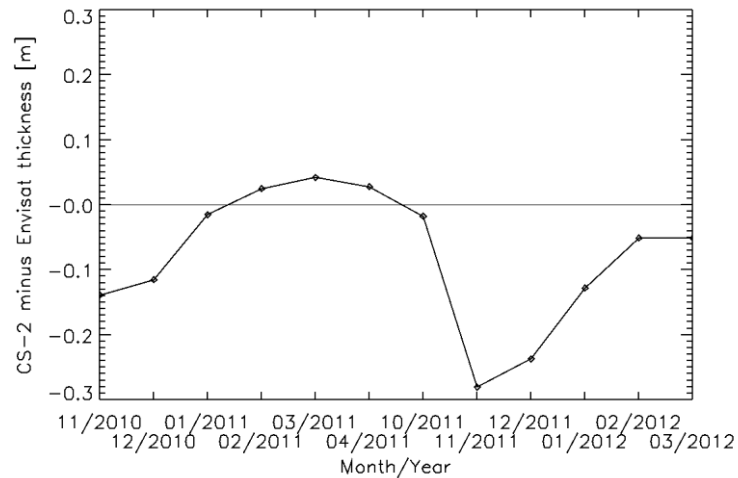
Sea-ice thickness

Figure 3-15: Time series of the hemispheric average sea-ice thickness difference CS2 minus Envisat for the Northern Hemisphere for the overlap period of CS-2 and Envisat. Only months October through April are used.

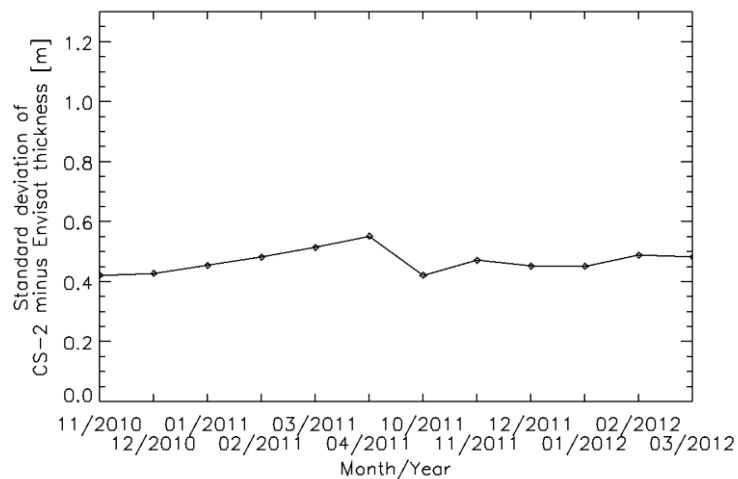


Figure 3-16: As Figure 3-15 but showing the sea-ice thickness difference standard deviation.

Figure 3-15 shows that for the Northern Hemisphere, the hemispheric average sea-ice thickness retrieved from CS-2 and Envisat agrees within 0.2 m except for Nov/Dec 2011. Absolute differences tend to be larger during late fall than during winter and early spring. The standard deviation of the freeboard difference is around 0.5 m (Figure 3-16).

Note that these are basically the times 10 versions of Figure 3-3 and Figure 3-4.

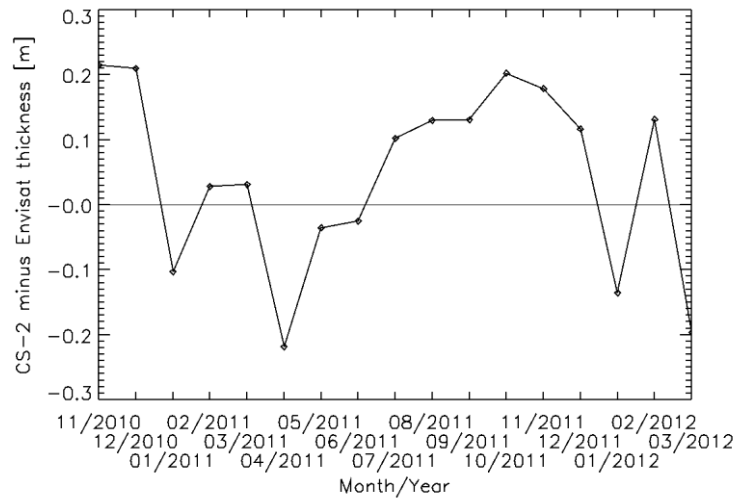


Figure 3-17: Time series of the hemispheric average sea-ice thickness difference CS2 minus Envisat for the Southern Hemisphere for the full overlap period of CS-2 and Envisat.

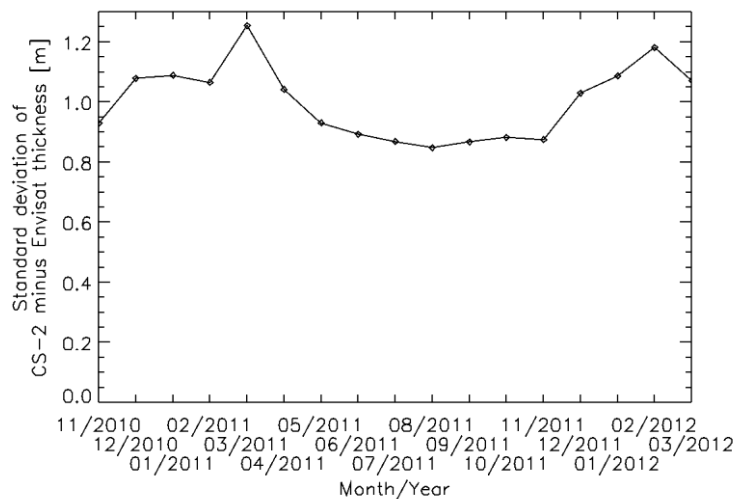


Figure 3-18: As Figure 3-17 but showing the sea-ice thickness difference standard deviation.

For the Southern Hemisphere (Figure 3-17), CS-2 and Envisat sea-ice thickness also mostly agree within 0.2 m. The standard deviation of the thickness difference is quite stable during winter months and into spring (November) around 0.9 m; it is larger than in the Northern Hemisphere (compare Figure 3-16). From late spring through late fall standard deviations are generally above 1 m (Figure 3-18). Note that these are basically the times 10 versions of Figure 3-5 and Figure 3-6.

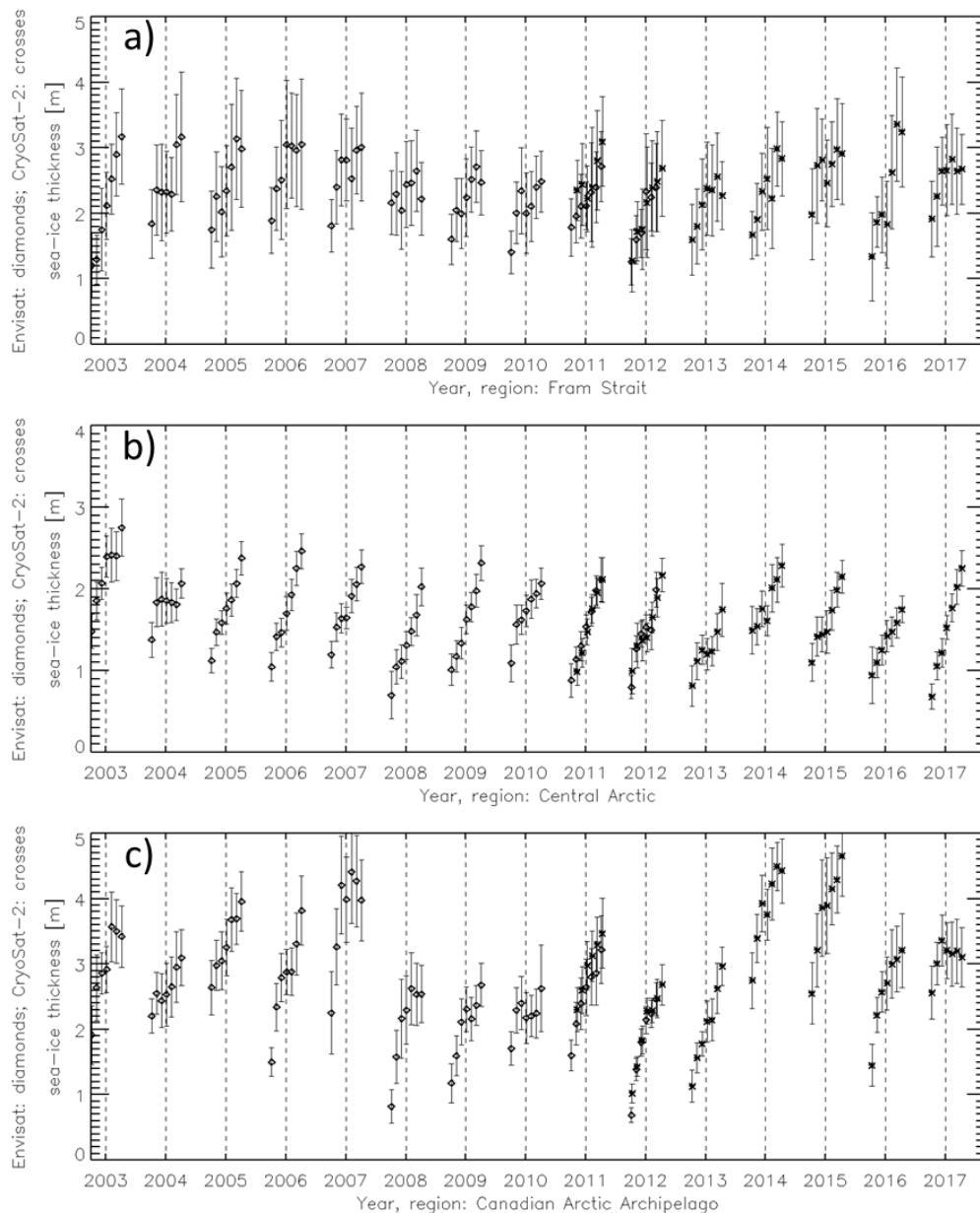


Figure 3-19: Time series of the regional mean sea-ice thickness for Envisat (diamonds) and CS-2 (crosses) for Northern Hemisphere regions Fram Strait, Canadian Arctic Archipelago, and Central Arctic (see Figure 3-1). Vertical bars denote plus/minus one standard deviation computed from a minimum of 3 and a maximum of 11x11 grid cells. Note the different scales of the y-axis.

In Figure 3-19 we show the entire time series of the sea-ice thickness for the seven regions in the Northern Hemisphere (compare Figure 3-1). The seasonal development of the sea-ice thickness seems to be reasonable in view of the different ice conditions. Unlike for the freeboard which does not need to increase necessarily during winter due to the reasons laid out in the context of Figure 3-7, sea-ice thickness increases during most of the winters for basically all six regions. Even in the region Fram Strait (FS), where ice conditions are dominated by the export of sea ice out of the Arctic Ocean, local changes in sea-ice thickness due to thermodynamic ice growth or

deformation are not completely mimicked by the properties of the sea ice upstream of the FS; that sea ice is of course also experiencing thickening during winter. Winters with minor sea-ice thickness increase in the FS are 2008/09 and 2010/11 (Figure 3-19 a)). Obviously, due to the presence of MYI ice, sea-ice thicknesses are largest in regions FS and CAA, followed by the Central Arctic (CeArc). Of note is the small increase in sea-ice thickness from higher late fall/early winter sea-ice thickness values in region SBS in 2014/15 (Figure 3-19 d)) and in region BGEP in 2013/14 and 2014/15 (Figure 3-19 g)) which presumably can be explained with the survival of FYI / import of MYI ice from the direction of region CAA.

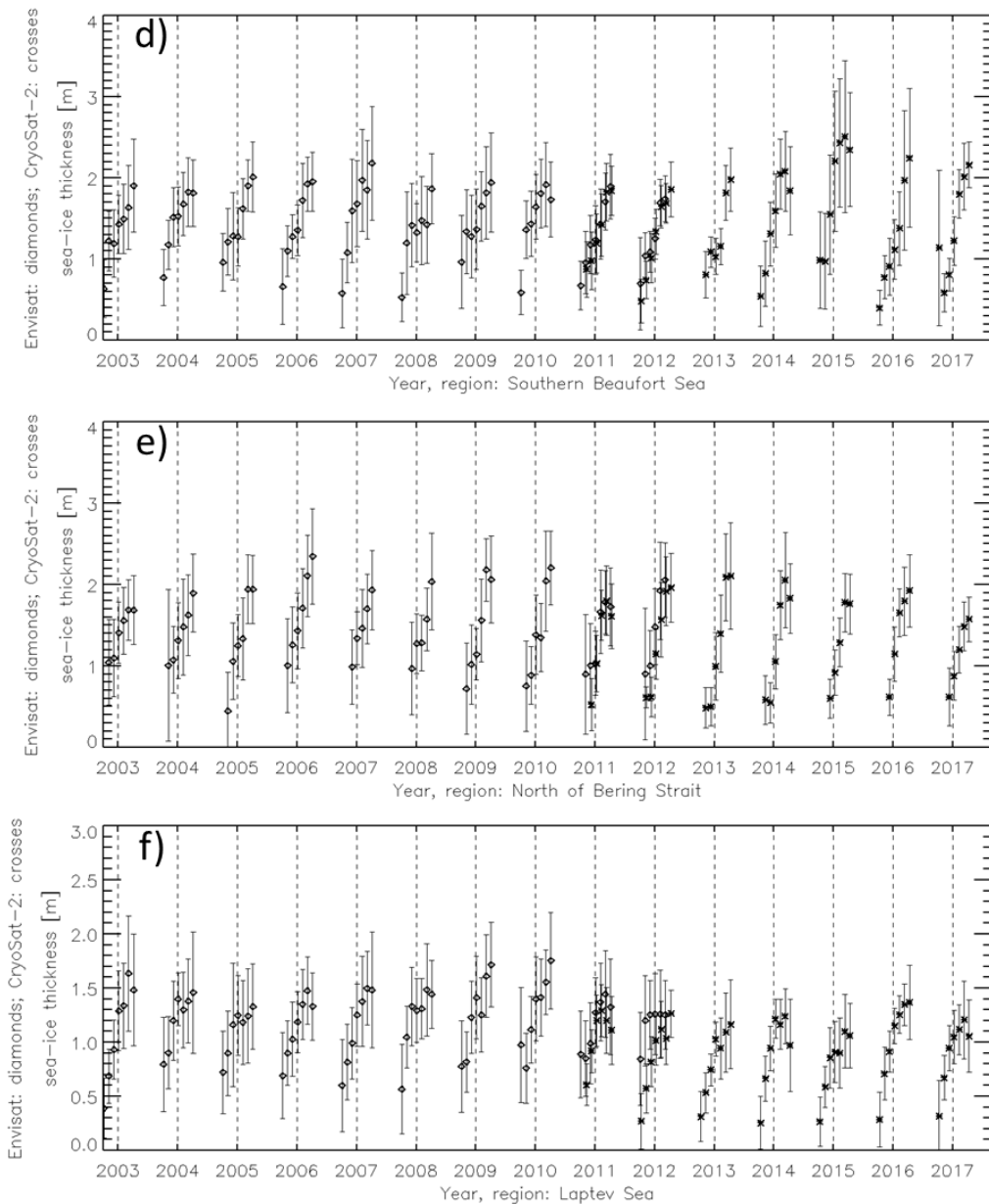


Figure 3-19 continued for Northern Hemisphere regions Southern Beaufort Sea, North of Bering Strait, and Laptev Sea (see Figure 3-1). Note the difference scales of the y-axis.

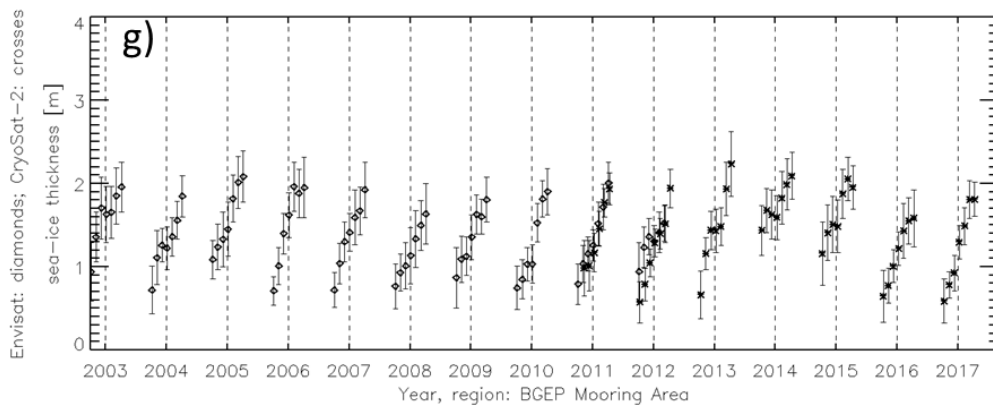


Figure 3-19 continued for Northern Hemisphere region BGEP mooring area (see Figure 3-1).

The time series suggest a smooth transition between Envisat and CS-2 for basically all regions except perhaps regions North of Bering Strait (NofBS) (Figure 3-19 e)) and Laptev Sea (LS) (Figure 3-19 f)). Until including winter 2009/10, typical late fall/early winter sea-ice thickness values in these region were between about 0.5 m to 0.8 m (or 1.0 m) – retrieved from Envisat. Starting with winter 2010/11 these values decrease to around 0.5 m or even below 0.5 m (see region LS) – retrieved from CS-2. While this could be the temporal trend with sea-ice thickness values at the beginning of winter decreasing, it could also be an effect of the change of sensors. Actually, Figure 3-19 e), f), and g) reveal that sea-ice thickness values from Envisat (diamonds) are located by between ~ 0.2 m and ~ 0.5 m above contemporary CS-2 values (crosses). This applies to 8 of the 12 months with valid overlapping data for region LS, to 4 months for region NofBS, and to 3 months for region BGEP. It seems to be more pronounced in the second winter of the overlap period (2011/12) and it seems to be more common for early winter months. We actually believe that smaller sea-ice thickness values at the beginning of winter, as are obtained with CS-2, are more reasonable but more comparisons are needed to prove this statement.

Table 3-5: Summary of the inter-comparison of the sea-ice thickness for the Northern Hemisphere for the seven regions shown in Figure 3-1: CAA: Canadian Arctic Archipelago, FS: Fram Strait, CeArc: Central Arctic, NofBS: North of Bering Strait, LS: Laptev Sea, SBS: Southern Beaufort Sea, and BGEP. Given is the average difference of the regional mean sea-ice thickness CS2 minus Envisat (SITDiff) and its standard deviation (SDEVofSITDiff), the difference CS2 minus Envisat of the regional sea-ice thickness standard deviation (SITSDEVDiff) and the number of months with valid data (maximum: 12).

	CAA	FS	CeArc	NofBS	LS	SBS	BGEP
SITDiff [m]	0.197	0.164	-0.018	-0.212	-0.264	-0.073	-0.128
SDEVofSITDiff [m]	0.144	0.178	0.108	0.177	0.187	0.118	0.160
SITSDEVDiff [m]	-0.012	0.131	0.030	-0.170	-0.133	-0.048	-0.017
NofMONTHS	12	12	12	10	12	12	12

The average differences CS2 minus Envisat sea-ice thickness of the seven regions summarized in Table 3-5 reflect the results of the average difference CS-2 minus Envisat freeboard (see Table 3-1). Positive differences, i.e. CS-2 sea-ice thickness exceeds Envisat sea-ice thickness, are observed for MYI dominated regions CAA and FS. Negative differences, i.e. Envisat sea-ice thickness exceeds CS-2 sea-ice thickness, are observed for FYI dominated regions NofBS and LS. Absolute differences for these four regions are between 0.16 m and 0.26 m. For the MYI dominated regions, a factor of 7 or 8 translates between freeboard difference and sea-ice thickness difference; for all other regions the average sea-ice thickness difference is 10 times the freeboard difference.

The largest variation in the sea-ice thickness difference is observed for regions FS, LS, NofBS and BGEP: almost 0.2 m – which is again similar to 10 times the variation in the freeboard difference (see Table 3-1). Variations in the sea-ice thickness difference are smaller for the other three regions with the minimum one observed for region Central Arctic (CeArc): 0.11 m and region SBS: 0.12 m.

Table 3-5 reveals finally, that also the difference in the variability of the sea-ice thickness values within the 11x11 grid cell boxes is driven by the variability of the respective freeboard values – regarding the sign as well as regarding the magnitude. For the basically FYI covered regions NofBS and LS the Envisat sea-ice thickness varies more than for CS-2. Absolute differences in the sea-ice thickness standard deviation are 0.13 m for LS and 0.17 m for NofBS; other regions exhibit differences < 0.05 m – except region FS, which shows the largest positive difference: 0.13 m, i.e. CS-2 sea-ice thickness varies more (in the 11x11 grid cell box) than Envisat. It seems straightforward to understand why region FS has such a large difference pointing to a more variable CS-2 than Envisat sea-ice thickness: the finer spatial resolution allows to resolve more different ice types and provides more different sea-ice thickness values. Why this difference is also large in regions NofBS and LS and, in addition, has a different sign, needs to be discussed.

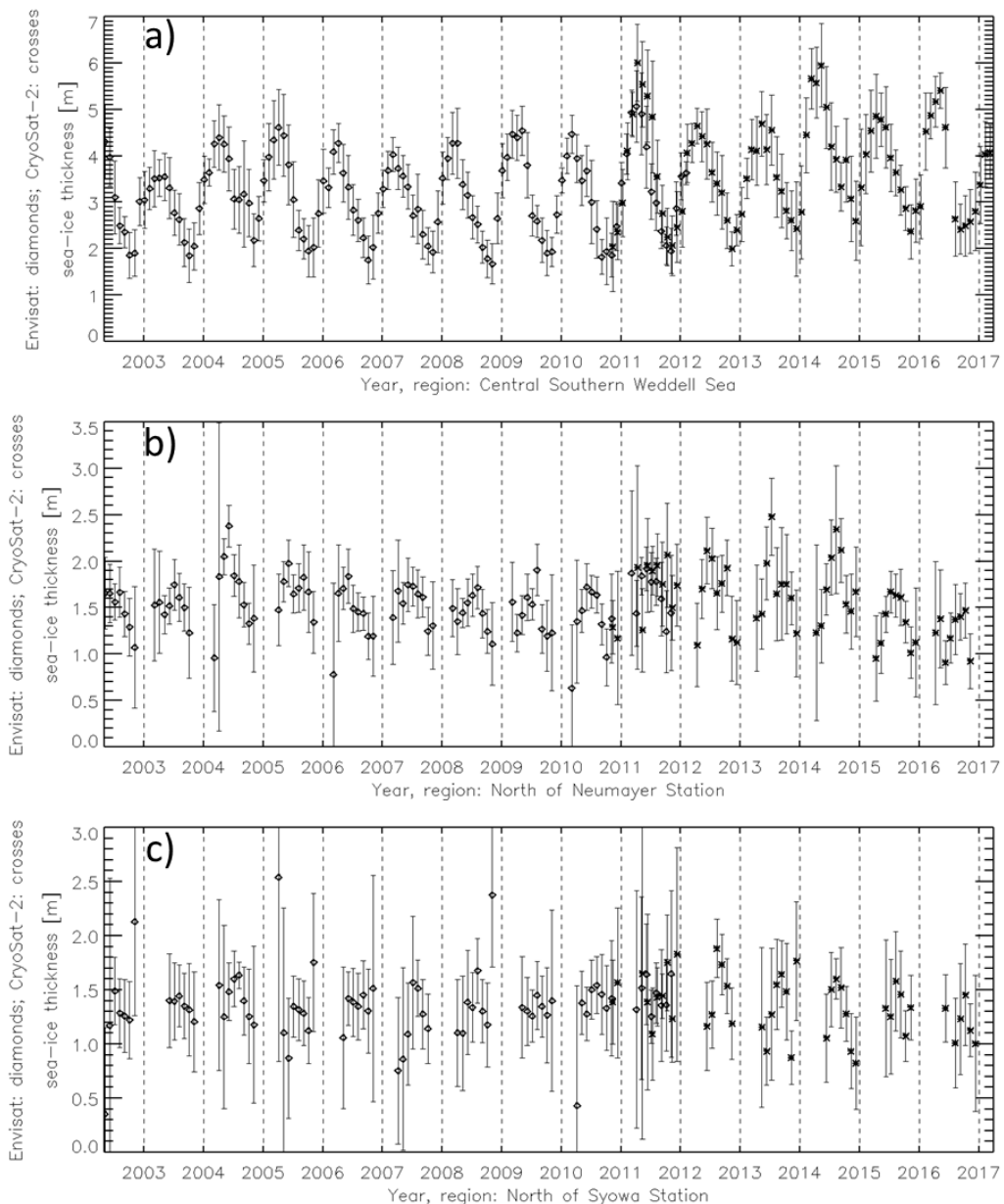


Figure 3-20: Time series of the regional mean sea-ice thickness for Envisat (diamonds) and CS-2 (crosses) for Southern Hemisphere regions Central Southern Weddell Sea, North of Neumayer Station, and North of Syowa Station (see Figure 3-2). Vertical bars denote plus/minus one standard deviation computed from a minimum of 3 and a maximum of 5x5 grid cells. Note the different scales of the y-axis.

According to the retrievals of Envisat and CS-2 the sea-ice thickness in the Southern Hemisphere regions does not increase too much during winter if it does increase at all. There is almost no seasonal cycle – in contrast to the Northern Hemisphere (see Figure 3-19). The main exception is the region depicted in the Weddell Sea (CSWS, Figure 3-20 a)) where thick old ice is replaced by thin young ice originating from the Ronne-Filchner Ice Shelf polynya and hence the sea-ice thickness decreases during winter until October/November. After that the sea-ice thickness in that region increases

until a maximum in March/April. It is challenging to explain this increase. One reason could be that due to summer melt the fraction of the thick old ice in that region increases at the expense of the thin younger ice. Another reason could be enhanced thickness gain due to deformation. However, no matter, which explanation holds it seems that the maximum sea-ice thickness of more than 4 m or even 5 m obtained by both Envisat and CS-2 is too large. One possible reason for this could be the usage of a snow depth product which – in comparison to snow depth buoy data of the AWI – seems to drastically under-estimate snow depth on sea ice.

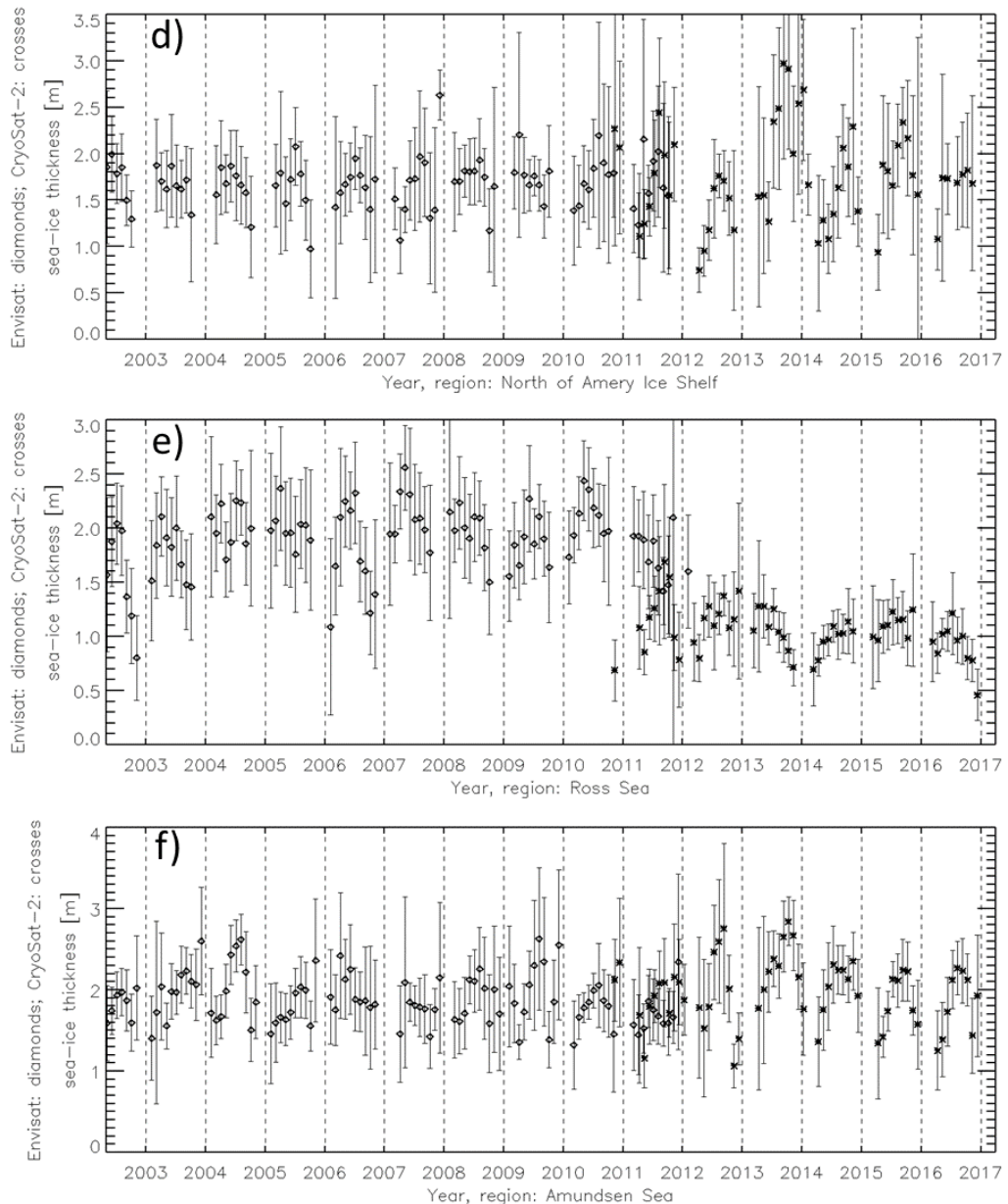


Figure 3-20 continued for Southern Hemisphere regions North of Amery Ice Shelf, Ross Sea, and Amundsen Sea (see Figure 3-2). Note the different scales of the y-axis.

One example for at least a few seasonal increases in sea-ice thickness is region North of Amery Ice Shelf (NofAIS) years 2010, 2012, and 2014

(Figure 3-20 d)). In most regions sea-ice thickness values are already around 1.5 m (North of Neumayer Station, NofNS, Figure 3-20 b)) or even higher (NofAIS) in early winter – despite the fact that these are regions dominated by FYI. Only for region North of Syowa Station (NofSS, Figure 3-20 c)) early winter sea-ice thickness values below 1.0 m are observed occasionally. It seems relatively likely that the sea-ice thickness is in general over-estimated by Envisat and CS-2 in early winter.

Still, the time series of the average regional sea-ice thickness in the Southern Hemisphere shown in Figure 3-20 illustrate that for most regions the transition between Envisat and CS-2 seems to be smooth; for single months differences between Envisat and CS-2 sea-ice thickness can easily exceed 0.5 m, however.

As has been discussed already in the context of Figure 3-8 e), Envisat seems to have serious problems with sea-ice conditions in region RS; this is reflected in way too thick sea ice with values between 1.0 m and above 2.5 m for the Envisat period in an area where smooth thin FYI generated in the Ross Ice Shelf polynya is dominating the sea-ice cover in most years. The much smaller sea-ice thickness values obtained with CS-2 for years 2011+ seem to be much more realistic for this region – but might still be too thick. We also list region NofAIS here because of the quite inconsistent sea-ice thickness values found for winter 2013 (Figure 3-20 d)). Note that during the overlap period sea-ice thickness values derived with Envisat and CS-2 in region NofAIS differ by more than 0.8 m for a few months and this difference has different signs.

Table 3-6: Summary of the inter-comparison of the sea-ice thickness for the Southern Hemisphere for the six regions shown in Figure 3-2: CSWS: Central Southern Weddell Sea, NofNS: North of Neumayer Station, NofSS: North of Syowa Station, NofAIS: North of Amery Ice Shelf, RS: Ross Sea, AS: Amundsen Sea. Given is the average difference of the regional mean sea-ice thickness CS2 minus Envisat (SITDiff) and its standard deviation (SDEVofSITDiff), the difference CS2 minus Envisat of the regional sea-ice thickness standard deviation (SITSDEVDiff) and the number of months with valid data (maximum: 17).

Region	CSWS	NofNS	NofSS	NofAIS	RS	AS
SITDiff [m]	0.397	0.116	0.045	0.092	-0.643	0.230
SDEVofSITDiff [m]	0.358	0.215	0.272	0.407	0.478	0.361
SITSDEVDiff [m]	0.184	0.087	0.060	0.028	-0.248	0.048
NofMONTHS	17	11	10	10	11	12

The average differences CS2 minus Envisat sea-ice thickness of the six regions summarized in Table 3-6 reflect the results of the average difference CS-2 minus Envisat freeboard (see Table 3-2). Positive differences, i.e. CS-2 sea-ice thickness exceeds Envisat sea-ice thickness, are observed for all regions but region RS with a maximum difference of ~0.4 m for region CSWS and a minimum of ~0.05 m for region NofSS. Negative differences, i.e. Envisat sea-ice thickness exceeds CS-2 sea-ice thickness, are only observed for region RS where the absolute difference exceeds 0.64 m. For

all regions the sea-ice thickness difference can be approximated by 10 times the freeboard difference (compare Table 3-2). The standard deviations of the sea-ice thickness difference are in line with those of the freeboard difference (see Table 3-2). The smallest variation in the differences of ~ 0.22 m is observed for region NofSS, the largest one occurs in region RS: 0.48 m. As with regard to the difference of spatial variabilities of the sea-ice thickness between CS-2 and Envisat we can also elaborate on Table 3-2 and have CS-2 providing a larger spatial variability of sea-ice thickness particularly for regions CSWS with absolute differences of ~ 0.25 m (Table 3-6) but also for regions NofNS: ~ 0.1 m, while for region RS Envisat provides the larger spatial variability: 0.25 m.

Sea-ice thickness uncertainty

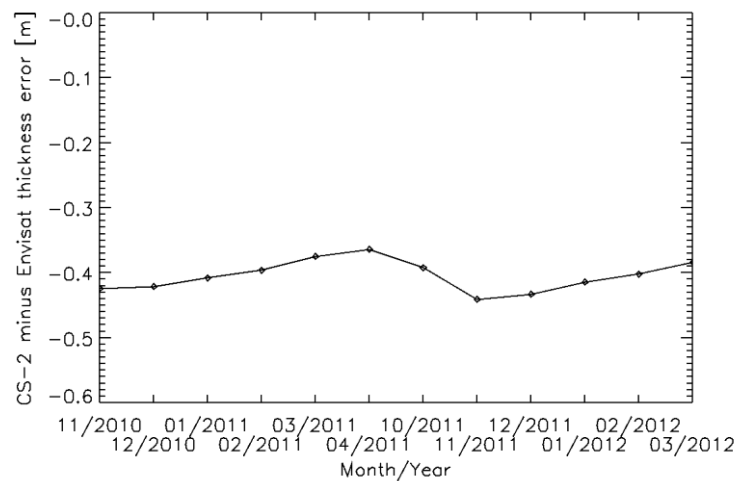


Figure 3-21: Time series of the hemispheric average sea-ice thickness uncertainty difference CS2 minus Envisat for the Northern Hemisphere for the overlap period of CS-2 and Envisat. Only months October through April are used.

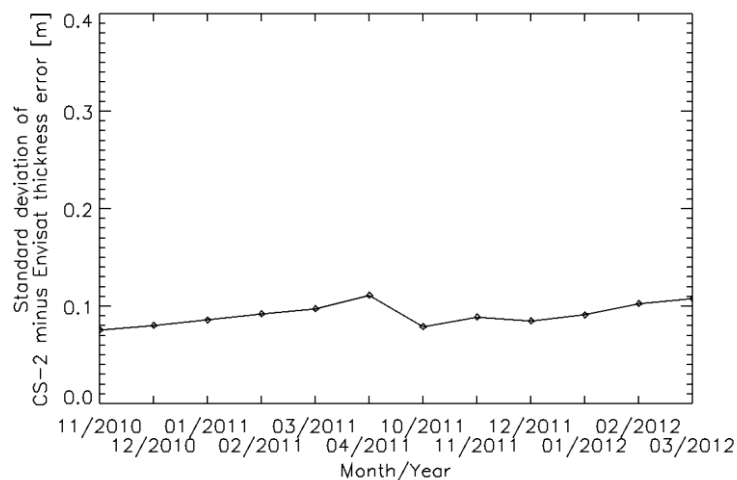


Figure 3-22: As Figure 3-21 but showing the sea-ice thickness uncertainty difference standard deviation.

Figure 3-21 shows the time series of the hemispheric average sea-ice thickness uncertainty difference and Figure 3-22 the respective standard deviation for the Northern Hemisphere. Figure 3-21 reveals that hemispheric average sea-ice thickness uncertainties are about 0.4 m larger for Envisat than for CS-2, i.e. 9-10 times larger than the freeboard uncertainty shown in Figure 3-10; the shape of the graphs of Figure 3-21 and Figure 3-10 are very similar. Like for the freeboard, the standard deviation of the sea-ice thickness uncertainty difference CS-2 minus Envisat is small and quite uniform around ~0.1 m (Figure 3-22).

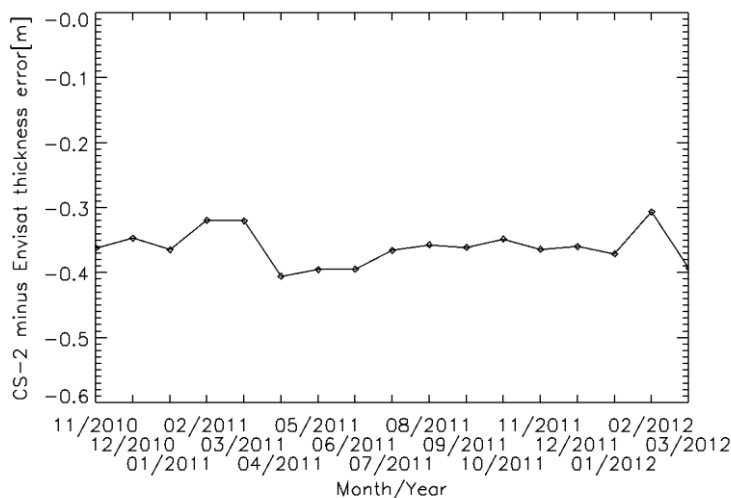


Figure 3-23: Time series of the hemispheric average sea-ice thickness uncertainty difference CS2 minus Envisat for the Southern Hemisphere for the full overlap period of CS-2 and Envisat.

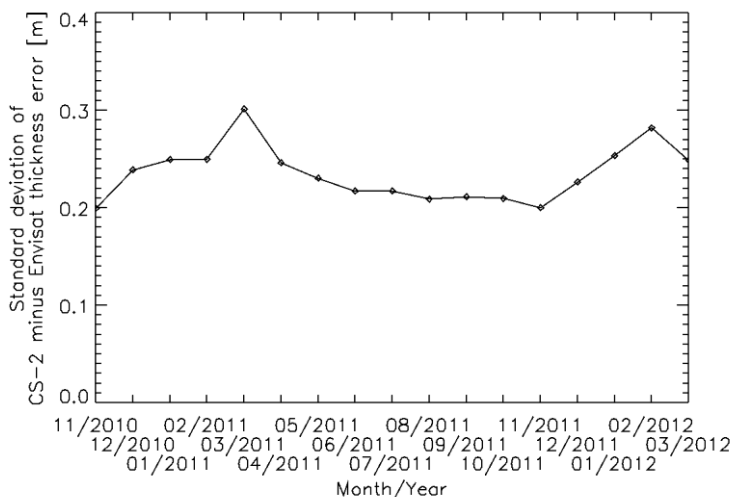


Figure 3-24: As Figure 3-23 but showing the sea-ice thickness difference standard deviation.

Figure 3-23 shows the time series of the hemispheric average sea-ice thickness uncertainty difference and Figure 3-24 the respective standard deviation for the Southern Hemisphere. Sea-ice thickness uncertainties

differences range between 0.3 m and 0.4 m at hemispheric scale, with the smaller uncertainty obtained with CS-2. The standard deviation of the hemispheric average sea-ice thickness uncertainty difference (Figure 3-24) is ~ 0.2 m during winter and slightly higher during summer – a factor of 10-12 compared to the respective standard deviation of the freeboard uncertainty difference (compare Figure 3-12).

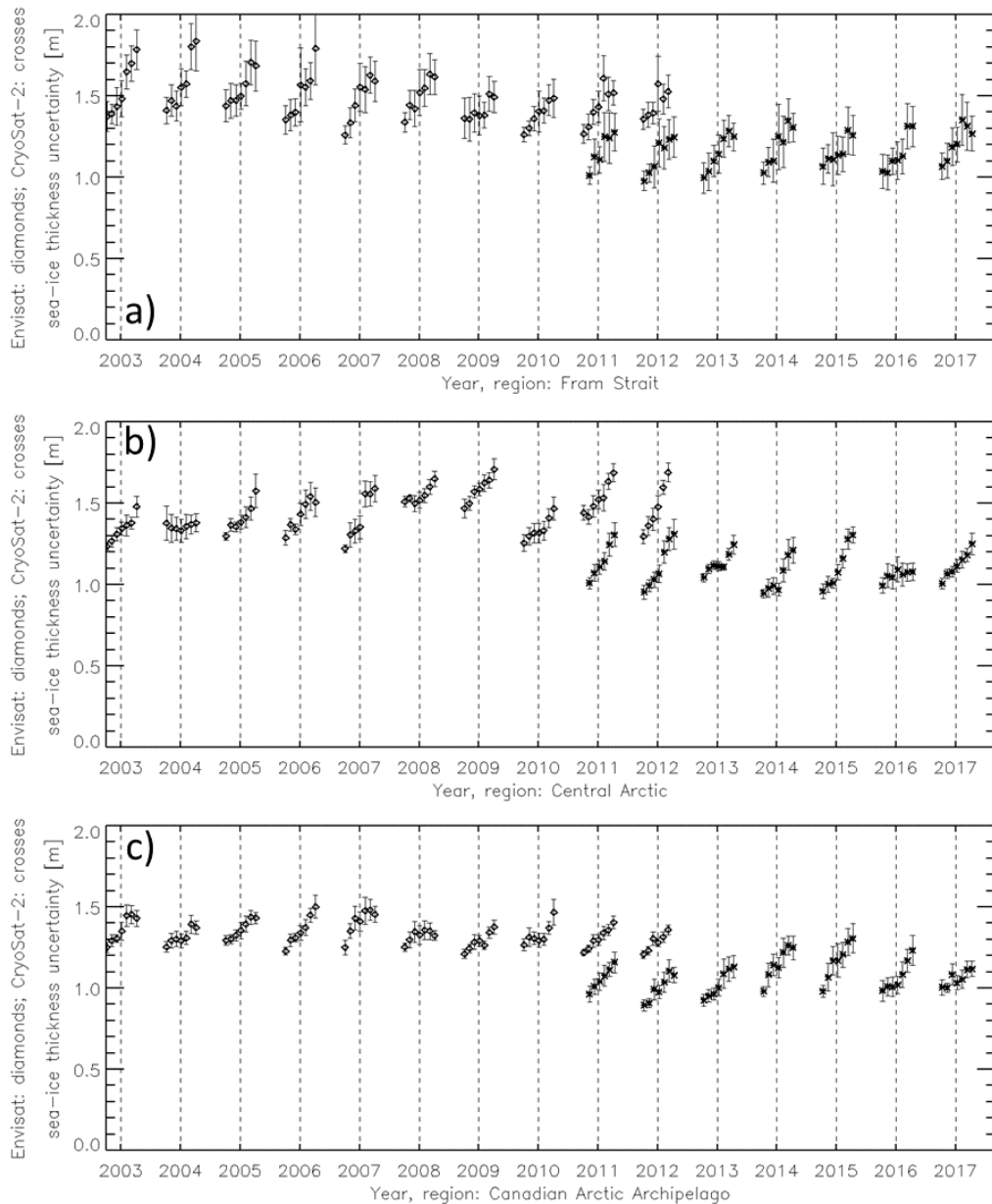


Figure 3-25: Time series of the regional mean sea-ice thickness uncertainty for Envisat (diamonds) and CS-2 (crosses) for Northern Hemisphere regions Fram Strait, Canadian Arctic Archipelago, and Central Arctic. Vertical bars denote plus/minus one standard deviation computed from a minimum of 3 and a maximum of 11x11 grid cells.

Figure 3-25 displays the time series of the regional mean sea-ice thickness uncertainty for the regions in the Northern Hemisphere. Sea-ice thickness

uncertainties are substantially above 1 m for Envisat (1.2 m to 1.8 m) and around 1 m (0.8 m to 1.4 m) for CS-2; during some winter seasons in some regions uncertainties might be larger than that, i.e. Central Arctic 2007/08 and 2008/09 (Figure 3-25 c)). It seems like uncertainties are on average larger for FYI dominated regions such as the Laptev Sea (Figure 3-25 f)) than for MYI dominated regions such as CAA (Figure 3-25 b)). We can observe a larger variation over winter for the MYI dominated regions than the FYI dominated regions, e.g. compare Laptev Sea with Central Arctic. For all seven regions we observe a considerable reduction in sea-ice thickness uncertainty from Envisat to CS-2. We note that also the regional sea-ice thickness uncertainties are about 10 times larger than the regional freeboard uncertainties.

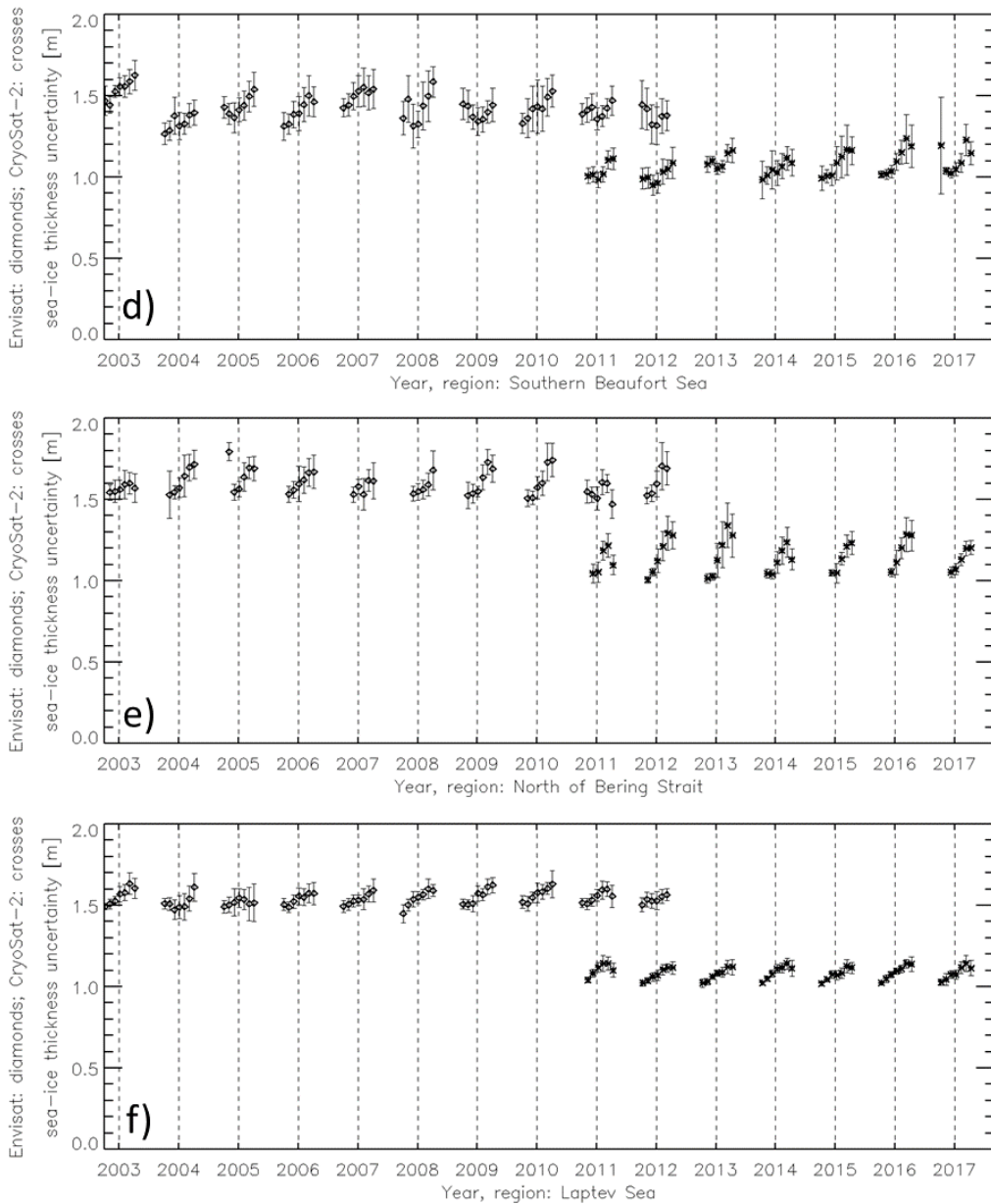


Figure 3-25 continued for Northern Hemisphere regions Southern Beaufort Sea, North of Bering Strait, and Laptev Sea.

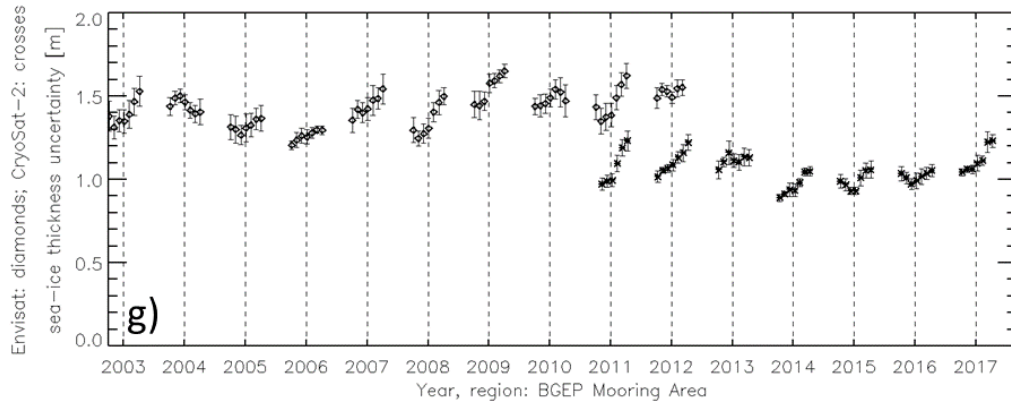


Figure 3-25 continued for Northern Hemisphere region BGEP mooring area.

Table 3-7: Summary of the inter-comparison of the sea-ice thickness uncertainty for the Northern Hemisphere: CAA: Canadian Arctic Archipelago, FS: Fram Strait, CeArc: Central Arctic, NofBS: North of Bering Strait, LS: Laptev Sea, SBS: Southern Beaufort Sea, BGEP: BGEP mooring area. Given is the average difference of the regional mean sea-ice thickness uncertainty CS2 minus Envisat (SITerrDiff) and its standard deviation (SDEVofSITerrDiff), the difference CS2 minus Envisat of the regional sea-ice thickness uncertainty standard deviation (SITerrSDEVDiff) and the number of months with valid data (maximum: 12).

Region	CAA	FS	CeArc	NofBS	LS	SBS	BGEP
SITerrDiff [m]	-0.280	-0.316	-0.391	-0.448	-0.461	-0.375	-0.413
SDEVofSITerrDiff [m]	0.028	0.043	0.023	0.051	0.016	0.041	0.037
SITerrSDEVDiff [m]	0.020	0.015	-0.004	-0.015	-0.016	-0.037	-0.021
NofMONTHS	12	12	12	10	12	12	12

Table 3-7 demonstrates that the absolute differences in the sea-ice thickness uncertainty between Envisat and CS-2 range between 0.28 m for region CCA and 0.46 m for region Laptev Sea. Clearly, Envisat sea-ice thickness uncertainties exceed CS-2 uncertainties and the difference is largest for FYI-dominated regions. The standard deviations of the uncertainty differences range between 0.02 m and 0.05 m and seem not to reflect any dependence on sea-ice type. The spatial variation of the sea-ice thickness uncertainties within regional boxes selected is between +/- 0.02m, except for region SBS: ~ 4 cm. We note that this difference is positive for MYI-dominated regions (CAA and FS) and negative for FYI-dominated regions.

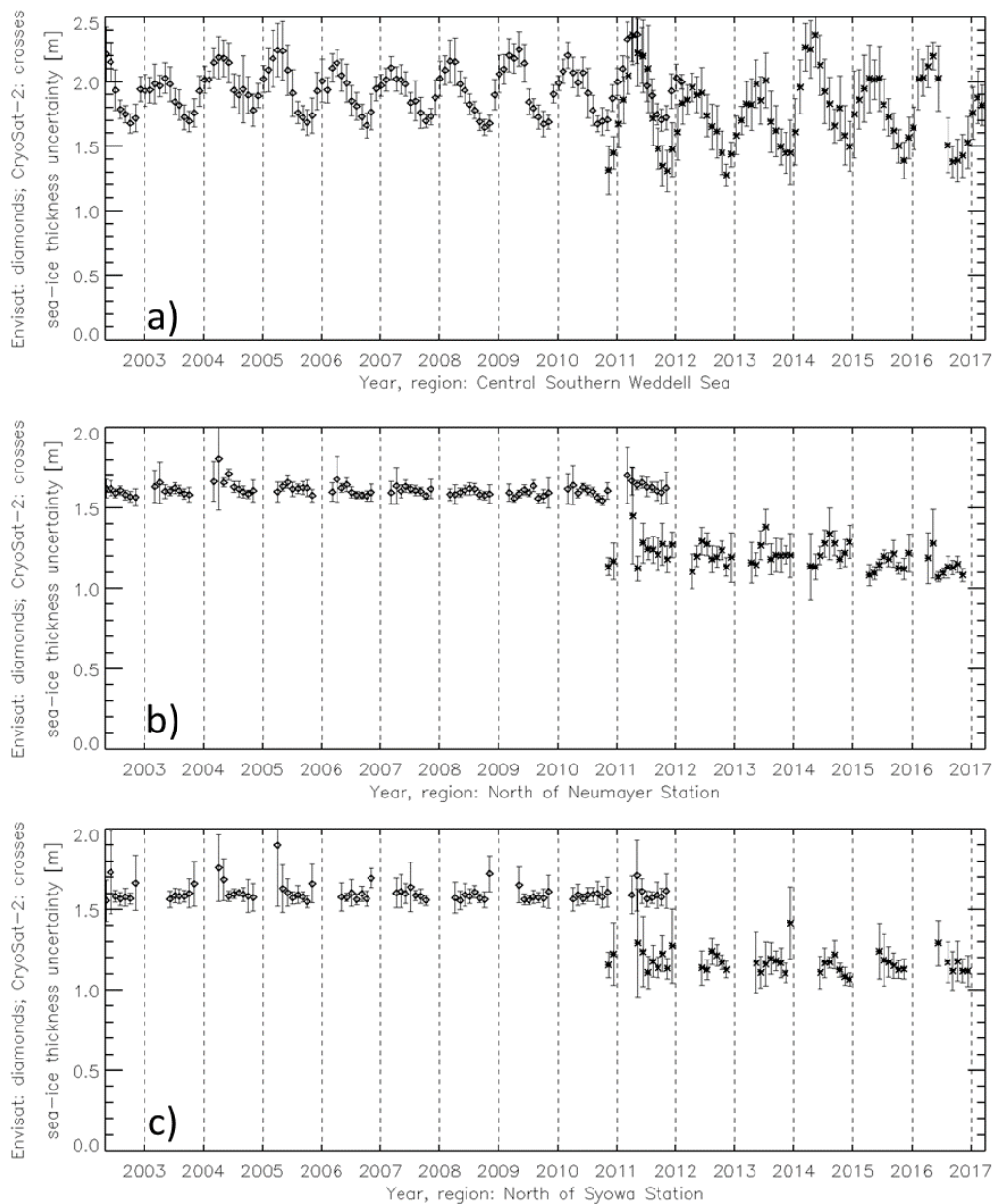


Figure 3-26: Time series of the regional mean sea-ice thickness uncertainty for Envisat (diamonds) and CS-2 (crosses) for Southern Hemisphere regions Central Southern Weddell Sea, North of Neumayer Station, and North of Syowa Station (see Figure 3-2). Vertical bars denote plus/minus one standard deviation computed from a minimum of 3 and a maximum of 5x5 grid cells.

In the Southern Hemisphere sea-ice thickness uncertainties take values around about 1.2 m for CS-2 and around 1.7 m for Envisat (Figure 3-26). Regions with a notable fraction of perennial / old ice, e.g., the Central Southern Weddell Sea (CSWS) and also the Amundsen Sea, reveal even larger uncertainties of up to > 2 m (Figure 3-26 a) and f)). We find a pronounced seasonal cycle in the sea-ice thickness uncertainties in region CSWS. We find a substantial reduction of the sea-ice thickness uncertainty from Envisat to CS-2.

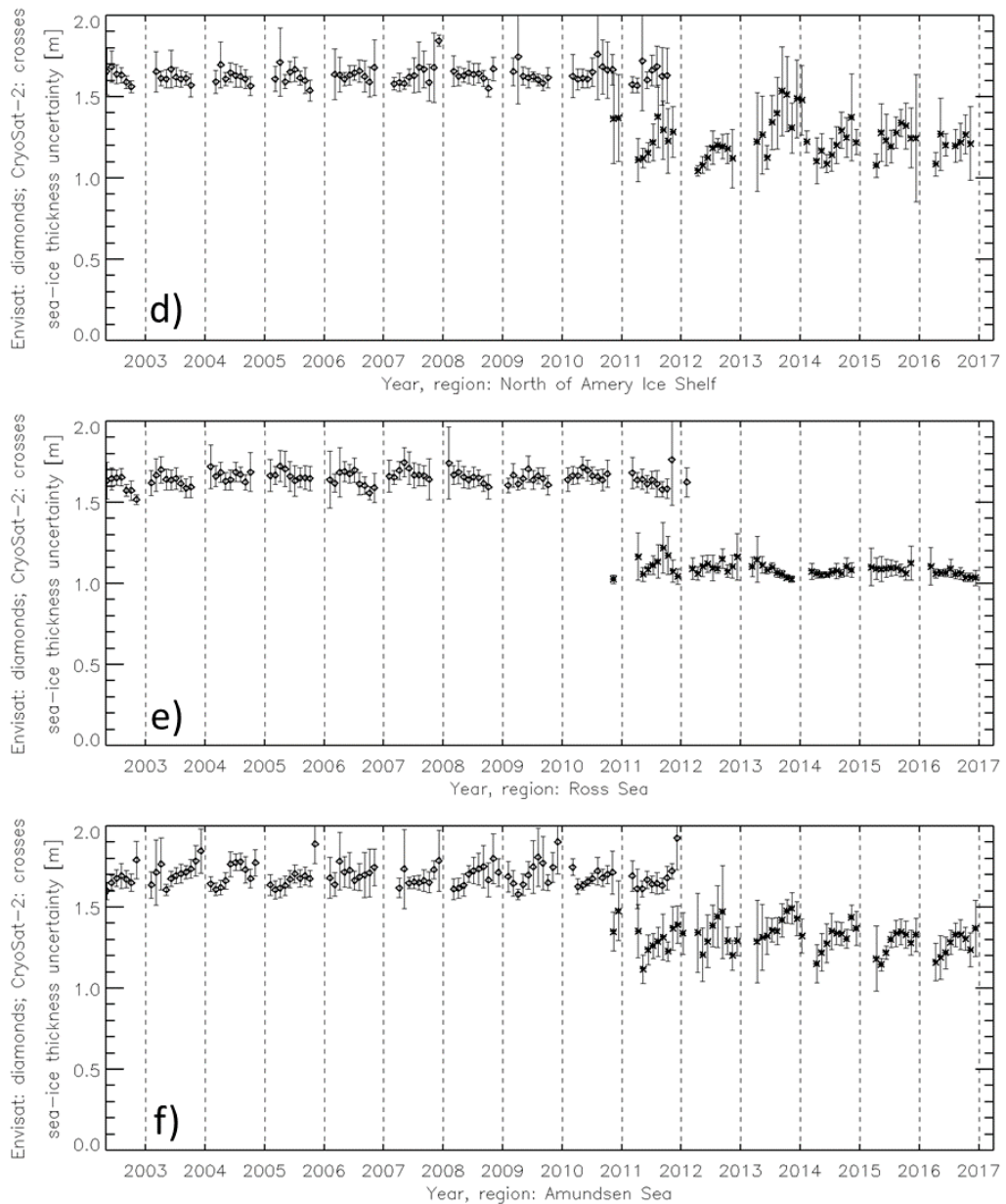


Figure 3-26 continued for Southern Hemisphere regions North of Amery Ice Shelf, Ross Sea, and Amundsen Sea (see Figure 3-2).

Table 3-8 illustrates how much sea-ice thickness uncertainty improves, on average, between the Envisat and the CS-2 period; the improvement is smallest for region CWSW: 0.22 m and largest for region Ross Sea: 0.53 m. For the remaining four regions the improvement is ~0.4 m. smooth this transition between Envisat and CS-2 is in the Southern Hemisphere in terms of the sea-ice thickness uncertainty. The standard deviation of the difference is largest in region CWSW: 0.13 m and smallest in the two other regions from the central and eastern Weddell Sea used, NofNS and NofSS: 0.07 and 0.06 cm. All regions but the Ross Sea show a positive difference of the uncertainty standard deviation between CS-2 and Envisat, i.e. CS-2 is having a more variable sea-ice thickness uncertainty than Envisat; values range between 0.03 m and 0.07 m. This difference is ~0 m in the Ross Sea.

Table 3-8: Summary of the inter-comparison of the sea-ice thickness uncertainty for the Southern Hemisphere for the six regions shown in Figure 3-2: CSWS: Central Southern Weddell Sea, NofNS: North of Neumayer Station, NofSS: North of Syowa Station, NofAIS: North of Amery Ice Shelf, RS: Ross Sea, AS: Amundsen Sea. Given is the average difference of the regional mean sea-ice thickness uncertainty CS2 minus Envisat (SITerrDiff) and its standard deviation (SDEVofSITerrDiff), the difference CS2 minus Envisat of the regional sea-ice thickness uncertainty standard deviation (SITerrSDEVDiff) and the number of months with valid data (maximum: 17).

Region	CSWS	NofNS	NofSS	NofAIS	RS	AS
SITerrDiff [m]	-0.221	-0.393	-0.406	-0.388	-0.534	-0.377
SDEVofSITerrDiff [m]	0.130	0.073	0.062	0.087	0.094	0.091
SITerrSDEVDiff [m]	0.073	0.044	0.060	0.035	-0.008	0.034
NofMONTHS	17	11	10	10	11	12

Additional Results

In this sub-section we provide values of the correlation, the number of valid data pairs, and the overall average differences in freeboard and its uncertainty as well as thickness and its uncertainty for the entire hemispheres for the overlap period Envisat CS-2.

All correlation values shown in the following figures and tables are computed assuming a linear relationship between the two data sets over a maximum number of 12 months for the Northern Hemisphere and 17 months for the Southern Hemisphere. Note (again) that for the Northern Hemisphere only months October through April are considered while for the Southern Hemisphere data from all months are used.

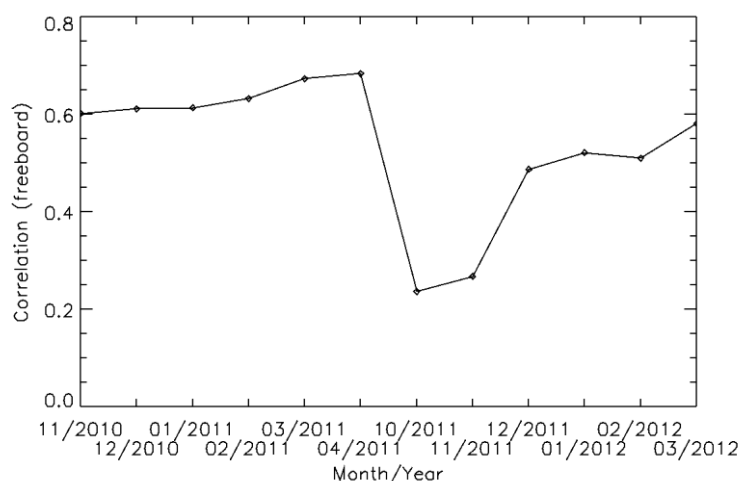


Figure 3-27: Time series of the correlation between valid freeboard values for the Envisat – CS-2 overlap period for the Northern.

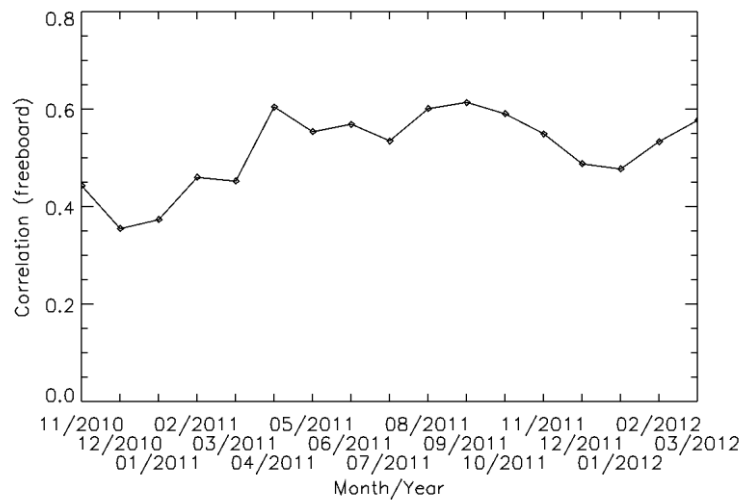


Figure 3-28: As Figure 3-27 but showing results for the Southern Hemisphere.

Figure 3-27 and Figure 3-28 illustrate that freeboard is only moderately correlated between Envisat and CS-2 in the monthly freeboard maps. In the Northern Hemisphere (Figure 3-27) the correlation varies between 0.25 and 0.65 without a seasonal cycle but with clearly better results for the first winter of overlap. In the Southern Hemisphere (Figure 3-28) we observe relatively constant correlation values of ~ 0.55 throughout the freezing season.

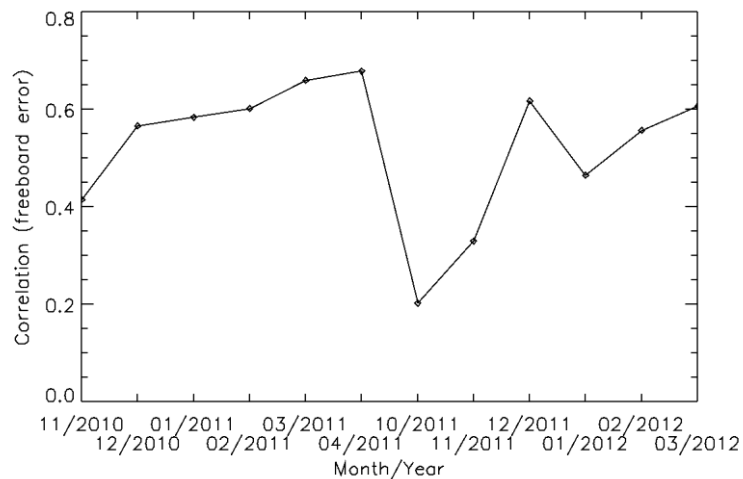


Figure 3-29: Time series of the correlation between valid freeboard uncertainty values for the Envisat - CS-2 overlap period for the Northern Hemisphere.

Figure 3-29 illustrates that the correlation between monthly maps of the freeboard uncertainty is similar to that found for the freeboard itself (Figure 3-27). In the Southern Hemisphere (Figure 3-30), correlations of freeboard uncertainties are more variable and smaller (around 0.45) than correlations of the freeboard itself (compare Figure 3-28).

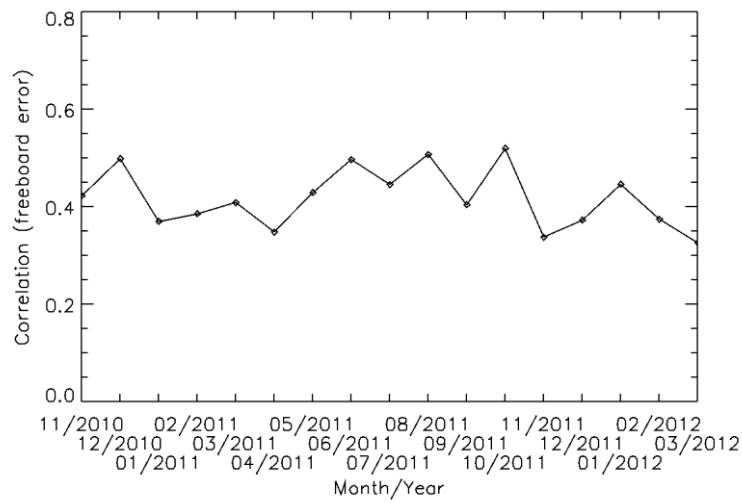


Figure 3-30: As Figure 3-29 but showing results for the Southern Hemisphere.

The correlation between sea-ice thickness maps obtained with Envisat and CS-2 in the Northern Hemisphere is as low as for the freeboard; it takes values between 0.25 and 0.65 (Figure 3-27) with higher values during the first overlapping winter and lower values during the second one. The correlation is notably larger in the Southern Hemisphere with values between 0.45 and 0.7 (Figure 3-32) and a mean during winter of ~ 0.65 .

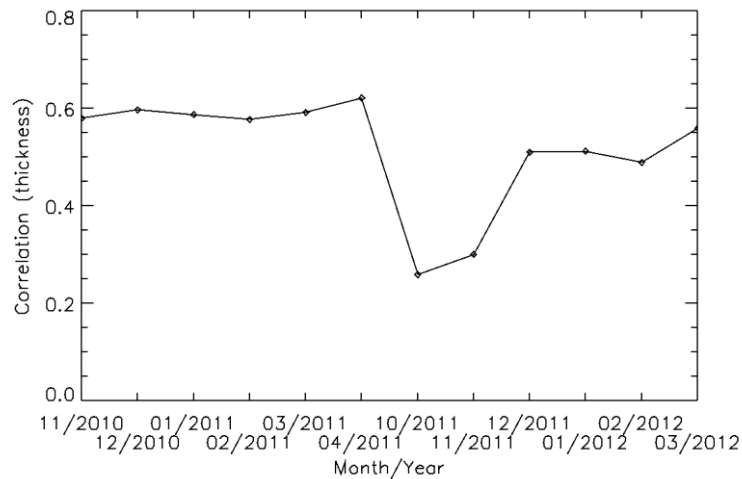


Figure 3-31: Time series of the correlation between valid sea-ice thickness values for the Envisat – CS-2 overlap period for the Northern Hemisphere.

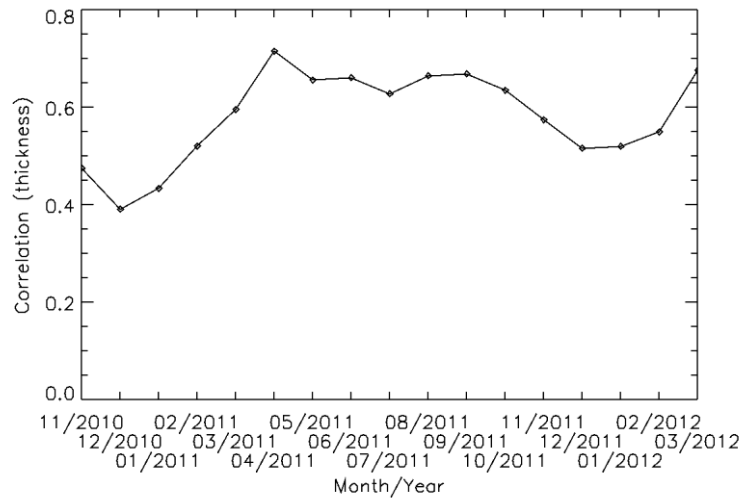


Figure 3-32: As Figure 3-31 but showing results for the Southern Hemisphere.

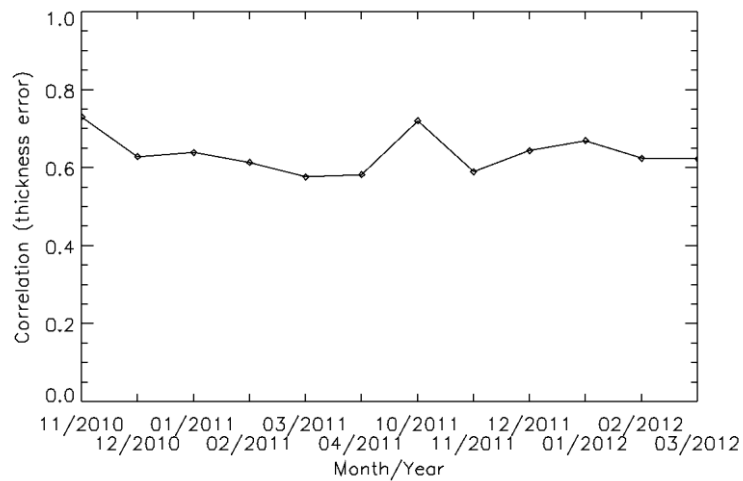


Figure 3-33: Time series of the correlation between valid sea-ice thickness uncertainty values for the Envisat – CS-2 overlap period for the Northern Hemisphere.

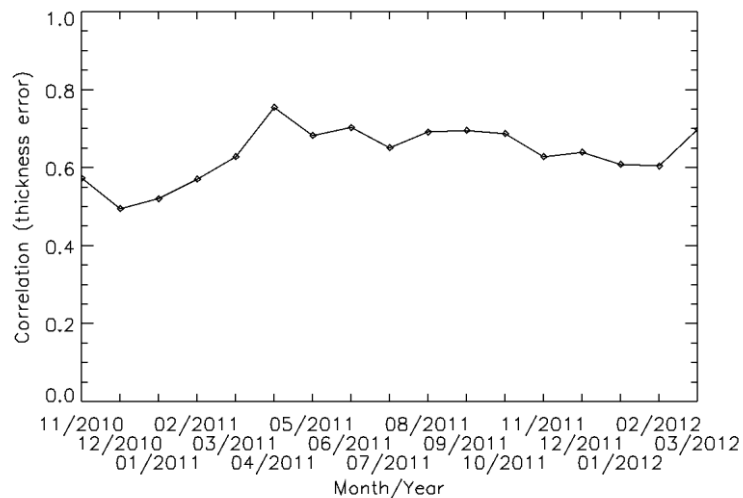


Figure 3-34: As Figure 3-33 but showing results for the Southern Hemisphere.

In contrast to Figure 3-31 and Figure 3-32, the correlation between sea-ice thickness uncertainty values based on Envisat and CS-2 is ~ 0.6 in the Northern Hemisphere. It is hence better correlated than the sea-ice thickness itself and also than the freeboard and freeboard uncertainty maps (Figure 3-27 through Figure 3-30). In the Southern Hemisphere, the correlation between the respective sea-ice thickness uncertainties is of the same order of magnitude with a winter-time average of ~ 0.65 – similar to the sea-ice thickness itself (compare Figure 3-32).

For the Northern Hemisphere, the number of valid data pairs varies between a low of ~ 2500 in October 2011 to a high of ~ 10200 in February 2011. For the Southern Hemisphere, the number of valid data pairs varies between a low of ~ 400 in February 2011 and a high of ~ 5400 in September 2011. Note that the data of the Southern Hemisphere have a grid resolution of 50 km compared to 25 km for the Northern Hemisphere and therefore the numbers given for the Southern Hemisphere would increase by a factor of 4 would a grid with 25 km resolution be used.

Summary

- The average hemispheric difference between CS-2 and Envisat is about 0.02 m for freeboard. It is around 0.1 m for sea-ice thickness.
- Hemispheric scale correlations of the four quantities between Envisat and CS-2 are relatively low: between 0.45 and 0.65
- On regional scale for the Northern Hemisphere, freeboard is overestimated by CS-2 compared to Envisat by 2-3 cm for regions with an applicable MYI fraction; in regions dominated by FYI, freeboard is underestimated by 2-3 cm by CS-2. This translates into a sea-ice thickness which is overestimated by CS-2 compared to Envisat by ~ 0.2 m for regions with an applicable MYI fraction; in regions dominated by FYI, sea-ice thickness is underestimated by CS-2 by ~ 0.2 m.
- A bit contradictory to that: Envisat seems to overestimate sea-ice thickness in FYI-dominated regions – particularly during early winter.
- On regional scale for the Southern Hemisphere, freeboard is overestimated by CS-2 compared to Envisat by between 1 cm and 5 cm for five of the six regions; the largest overestimation is observed for the region selected in the southwestern Weddell Sea which has the highest MYI fraction of all six regions. In contrast, for region Ross Sea CS-2

underestimates freeboard by about 7 cm compared to Envisat. The time series reveals a jump in freeboard between both sensors. This translates into respective sea-ice thickness overestimations by CS-2 by between 10 and 50 cm for the five above-mentioned regions. For region Ross Sea, sea-ice thickness is underestimated by CS-2 by about 50 cm compared to Envisat. The location of region Ross Sea suggests that the CS-2 estimates are more realistic.

- In the Southern Hemisphere regions, freeboard and sea-ice thickness and reveal a smooth transition between Envisat and CS-2 period for four to five of the six regions; region Ross Sea has a jump in freeboard and sea-ice thickness when transiting from Envisat to CS-2
- Overall we find considerable improvement of the uncertainty of freeboard and also sea-ice thickness from Envisat to CS-2. The improvement in freeboard uncertainty is ~ 0.05 m uniformly across regions and hemispheres. The improvement in sea-ice thickness uncertainty is more variable and depends on region and ice type. It can range between 0.2 m and 0.5 m.
- Overall, sea-ice thickness values seem to be more realistic in the Northern than in the Southern Hemisphere. This applies to the seasonal cycle but more so to the values at the beginning of the freezing season which almost without exception seem to be too large (by about 0.5 m to 1.0 m) in the Southern Hemisphere. In addition, mean monthly sea-ice thickness for the region selected in the southwestern Weddell Sea varies between ~ 1.5 m and over > 6 m which is too thick.

3.1 Evaluation of the SICCI 2 sea-ice freeboard (SIF) product

In the following analysis results from NASA Operation IceBridge (OIB) snow radar and airborne topographic Mapper (ATM), has been used. The ATM is a green laser, which is presumed to measure the snow surface, thus giving the total freeboard (sea-ice freeboard + snow depth) F_{total} . This combined with the snow depth SD obtained from the snow radar provides directly a measure of the sea-ice freeboard (SIF) F_{SI} for direct evaluation of SICCI-2 which we used; we discarded negative SIF values resulting from $SD > F_{total}$.

$$F_{SI} = F_{total} - SD$$

OIB data has been collected in each Arctic spring season (March & April) since 2009 to present, and does provide a seasonal evaluation. Here we use the official level 4 Sea Ice Freeboard, Snow Depth, and Thickness product (IDCSI4) for the period 2009-2013 downloaded at nsidc.org, together with the inter-mediate Quick Look (QL) product covering 2014-2016. Thus, OIB provides data in the overlap period between ENVISAT and CryoSat (2011-2012).

The OIB data provides along-track measurements with a horizontal resolution of 40 m. In order to compare with SICCI-2 SIF the OIB observations have been prepared by averaging them over 50 km sections along-track. If all samples are available this will include an average of 1250 points.

For each of the 50 km averaged OIB data points we have collocated the corresponding SICCI2 satellite data by averaging all observations which fall into a search radius of 25 km centered at the respective 50 km OIB section – for both SICCI-2 Envisat and CS-2 data.

As the SICCI-2 SIF gridded products are monthly products we take all measurements within ± 15 days of the OIB observation date. For each OIB measurement we end up having in the order of 500-1000 satellite points depending on latitude.

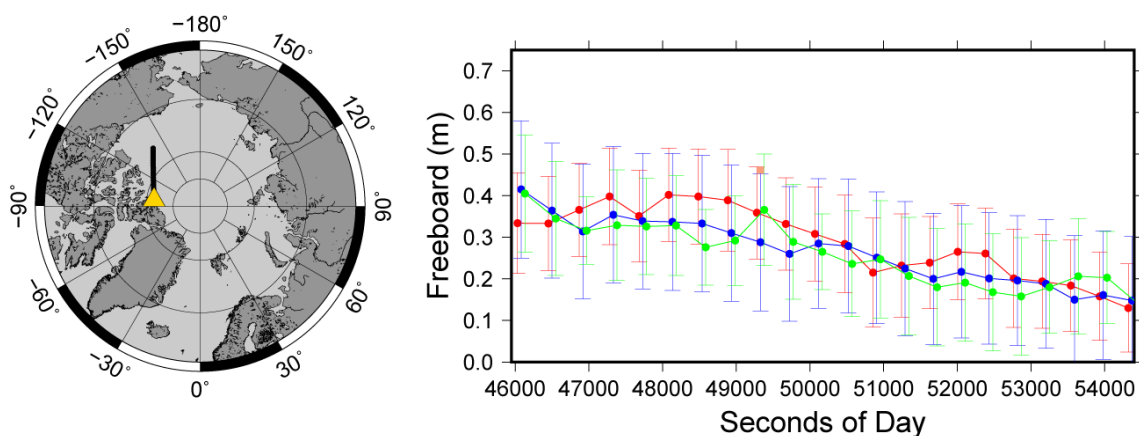


Figure 3-35: Example of along-track intercomparison of collocated SIF from OIB (green), Envisat (blue) and CS-2 (red) from March 16, 2011.

As an example the along-track sea-ice freeboard from OIB flight on March 16, 2011, is shown in Figure 3-35: OIB (green), Envisat (blue) and CS-2 (red). Along this particular track we find a high correlation between OIB and Envisat SIF, whereas CS-2 tends to overestimate SIF slightly. However, all estimates agree within the expected uncertainties.

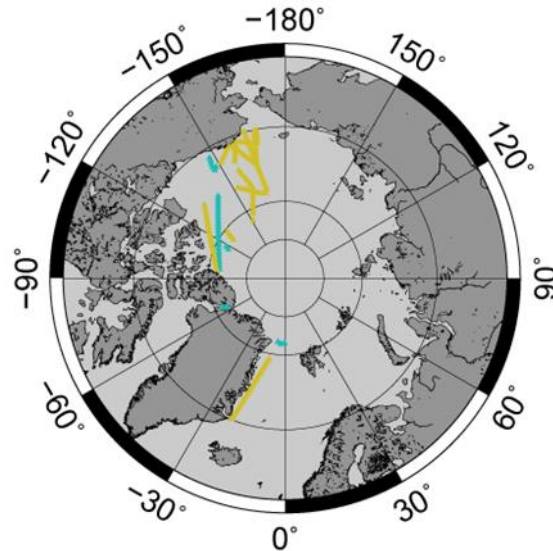


Figure 3-36: Location of all OIB tracks used in the comparison for the overlap period between Envisat and CS-2 shown in Figure 3-37.

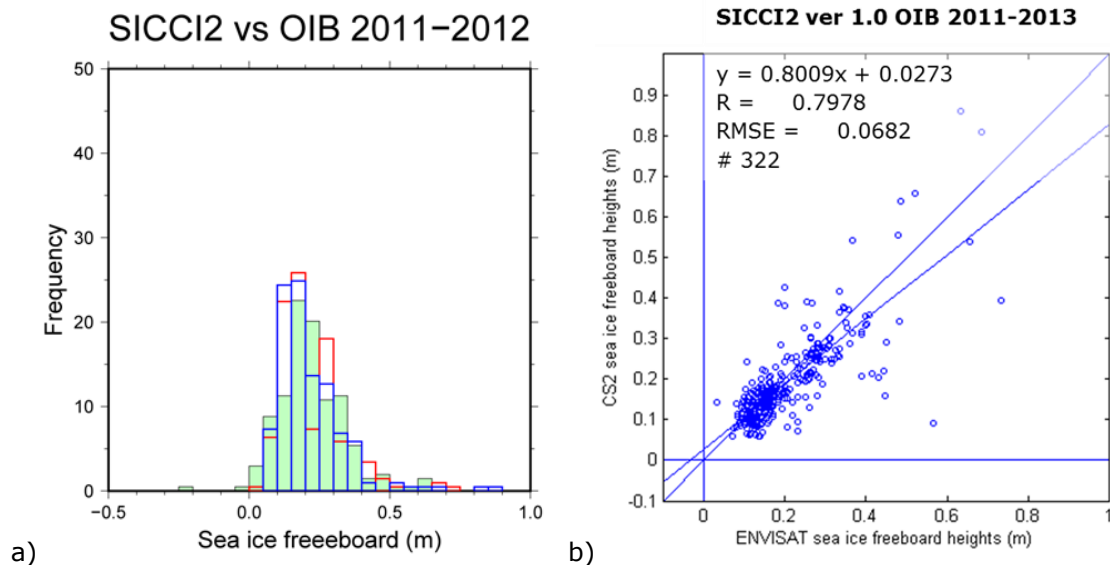


Figure 3-37: Comparison of the data pairs from location shown in Figure 3-36; a) histogram of collocated SIF from OIB (green), Envisat (blue) and CS-2 (red); b) scatterplot of CS-2 vs Envisat SIF in the overlap period (i.e. from the red and blue parts of the histogram in a)) with, from top to bottom, the linear regression line equation, the linear correlation coefficient R, the root mean squared error (RMSE), and the count of valid data #.

If we look at the histogram (Figure 3-37 a) in the overlap period (2011-2012) between Envisat and CS-2 we find an almost perfect match between OIB and SICCI2 SIF, which is also reflected in the mean and mode values presented in Table 3-9. Further the scatterplot between Envisat and CS-2, Figure 3-37 b), shows an excellent correlation of 0.8 with RMSE 0.07 m.

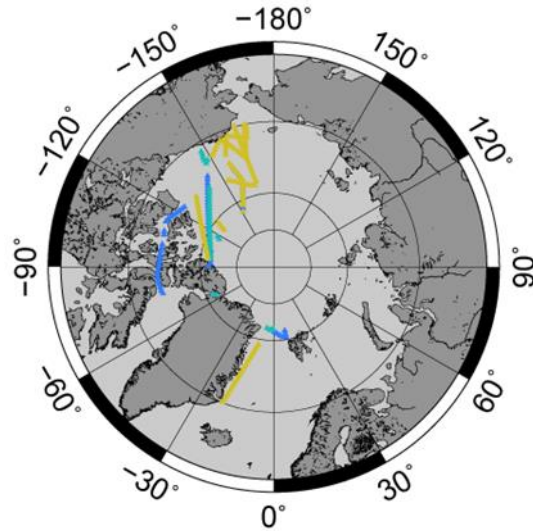


Figure 3-38: Location of all OIB tracks from 2009-2012 used in the comparison for the overlap period with Envisat shown in Figure 3-39.

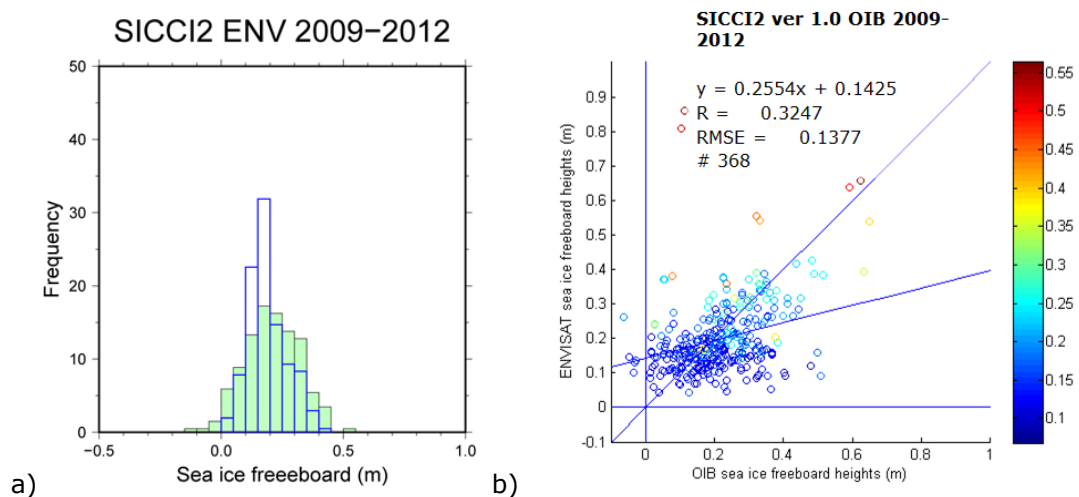


Figure 3-39: As Figure 3-37 but using only the official level 4 OIB data overlapping with Envisat, i.e. 2009-2012, which locations are given in Figure 3-38. Colors in b) denote the SICCI-2 SIF standard deviation in meters.

This is not quite consistent if we look into the freeboard distribution of all OIB data in the Envisat (2009-2012) and CS-2 (2011-2013, 2011-2016 including QL) shown in Figure 3-39, Figure 3-41, and Figure 3-43. We see in general that CS-2 tends to overestimate OIB SIF, whereas Envisat tends to underestimate it. This tendency is also reflected in the differences in mean and mode (Table 3-9) and by a relative low correlation of ~ 0.56 for CS-2 vs.

OIB and only 0.32 for Envisat vs. OIB (see image b) in Figure 3-39, Figure 3-41, and Figure 3-43).

In general, it has been concluded that a lower correlation of satellite altimetry derived freeboard and thicknesses compared with OIB is found compared to other evaluation data, such as upward looking sonars and/or AEM sea ice thicknesses ([RD-06], [RD-07]).

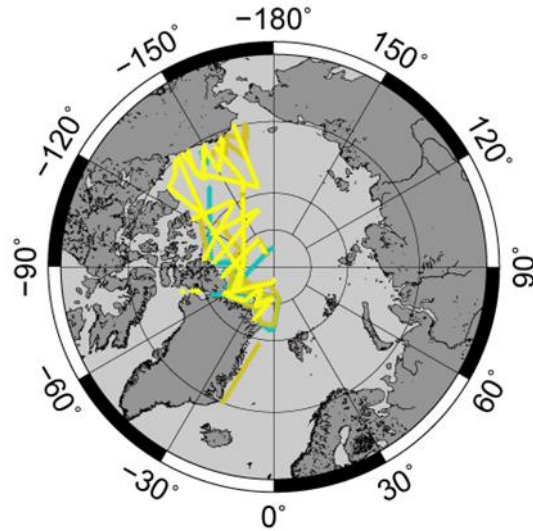


Figure 3-40: Location of all OIB tracks from 2011-2013 used in the comparison for the overlap period with CS-2 shown in Figure 3-41.

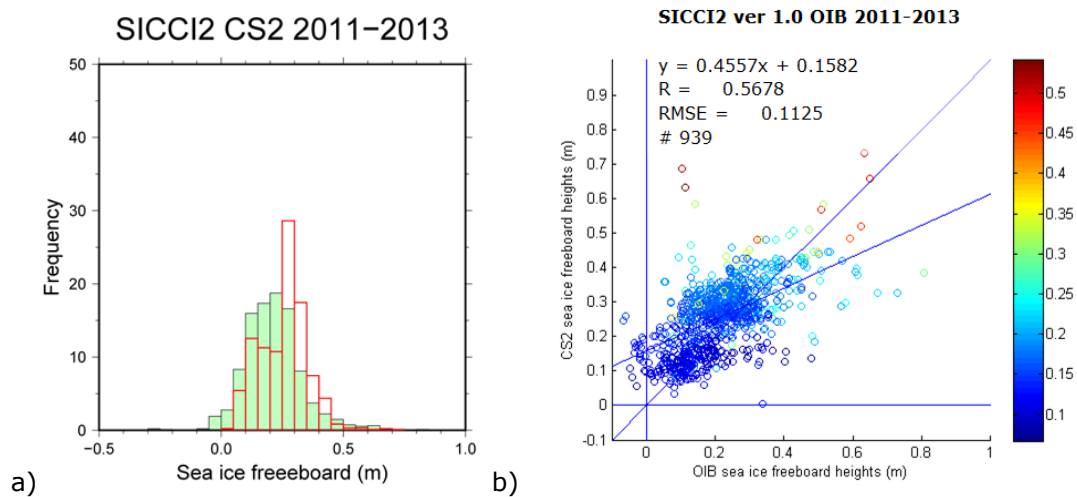


Figure 3-41: As Figure 3-37 but using only the official level 4 OIB data overlapping with CS-2, i.e. 2011-2013, which locations are given in Figure 3-40. Colors in b) denote the SICCI-2 SIF standard deviation in meters.

However, in our cases the coverage of data is not overlapping. The comparison Envisat/OIB primarily is in the FYI region north of Canada, while the comparison CS-2/OIB covers both, FYI regions north of Canada and MYI regions north of Greenland.

The color scale in image b) of Figure 3-39, Figure 3-41, and Figure 3-43 is the standard deviation of all CS-2/Envisat SIF values within the 25 km search radius around the respective OIB section center. It is seen that a lower standard deviation is related with low freeboard values and vice versa. This fits well with the fact that thicker sea ice is rougher resulting in a larger variation in sea-ice freeboards (standard deviation) than thinner sea ice.

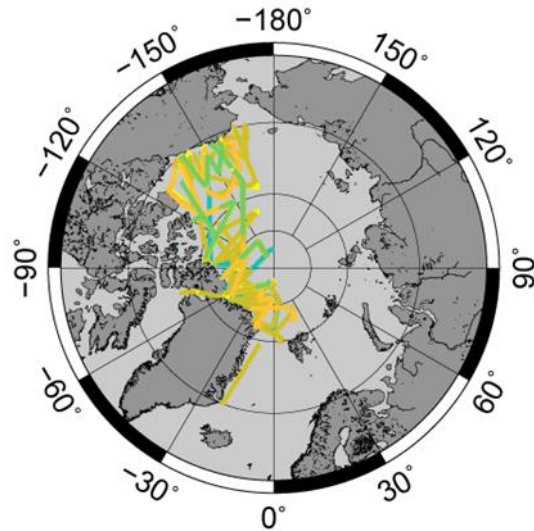


Figure 3-42: Location of all OIB tracks from 2011-2016 used in the comparison for the overlap period with CS-2 shown in Figure 3-43.

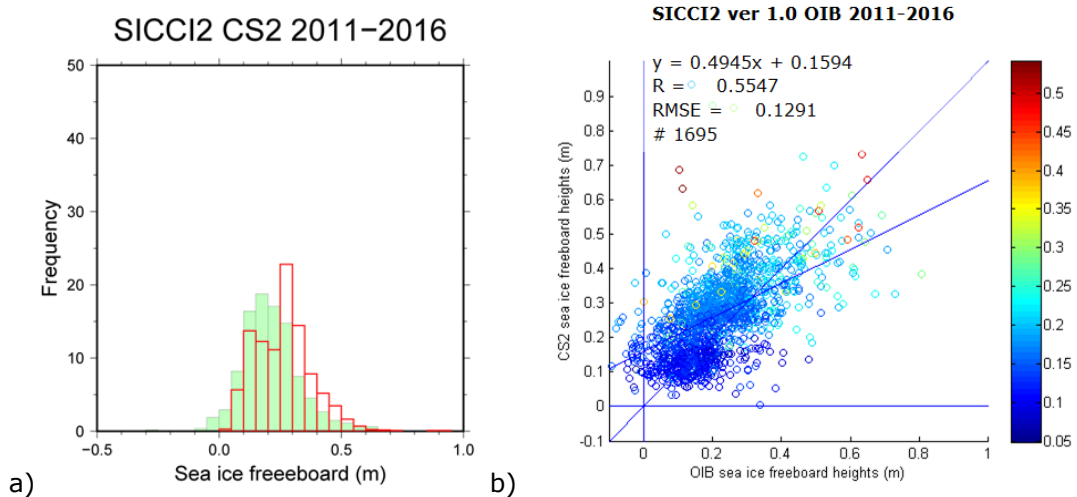


Figure 3-43: As Figure 3-37 but using the official level 4 and the quicklook OIB data overlapping with CS-2, i.e. 2011-2016, which locations are given in Figure 3-42. Colors in b) denote the SICCI-2 SIF standard deviation in meters.

Table 3-9: Statistics of the sea-ice freeboards presented in Figure 3-37, Figure 3-39, Figure 3-41, and Figure 3-43.

Period	SICCI-2 CS-2		SICCI-2 Envisat		OIB	
	Mean	Mode	Mean	Mode	Mean	Mode
2011-2013	0.26 m	0.28 m			0.22 m	0.19 m
2011-2016*	0.26 m	0.27 m			0.21 m	0.19 m
2009-2012			0.20 m	0.17 m	0.22 m	0.20 m
2011-2012	0.22 m	0.16 m	0.21 m	0.17 m	0.23 m	0.20 m

*Including OIB quicklooks

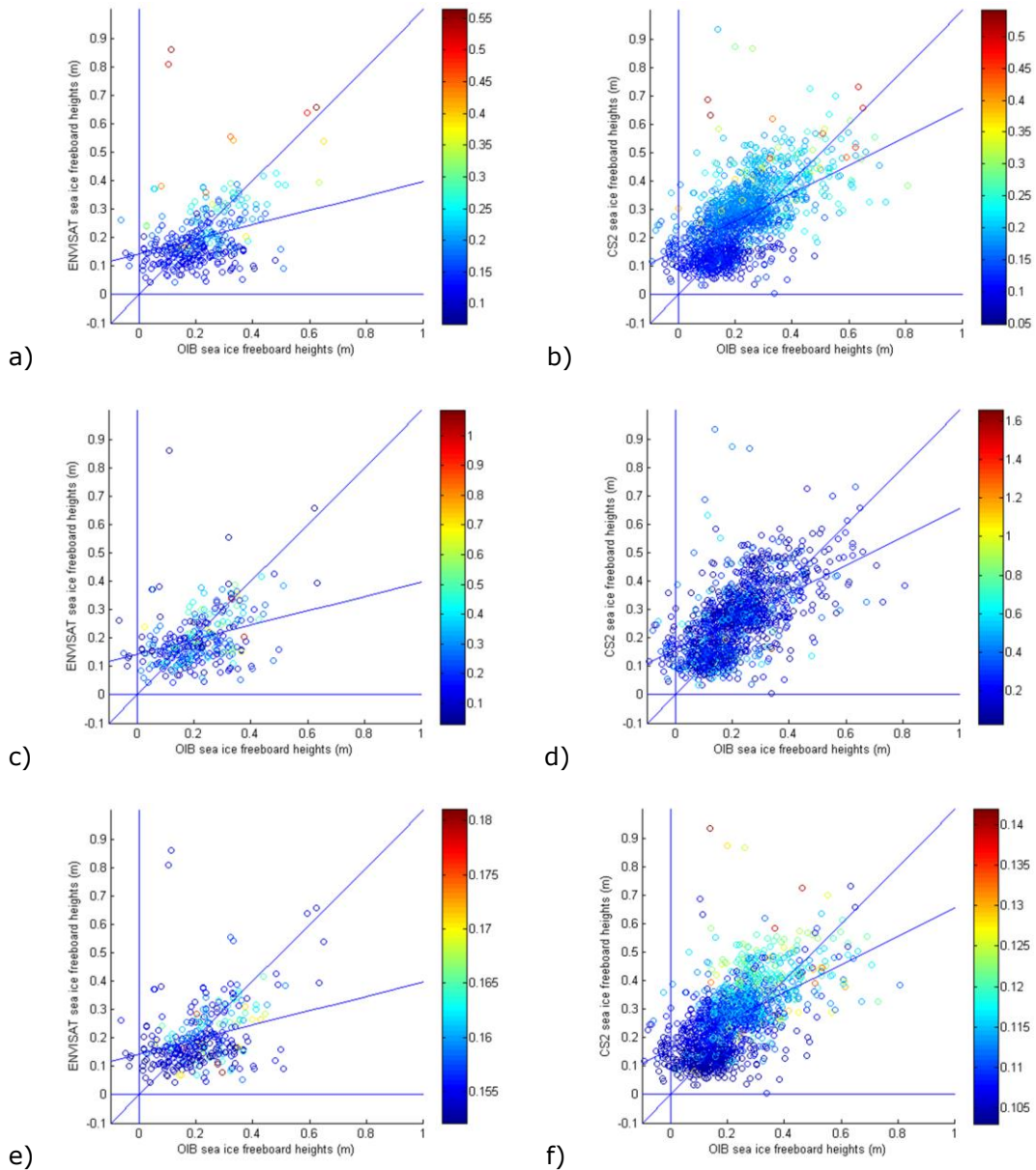


Figure 3-44: Comparison of different freeboard variation parameters for the OIB – Envisat overlap (2009-2012, left column) and the OIB – CS-2 overlap (2011-2016, right column): a) & b) colors denote the SICCI-2 SIF standard deviation in meters; c) & d) colors denote roughness from the OIB product; e) & f) colors denote the SIF retrieval uncertainty from the SICCI-2 SIF product. Note the different y-axis scales.

In Figure 3-44 we color coded the SIF value pairs OIB-SICCI-2 Envisat (left column) and OIB-SICCI-2 CS-2 (right column) with different parameters giving information about surface roughness and/or uncertainty of the SIF data. We find that the roughness parameter from the OIB product (c,d) has not too much in common with the SICCI-2 SIF standard deviation (a,b) or the SICCI-2 SIF retrieval uncertainty (e,f). We note that this OIB roughness parameter is larger for collocated SICCI-2 Envisat SIF than CS-2 SIF. We find an increase of SIF retrieval uncertainty with increasing SIF (e,f) which looks relatively similar to the increase in SICCI-2 SIF standard deviation, except that the latter is larger by a factor of 3 to 4.

3.2 Evaluation / Inter-comparison with in situ measurements from North-Pole (NP) drifting stations

Russian (previous Soviet) manned North Pole drifting ice stations (NP) have been carried out by the Arctic and Antarctic Research Institute (AARI) for several decades. During the usually year-long drift in the Arctic Ocean a wide range of oceanographic, meteorological, and geophysical measurements are collected. Data include measurements of snow and ice properties which can be used to validate satellite estimates of sea ice thickness. For the validation of the SICCI SIT prototype data we used measurements from NP-37 (2009/2010), NP-38 (2010/2011), and NP-39 (2011/2012) which were drifting in the Beaufort and Chukchi Sea between 76°N and 83°N.

Similar to SICCI project phase 1 (see [RD-05]) we evaluated the SICCI-2 SIT product with in-situ sea-ice thickness measurements obtained during these stations.

Data from the Russian North Pole drifting stations NP-37 (2009/2010) and NP-39 (2011/2012) were used for validation of SICCI freeboard and thickness prototype (see Figure 3-45 and Table 3-10). Data from the station NP-38 (2010/2011) will be used later for validation of sea ice thickness only.

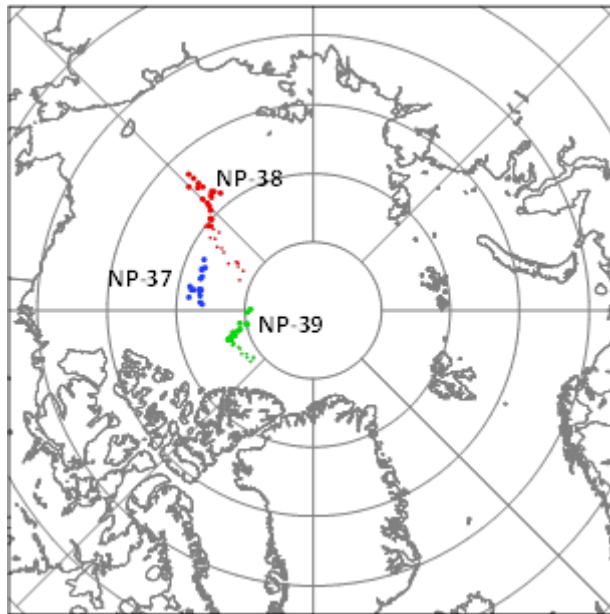


Figure 3-45: Location of the drifting stations NP-37, NP-38 and NP-39 collocated with Envisat and Cryosat-2 measurements (large circles – October to April, small circles – May to Sep).

Sea ice measurements on the drifting ice floe have been conducted every 10 days in a 100 m x 100 m polygon every 20 m (See Figure 3-46). For the NP-37 and NP-39 only the center sections have been measured every 10 days (for the NP-37 every 10 m), while the entire polygon has only been sampled once a month on the NP-37 and with three gaps over collocation period for the NP-39.

Table 3-10: Periods of collocation of the North Pole drifting stations NP-37, NP-38 and NP-39 with SICCI SIT prototype derived from Envisat and Cryosat-2 measurements. Parameters measured on the drifting stations are listed.

NP station	Satellite	Period of collocation	Parameters
NP-37	Envisat	Oct 2009 – Apr 2010	Freeboard, thickness, snow depth
NP-38	Envisat	Oct 2010 – Apr 2011	Thickness, snow depth
	Cryosat-2	Oct 2010 – Apr 2011	
NP-39	Cryosat-2	Nov 2011 – Apr 2012	Freeboard, thickness, snow depth

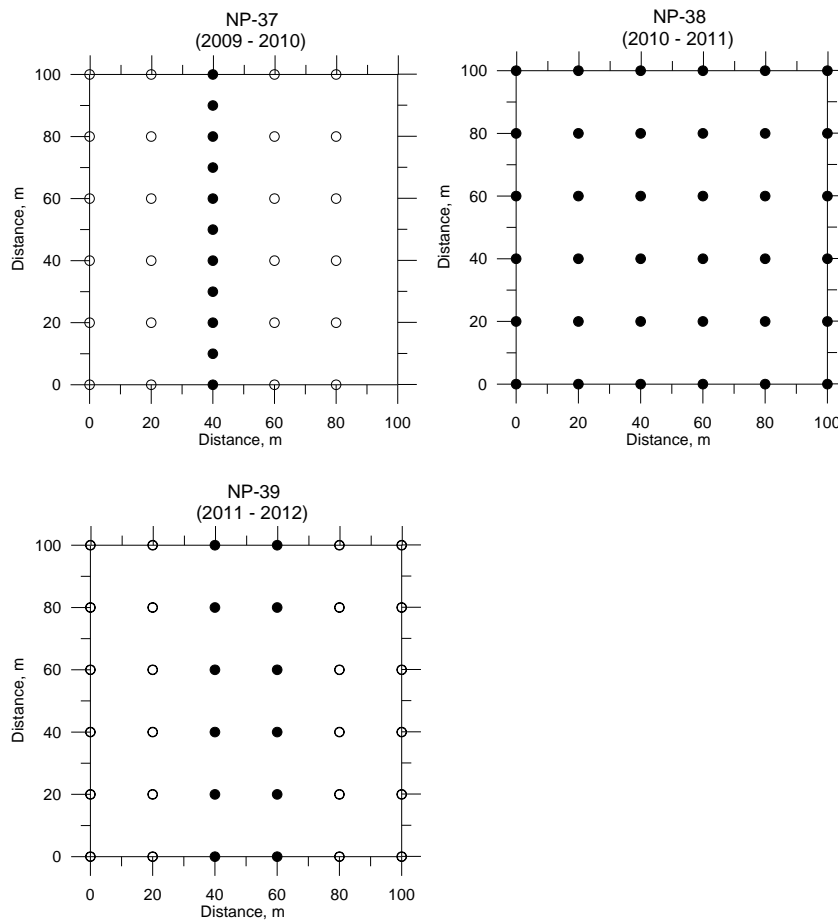


Figure 3-46: Measurement points along the polygon of the North Pole drifting stations NP-37, NP-38 and NP-39. Filled circles indicate locations of the measurements sampled every 10 days. Unfilled circles are locations of the measurements sampled every month for the NP-37 or with few gaps for the NP-39.

The collocated freeboard measurements from the NP-37 and the freeboard averaged within 25 km grid cell from SICCI-2 Envisat product are presented in Figure 3-47. The SICCI-2 sea-ice freeboard is larger than the in-situ measurements by 6.7 cm with standard deviation (S.D.) of the difference of 3.8 cm along the central section of the polygon, and by 5.1 cm with S.D. of 3.2 cm for the entire polygon. In order to evaluate the effect of the scale used for spatial averaging on the observed differences the mean freeboard from the grid cells located within 50 km radius from the drifting station is estimated. In this case the differences (and its S.D.) between in-situ measurements and SICCI-2 Envisat products are 6.7 cm (2.7 cm) and 4.4 cm (2.8 cm) for the central section and the entire polygon respectively. Figure 3-47 also shows that the effect of different scale for spatial averaging is random and freeboard estimates do not vary significantly.

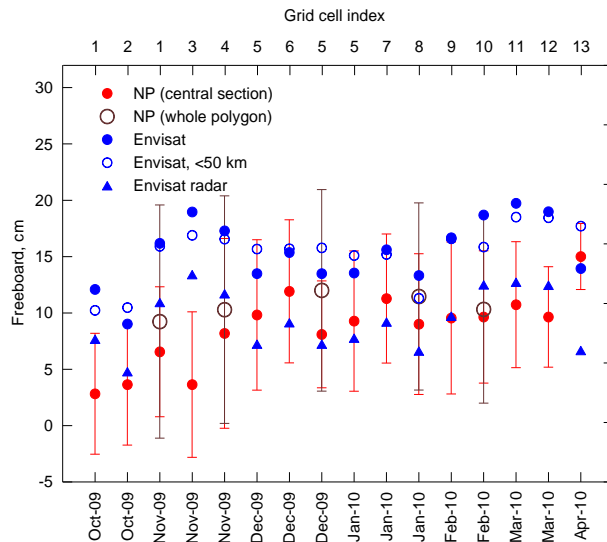


Figure 3-47: Freeboard measurements from the NP-37 collocated with sea-ice freeboard from SICCI-2 gridded Envisat product. Top x-axis represents the grid cells (named by numbers) of SICCI-2 SIT product where the NP station was located.

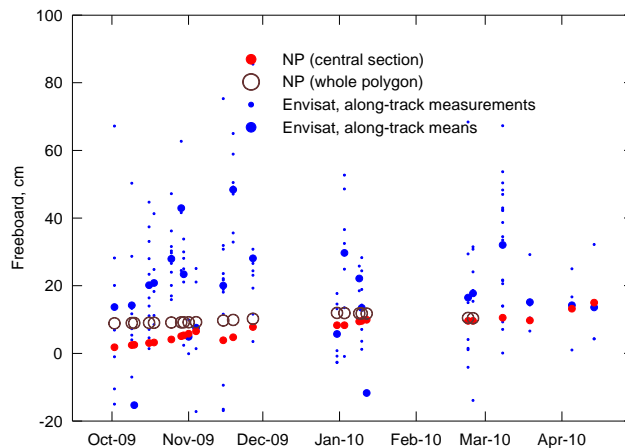


Figure 3-48: Freeboard measurements from the NP-37 collocated with individual along-track sea-ice freeboard from SICCI-2 Envisat product.

Since the observed discrepancies can reflect the difference between local freeboard measured around NP-37 and the mean values over large area of grid cells the individual altimeter measurements along the satellite track within ± 2 km and ± 1.5 hours of the station were considered (Figure 3-48). The corresponding sea-ice freeboard values from the NP-37 have been obtained by interpolation to the collocated dates. The orbit-mean freeboards for the selected satellite tracks overestimate in-situ measurements on average by 10.7 cm for the central section and by 7.5 cm for the entire polygon respectively, i.e. even larger than the gridded means.

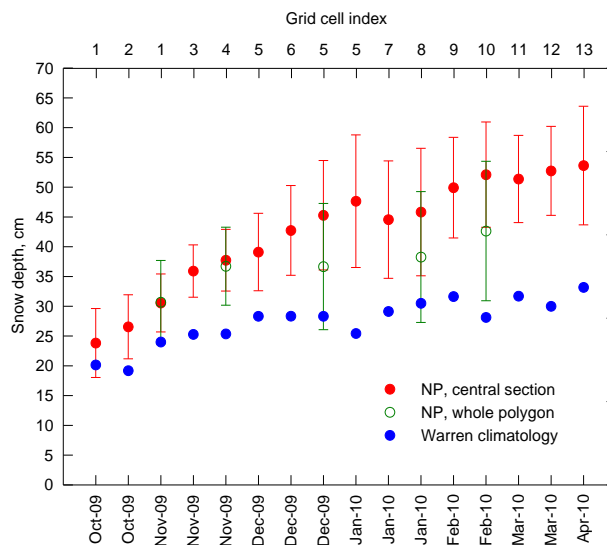


Figure 3-49: Collocated snow depth as used in the SICCI-2 SIT product from climatological values ([RD-08]) and in-situ measurements scaled for sea-ice type and in situ measurements from NP-37. See Figure 3-47 for top x-axis explanation.

The freeboard estimates in the SICCI-2 product take into account the lower propagation speed in the snow by adding a correction for snow depth calculated as $0.22h_{sn}$, where h_{sn} is snow depth. As the values of h_{sn} are taken from snow climatology ([RD-08]) this correction may be a source of uncertainty in the freeboard retrieval. Figure 3-49 shows that snow depth measured on the NP-37 is larger and the difference with respect to climatological snow depth for the collocated grid cells increases over winter season 2009/2010 from few cm to about 20 cm and 15 cm for the central section and the entire polygon respectively. This is equivalent to additional correction by up to 4-5 cm in the end of winter, which would increase the observed freeboard differences. However, it can be noted that significant difference between the mean snow depths along the central section of the polygon and over the entire polygon indicates large spatial variability of snow depth even within a small area of 100×100 m.

The collocated freeboard measurements from the NP-39 and the freeboard from the SICCI Cryosat-2 gridded product are presented in Figure 3-50. The sea-ice freeboard from the SICCI-2 product is larger than the in-situ measurements by 22.0 cm (S.D. 4.0 cm) and 20.3 cm (S.D. 5.1 cm) along the central section and the entire polygon respectively. The scale for spatial averaging has insignificant impact on the Cryosat-2 freeboard collocated with the NP-39.

Freeboards from the individual measurements near the NP-39 within ± 2 km and ± 1.5 hours (Figure 3-51) also overestimate in-situ data by 27.9 cm and 26 cm for the central section and for the entire polygon, respectively.

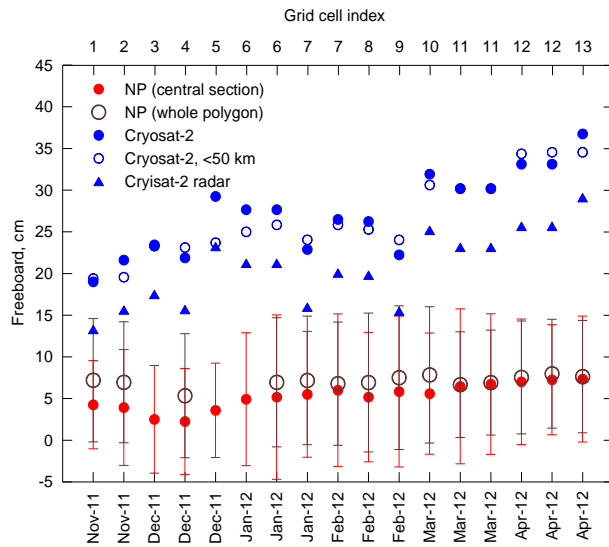


Figure 3-50: Collocated freeboard measurements from SICCI-2 Cryosat-2 gridded product and in-situ measurements from NP-39. Top x-axis represents the grid cells (named by numbers) of SICCI-2 SIT product where the NP station was located.

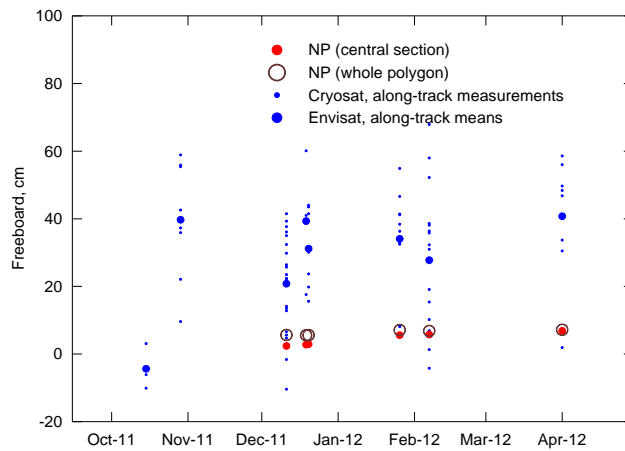


Figure 3-51: Freeboard measurements from the NP-39 collocated with individual along-track sea-ice freeboard from SICCI-2 Envisat product.

Snow depth measured on the NP-39 in winter 2011/2012 and climatological snow depth for the collocated grid cells are very close (Figure 3-52). Although NP-39 data gives slightly larger growth of snow depth over winter season the most of the differences are within 5 cm implying that offset of the freeboard correction for snow depth is within ~1 cm.

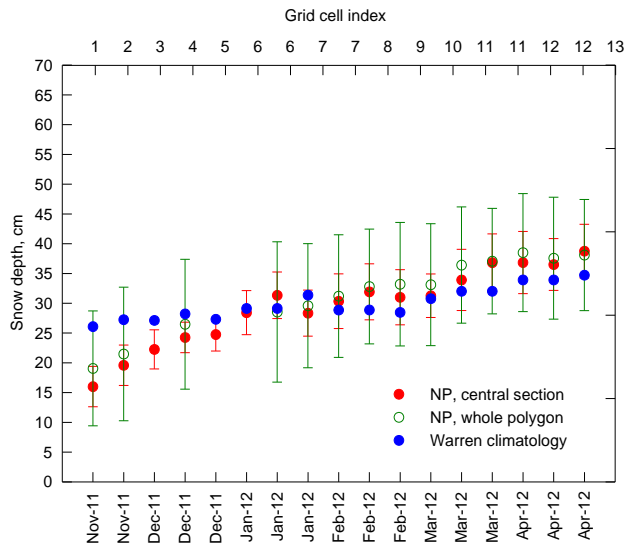


Figure 3-52: Collocated snow depth as used in the SICCI SIT prototype from climatological values ([RD-08]) and in-situ measurements from NP-39. Top x-axis represents the grid cells (named by numbers) of SICCI-2 SIT product where the NP station was located.

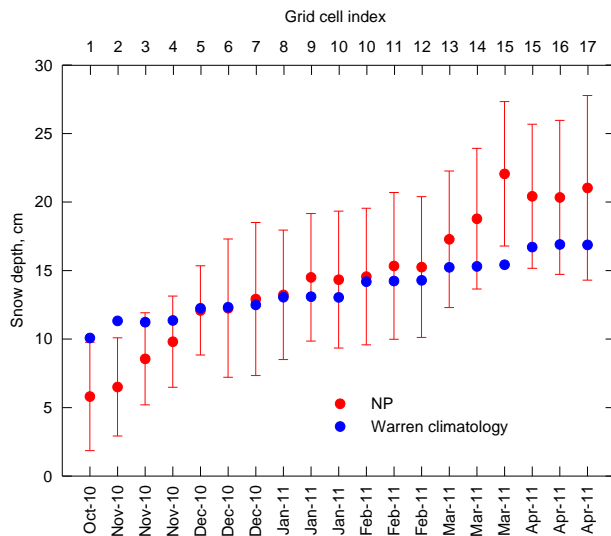


Figure 3-53: Collocated snow depth as used in the gridded SICCI SIT prototype from climatological values ([RD-08]) scaled for sea ice type and in-situ measurements from NP-38. Spatial scale on the top represents the grid cells (named by numbers) of SICCI SIT product where drifting station was located.

The NP-38 has been operating during winter 2010/2011 and data from this station can be collocated with both Envisat and Cryosat-2 measurements. However, NP-38 provides only one freeboard measurement in the beginning of its operation on 7th of November 2010. The freeboard of 7.4 cm measured on the station is in a good agreement with monthly mean freeboards of 4.0 cm and 6.3 cm retrieved from Envisat and Cryosat-2 respectively for the collocated grid cell. Snow depth measured on the NP-38 and climatological snow depth for the collocated grid cell are in agreement

within 5 cm although in-situ data again shows larger growth rate during winter season (Figure 3-53).

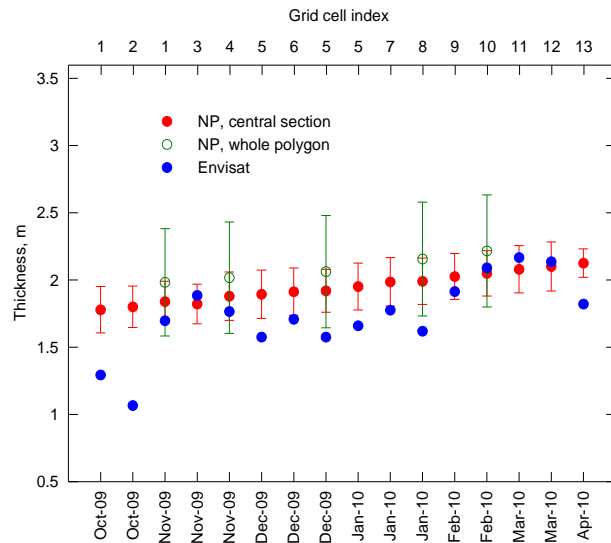


Figure 3-54: Collocated sea ice thickness from in-situ measurements on the drifting station NP-37 and SICCI SIT Envisat gridded product. Spatial scale on the top represents the grid cells (named by numbers) of SICCI SIT product where drifting station was located.

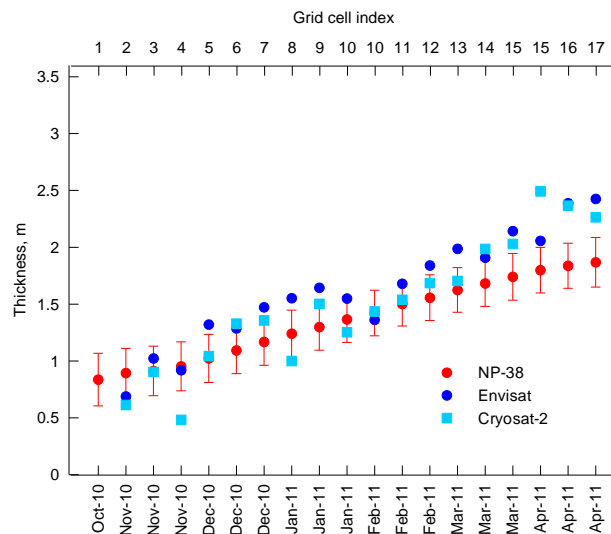


Figure 3-55: Figure 3-54 but for NP-38 and the Envisat and CryoSat-2 SIT products.

The collocated SIT from the gridded SICCI-2 product and the in-situ measurements are shown in Figure 3-54 through Figure 3-56 for all three NP stations. Sea-ice thickness estimates derived from Envisat are smaller than SIT measurements on the NP-37 on average by 0.21 m (S.D. = 0.22 m) for the central section and by 0.34 m (S.D. = 0.17 m) for the entire polygon (Figure 3-54). The SIT from Envisat and Cryosat-2 is larger than those measured on the NP-38 by 0.21 m (S.D. = 0.22 m) and 0.11 m (S.D. = 0.29 m) respectively (Figure 3-55). The SIT from Cryosat-2 is larger than measurements on the NP-39 by 1.23 m (S.D. = 0.24 m) and 1.17 m (S.D. = 0.24 m).

= 0.25 m) for the central section and the entire polygon, respectively (Figure 3-56).

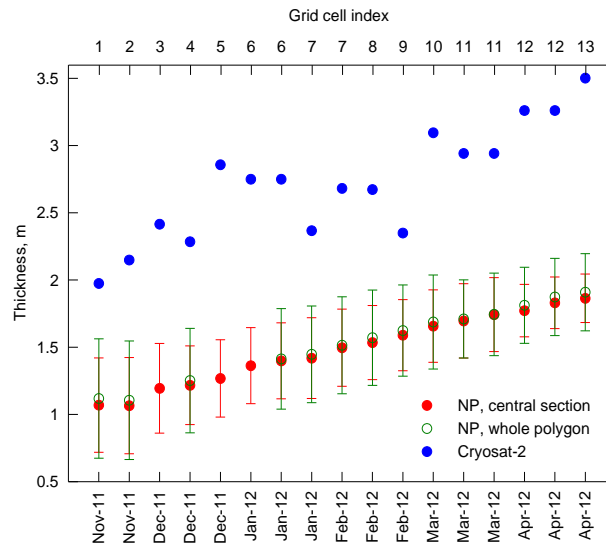


Figure 3-56: As Figure 3-54 but for NP-39 and the CryoSat-2 SIT product.

Thickness overestimation from Cryosat-2 as compared to in-situ measurements (Figure 3-56) is caused, apparently, by the larger freeboard values retrieved from this radar altimeter. A good agreement between in-situ data from the NP-38 and satellite-derived thicknesses (Figure 3-55) likely represents consistency in freeboards measured on the station’s polygon and those derived from Envisat and Cryosat-2. Slightly smaller thickness from Envisat product as compared NP-37 data for the most of collocated points (Figure 3-54) can be attributed to underestimation of snow depth used to convert freeboard to thickness (Figure 3-49). Larger discrepancy by 0.5 and 0.7 m for the first two points can be explained by the uncertainty of sea-ice density, which is also used for freeboard-to-thickness conversion. This is confirmed when evaluating the sea-ice density from the sea-ice freeboard, thickness and snow depth measured on the drifting stations and using isostatic equilibrium equation as

$$\rho_i = \frac{\rho_w (h_i - h_f) - h_{sn} \rho_{sn}}{h_i},$$

where h_i – sea-ice thickness, h_f – sea-ice freeboard, and h_{sn} – snow depth. Water density (ρ_w) is taken equal to 1024 kg/m³, snow density (ρ_{sn}) is taken from snow climatology ([RD-08]). Figure 3-57 shows that sea-ice density estimated from the measurements on NP-37 is rapidly decreasing in October-November from the values of much higher than even those typical for the FYI to the densities of 890-910 kg/m³, which are closer to the values characteristic of the MYI. For the whole polygon sea-ice densities in the beginning of winter season are lower than for central section, but still much higher than it could be expected for the MYI floe, where the drifting station was established. Thus, seasonal changes of sea-ice density and its anomalously large values in October could be a reason for larger underestimation of sea-ice thickness in the Envisat product as compared to the in-situ data for the first two points in Figure 3-54. (Note that the first point in Figure 3-57 is related to the measurements conducted on September 28th and this point is not included in Figure 3-48, Figure 3-50,

and Figure 3-54). For the NP-39 (Figure 3-58) a decrease in density in the beginning of winter is less pronounced and observed only for the central section of the polygon. The most of sea-ice density estimates over the whole winter season ranges between 915 kg/m³ and 925 kg/m³, i.e. values expected rather for the FYI. However, application of these higher sea-ice density values when estimating SIT from freeboard would result in an even larger overestimation of the Cryosat-2 product as compared to the in-situ measurements on the NP-39.

The MYI fraction used in the SICCI-2 SIT product indicates predominantly MYI within the grid cells collocated with NP-37 and NP-39. Ice density of 919 kg/m³ estimated using this approach for NP-38 for the measurement on 7th of November is in agreement with the values used in SICCI-2 SIT product where only FYI is indicated for the collocated grid cells.

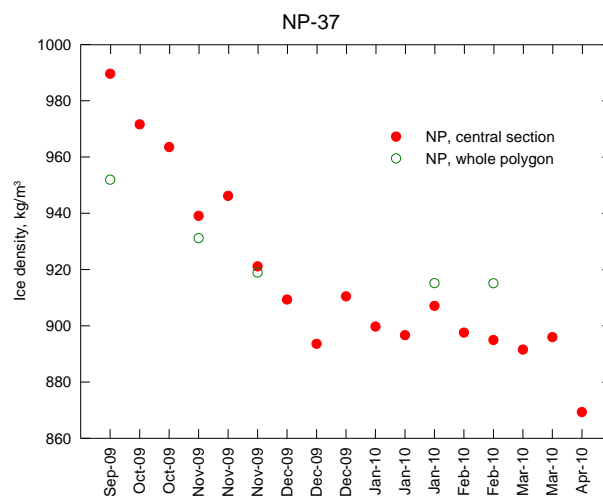


Figure 3-57: Sea-ice density estimated with the equation given above using measurements of sea-ice freeboard, thickness and snow depth on the North Pole drifting station NP-37.

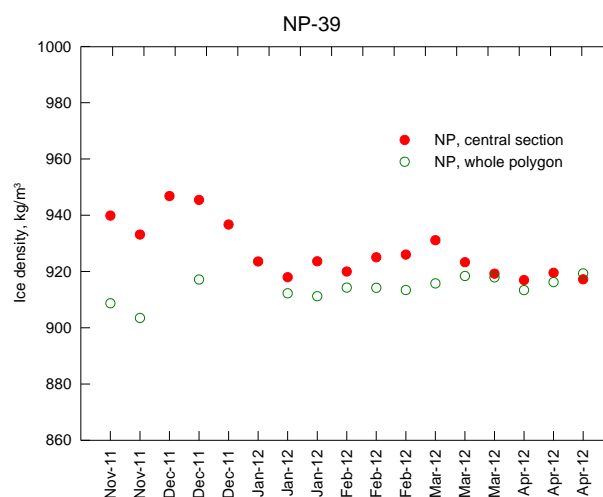


Figure 3-58: As Figure 3-57 but using data from NP-39.

3.3 SIT evaluation with other in-situ measurements

The SICCI-2 sea-ice thickness (SIT) data set v09 has been evaluated with a few in-situ SIT measurements in the Southern Hemisphere. We used the ASPeCt-BIO data collection [RD-09] of in-situ observations of the sea-ice thickness from in-situ drillings around Antarctica; data overlapping with the SICCI-2 SIT data set are from years 2002 through 2007. Figure 3-59 shows the locations from which we have taken in-situ observations of the SIT from the ASPeCt-BIO data set.

Note that the in-situ data are very local and comprise relatively few, if not just one, SIT measurement at one specific location.

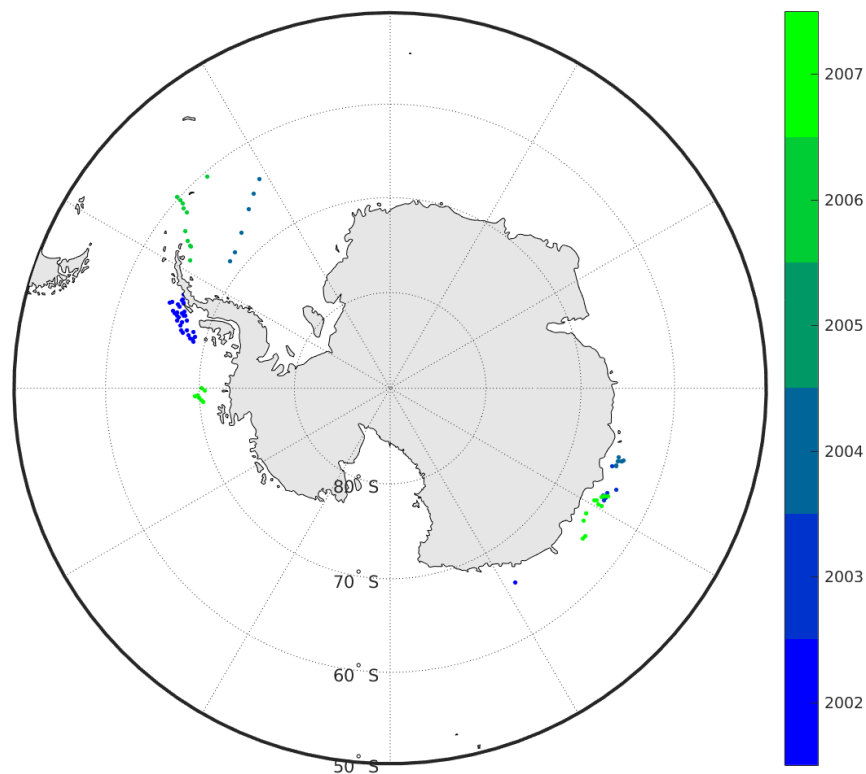


Figure 3-59: Locations of in situ SIT observations from drillings taken from the ASPeCt-BIO data set. Symbols are color-coded according to the year in the observation was made

In situ data locations were collocated with satellite data as follows: For each SICCI-2 SIT product grid cell (25 km x 25 km and 50 km x 50 km for the Northern and Southern Hemisphere, respectively) we seek for contemporary in situ data within a search radius of 13 km (26 km for the Southern Hemisphere) for data within the respective SIT product month. If we find more than one valid observation then we average these for the respective SICCI-2 grid cell. In order to reduce the scatter of the observation data

pairs we averaged the SIT and TSIT values over bins half a meter wide, i.e. > 0 to ≤ 0.5 m; > 0.5 m to ≤ 1.0 m, etc., using the in-situ data as reference. Uncertainties from the SICCI-2 SIT product and, if available, standard deviations of the observations were averaged accordingly.

Figure 3-60 suggests, in agreement with Figure 3-64 and the ANTXXIX/7 part of Figure 3-66 that SICCI-2 SIT overestimates SIT from other observations. The majority of the data pairs is located above the line of 1-to-1 agreement. Without the three data pairs below the 1-to-1 line for in-situ SIT > 2.5 m the comparison suggests a constant positive bias of about 1 m.

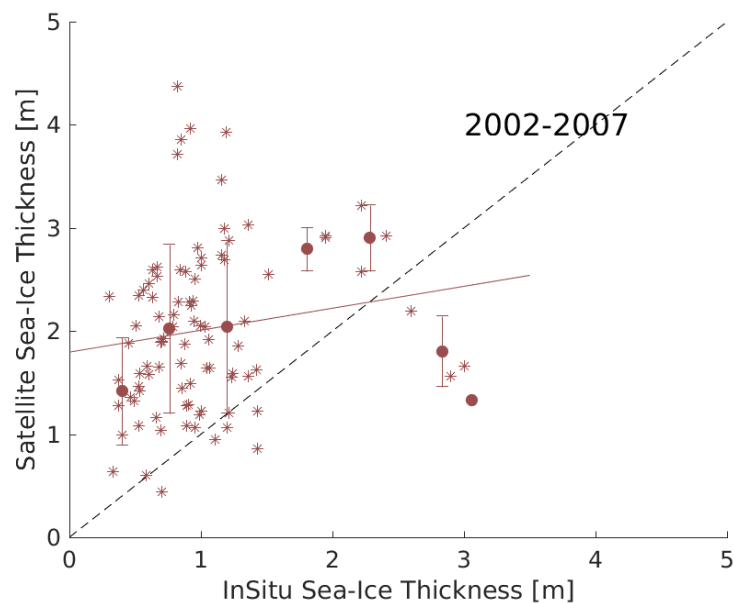


Figure 3-60: Comparison between ASPeCt-BIO [RD-09] in situ SIT (x-axis) and SICCI-2 SIT (y-axis) using data from 2002-2007, i.e. from the Envisat period of the SICCI-2 SIT product. Filled circles denote the 0.5 m – wide bin averages over data from both expeditions. Through these a linear regression is computed (solid line). The dashed line is the line of 1-to-1 agreement.

In summary: An inter-comparison of SICCI-2 SIT data and in situ observations of the SIT taken from the ASPeCt-BIO data set confirms the notion that SICCI-2 SIT tends to be positively biased when compared to independent SIT observations.

3.4 SIT evaluation with EM observations

The SICCI-2 sea-ice thickness (SIT) data set v09 has been evaluated with airborne electromagnetic (EM) sounding data of the total (sea ice plus snow) sea-ice thickness (TSIT) in the Northern and Southern Hemisphere.

For the Northern Hemisphere we used AEM data from years 2003 through 2014 [RD-10] of the following campaigns / programs: ARKXIX/1ab (2003) [RD-11]; SEDNA (2007) [RD-12]; NP_07 (2007) [RD-13]; TransDrift (2008) [RD-14]; SIZONet 2007-2014 [RD-15]; PAMARCMIP 2009+2012 [RD-15]; BREA 2013 [RD-16]. The majority (> 95%) of these AEM data was acquired in April; the rest was acquired in March.

For the Southern Hemisphere we used AEM data from the ISPOL (2004/05) [RD-17] and WWOS (2006) [RD-18] as well as of the ANTXXIX/6 and ANTXXIX/7 expeditions (2013) of the R/V Polarstern into the Southern Ocean ([RD-19; RD-20]; data provided by Stefan Hendricks, AWI, Bremerhaven, Germany).

Note that the AEM data are the mean total sea-ice thickness (TSIT) over the typically used flight pattern and hence represent the TSIT of flight segments between ~ 20 km and ~ 50 km length.

AEM data locations were collocated with satellite data as follows: For each SICCI-2 SIT product grid cell (25 km x 25 km and 50 km x 50 km for the Northern and Southern Hemisphere, respectively) we seek for contemporary AEM data within a search radius of 13 km (26 km for the Southern Hemisphere) for data within the respective SIT product month. If we find more than one valid observation then we average these for the respective SICCI-2 grid cell. Standard deviations of TSIT provided for the Northern Hemisphere data were averaged accordingly if needed.

In order to reduce the scatter of the observation data pairs we averaged the SIT and TSIT values over bins half a meter wide, i.e. > 0 to ≤ 0.5 m; > 0.5 m to ≤ 1.0 m, etc., using the AEM data as reference. Uncertainties from the SICCI-2 SIT product and, if available, standard deviations of the observations were averaged accordingly.

Northern Hemisphere

The locations from which we were able to use AEM data within the months October through April in the Northern Hemisphere are shown in Figure 3-61.

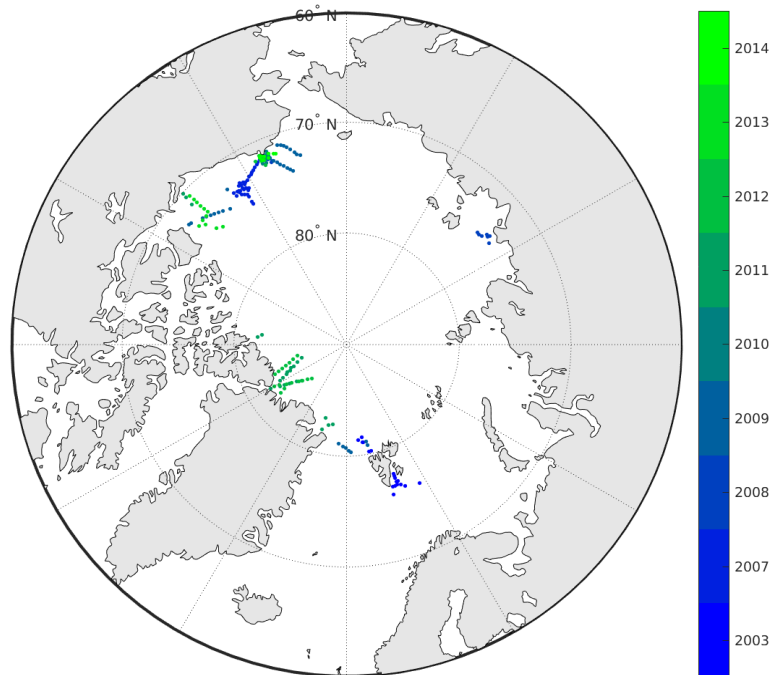


Figure 3-61: Locations of AEM measurements used for the SICCI-2 SIT product evaluation in the Northern Hemisphere. Symbols are color-coded according to the year in which the AEM data were acquired.

AEM observations relevant for our evaluation in the Northern Hemisphere are located near Fram Strait, in the Lincoln Sea and in the southern Beaufort and Chukchi Seas.

Figure 3-62 shows the results of the evaluation for the Northern Hemisphere. The agreement between SICCI-2 SIT and AEM TSIT seems reasonable in general. The slope of a linear regression between both data sets is ~ 0.75 and the intercept is ~ 0.7 m. It seems like the agreement between CS-2 SIT and AEM TSIT is considerably better than the agreement between Envisat SIT and AEM TSIT; CS-2 – AEM data pairs stretch much better along the 1-to-1 line (black dashed line) than the Envisat – AEM data pairs. A linear regression between CS-2 and AEM data results in a slope of ~ 0.875 with an intercept close to zero. Keeping in mind that AEM data represent total SIT, i.e. include the snow depth, then a little underestimation of TSIT by SIT is in line with the expectations. In contrast, the linear regression between Envisat and AEM data results in a slope of ~ 0.25 with an intercept of ~ 1.5 m.

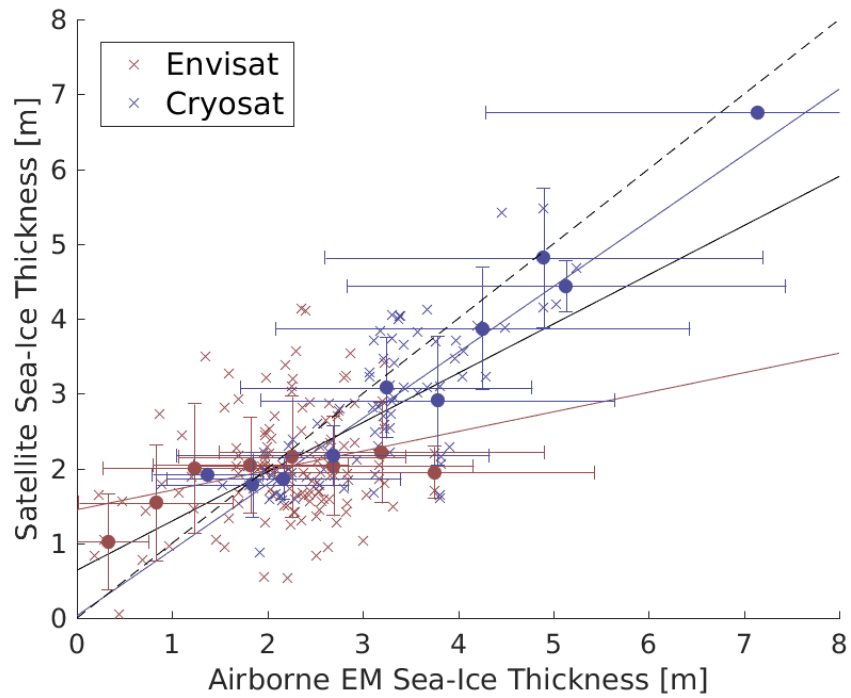


Figure 3-62: Comparison between Envisat (red symbols) and CS-2 (blue symbols) SICCI-2 SIT and AEM TSIT. Crosses denote single co-located data pairs. Filled circles denote 0.5 m – bin wide averages of SIT and TSIT of the respective satellite data set. For bars see the text. Dashed black line denotes the 1-to-1 agreement. The colored solid lines denote the linear regressions for the respective data sets; the black solid line denotes the regression over all.

Southern Hemisphere

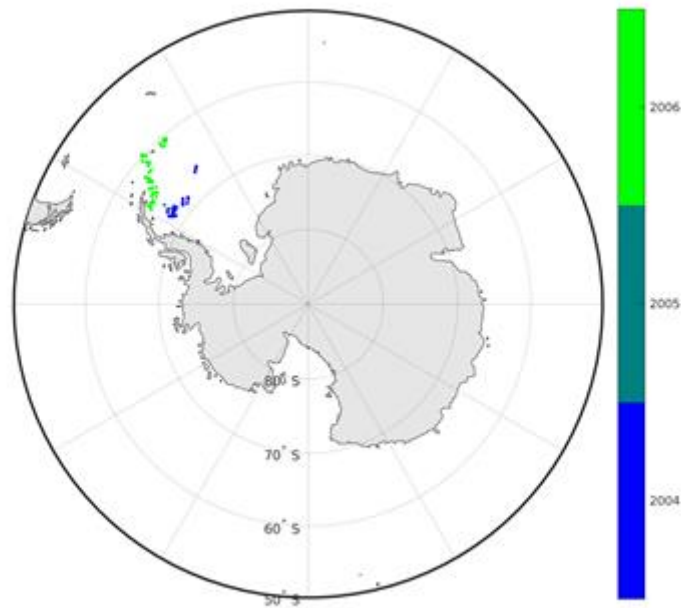


Figure 3-63: Locations of AEM observations during ISPOL (Nov 13 2004 through Jan 4 2005) and WWOS (Sep/Oct 2006).

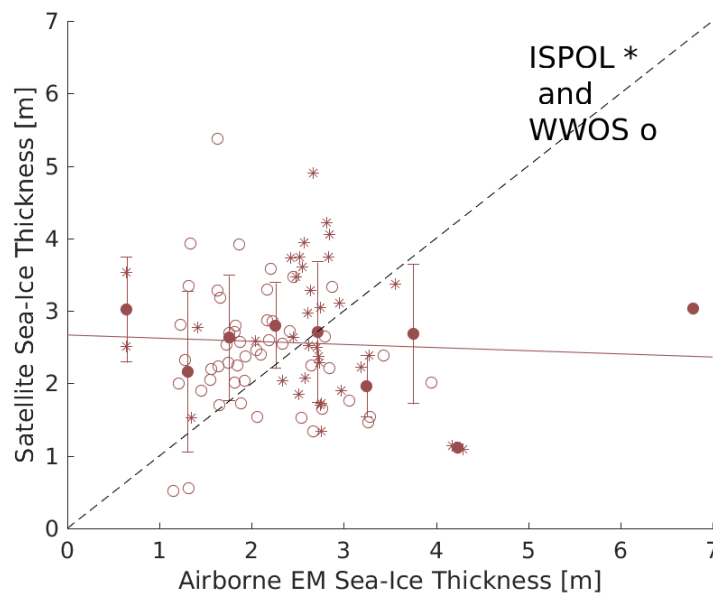


Figure 3-64: Comparison between AEM total SIT (x-axis) and SICCI-2 SIT (y-axis) for WWOS and ISPOL, i.e. for the Envisat data period of the SICCI-2 SIT product. Stars and open circles denote the co-located observations. Filled circles denote the 0.5 m – wide bin averages over data from both expeditions. Through these a linear regression is computed (solid line). The dashed line is the line of 1-to-1 agreement.

We separate between ISPOL and WWOS and the two ANTXXIX cruises because the latter overlap with CS-2 data and also took place during winter.

Note that all these cruises too place in the Weddell Sea and can hence not represent sea-ice conditions in other parts of the Southern Ocean.

The agreement between SICCI-2 SIT and AEM TSIT is poor (Figure 3-64). There is little indication for a SIT increase when TSIT increases and vice versa. The overall linear regression even has a slightly negative slope – as a result of the scatter. For WWOS for example SICCI-2 SIT values range between ~ 0.5 m and ~ 5.5 m in the TSIT bin 1m to 2 m, while in the TSIT bin 3 m to 4 m SICCI-2 SIT values range between ~ 1.5 m and ~ 2.5 m. For ISPOL, most of the data pairs fall into the range AEM TSIT 2 m to 3 m; here SICCI-2 SIT ranges between ~ 1 m and ~ 5 m. In addition to that data pairs exist, where AEM TSIT is ~ 4 m but SICCI-2 SIT is just ~ 1 m and vice versa where AEM TSIT is ~ 0.5 m but SICCI-2 SIT is ~ 3 m.

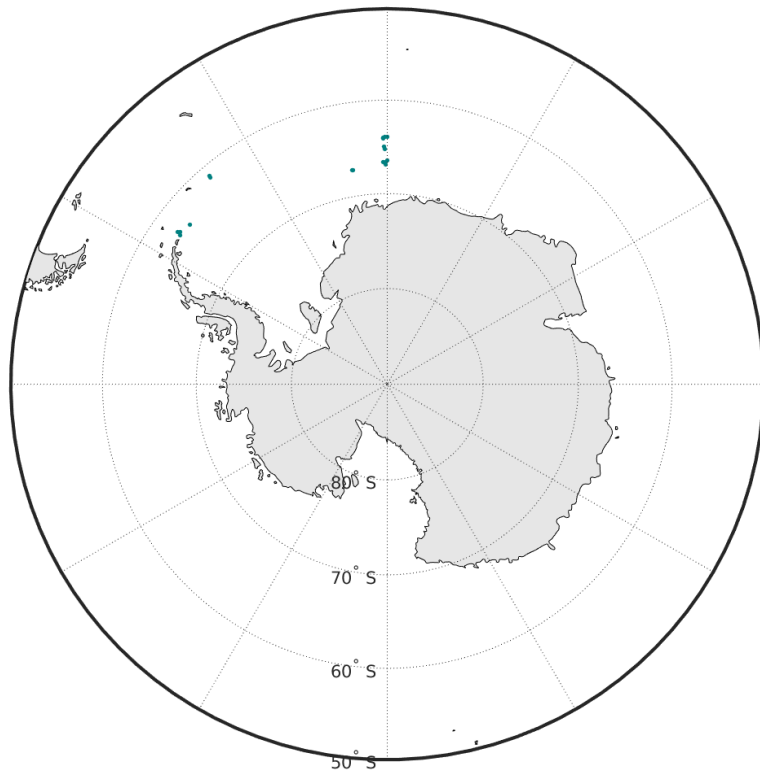


Figure 3-65: Location of AEM observations during ANTXXIX/6 and ANTXXIX/7.

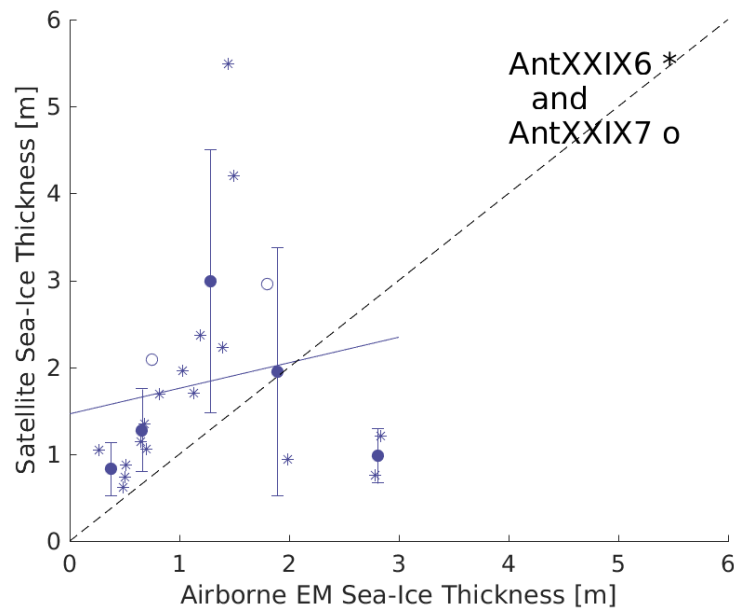


Figure 3-66: Comparison between AEM total SIT (x-axis) and SICCI-2 SIT (y-axis) for ANTXXIX/6 and 7, i.e. from the CS-2 data period of the SICCI-2 SIT product. Stars and open circles denote the co-located observations for ANTXXIX/6 and ANTXXIX/7, respectively. Filled circles denote the 0.5 m – wide bin averages over data from both expeditions. Through these a linear regression is computed (solid line). The dashed line is the line of 1-to-1 agreement.

The number of co-located SIT values from the ANTXXIX6 and /7 cruises is quite low and it is difficult to derive any solid conclusion from that (Figure 3-66). For ANTXXIX/7 only two data pairs are available which both suggest an overestimation of TSIT by ~ 1 m. For ANTXXIX/6 some more data pairs are available. Those with an AEM TSIT below ~ 1.5 m agree reasonably well – even though again SICCI-2 SIT overestimates AEM TSIT. For AEM TSIT > 1.5 m, however, the tentative agreement breaks down completely with an overestimation by 4 m close to 1.5 m AEM TSIT and an underestimation by almost 2 m for AEM TSIT of ~ 2.8 m.

Summary

For the Northern Hemisphere, SICCI-2 SIT and airborne electromagnetic (EM) measurements of the total (sea ice plus snow) sea-ice thickness (TSIT) are in reasonable agreement in general. This reasonable agreement comes from a very good agreement for the CS-2 part of the period where a linear regression with almost zero intercept and a slope close to 0.9 fits perfectly well with the fact that TSIT $>$ SIT. The agreement between Envisat SIT and airborne EM (AEM) measurements is poor with a clear underestimation of TSIT by the SICCI-2 product.

For the Southern Hemisphere, SICCI-2 SIT and AEM TSIT measurements have far less in common than in the Northern Hemisphere. It is difficult to obtain useful conclusions from the AEM data of only four cruises, which all took place in the Weddell Sea. One could get the idea that CS-2 performs better than Envisat but even if so it is likely that SICCI-2 SIC is positively biased compared to AEM TSIT.

3.5 SIT validation with moored ULS

Upward looking sonars (ULS) observe sea-ice draft, the part of the ice under the water level, which can be used for validation of the SICCI SIT prototype product.

In the Arctic moored ULS data are available for basically two sites. One is the Beaufort/Chukchi Sea (Figure 3-67) where the Beaufort Gyre Exploration Project (BGEP) has been taking place since 2003. Four moored ULS measured sea-ice draft in the period from 2003 to 2015. BGEP ULS data are available at <http://www.whoi.edu/page.do?pid> [RD-21; RD-22]. The other location is the Fram Strait (Figure 3-68) where ULS observations have been carried out since the 1990ties and are available via the Norsk Polar Institute (NPI) in Tromso, Norway [RD-23].

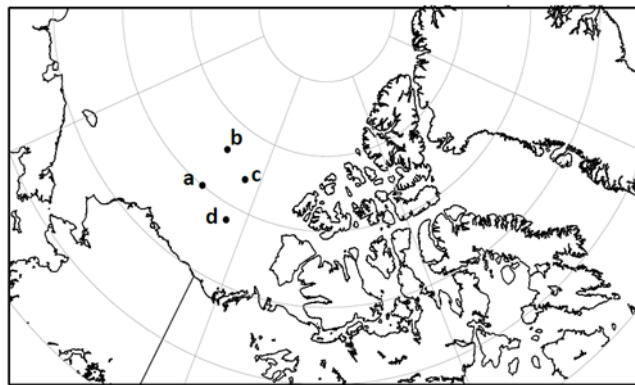


Figure 3-67: Location of ULS moorings from the Beaufort Gyre Exploration Project (BGEP).

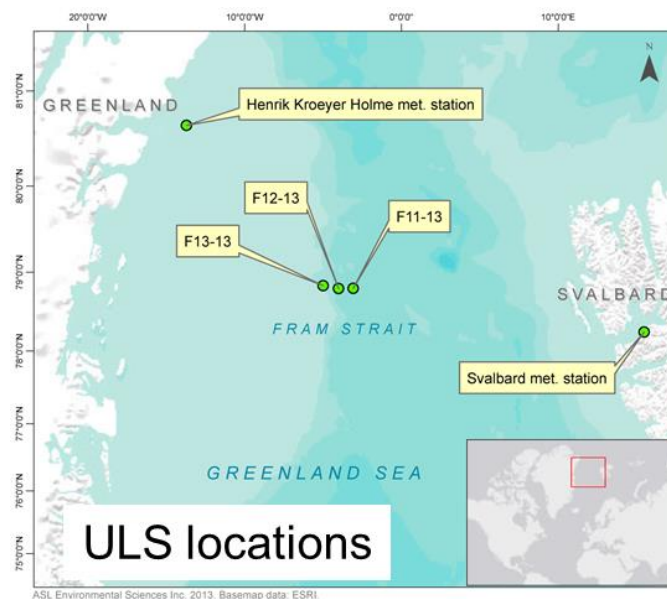


Figure 3-68: Location of the moored ULS in the Fram Strait between Svalbard and Greenland owned by the Norwegian Polar Institute (NPI) (taken from [RD-23], see also [RD-24]).

In the Antarctic, moored ULS are located in the Weddell Sea as described in Behrendt et al. [RD-25] and are available via the PANGAEA data base: doi:10.1594/PANGAEA.785565.

The advantage of ULS observations is that they provide information about the temporal evolution of the sea-ice thickness (by means of the measured draft) at the location of the mooring. When combined with sea-ice drift information one can also extract information about the sea-ice thickness distribution upstream of the mooring location (e.g. Hansen et al. [RD-24]).

BGEP Results

Upward looking sonars (ULS) observe sea ice draft, the part of the ice under the water level, which can be used for validation of the SICCI-2 SIT product data. Here we used data from the Beaufort Gyre Exploration Project (BGEP) where four (a, b, c and d) moored ULS measured sea ice draft over the period from 2003 to 2015. The approximate location of the moorings is indicated in Figure 3-67. Over the whole period considered the mooring 'a' provides ULS measurements for all 12 winter seasons, mooring 'b' has the gaps in winters 2005/2006 and 2009/2010, the measurements for winters 2003/2004 to 2007/2008 are available from mooring 'c', and for winters 2007/2008 to 2014/2015 from mooring 'd'.

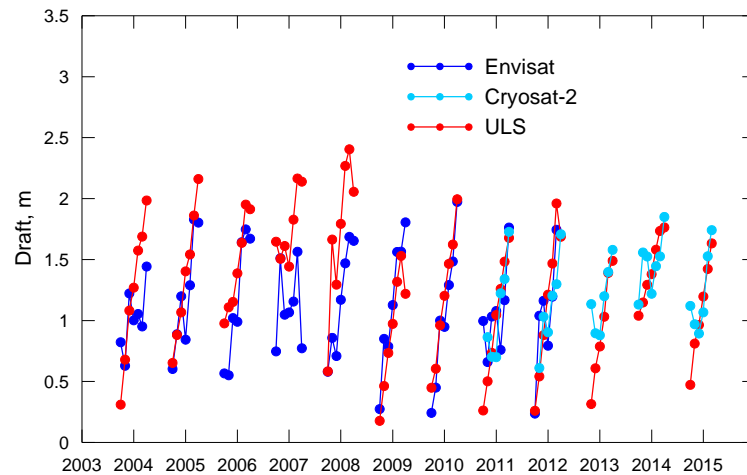


Figure 3-69: Monthly mean sea-ice draft measurements from the BGEP ULS moorings and sea-ice draft estimates from collocated grid cells from the SICCI-2 SIT product for ULS at mooring location 'a'.

In Figure 3-69 through Figure 3-73 monthly mean sea-ice draft measurements from the four moorings (Figure 3-69 to Figure 3-72) and their mean (Figure 3-73) are compared with SICCI-2 SIT product sea-draft estimates from the collocated grid cells and a mean of the grids within large area of moorings location (70° to 82° N by 130° to 160° W), respectively. Sea-ice draft has been calculated from the SICCI SIT product as a difference between SIT and sea-ice freeboard. In order to account for inclusion of the open water in the ULS data the draft from the SICCI SIT product has been multiplied by the sea-ice concentration.

The corresponding differences between SICCI-2 and ULS sea-ice draft (SICCI-2 – ULS) are presented in Figure 3-74 through Figure 3-78.

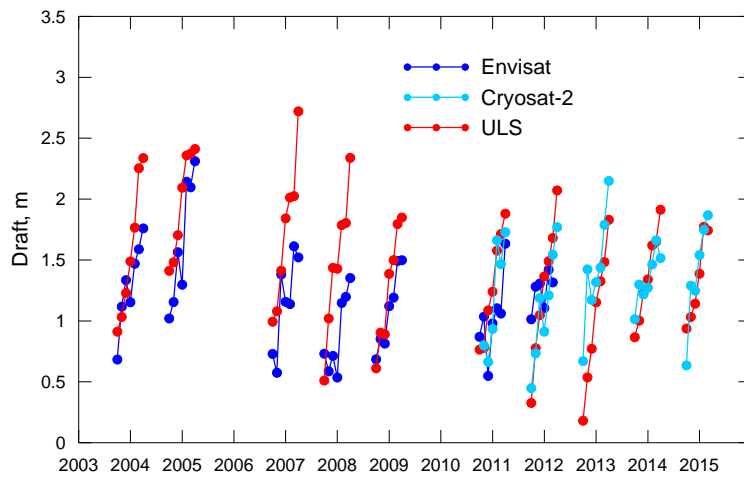


Figure 3-70: As Figure 3-69 but for ULS at mooring location 'b'.

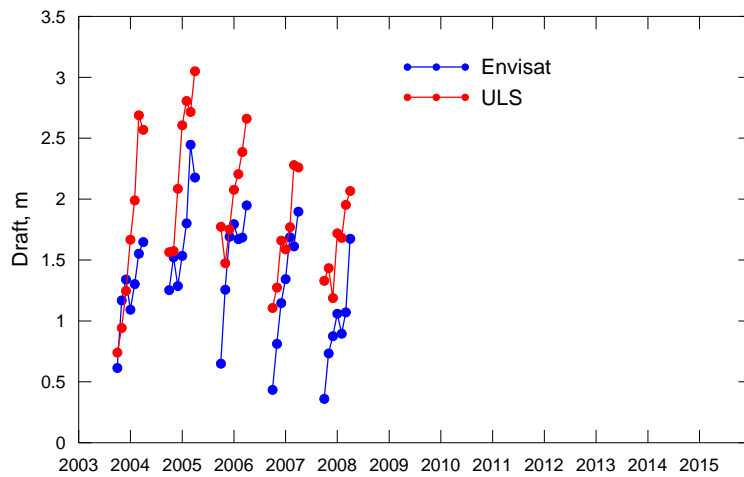


Figure 3-71: As Figure 3-69 but for ULS at mooring location 'c'.

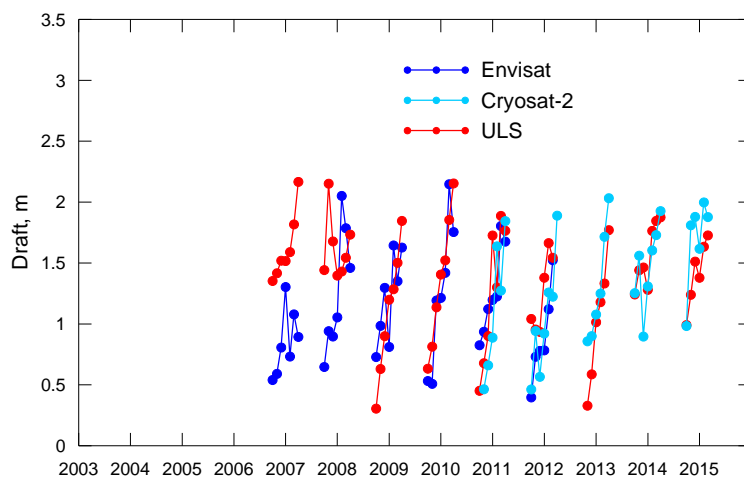


Figure 3-72: As Figure 3-69 but for ULS at mooring location 'd'.

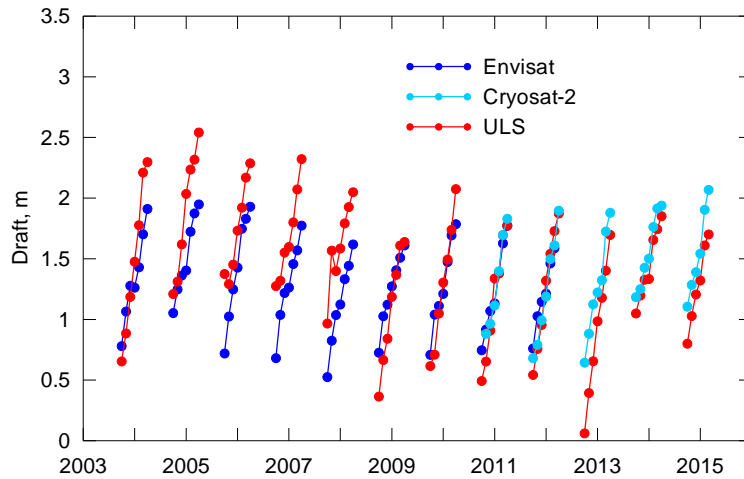


Figure 3-73: Mean sea-ice draft of four BGEP ULS moorings and a mean sea-ice draft estimated from the grid cells of SICCI-2 SIT product covering sector of moorings' location (70° to 82° N by 130° to 160° W).

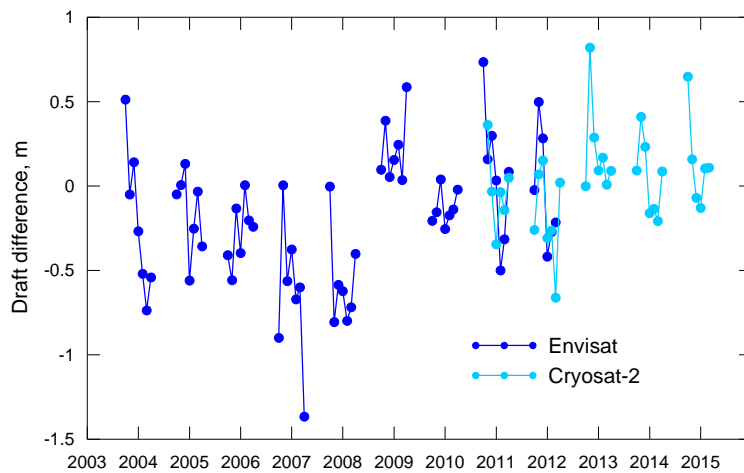


Figure 3-74: Difference monthly mean SICCI-2 sea-ice draft minus BGEP ULS sea-ice draft for ULS at mooring location 'a' (see Figure 3-69).

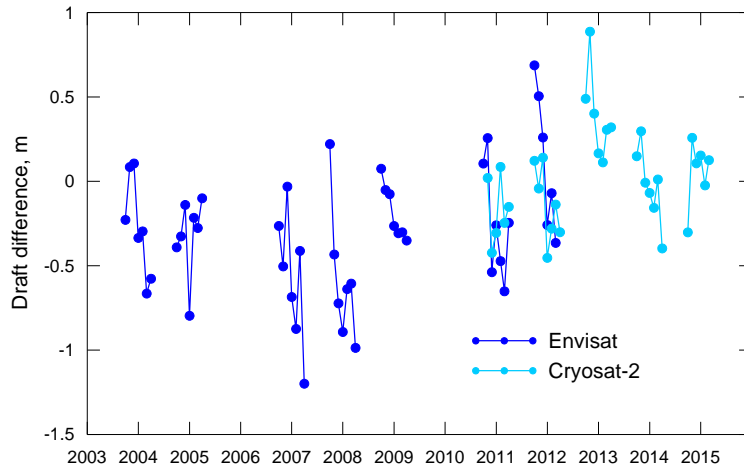


Figure 3-75: As Figure 3-74 but for ULS at mooring location 'b'.

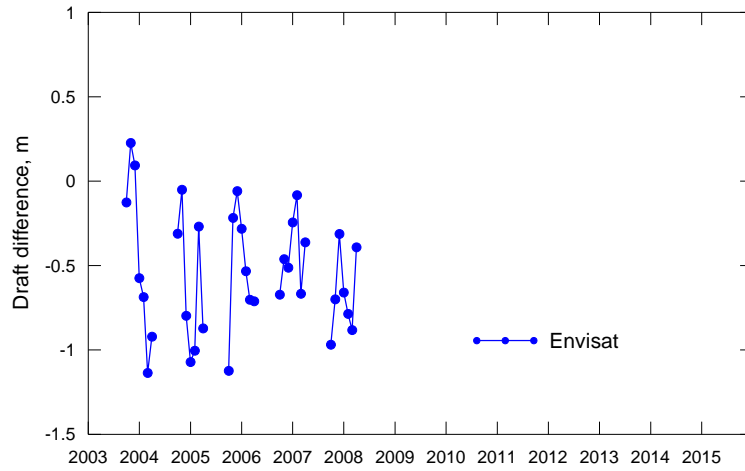


Figure 3-76: As Figure 3-74 but for ULS at mooring location 'c'.

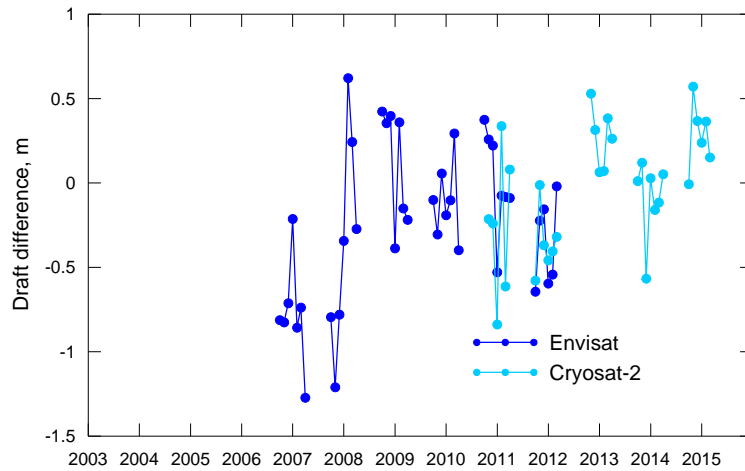


Figure 3-77: As Figure 3-74 but for ULS at mooring location 'd'.

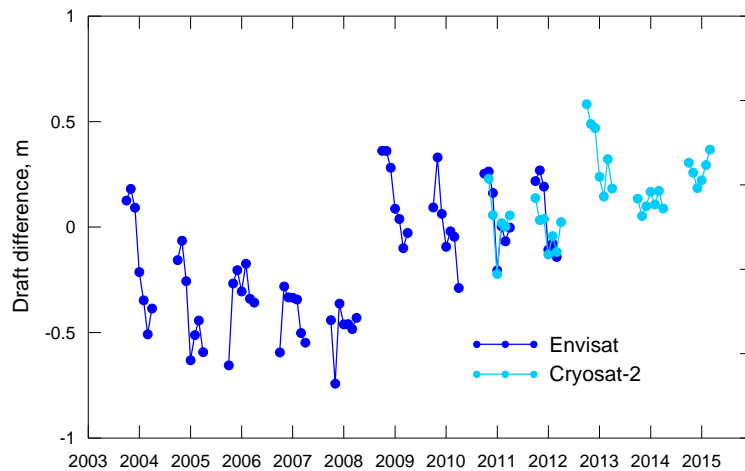


Figure 3-78: As Figure 3-74 but using the average of all four moorings and the sector of moorings' location (70° to 82° N by 130° to 160° W) (compare Figure 3-73).

The SICCI-2 SIT product predominantly underestimates sea-ice draft on average by 35 cm (S.D. = 21 cm) for winters 2003/2004 to 2007/2008, and overestimates it by 11 cm (S.D. = 18 cm) for winters 2008/2009 to 2014/2015 over the large sector (Figure 3-73 and Figure 3-78). Overall, the mean difference for the whole period is -17 cm (S.D. = 29 cm) for Envisat, 15 cm (S.D. = 18 cm) for Cryosat-2 and -6 cm (S.D. = 30 cm) for the entire dataset.

The observed shift in the differences in 2008 can be linked to the uncertainty of snow depth estimates applied to convert freeboard to thickness. In the SICCI-2 SIT product snow depth is derived from Warren et al. ([RD-08]) for MYI and 50% of those values for FYI as an assessment of present-day snow depth derived from airborne Operational Ice Bridge (OIB) measurements ([RD-26]). However OIB observations provide data starting from 2009 and a found relation may be not representative for the earlier period. Mixture of FYI and MYI observed in the area of BGEP mooring location enhances the uncertainty of the snow depth used in SICCI-2 SIT product and could, in particular, lead to snow depth underestimation for the period before 2008, and, consequently, to underestimation of SIT retrievals. Another feature of the observed differences is their decrease from autumn to spring for most of winter seasons that could be explained by underestimation of climatological snow depth growth during winter season as observed from comparison with NP data.

NPI-ULS Results

Similar to SICCI phase 1 and published literature (e.g. Hansen et al. [RD-24]) sea-ice draft measured by the ULS will be converted into sea-ice thickness by applying a constant conversion factor of 1.136.

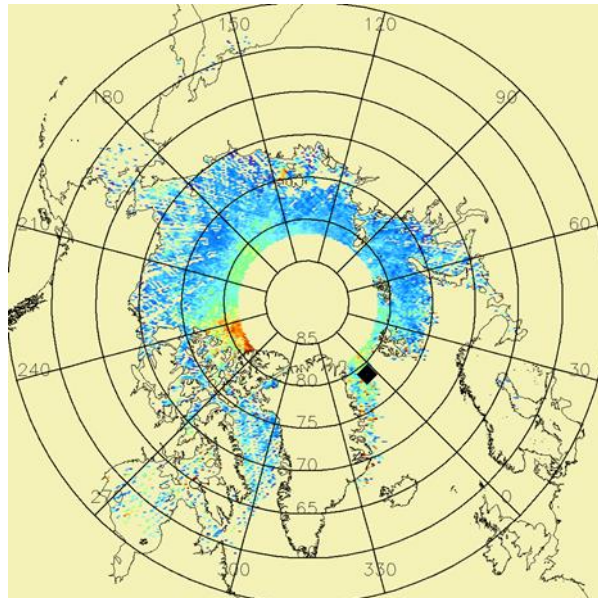


Figure 3-79: Location of the moorings from which we used ULS data from the NPI mooring location in the Fram Strait. The background is the SICCI-2 SIT from Envisat from February 2003.

For the NPI ULS we have monthly data of mean and modal sea-ice thickness. The sea-ice thickness is converted from the sea-ice draft observed via a constant conversion factor which is based on in-situ drillings. It does not take into account seasonal changes in snow or sea-ice density and snow depth. It might also be biased towards level ice conditions as drillings are much easier to perform over level sea ice. Details about data processing as well as precision and accuracy are given, e.g., in Hansen et al. [RD-24]. The sea-ice thickness given is a true sea-ice thickness, i.e. periods of open water were excluded from the data.

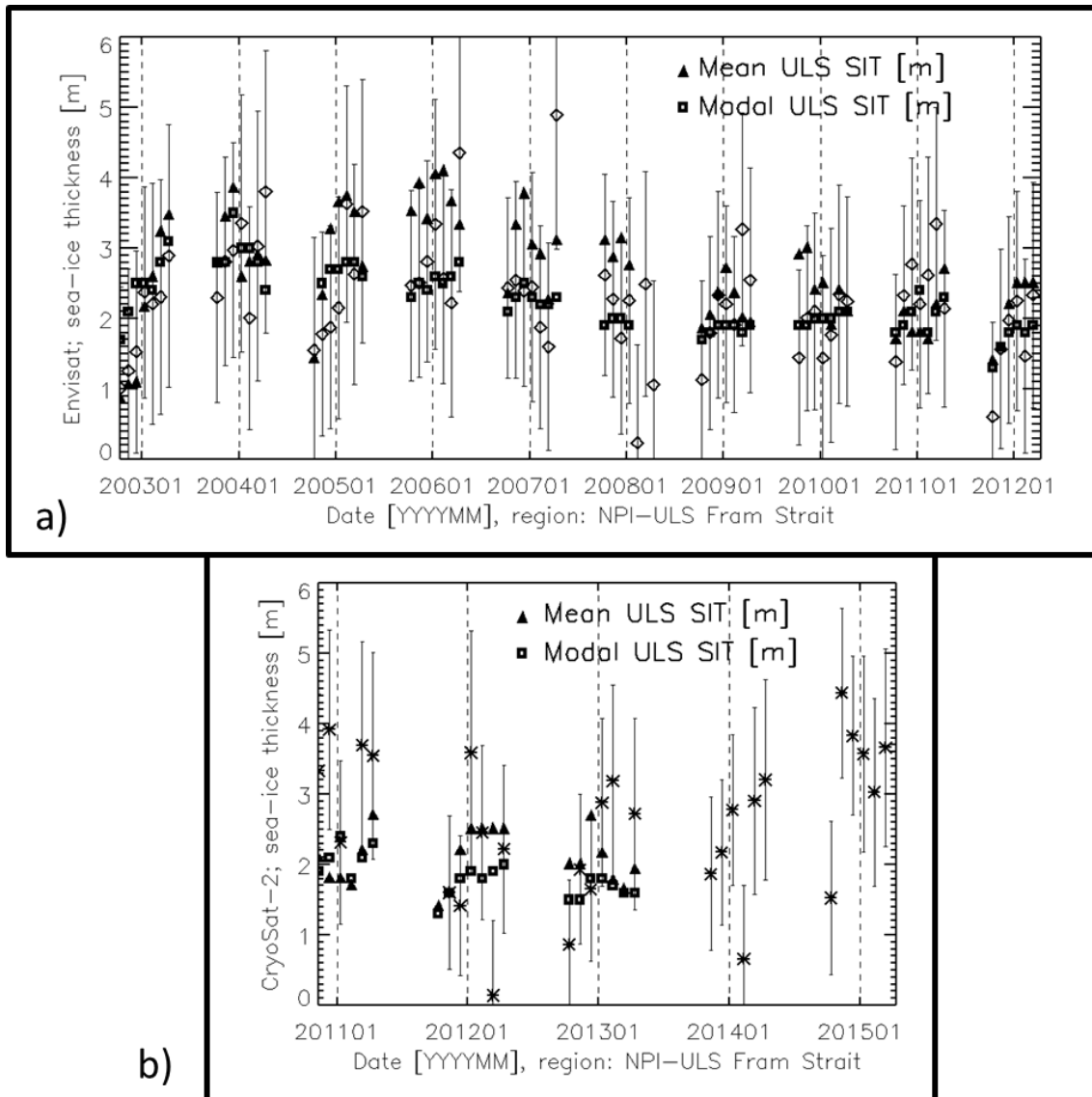


Figure 3-80: Time series of the SICCI-2 SIT derived from Envisat (top, diamonds) and CS-2 (bottom, stars) and the co-located NPI ULS based monthly SIT estimates; mean and modal SIT values are given by triangles and squares, respectively. Error bars given denote the SICCI-2 SIT retrieval uncertainty.

SICCI-2 Envisat SIT tends to agree relatively well with the NPI ULS SIT data (Figure 3-80 a). This applies in particular for the modal ULS SIT which is mostly falling within the range given by the SIT retrieval uncertainty. Mean

ULS Sit data often also fall into this range but also have the tendency to be larger than SICCI-2 SIT. The agreement between SICCI-2 CS-2 SIT and NPI ULS SIT data seems to be less good (Figure 3-80 b). The fraction of modal NPI ULS SIT falling outside the SICCI-2 SIT range is larger than for Envisat SIT; CS-2 SIT data seem exceeding mean NPI ULS SIT more often than for Envisat.

The combined time-series given in Figure 3-81 (a) illustrates the less good agreement between SICCI-2 and ULS data for the CS-2 measurement period. Note in this context that the difference CS-2 minus Envisat SIT for the grid cell co-located with the NPI ULS location for the 10 months of overlap is $0.31\text{m} \pm 1.08\text{m}$, i.e. CS-2 is over-estimating SIT relative to Envisat.

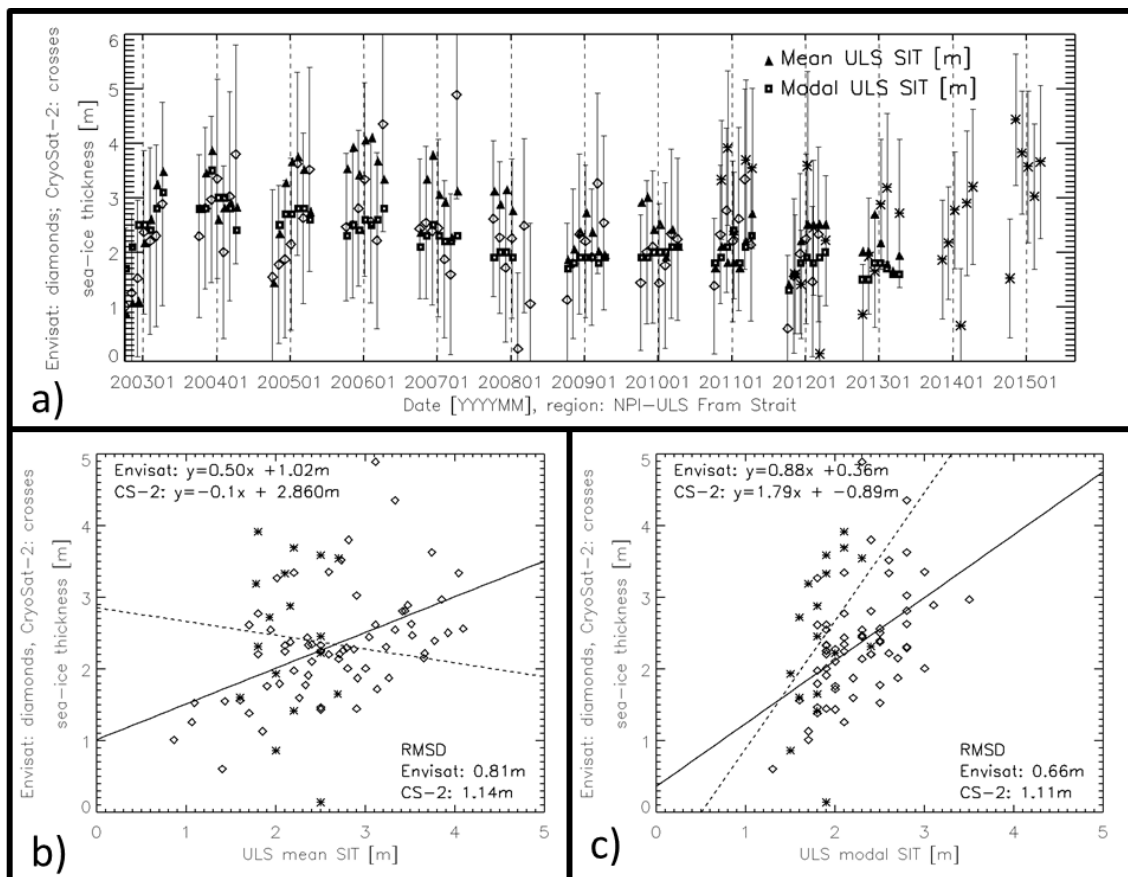


Figure 3-81: Combined time-series of SICCI-2 SIT (Envisat: diamonds, CS-2: crosses) and NPI ULS SIT (mean and modal SIT given by triangles and squares, respectively) (top). Scatterplots between mean (left) and modal (right) ULS SIT and mean SICCI-2 SIT for Envisat data (diamonds) and CS-2 data (stars) together with the lines (solid for Envisat, dashed for CS-2) and equations of a linear regression and the RMSD values (bottom).

The scatterplots (Figure 3-81 b,c) confirm the observations made in Figure 3-80 and Figure 3-81a); agreement between Envisat SIT and ULS SIT is considerably better than for CS-2 SIT with a RMSD: 0.81 m for mean ULS SIT and 0.69 m for modal ULS SIT, being smaller than the typical SICCI-2 SIT retrieval uncertainty. The SIT point cloud resembles more correlation between the two SIT data sets for Envisat than for CS-2. The few CS-2 SIT

data spread over a far larger SIT range: 0.2 m to 3.9 m than the corresponding ULS SIT data: 1.6 m to 2.7 m for mean SIT and 1.5 m to 2.4 m for modal SIT, explaining the poor correlation and poor linear relationship. Note that the linear regression improves somewhat when comparing SICCI-2 Envisat SIT with modal instead of mean ULS SIT values.

We observe a decrease in mean and modal NPI ULS SIT from Envisat period data to CS-2 period data: mean ULS_envisat: (2.64 ± 0.76) m to mean ULS_cs2: (2.17 ± 0.34) m; modal ULS_envisat: (2.07 ± 1.56) m to modal ULS_cs2: (1.86 ± 0.26) m. In contrast, the SICCI-2 data show a slight increase from (2.39 ± 0.80) m to (2.43 ± 1.06) m.

AWI-ULS Results

For the Southern Hemisphere we used ULS data of the moorings in the Weddell Sea operated by the Alfred Wegener Institute for Polar and Marine Research (AWI), Bremerhaven, Germany. Figure 3-82 illustrates the location of the ULS moorings.

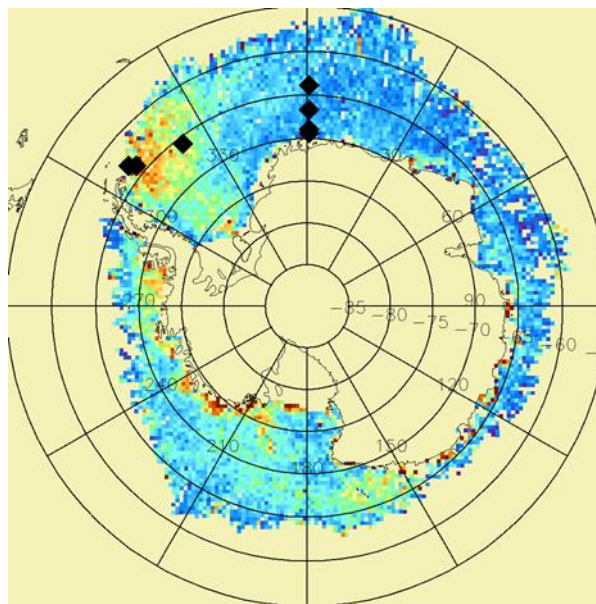


Figure 3-82: AWI mooring locations in the Weddell Sea. Moorings in the western Weddell Sea are, from left to right, AWI-206, AWI-207, and AWI-208; moorings in the eastern Weddell Sea along the Greenwich meridian are, from north to south, AWI-229, AWI-231, AWI-232, and AWI-233. The background is given by sea-ice draft (right, September 2002).

For the AWI ULS we have monthly data of the mean sea-ice draft and its standard deviation. Derivation of sea-ice draft from the ULS measurements is described in Behrendt et al. [RD-25]; this is for the original processing only, though. The monthly data are part of this data set: http://psc.apl.uw.edu/sea_ice_cdr/Sources/awi_weddell_sea.html. For this data set with monthly temporal resolution the time-mean sea-ice draft is given, i.e. open water observations are NOT excluded.

The AWI ULS data set overlaps only with Envisat SICCI-2 sea-ice thickness data; hence no comparison is carried out with the CS-2 sea-ice thickness data. For every AWI ULS location (Figure 3-82) the closest SICCI-2 SIT grid cell (50 km by 50 km grid resolution) is taken. We keep the ULS AWI data as they are and i) compute the sea-ice draft from the SICCI-2 data by subtracting the SICCI-2 sea-ice freeboard from the SICCI-2 sea-ice thickness and by ii) converting the true sea-ice draft into a grid-cell mean sea-ice draft by multiplying the value with the sea-ice concentration. All data required can be taken from the SICCI-2 SIT data product.

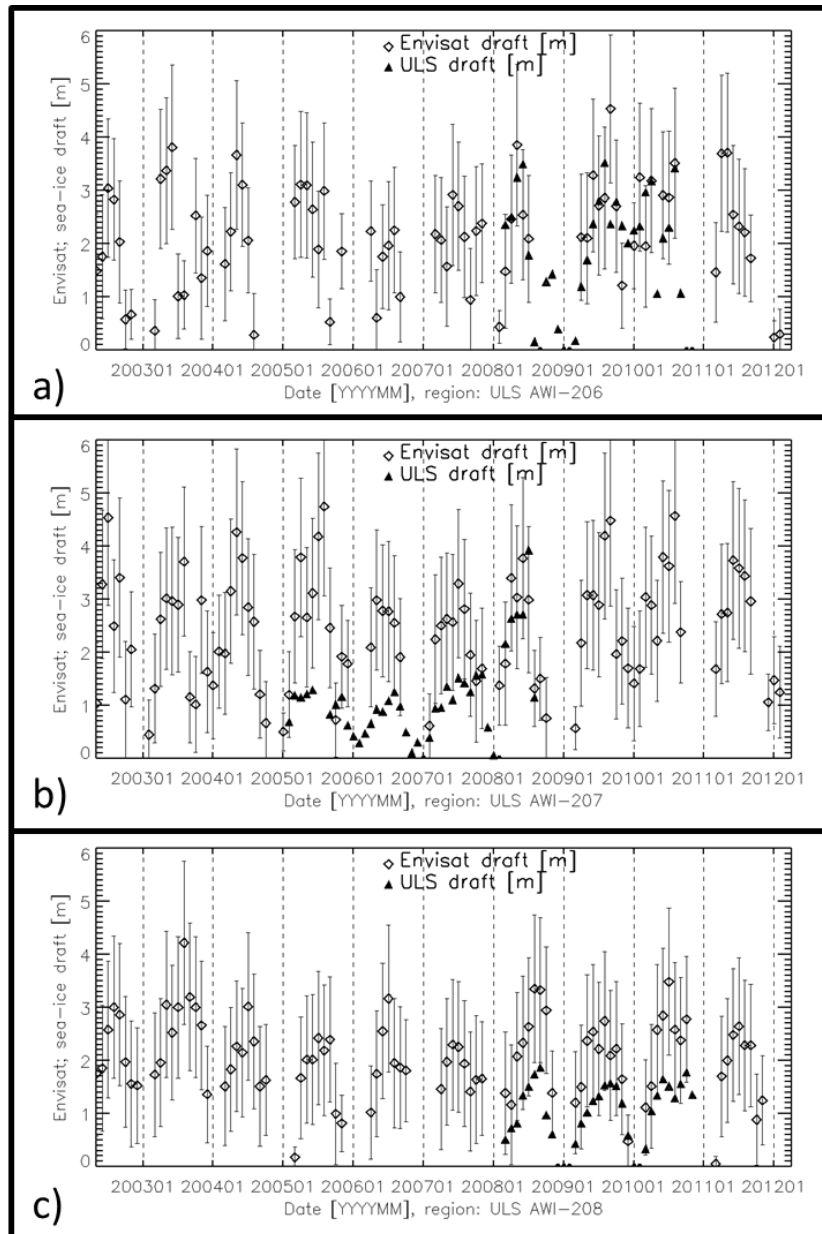


Figure 3-83: Time series of the monthly grid-cell mean sea-ice draft obtained from SICCI-2 SIT data (diamonds) and estimated from AWI ULS data (triangles) for the three AWI ULS in the western Weddell Sea. Error bars denote the sea-ice draft retrieval uncertainty computed as the root mean squared sum of the retrieval

uncertainties of SIT and sea-ice freeboard; the uncertainty in sea-ice concentration is not taken into account.

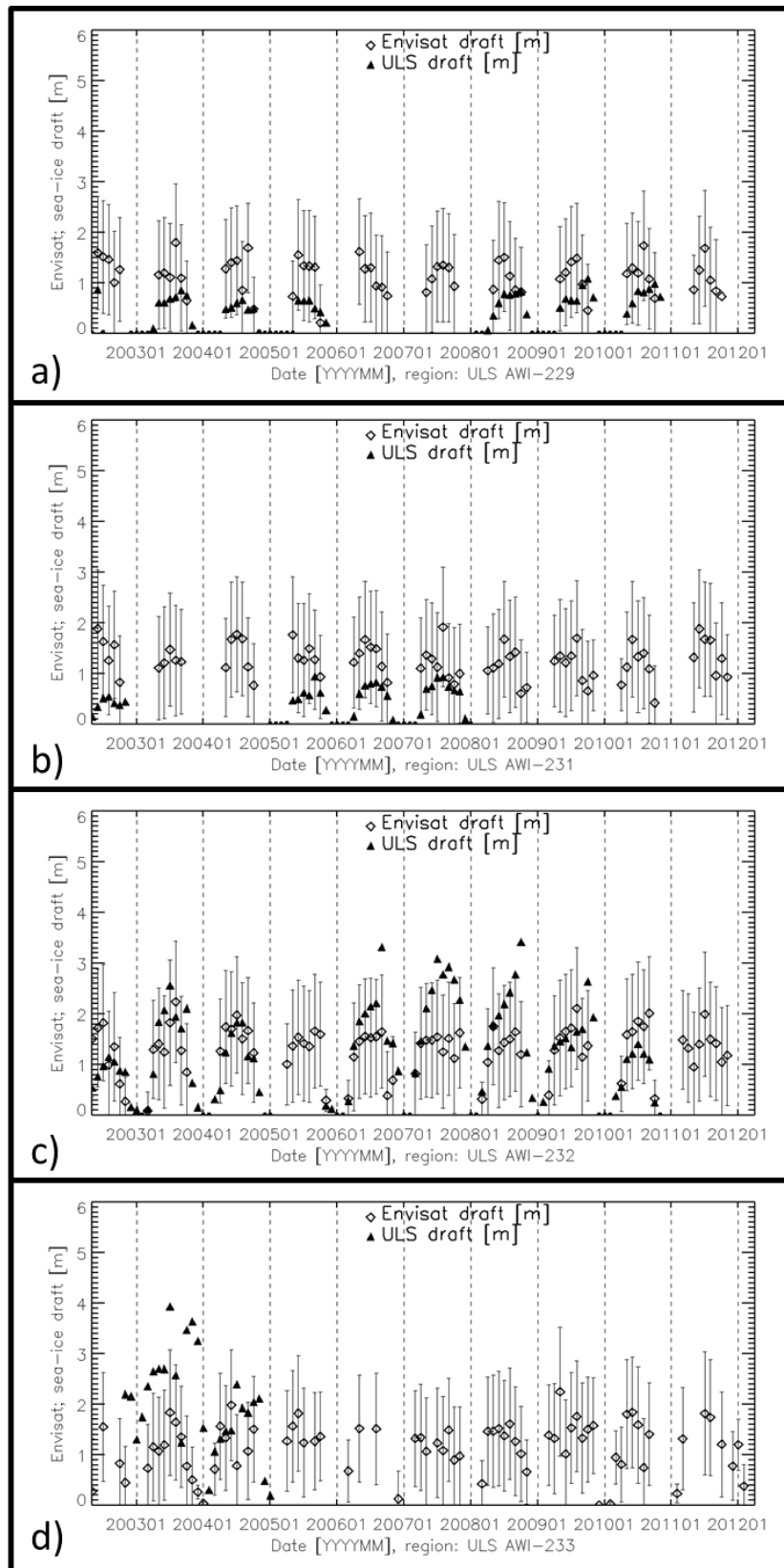


Figure 3-84: As Figure 3-83 but for the four AWI ULS locations in the eastern Weddell Sea along the Greenwich meridian (see Figure 3-82).

For the western Weddell Sea (Figure 3-83), the region with a potentially large influence of perennial (multiyear) sea ice drifting north along the Antarctic Peninsula, we find only some agreement between Envisat and ULS sea-ice draft. For AWI-206 (a), the most western located ULS, about half of the ULS sea-ice draft (SID) data fall into the SID range given by the SICCI-2 values and their error bars. At that location data from the year 2010 mostly show ULS SID below SICCI-2 SID. This under-estimation is common for the other two AWI ULS in this region: AWI-207 (b) and AWI-208 (c), the latter being located substantially further east (compare Figure 3-82). The under-estimation is between 1 and 2 meters at these two AWI ULS – except for AWI-2007 in the year 2008, where ULS SID again tends to fall into the SICCI-2 SID range.

For the eastern Weddell Sea (Figure 3-84), a region dominated by seasonal sea ice, we find ULS sea-ice drafts which are systematically between 0.5 and 1 m smaller than SICCI-2 based SID at the two northern AWI ULS sites AWI-229 (a) and AWI-231 (b). Agreement between SICCI-2 SID and AWI ULS SID is substantially better for the two southern AWI ULS sites AWI-232 (c) and AWI-233 (d). Note that we were taking SICCI-2 SID data from one grid cell further to the east (50 km distance) of AWI-232 because otherwise we would only have had four valid SICCI-2 SID data points. Since sea-ice motion in that region can be expected to be westward the mistake we are making by this should be relatively small. We find that AWI ULS data of some years mostly fall within the SICCI-2 SID range, e.g. for year 2004. In contrast to the two northern AWI ULS sites we find that ULS SID is larger than SICCI-2 SID at AWI-232, e.g. for years 2008 and 2009, and also for AWI-233 in year 2003.

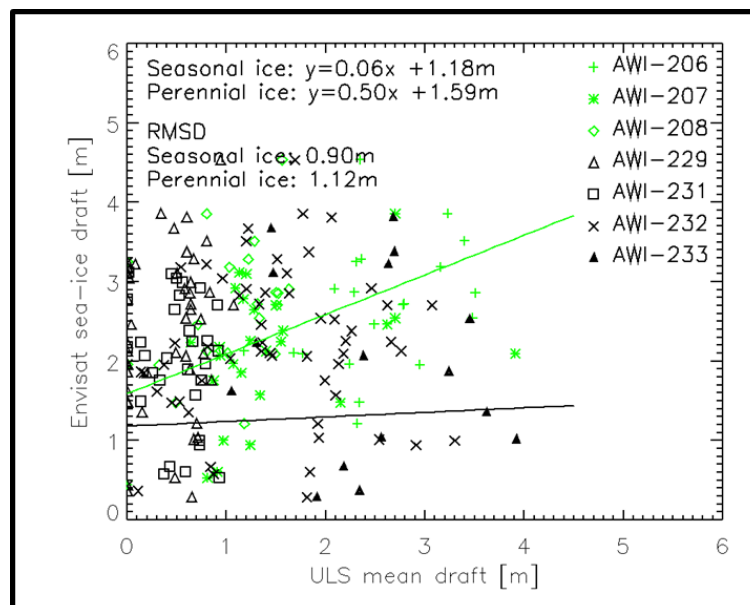


Figure 3-85: Scatterplot between mean ULS sea-ice draft and mean SICCI-2 sea-ice draft based on Envisat data only. Different AWI ULS sites are denoted by different symbols, those in the western Weddell Sea (dominated by perennial sea ice) are given in green; those in the eastern Weddell Sea (seasonal sea ice) are given in black.

Superposed are lines of the linear regression between the sea-ice draft data sets separately for seasonal sea ice (black) and perennial sea ice (green) AWI ULS sites. Sea-ice draft values < 0.2 m have been excluded from the regression analysis.

This regionally and temporally contrasting agreement between ULS SID and SICCI-2 SID is illustrated further in Figure 3-85 which shows the scatterplot between the two data sets together with the lines and equations of a linear regression and the RMSD. Regression and RMSD are computed only for SID values > 0.2 m. For this step we also grouped SID values into seasonal sea ice, AWI-229 through AWI-233, and perennial sea ice, AWI-206 through AWI-208; one may simply name it western and eastern Weddell Sea as well. From that analysis we find some relationship between AWI ULS SID data and SICCI-2 SID for the perennial sea ice / western Weddell Sea while there seems to be no relationship for the seasonal sea ice / eastern Weddell Sea.

Note that computing the mean sea-ice draft would have resulted in the opposite result: Perennial ice: AWI ULS: (1.59 ± 0.84) m versus SICCI-2: (2.35 ± 0.79) m; seasonal ice: AWI ULS: (1.30 ± 0.84) m versus SICCI-2: (1.20 ± 0.42) m. According to these numbers the difference between mean sea-ice draft values is much smaller for seasonal ice: 0.10 m than for perennial ice: 0.76 m.

Summary

The gridded SICCI-2 sea-ice thickness (SIT) product has been compared with data from moored upward looking sonar (ULS) data other than the BGEP sites. For the Northern Hemisphere we used the ULS data from the Fram Strait provided by NPI [RD-23]. These are – like the SICCI-2 SIT values – true estimates of the sea-ice thickness, i.e. exclude the open water influence. Here a constant conversion factor is used to convert the ULS sea-ice draft observations into SIT. For the Southern Hemisphere we used the ULS data from the Weddell Sea provided by AWI [RD-25] but modified at http://psc.apl.uw.edu/sea_ice_cdr/Sources/awi_weddell_sea.html from daily observations into monthly mean sea-ice draft data which **include** open water measurements. We tried to take into account this fact by convert the SICCI-2 data also into grid-cell mean values by multiplication with the sea-ice concentration also provided with the SIT product. In order to be able to compare sea-ice drafts we computed the sea-ice draft from the SICCI-2 data by subtracting sea-ice freeboard from SIT.

- For the Northern Hemisphere, agreement between ULS and SICCI-2 SIT data seems to be better for the Envisat period than the CS-2 period. While the mean Envisat SICCI-2 SIT value lies between modal and mean ULS SIT values, the mean CS-2 SICCI-2 SIT value exceeds both ULS SIT values.
- For the Southern Hemisphere, agreement between ULS and SICCI-2 SIT data seems to be better for regions with (at least) some multiyear (or perennial) sea ice, i.e. the western Weddell Sea, than for regions dominated by seasonal sea ice, i.e. the eastern Weddell Sea.
- Note that we have compared a point measurement (more or less) with sea-ice thickness estimates representative of a 25 km by 25 km (Northern Hemisphere) or 50 km by 50 km (Southern Hemisphere).
- Note that ULS SIT data of the Northern Hemisphere were converted from the sea-ice draft observations using a constant, empirically

derived conversion factor which is certainly biased towards conditions encountered for level ice (see [RD-23]).

- Note that ULS sea-ice draft data of the Southern Hemisphere were only available as monthly grid-cell mean value, i.e. periods of ULS measurements with open water were included. Even though we tried to take this into account by converting the SICCI-2 data into a grid-cell mean value as well and therefore compare two grid-cell mean data sets it can be expected that the different scales involved in this comparison could lead to a systematic positive bias in the SICCI-2 sea-ice draft. Another point which makes the evaluation for the Southern Hemisphere more problematic as well is that we assume that the sea-ice freeboard, which we use to compute sea-ice draft from the SIT data is correct. We know that sea-ice freeboard might be biased thanks to a yet unknown bias in snow depth.

3.6 SICCI-2 SIT evaluation with ICESat SIT data

Part I: Comparison to the ICESat SIT product from NSIDC

The SICCI-2 sea-ice thickness (SIT) data set has been compared with the ICESat SIT data set for the Arctic produced at NSIDC and available from NSIDC <https://nsidc.org/data/NSIDC-0393/versions/1> [RD-27].

The Ice, Cloud and land Elevation Satellite (ICESat) carried the Geoscience Laser Altimeter System (GLAS), a laser altimeter capable to measure the total (sea ice + snow) freeboard. ICESat measured discontinuously. Typically, the laser altimeter was switched on for three about 35-days long periods every year. For the Arctic, ICESat SIT is taken for late fall / early winter periods, i.e. October/November, and late winter periods, i.e. February/March or March/April. For the comparison, data of each ICESat measurement period (see Table 3-11), which extend over two months (except ON03 which starts even in September), we initially take SICCI-2 SIT data from these two months, that is from October and November and from February and March, and for 2007 from March and April. Later we restrict the data from Envisat to those months which have a major overlap with the ICESat measurement period. The inter-comparison is limited to the Northern Hemisphere and to the Envisat part of the SICCI-2 SIT product.

Table 3-11: ICESat measurement periods. Acronyms ON, FM and MA refer to October/November, February/March and March/April, respectively, while 03, 04, ..., 08 refer to the year.

2003/04		2004/05		2005/06		2006/07		2007/08	
ON03	Sep. 25- Nov. 19	ON04	Oct. 3- Nov. 8	ON05	Oct. 21- Nov. 24	ON06	Oct. 25- Nov. 27	ON07	Oct. 2- Nov. 5
FM04	Feb. 17- Mar. 21	FM05	Feb. 17- Mar. 24	FM06	Feb. 22- Mar. 27	MA07	Mar. 12- Apr. 14	FM08	Feb. 17- Mar. 21

ICESat and Envisat SIT data are co-located by finding the ICESat grid cell which is closest to the respective Envisat grid cell using a search radius of 0.25 degrees. Note that the Envisat data are on the EASE2 grid while ICESat data are projected onto the NSIDC polar-stereographic grid with tangential plane at 70 degrees N.

During the October/November ICESat measurement periods the sea-ice extent increased. But also during the late winter periods sea-ice extent varied – albeit not in the Arctic Ocean itself, the region of our main interest. In order to take these variations into account we compute the arithmetic mean of the co-located Envisat SIT values of the two months with overlapping ICESat SIT data in case two Envisat SIT values are available; otherwise we just use one Envisat SIT value. Consider a co-located grid cell is open water in October but sea ice in November. Then the comparison is done with the value of November. If in both months an Envisat SIT value exists, then we average over both – provided that we have an overlap of at least ten days with the respective month. We refer to Table 3-12 for start and end days of the respective averaging periods.

Table 3-12: ICESat measurement periods and periods from which Envisat data are used for the inter-comparison shown in this section (compare Table 3-11).

Sensor	ICESat		Envisat	
	start	end	start	end
ON03	Sep. 25	Nov. 19	Oct. 01	Nov. 30
FM04	Feb. 17	Mar. 21	Feb. 01	Mar. 31
ON04	Oct. 03	Nov. 08	Oct. 01	Oct. 31
FM05	Feb. 17	Mar. 24	Feb. 01	Mar. 31
ON05	Oct. 21	Nov. 24	Nov. 01	Nov. 30
FM06	Feb. 22	Mar. 27	Mar. 01	Mar. 31
ON06	Oct. 25	Nov. 27	Nov. 01	Nov. 30
MA07	Mar. 12	Apr. 14	Mar. 01	Apr. 30
ON07	Oct. 02	Nov. 05	Oct. 01	Oct. 31
FM08	Feb. 17	Mar. 21	Feb. 01	Mar. 31

We excluded sea-ice thickness values above 5 m from the analysis – justified by the fact that the largest sea-ice thickness typically occurs north of Greenland, an area which is not covered by Envisat data and that very few sea-ice thickness values actually fall into the category > 5 m.

In order to have the possibility to limit the analysis to the Arctic Ocean we used the standard NSIDC sections of the Arctic Ocean (available e.g. ftp://sidacs.colorado.edu/pub/DATASETS/seaice/polar-stereo/tools/region_n.msk) Here we used the sector “arctic ocean” which excludes seas like the Greenland and Kara Seas as well as the Canadian Arctic Archipelago. This way we are able to exclude those areas from the inter-comparison where the SICCI-2 SIT is based on less valid snow depth estimates due to the limited regional validity of the Warren et al. ([RD-08]) snow depth climatology used.

We only used data where the SICCI-2 SIT product quality flag indicates a “0”, i.e. nominal retrieval.

In order to investigate whether potential differences in SIT between the two products are associated with ice type, we also read the ice type from the SICCI-2 SIT product. We repeat the inter-comparison by, for the first-year ice (FYI) case, only using grid cells with more than 85% FYI concentration. Conversely, for the multiyear ice (MYI) case, we only use grid cells with more than 85% MYI concentration.

First we focus on the comparison using all data. Figure 3-86 and Figure 3-87 exemplify the SIT distribution of the two data sets for periods ON03 and FM04, respectively, in images a) and b). It is obvious that for period ON03 the NSIDC ICESat SIT is noisier than the SICCI-2 Envisat SIT data set and that the latter provides larger SIT values over the majority of the area where both data sets have valid data. This becomes more evident in the difference map (image d) showing red tones = overestimation of Envisat SIT relative to ICESat. At the same time, however, we find a substantial fraction – at least one third – where the opposite applies, blue tones, and where Envisat SIT is smaller than ICESat SIT. This seems to apply primarily to those areas where MYI is present. Overall, we find that Envisat

underestimates ICESat by 0.23 m (image c) with a standard deviation and RMSD both ~ 0.8 m.

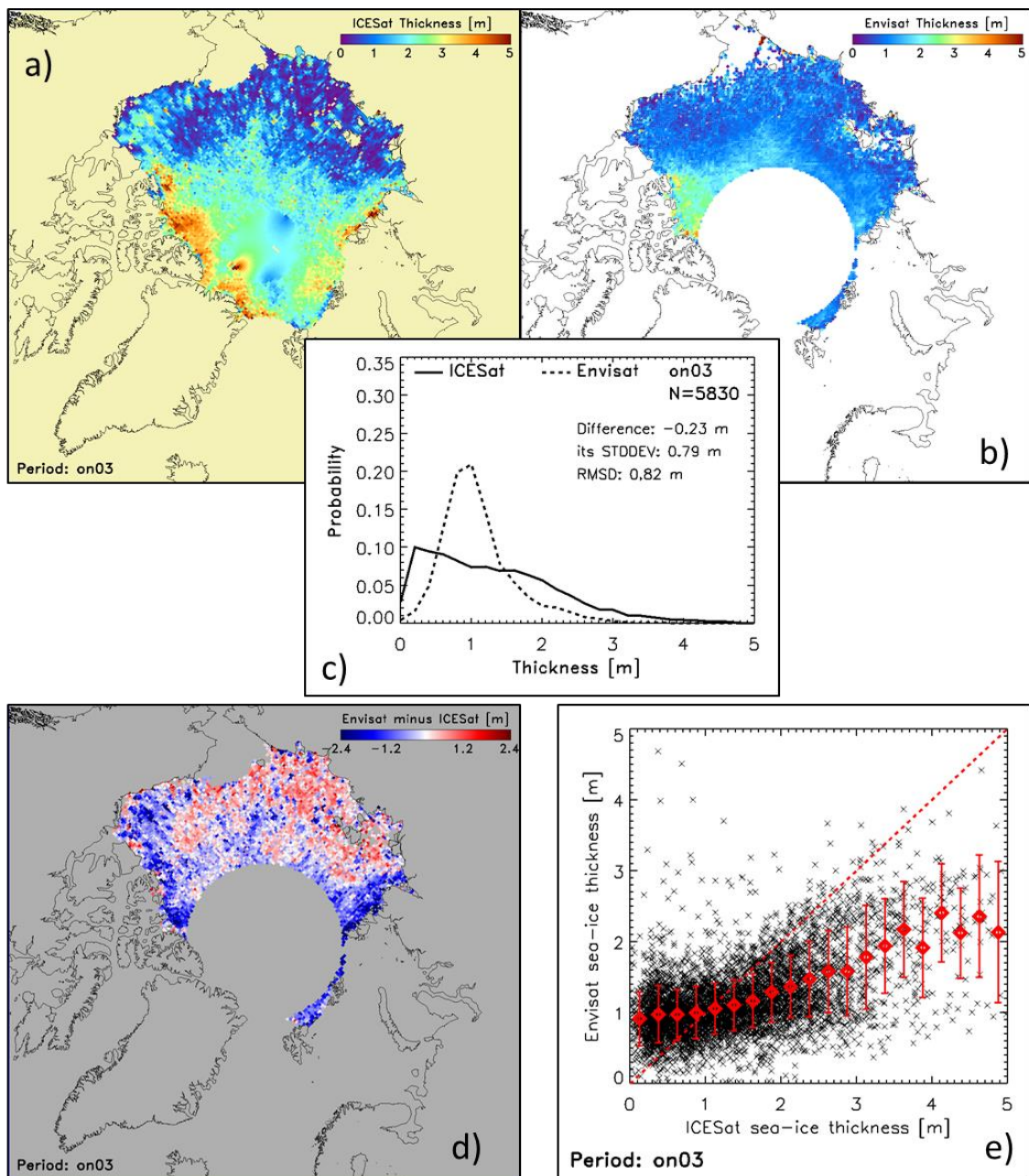


Figure 3-86: Inter-comparison of NSIDC ICESat versus SICCI-2 Envisat sea-ice thickness (SIT) for ICESat measurement period ON03 (see Table 3-11). a) ICESat SIT, note that SIT values are interpolated over the polar data gap; b) Envisat SIT, the white circular disk denotes the polar data gap; d) Difference Envisat minus ICESat SIT; c) histograms of the SIT from both sensors for coinciding grid cells together with the count of data pairs "N", the root mean squared difference "RMSD" as well as the mean difference and its standard deviation; e) scatterplot of all co-located SIT values (black crosses) superposed by the mean Envisat SIT per 0.2 m ICESat SIT bin. The error bars denote plus/minus one standard deviation. The red dashed line is the 1-to-1 fit line.

The scatterplot (Figure 3-86 e) shows that Envisat is overestimating ICESat SIT at SIT values $< \sim 1$ m and underestimating ICESat SIT at SIT $> \sim 1$ m. While there is substantial scatter in the single values, the mean Envisat SIT binned to 0.2 m wide ICESat SIT bins (red symbols) seems to follow a linear relationship albeit with a slope less than ~ 0.3 and an intercept close to 1 m. We note that the shape of the histograms is also quite different. The Envisat histogram has a distinct, relatively narrow distribution with only a short tail towards thick sea ice. The ICESat histogram has a very broad distribution with no clearly defined peak or modal value and a long tail towards thicker sea ice.

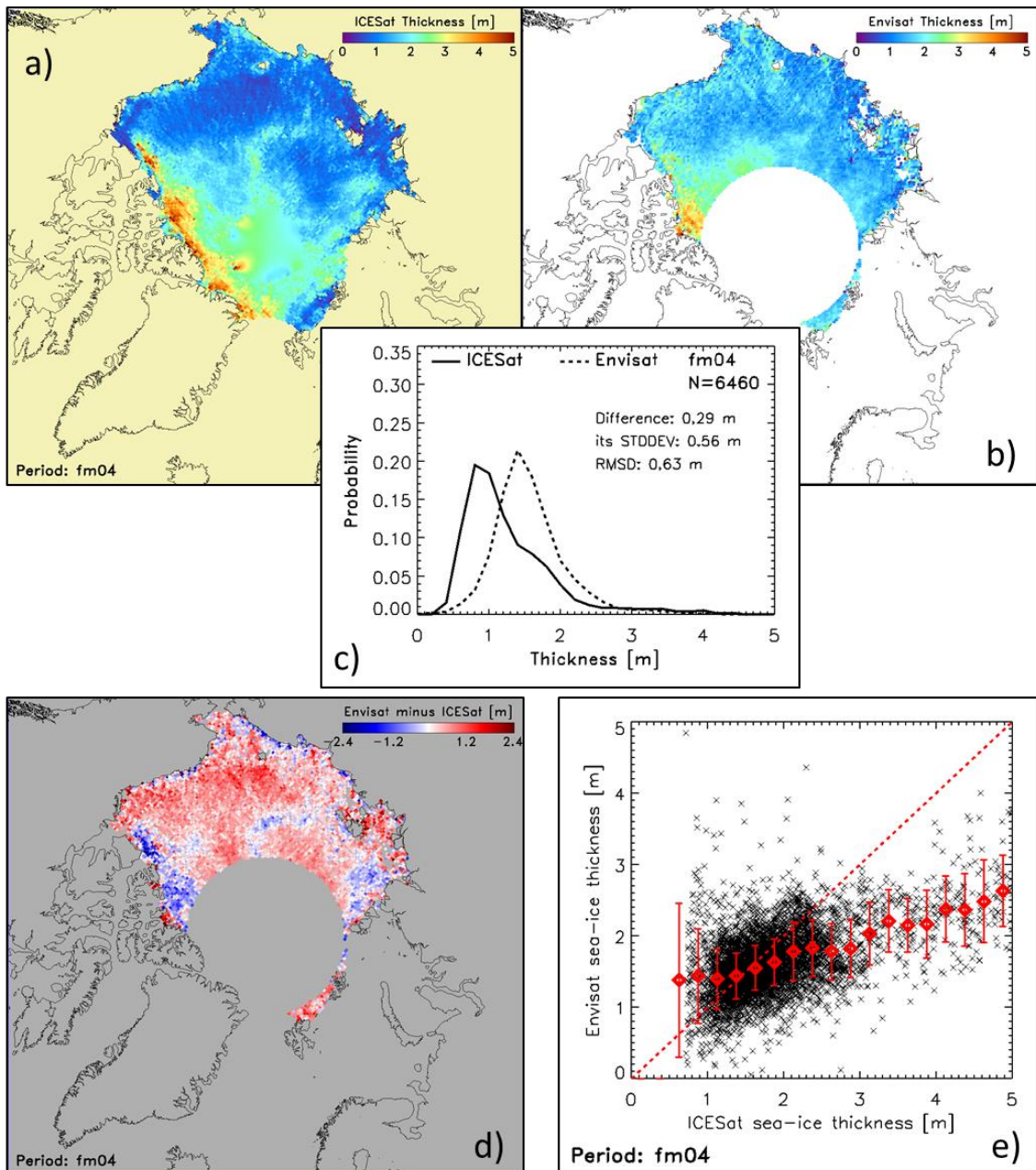


Figure 3-87: As Figure 3-86 but for ICESat measurement period FM04 (see Table 3-11).

For FM04 (Figure 3-87), the SIT distributions are similar and both noisy to the same degree; a substantial portion of the images a) and b) shows Envisat SIT larger than ICESat SIT which is illustrated well by the difference map (image d), which is mostly in red = Envisat > ICESat and only relatively few patches – possibly partly MYI – exhibit Envisat < ICESat (in blue). The shapes of the histograms (Figure 3-87 c) are much more similar than for the ON03 period (Figure 3-86 c) which is also expressed by a considerably smaller RMSD and standard deviation of the difference of ~ 0.6 m compared to ~ 0.8 m. The mean difference has shifted sign and is now positive at ~ 0.3 m, i.e. Envisat is overestimating ICESat. The scatterplot (Figure 3-87 e) reveals improved agreement between Envisat and NSIDC ICESat SIT but still the slope of a linear regression through the 0.2m bin averaged SIT would be only about 0.5 (not shown).

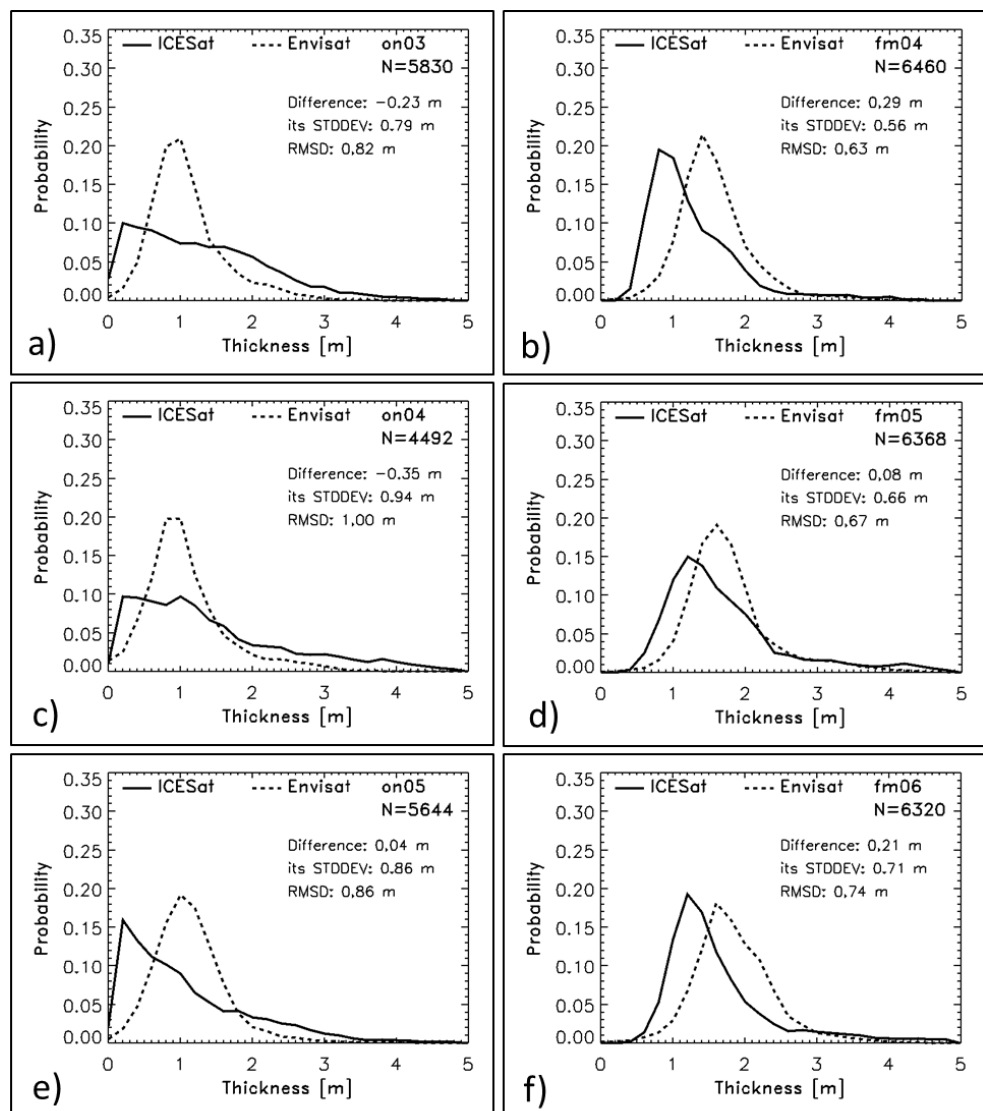


Figure 3-88: Histograms of the NSIDC ICESat SIT and the SICCI-2 Envisat SIT for the Arctic Ocean for late fall (ON periods, left column) and winter (FM periods, right column) for winters 2003/04 through 2005/06. In each image the number of valid data pairs, the mean difference Envisat minus ICESat SIT and its standard deviation and the RMSD is given (see also Table 3-13).

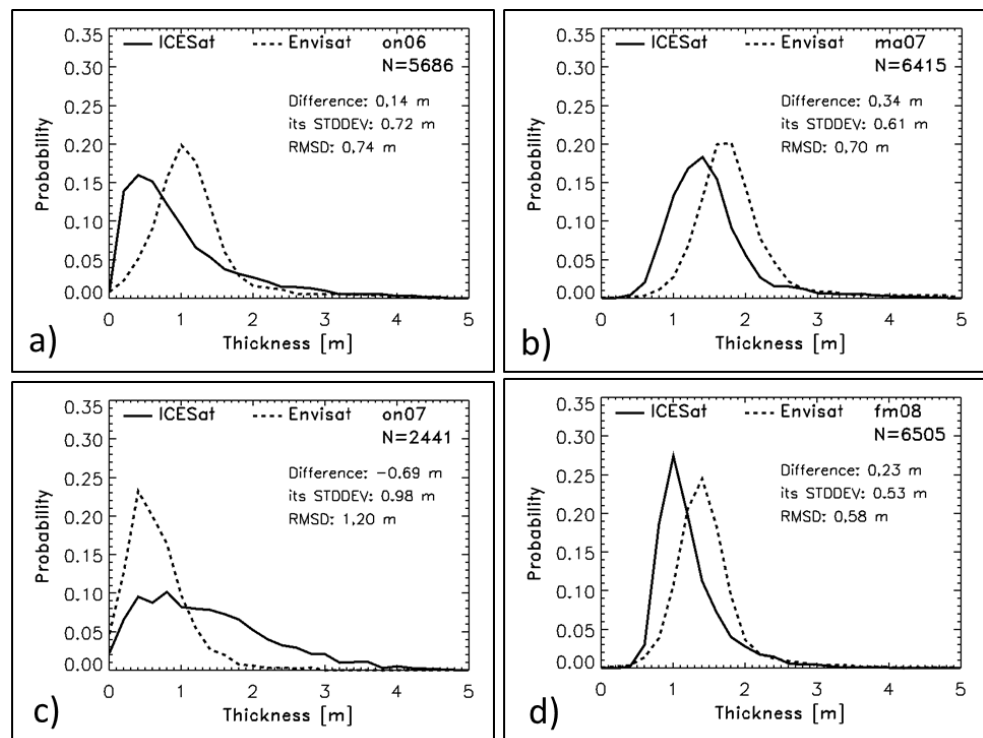


Figure 3-88 continued for winters 2006/07 and 2007/08.

Figure 3-88 presents the histograms of the two co-located SIT values for all ICESat measurement periods – ON (left column) and FM (right column). We find that common to the ON periods are i) a very low modal SIT in the NSIDC ICESat SIT and ii) a long tail towards thicker SIT values while SICCI-2 Envisat SIT has a comparably small tail towards thick SIT and a much more pronounced modal SIT value than NSIDC ICESat SIT. For FM periods, we find a much better agreement between the histograms in shape and also in the position of the modal value. Without exception both the mean and the modal SIT value are higher for Envisat than the NSIDC ICESat data set. We find a considerable reduction of the standard deviation of the mean and of the RMSD between ON- and FM-periods. We refer to Table 3-13 for a summary of the results.

That histograms only provide half of the story could be guessed by the scatterplots shown as image e) of Figure 3-86 and Figure 3-87. In Figure 3-89 we show the corresponding scatterplots for all ICESat measurement periods. The first impression we obtained from Figure 3-86 e) and Figure 3-87 e) is confirmed here. SICCI-2 Envisat SIT overestimates NSIDC ICESat SIT for SIT values about below ~ 1 m and underestimates it above that threshold for ON-periods. For FM-periods, the overestimation of NSIDC ICESat SIT by SICCI-2 Envisat SIT extends to up to 1.5 m to 2 m. Actually there is a data point cloud which does not allow any conclusion about agreement, e.g. FM06 (Figure 3-89 f) and MA07 (Figure 3-89 cont. b). The agreement between the two SIT data sets improves for SIT values $> \sim 2$ m. See our discussion about the results using only MYI further down.

The difference maps shown in Figure 3-90 finally illustrate how the differences (or regions of over- or underestimation) distribute across the Arctic Ocean.

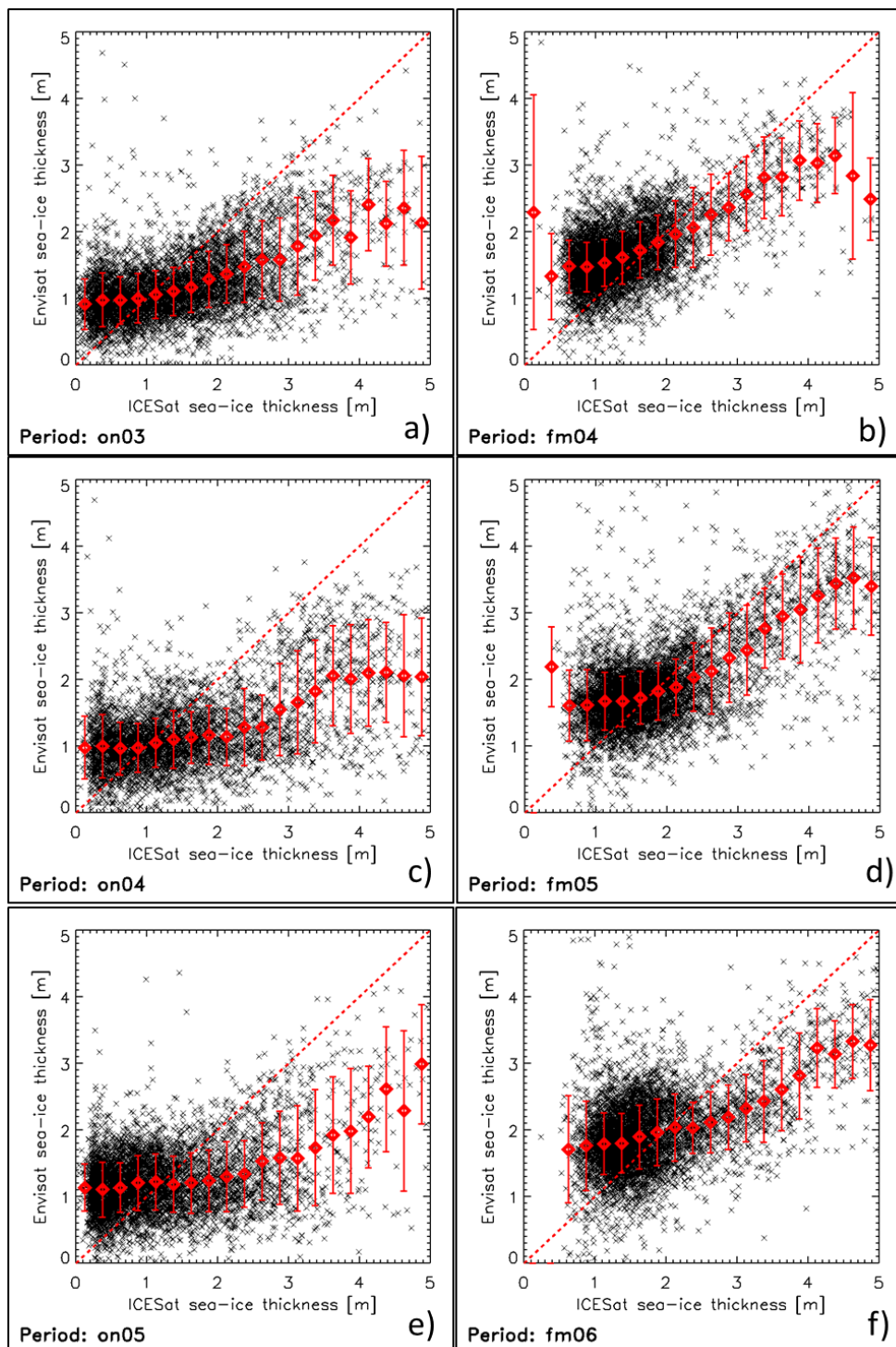


Figure 3-89: Scatterplot of individual data pairs SICCI-2 Envisat versus NSIDC ICESat SIT (black crosses) and mean Envisat SIT values derived for 0.2 m wide ICESat SIT bins starting with 0.0 m to 0.2 m (red diamonds). Error bars denote one standard deviation; the dashed red line denotes a 1-to-1 fit line. Like in Figure 3-88, the left (right) column is for ON (FM) periods for winters 2003/04 through 2005/06.

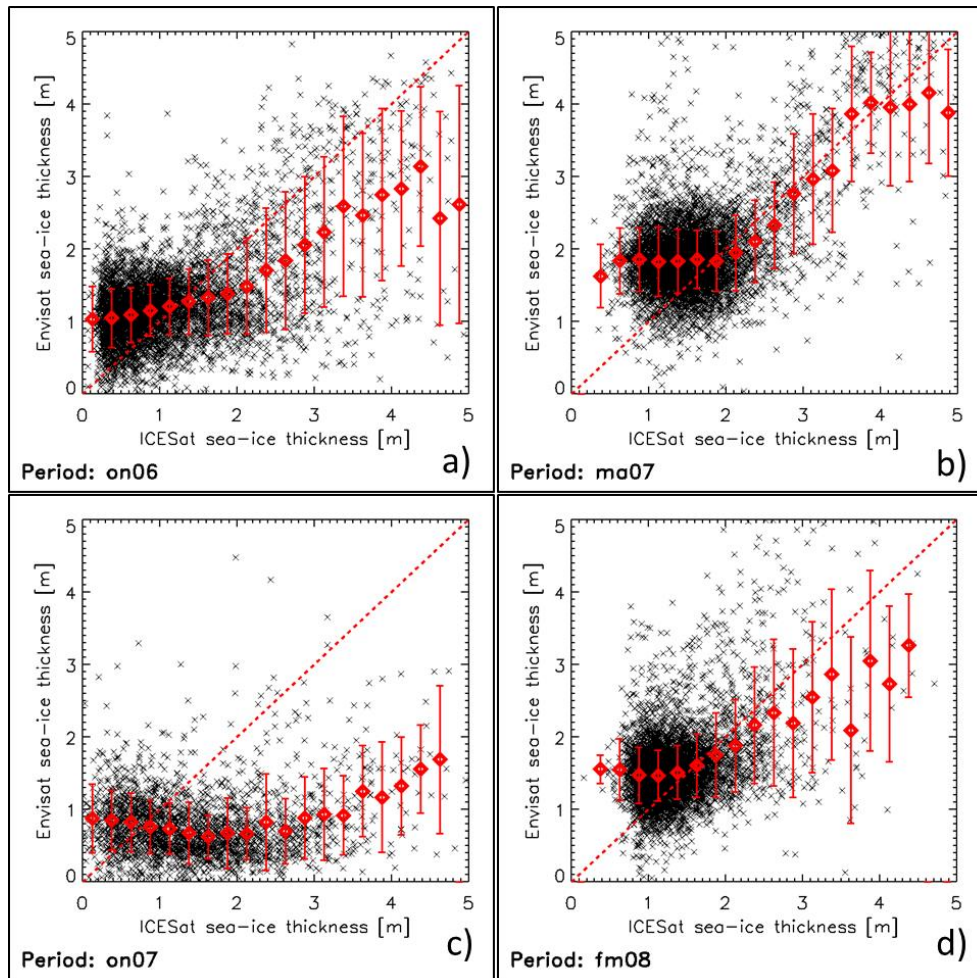


Figure 3-89 continued for winters 2006/07 and 2007/08.

Table 3-13: Per period mean SICCI-2 Envisat SIT, NSIDC ICESat SIT, the difference Envisat minus ICESat, the RMSD, the linear correlation, and the count N of collocated data pairs. Bold numbers at the end provide the averages over all ON, all FM, and all ON and FM values. Standard deviations 1σ given at the end are the averages of the respective values of the previous rows.

Period	$SIT_{ENV} \pm 1\sigma$	$SIT_{ICE} \pm 1\sigma$	$SIT_{DIFF} \pm 1\sigma$	RMSD	Corr	N
ON03	1.20±0.52	1.42±0.94	-0.23±0.79	0.82	0.53	5830
FM04	1.67±0.51	1.39±0.67	0.29±0.56	0.63	0.58	6460
ON04	1.18±0.58	1.53±1.08	-0.35±0.94	1.00	0.50	4492
FM05	1.89±0.63	1.81±0.83	0.08±0.66	0.67	0.62	6368
ON05	1.23±0.50	1.20±0.89	0.04±0.86	0.86	0.34	5644
FM06	1.95±0.57	1.74±0.77	0.21±0.71	0.74	0.47	6320
ON06	1.26±0.62	1.12±0.83	0.14±0.72	0.74	0.53	5686
MA07	1.94±0.61	1.61±0.61	0.34±0.61	0.70	0.50	6415
ON07	0.77±0.46	1.46±0.91	-0.69±0.98	1.20	0.08	2441
FM08	1.56±0.49	1.33±0.47	0.23±0.53	0.58	0.38	6505
ONs	1.13±0.54	1.35±0.93	-0.22±0.86	0.92	0.40	
FMs	1.80±0.56	1.58±0.67	0.23±0.61	0.67	0.51	
All	1.47±0.55	1.46±0.80	0.01±0.73	0.80	0.45	

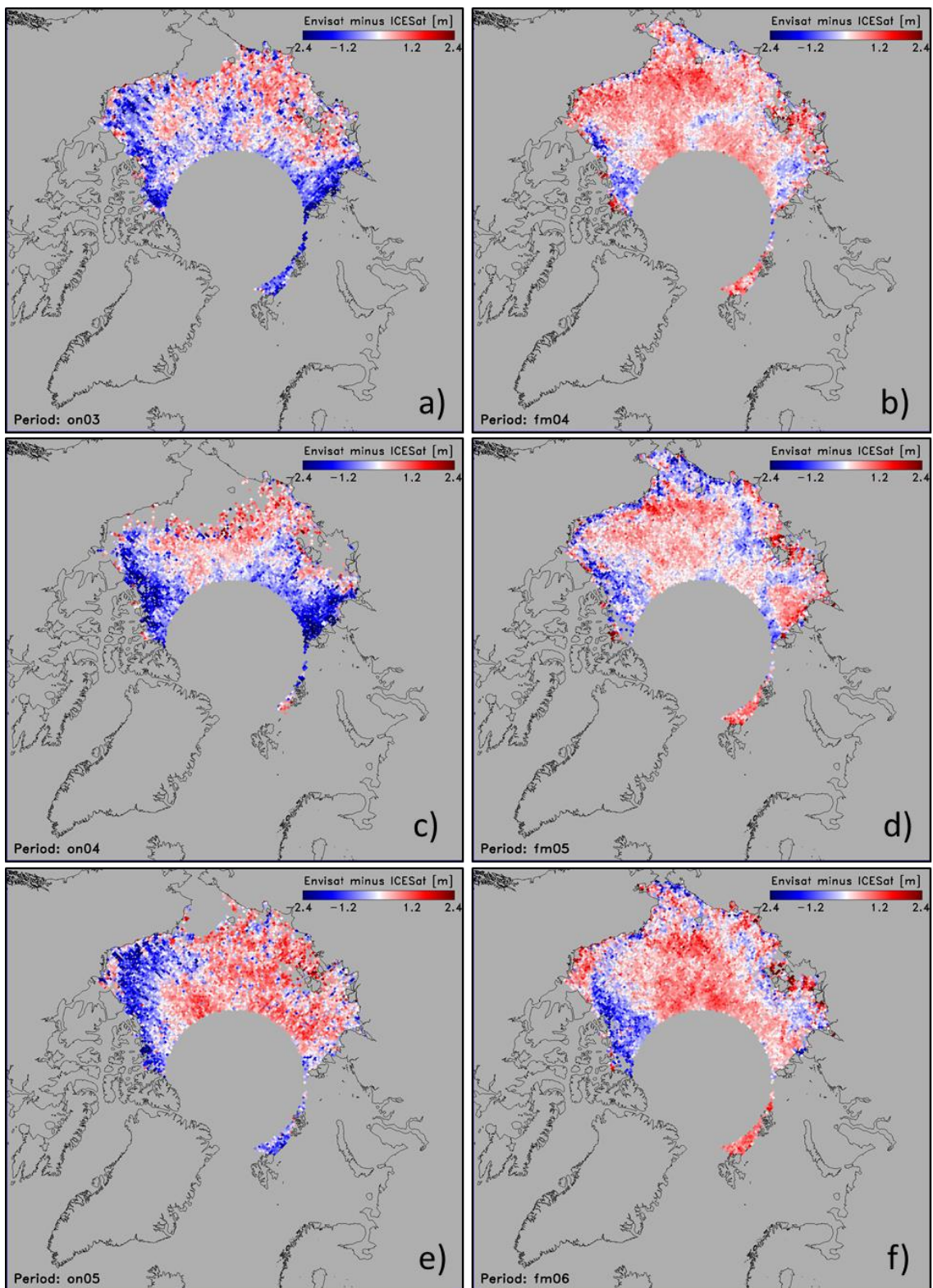


Figure 3-90: Distribution of the difference SICCI-2 Envisat minus NSIDC ICESat SIT for ON periods (left) and FM periods (right) for winters 2003/04 through 2005/06 (from top to bottom).

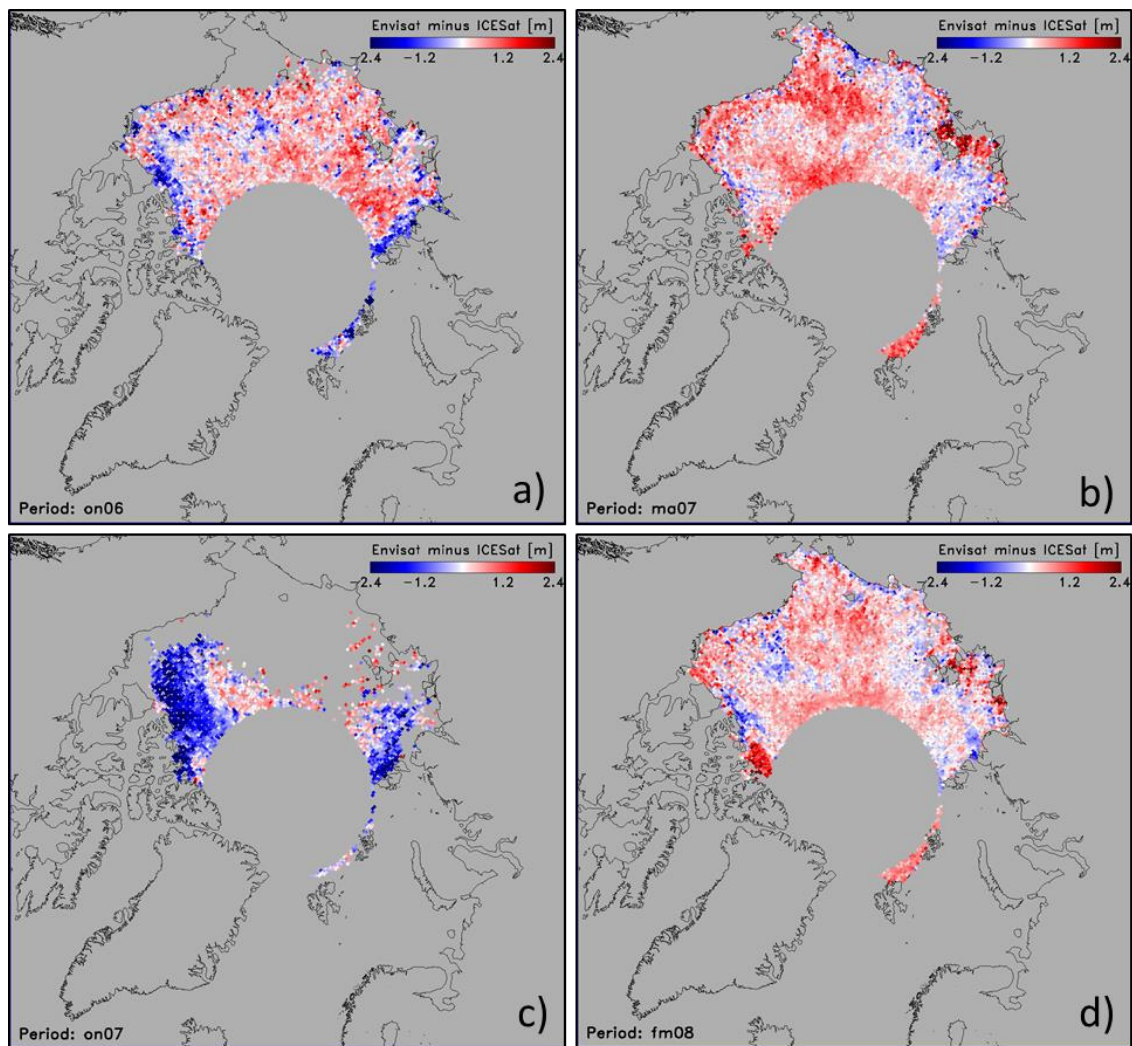


Figure 3-90 continued for winters 2006/07 and 2007/08.

We find a larger fraction of negative differences, i.e. SICCI-2 Envisat SIT < NSIDC ICESat SIT during the ON-periods than during the FM-periods (Figure 3-90, compare left and right column). We state that the majority of the differences is not small but has absolute values above 0.5 m. Maximum absolute differences between the two SIT data sets reach or even exceed 2 m during ON-periods and remain a bit smaller during FM-periods.

“Hot spots” for negative differences, i.e. SICCI-2 Envisat SIT < NSIDC ICESat SIT are MYI areas north of the Canadian Arctic Archipelago as well as northeast of Severnaya Zemlya. Particularly during FM-periods we also observed a band of negative differences along the Eurasian Shelf. We find wide-spread positive differences, i.e. SICCI-2 Envisat SIT > NSIDC ICESat SIT in the Chukchi Sea and north of it for most FM-periods. Another area of pronounced positive differences is the southern Laptev Sea.

Overall, i.e. averaged over the entire Arctic Ocean and all 10 ICESat measurement periods, the mean difference SICCI-2 Envisat minus NSIDC ICESat SIT is ~ 0.01 m. The mean difference for ON-periods is -0.22 m, i.e. NSIDC ICESat SIT over-estimates SICCI-2 Envisat SIT. This is almost perfectly balanced by a difference of $+0.23$ m for FM-periods, i.e. NSIDC ICESat SIT under-estimates SICCI-2 Envisat SIT (Table 3-13); the

difference between the two SIT data sets changes by 0.45 m from ON- to FM-periods. The overall correlation increases from 0.4 to ~ 0.5 between ON- and FM-periods. The overall RMSD and standard deviation of the SIT difference decreases from ~ 0.9 m (ON-periods) to ~ 0.65 m (FM-periods).

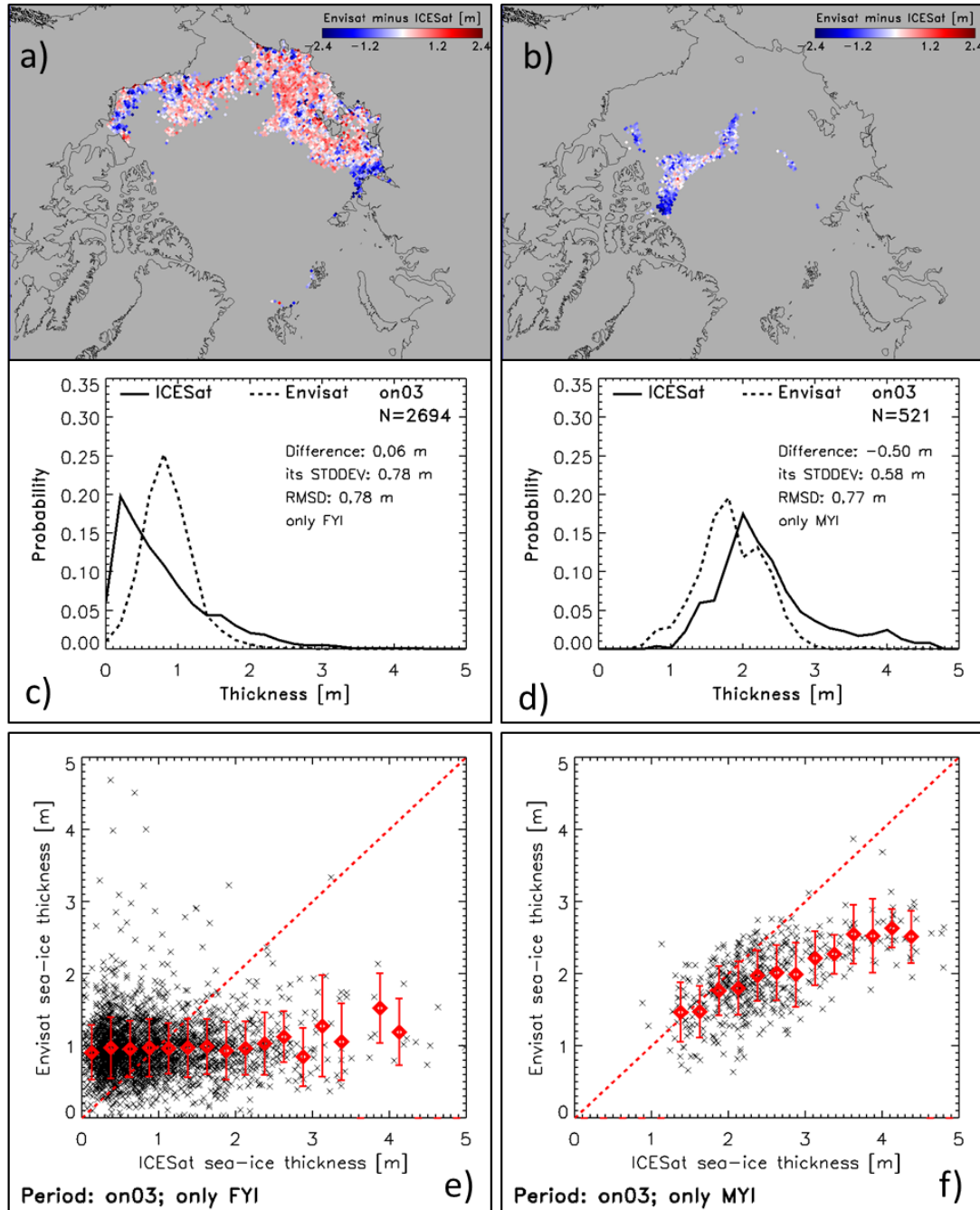


Figure 3-91: Comparison of SICCI-2 Envisat SIT and NSIDC ICESat SIT for grid cells with FYI concentration > 85% (left column) and MYI concentration > 85% (right column) for ON03. Difference SICCI-2 Envisat SIT minus NSIDC ICESat SIT for a) > 85% FYI and b) > 85% MYI; histograms (c,d) and scatterplots (e,f) of the respective sub-sets of the data sets (compare Figure 3-88 and Figure 3-89).

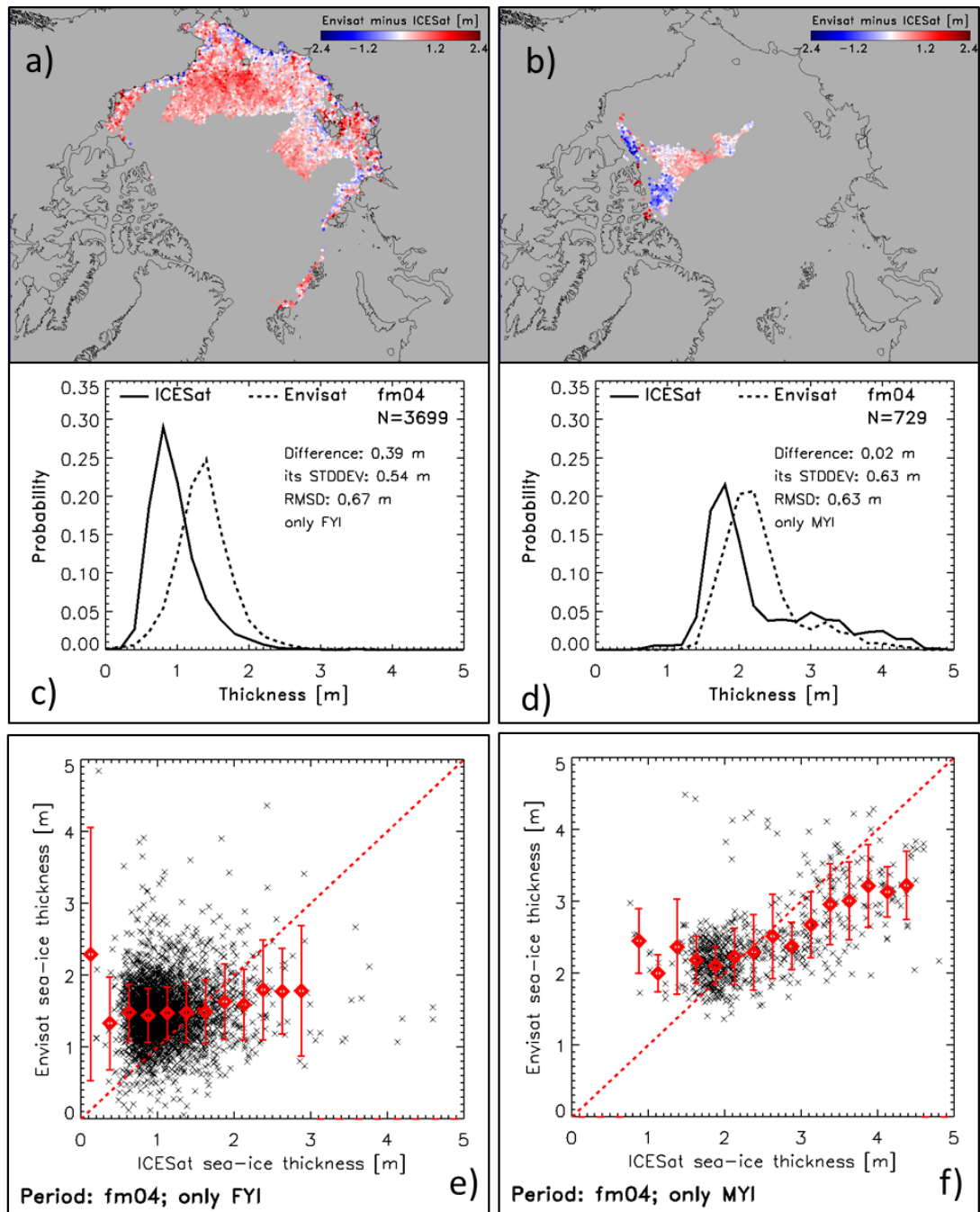


Figure 3-92: As Figure 3-91 but for FM04.

In the following we repeat the analysis constraining the data pairs to either > 85% MYI or > 85% FYI. Figure 3-91 and Figure 3-92 illustrate how the results of the inter-comparison of the two datasets change.

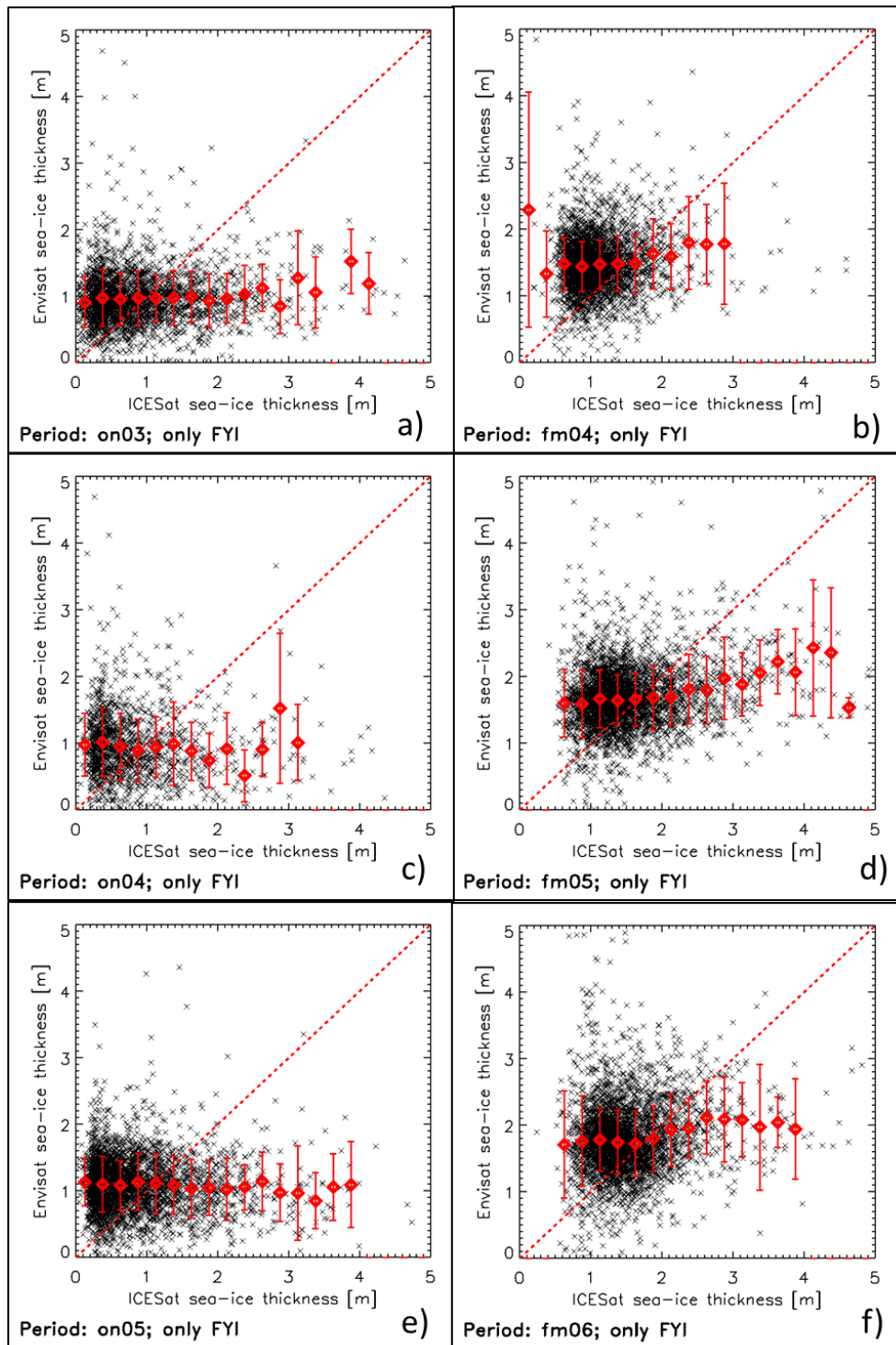


Figure 3-93: As Figure 3-93 but for > 85% FYI concentration.

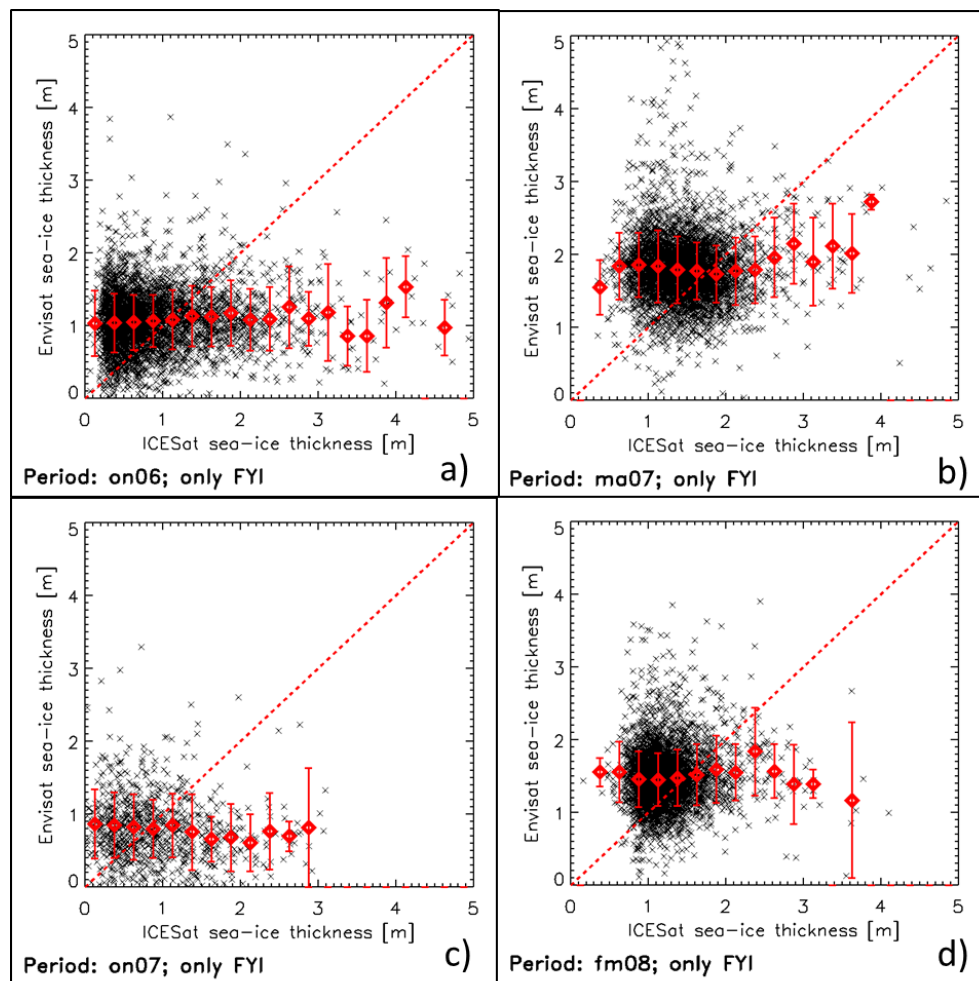


Figure 3-93 continued for winters 2006/07 and 2007/08.

We find that the agreement between SICCI-2 Envisat SIT and NSIDC ICESat SIT is quite poor for FYI, while for MYI the agreement is substantially better. For MYI, the difference between the two datasets is predominantly negative (Figure 3-91 b) and reasonable agreement is only achieved in the SIT range between 1.5 m and 2.5 m (Figure 3-91 f). For FM04, the agreement is reasonable for the SIT range between 1.5 m and 4.0 m – still with a tendency of SICCI-2 Envisat SIT to underestimate NSIDC ICESat SIT at higher SIT values (Figure 3-92 f); see Figure 3.6.9 for the other periods. We note that for MYI the SIT values are within the expected range.

This does not apply for FYI. Both data sets reveal SIT > 1.5 m (> 2.0 m) for a substantial fraction of the co-located grid cells for ON03 (Figure 3-91 c) (FM04 (Figure 3-92 c)), hence pointing to a substantial overestimation of the actual FYI thickness; see also Figure 3-93. There is no relationship between SICCI-2 Envisat SIT and NSIDC ICESat SIT in the scatterplots (Figure 3-91 e), Figure 3-92 e), and Figure 3-93) – except that SICCI-2 Envisat SIT is quasi-constant for the entire NSIDC ICESat SIT range for FYI.

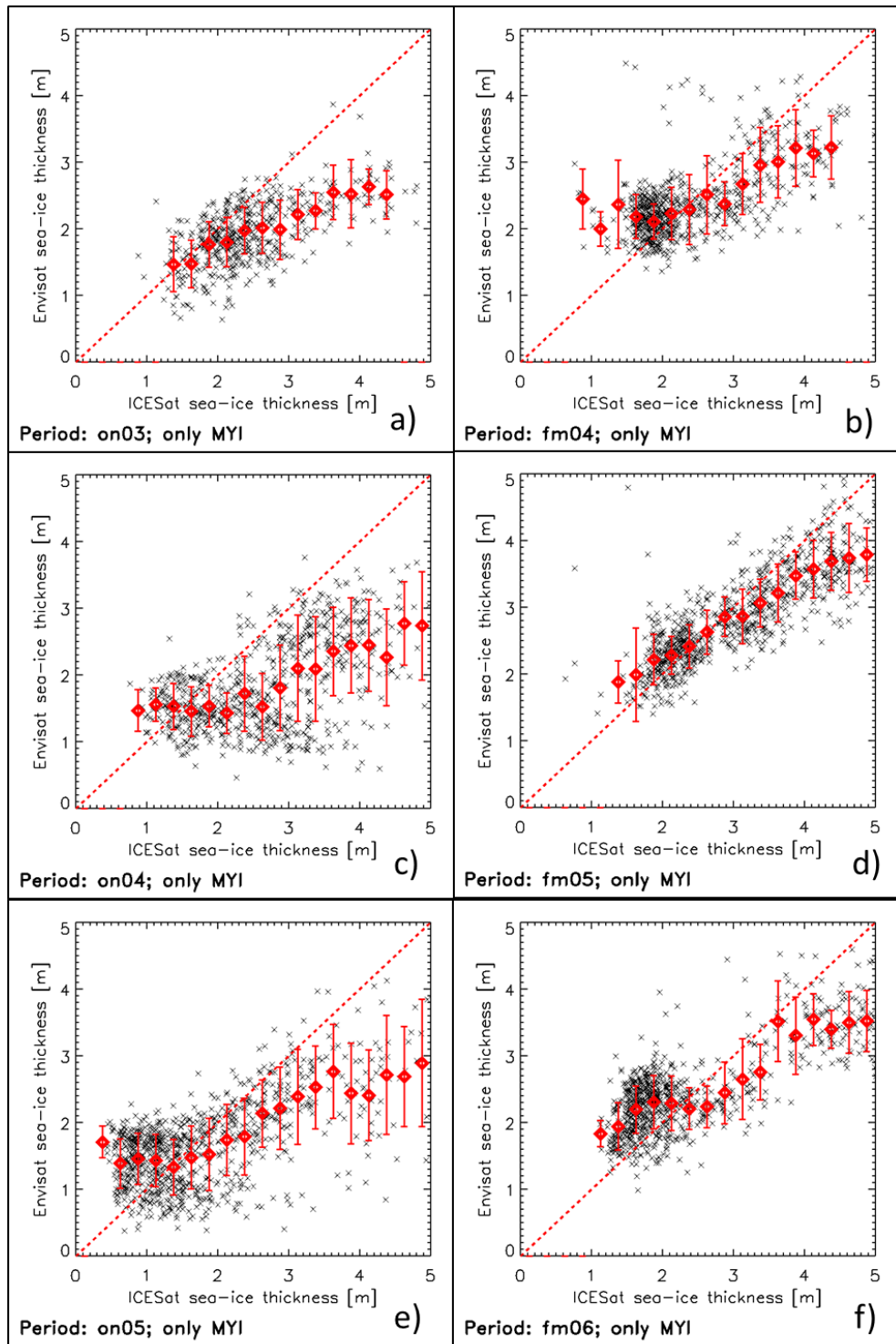


Figure 3-94: As Figure 3-89 but for > 85% MYI concentration.

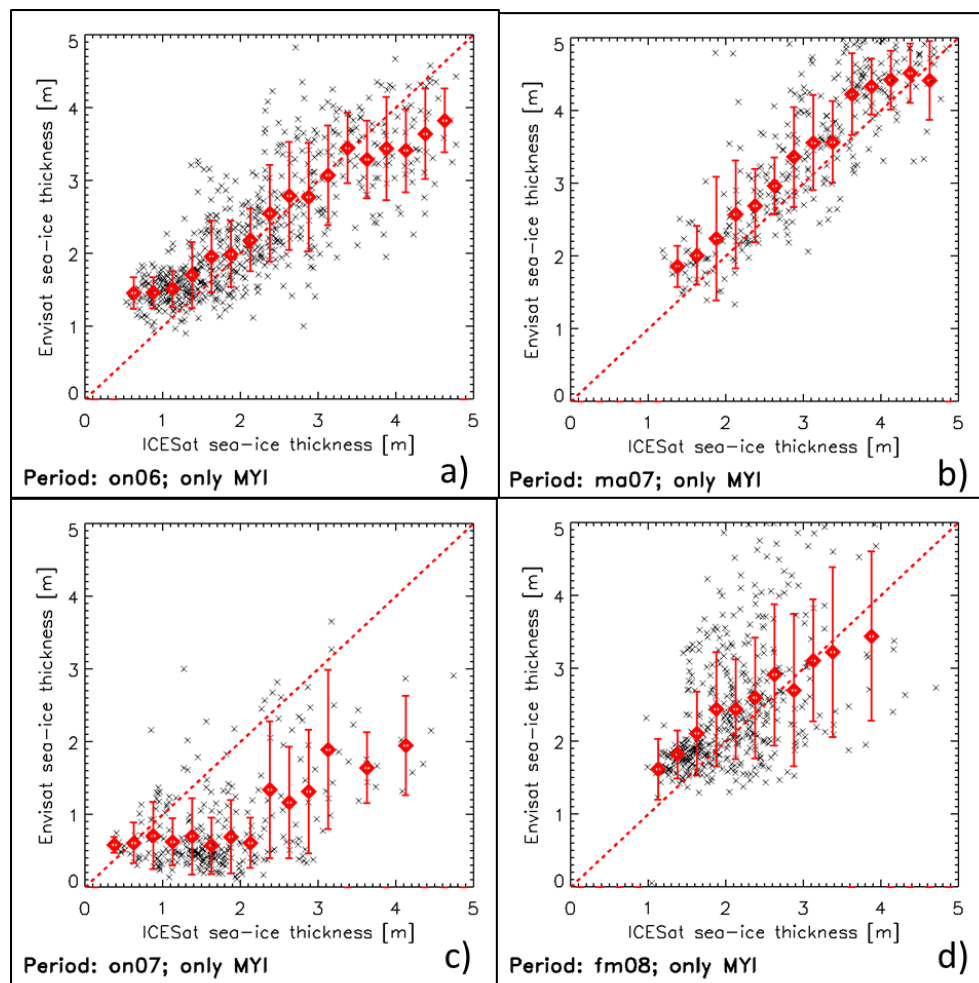


Figure 3-94 continued for winters 2006/07 and 2007/08.

Table 3-14: Same as Table 3-13 but for > 85% FYI concentration.

Period	SIT _{ENV} ±1σ	SIT _{ICE} ±1σ	SIT _{DIFF} ±1σ	RMSD	Corr	N
ON03	0.97±0.40	0.91±0.69	0.06±0.78	0.78	0.06	2694
FM04	1.48±0.41	1.09±0.40	0.39±0.54	0.67	0.09	3699
ON04	0.96±0.51	0.79±0.63	0.17±0.83	0.85	-0.06	1443
FM05	1.68±0.46	1.52±0.61	0.16±0.69	0.71	0.18	3906
ON05	1.10±0.41	0.84±0.65	0.25±0.79	0.83	-0.05	3504
FM06	1.79±0.52	1.49±0.51	0.30±0.68	0.75	0.12	4006
ON06	1.07±0.40	0.90±0.64	0.17±0.73	0.75	0.08	4107
MA07	1.80±0.45	1.47±0.45	0.34±0.64	0.72	-0.01	4710
ON07	0.81±0.45	0.89±0.59	-0.09±0.78	0.78	-0.10	875
FM08	1.48±0.39	1.21±0.35	0.27±0.51	0.57	0.06	4695
ONs	0.98±0.43	0.87±0.64	0.12±0.78	0.80	-0.02	
FMs	1.65±0.45	1.36±0.46	0.29±0.61	0.68	0.09	
All	1.31±0.44	1.11±0.55	0.20±0.70	0.74	0.03	

Table 3-15: Same as Table 3-13 but for > 85% MYI concentration.

Period	SIT _{ENV} ±1σ	SIT _{ICE} ±1σ	SIT _{DIFF} ±1σ	RMSD	Corr	N
ON03	1.93±0.46	2.44±0.72	-0.50±0.58	0.77	0.59	521
FM04	2.39±0.54	2.37±0.79	0.02±0.63	0.63	0.61	729
ON04	1.84±0.67	2.63±0.94	-0.80±0.83	1.15	0.51	696
FM05	2.83±0.67	2.97±0.93	-0.15±0.54	0.56	0.82	800
ON05	1.68±0.64	1.77±1.00	-0.09±0.80	0.81	0.59	900
FM06	2.42±0.61	2.28±0.98	0.13±0.67	0.68	0.74	820
ON06	2.30±0.87	2.17±1.02	0.13±0.61	0.63	0.80	655
MA07	3.41±0.99	3.04±0.88	0.37±0.56	0.68	0.82	324
ON07	0.85±0.66	1.78±0.80	-0.93±0.74	1.19	0.50	293
FM08	2.40±0.83	2.08±0.62	0.32±0.77	0.83	0.46	475
ONs	1.72±0.73	2.16±0.66	-0.44±0.71	0.91	0.60	
FMs	2.69±0.73	2.55±0.84	0.14±0.63	0.68	0.68	
All	2.21±0.70	2.35±0.87	-0.15±0.67	0.80	0.65	

The summary of the results for the comparison of SICCI-2 Envisat SIT and NSIDC ICESat SIT, constrained to FYI or MYI, compiled in Table 3-14 and Table 3-15, reveals:

- Poor correlation between the two data sets for FYI regions
- Reasonable correlation between the two data sets for MYI regions
- Increase in the overall period-mean SIT difference for FYI regions but decrease for MYI regions
- An overall over- (under-) estimation of NSIDC ICESat SIT by the SICCI-2 Envisat data set by 0.2 m (-0.15 m) with an over-estimation of FYI SIT in both periods and a switch from under- to over-estimation of MYI SIT from ON- to FM-periods.
- A slightly smaller (realistic) ice growth between ON- and FM-periods for FYI than MYI (0.5 m versus 0.4 m) for NSIDC ICESat SIT (Table 3-14) but an unrealistic magnitude in ice growth between ON- and FM-periods for MYI: almost 1.0 m compared to 0.7 m for FYI, for SICCI-2 Envisat SIT (Table 3-15).
- A moderate range of SIT differences for FYI: -0.09 m to +0.25 m for ON-periods and +0.16 m to +0.39 m for FM-periods (Table 3-14)
- A large range of SIT differences for MYI, particularly for the ON-periods: -0.93 m to +0.13 m for ON-periods and -0.15 m to +0.37 m for FM-periods (Table 3-15).

The large SIT differences observed for MYI regions could be caused by a local bias in the MYI concentration data set used. Figure 3-95 illustrates ICESat and Envisat SIT of periods ON04 and ON07, i.e. those periods with the largest SIT difference for MYI regions (Table 3-15). The areas encircled by the black circle are the regions of concern. We can observe quite thick sea ice in these regions in the ICESat data – particularly for period ON04. In this area, during ON04, Envisat SIT is large compared to outside of the circle; this is good news. But for ON07, both large and low SIT compared to the outside of the circle is observed. Apparently, and this is where the red arrow points to, even though MYI concentrations in these areas should be close to 100%, the > 85% MYI SIT maps shown in the bottom row of Figure 3-95 have data gaps here, indicating that the MYI concentration is < 85% here. It is likely that this had an impact on the retrieved SIT.

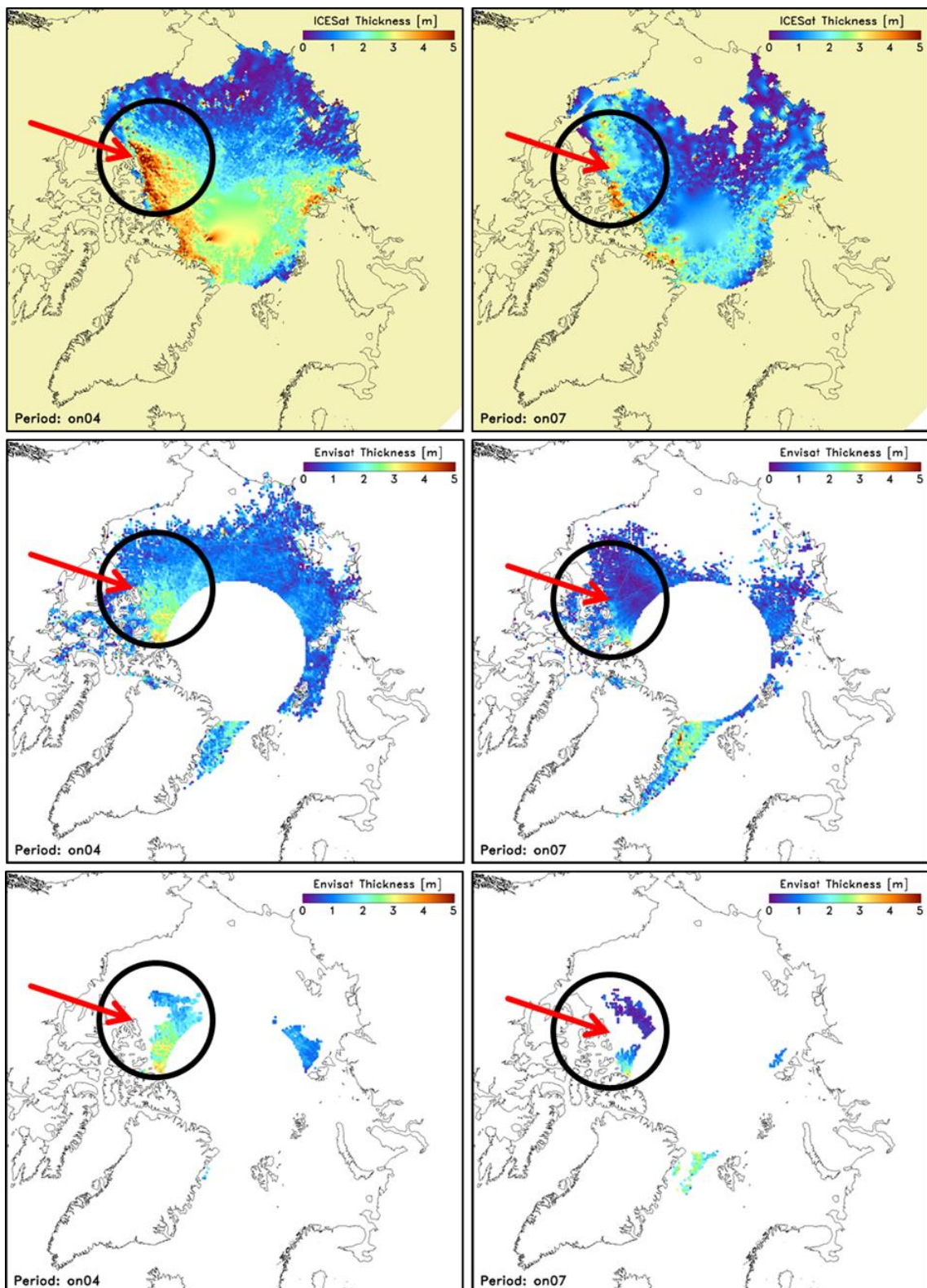


Figure 3-95: Top: NSIDC ICESat SIT for periods ON04 and ON07; middle: SICCI-2 Envisat SIT for these periods; bottom: SICCI-2 Envisat SIT for grid cells with > 85% MYI concentration. See text for black circles and red arrows.

Part II: Comparison to the ICESat SIT product from JPL

The SICCI-2 sea-ice thickness (SIT) data set v09 has been compared with the ICESat SIT data set for the Arctic available from Ron Kwok, JPL, via https://rkwok.jpl.nasa.gov/icesat/register_form.html.

The main differences between this ICESat data set and the NSIDC data set are a slightly different freeboard retrieval and, more importantly, a different snow-depth parameterization as described in Kwok and Cunningham [RD-28]. In the JPL ICESat SIT data set snow depth is parameterized via accumulation of snow on sea ice taken from ECMWF model data, taking information of sea-ice drift into account and accumulating snow only on sea ice of at least 50% sea-ice concentration. In addition, in order to avoid negative sea-ice freeboard and to take into account the varying fractions of leads, the snow depth is scaled with the ratio between the measured freeboard and the constructed snow depth; this approach is similar to but more mature than the approach used in the NSIDC ICESat sea-ice thickness data set ([RD-28]).

All elements of this inter-comparison, i.e. co-location, selection of multiyear ice (MYI) and first-year ice (FYI) areas, etc. are carried out the same way as was done for the comparison with the NSIDC ICESat sea-ice thickness product.

Figure 3-96 and Figure 3-97 illustrate the differences in the sea-ice thickness (SIT) distribution between JPL ICESat and SICCI-2 Envisat for ICESat measurement periods ON03 and FM04, respectively. These figures are similar to Figure 3-86 and Figure 3-87. Note that we kept the color legend of the SIT maps at the top as well as the SIT range in the histograms and the scatterplot the same in order to ease the inter-comparison with those figures. We changed the color legend of the difference Envisat minus ICESat (bottom left) from an absolute difference of 2.4 m to an absolute difference of 4.0 m because maximum differences are considerably larger.

Figure 3-96 and Figure 3-97 reveal relatively small difference over much of the sea-ice cover (image d) but illustrate at the same time that SICCI-2 Envisat SIT underestimates JPL ICESat SIT substantially, by 2 m or more, in the area north of the Canadian Arctic Archipelago (images d,e). For ON03 (Figure 3-96 c) the histogram suggest a better agreement between the two data sets than for NSIDC ICESat SIT (Figure 3-86 c) and also for FM04 the agreement looks almost perfect (Figure 3-97 c). But the scatterplots again point out that – like found for NSIDC ICESat SIT (Figure 3-86 e) and Figure 3-87 e)) – SICCI-2 Envisat SIT underestimates ICESat SIT for thick sea ice (SIT > ~1.0 m) and overestimates it for thin sea ice – if present. We note, that in contrast to Figure 3-86 e) and Figure 3-87 e) the respective scatterplots in Figure 3-96 and Figure 3-97 do not show any ICESat SIT < 0.6 m.

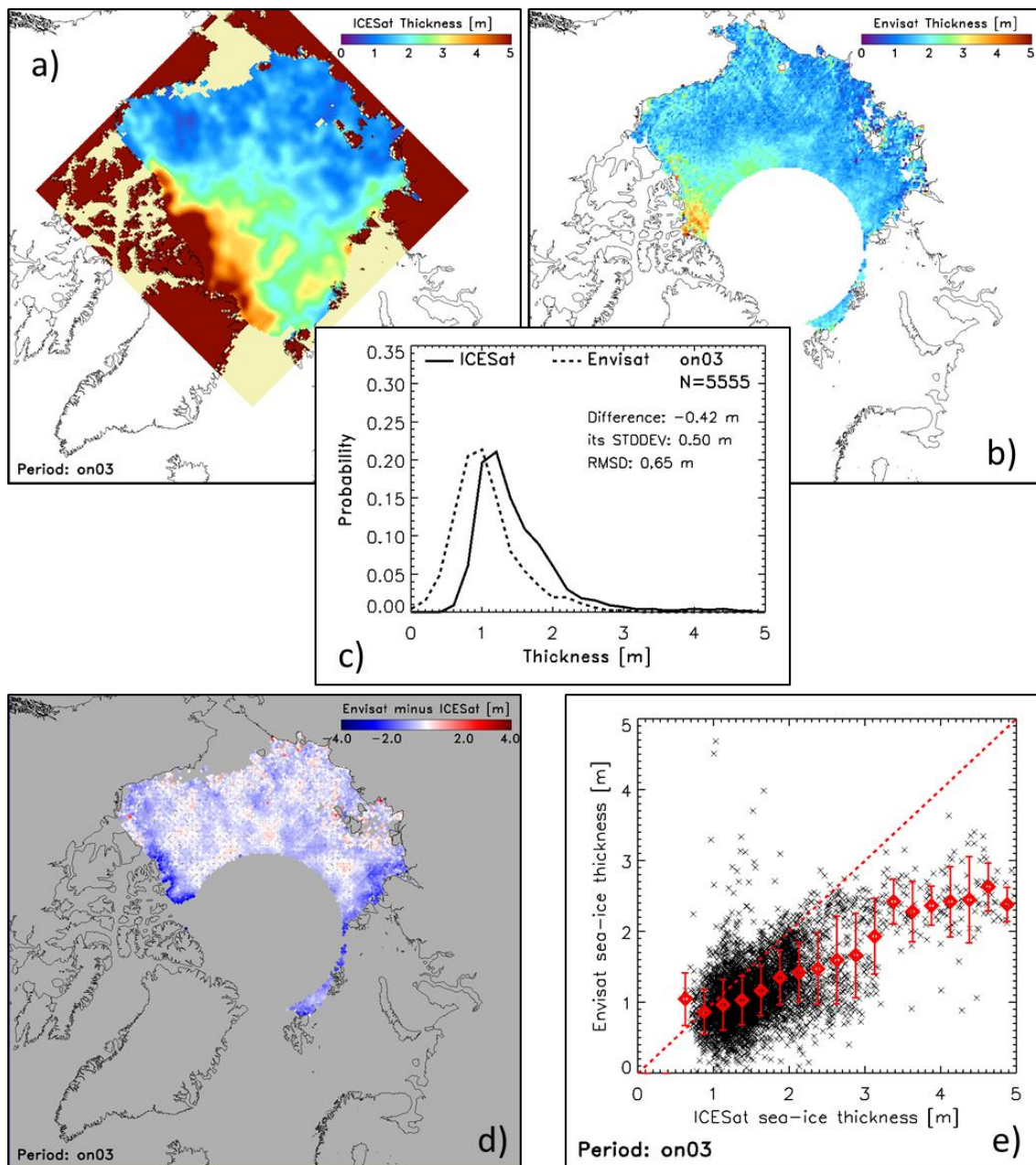


Figure 3-96: Inter-comparison of JPL ICESat versus SICCI-2 Envisat sea-ice thickness (SIT) for ICESat measurement period ON03 (see Table 3-11). a) ICESat SIT, note that SIT values are interpolated over the polar data gap; b) Envisat SIT, the white circular disk denotes the polar data gap; d) Difference Envisat minus ICESat SIT; c) histograms of the SIT from both sensors for coinciding grid cells together with the count of data pairs "N", the root mean squared difference "RMSD" as well as the mean difference and its standard deviation; e) scatterplot of all co-located SIT values (black crosses) superposed by the mean Envisat SIT per 0.2 m ICESat SIT bin. The error bars denote plus/minus one standard deviation. The red dashed line is the 1-to-1 fit line. Note the increase in range of the SIT difference from -2.4 m ... 2.4 m (Figure 3-86) to -4.0 m ... 4.0 m here.

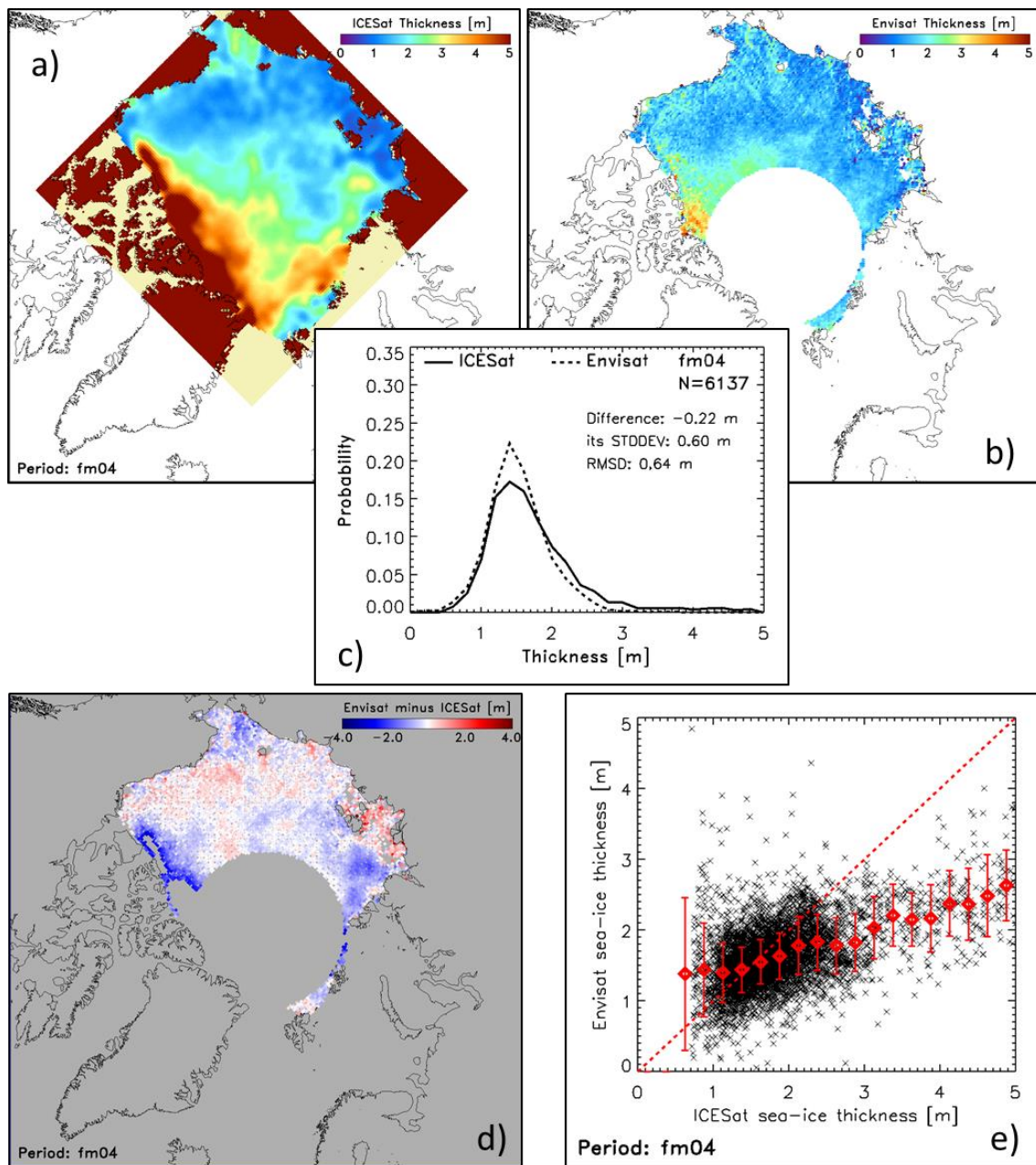


Figure 3-97: As Figure 3-96 but for ICESat measurement period FM04.

Before we look in detail at histograms and scatterplots of the kind shown in Figure 3-96 and Figure 3-97 for all ICESat periods (see Table 3-11) we show a comparison of the difference maps for ON- (Figure 3-98) and FM-periods (Figure 3-99).

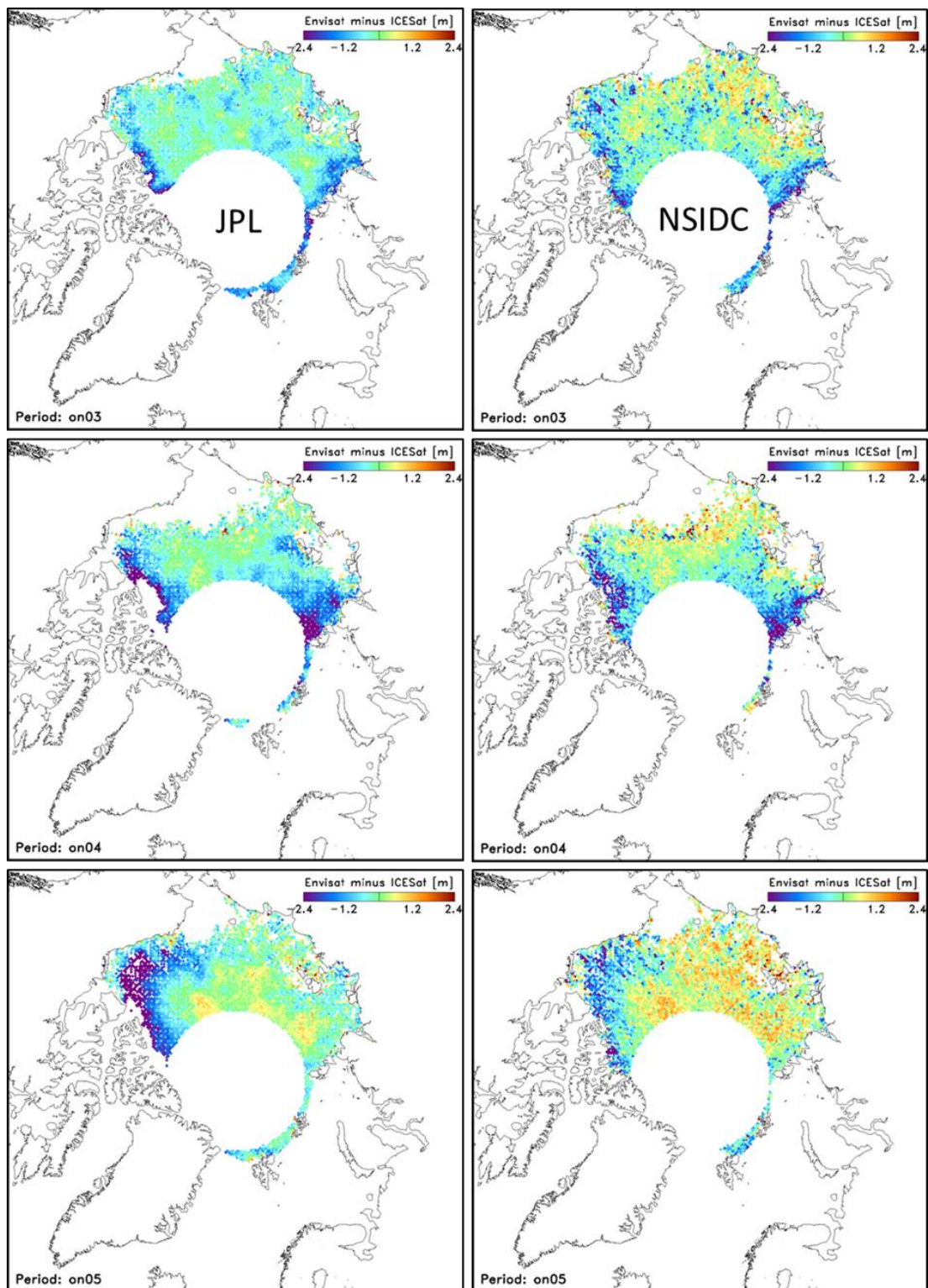


Figure 3-98: Maps of the SIT difference Envisat minus ICESat using the JPL product (left) and the NSIDC product (right) for periods ON03, ON04, and ON05.

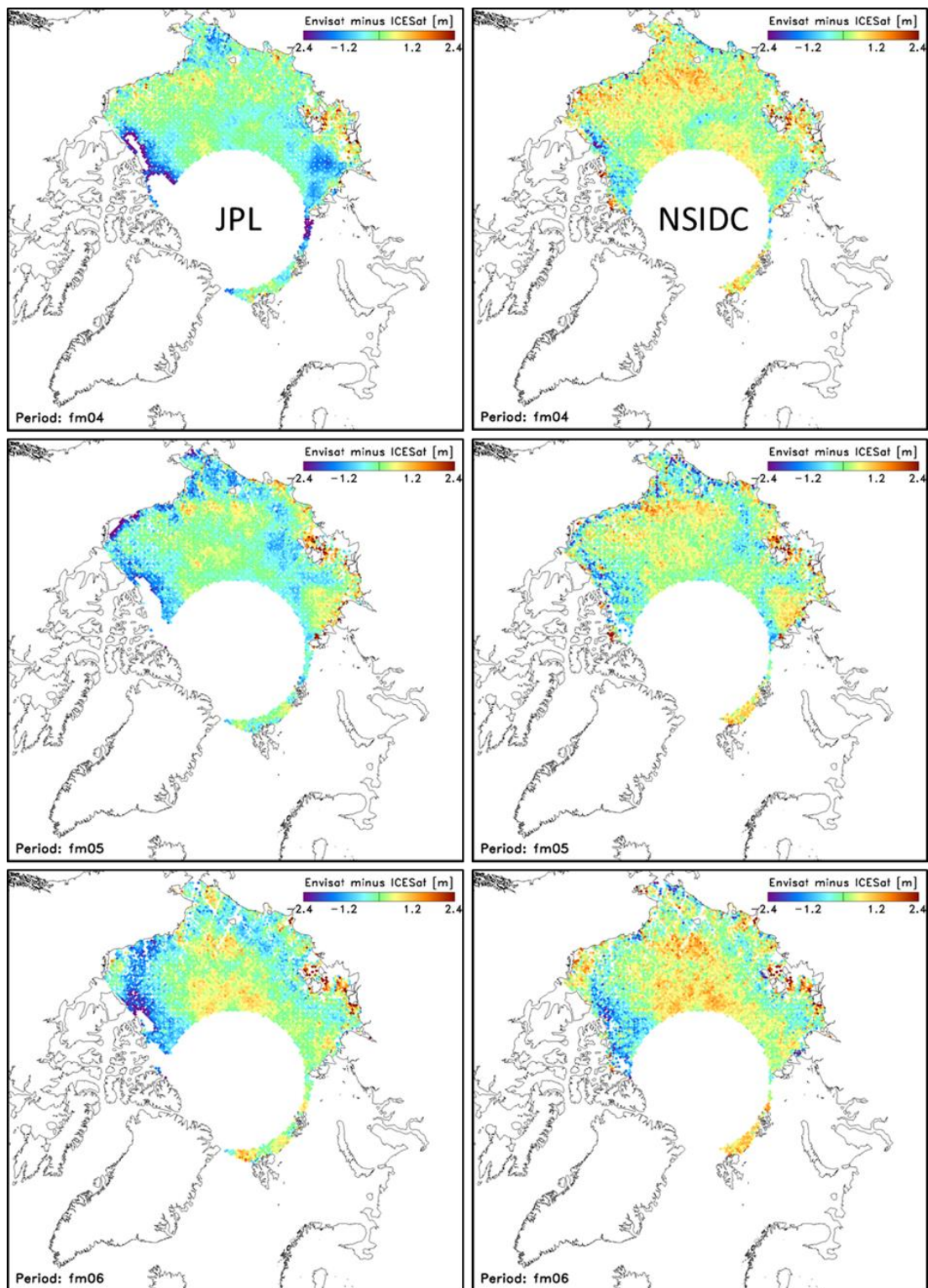


Figure 3-99: As Figure 3-98 but for periods FM04, FM05, and FM06.

The difference maps shown in Figure 3-98 and Figure 3-99 illustrate the different degree of smoothing in the ICESat products; clearly the JPL ICESat SIT product is smoother than the NSIDC ICESat SIT product which results in more scatter and noise in the difference maps involving the NSIDC product. The general spatial distribution of positive and negative SIT differences is

similar for both ICESat SIT products. Positive differences, i.e. SICCI-2 Envisat SIT > ICESat SIT, are more pronounced and more widespread when using the NSIDC ICESat SIT data. This applies in particular for ON-periods (Figure 3-98) but also for FM-periods (Figure 3-99).

The differences with the JPL ICESat SIT product seem to be greener and positive differences less often exceed 1.2 m (orange). At the same locations with negative differences, i.e. ICESat SIT exceeds SICCI-2 Envisat SIT, are more widespread in the JPL ICESat SIT difference maps. Also the maximum negative differences are larger. While NSIDC ICESat SIT difference maps show almost no grid cells with differences < -2.4 m there are substantial areas where JPL ICESat SIT difference maps show values < -2.4 m; these are the white patches north of the Canadian Arctic Archipelago – particularly pronounced in ON04 and ON05 as well as FM05 and FM06. Hence, in summary, difference maps between two different ICESat SIT data sets and SICCI-2 Envisat SIT show a similar spatial distribution of positive and negative differences but less pronounced positive than negative differences when comparing JPL and NSIDC SIT products. Overall biases between JPL ICESat SIT and SICCI-2 Envisat SIT can be expected to be more negative than for the NSIDC product. The overall bias for FYI can be expected to be less positive for JPL compared to NSIDC while the overall bias for MYI can be expected to be even more negative for JPL than for NSIDC.

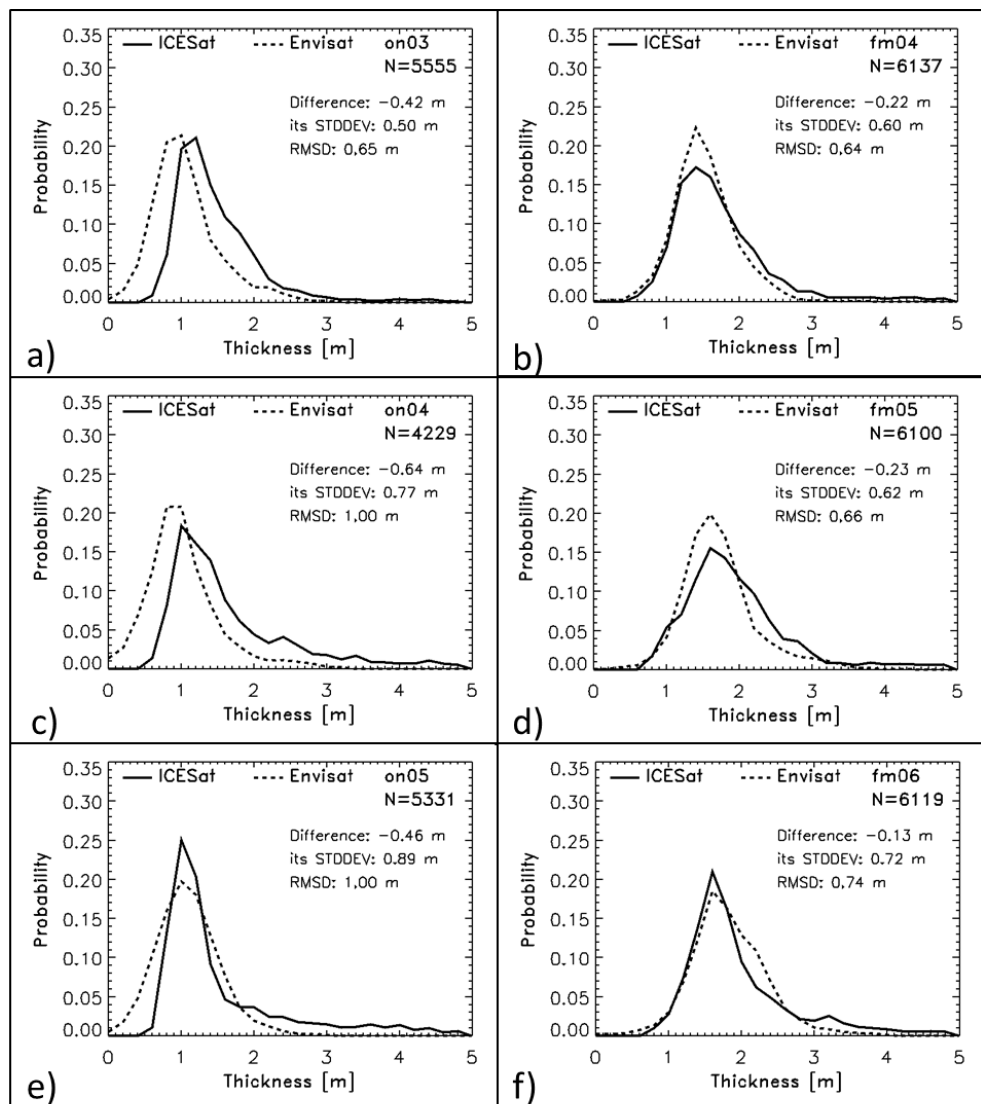


Figure 3-100: Histograms of JPL ICESat SIT and SICCI-2 Envisat SIT for the Arctic Ocean (compare Figure 3-88) for ON-periods (left column) and FM-periods (right column) for winters 2003/04 through 2005/06. In each image the count of valid data pairs "N", the mean difference Envisat minus ICESat SIT and its standard deviation and the root mean squared difference "RMSD" is given.

For FM-periods, histograms of co-located Arctic Ocean JPL ICESat and SICCI-2 Envisat SIT compare very well with similar modal SIT values, and similar distributions at the lower and upper end of the histograms (Figure 3-100, right column). There seems to be a slightly higher probability for SIT < 0.6 m in the Envisat data. For FM-periods the largest difference is found for FM08 where modal values agree but JPL ICESat SIT is shifted towards higher SIT values with a steeper increase left of the mode and a slower decrease right of the mode (Figure 3-100 continued d).

For ON-periods, the agreement between JPL ICESat and SICCI-2 Envisat SIT is less good; JPL ICESat SIT has more thick ice and less thin ice than Envisat SIT. While JPL ICESat SIT < 0.4 is practically absent for ON-periods, ENVISAT SIT has a considerable fraction of grid cells with SIT < 0.4 m (Figure 3-100, left column). The lack of thin sea ice in the JPL ICESat SIT

product is in stark contrast to the NSIDC ICESat SIT product which showed a considerable fraction of SIT < 0.4 (compare Figure 3-88, left column). Like for the NSIDC ICESat SIT product period ON07 is extreme in terms of disagreement with two completely shifted histograms.

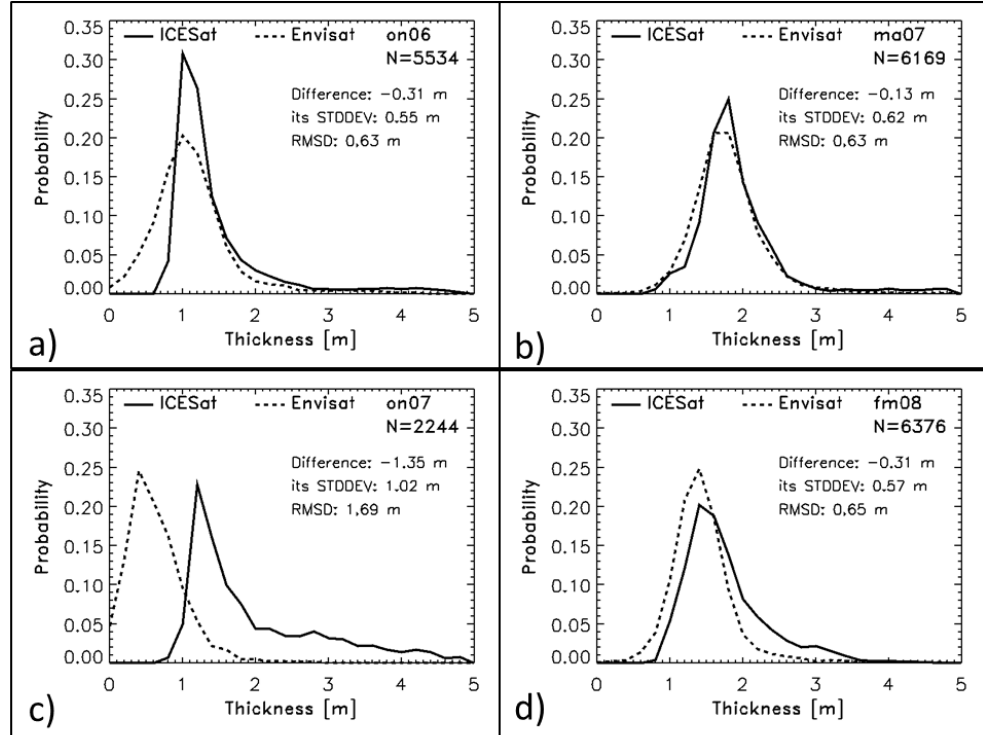


Figure 3-100 continued for winters 2006/07 and 2007/08.

Table 3-16: Per period mean SICCI-2 Envisat SIT, JPL ICESat SIT, the difference Envisat minus ICESat, the RMSD, the linear correlation, and the count N of collocated data pairs. Bold numbers at the end provide the averages over all ON, all FM, and all ON and FM values. Standard deviations 1σ given at the end are the averages of the respective values of the previous rows.

Period	SIT _{ENV} ±1σ	SIT _{ICE} ±1σ	SIT _{DIFF} ±1σ	RMSD	Corr	N
ON03	1.17±0.48	1.59±0.62	-0.42±0.50	0.65	0.61	5555
FM04	1.62±0.44	1.84±0.68	-0.22±0.60	0.64	0.49	6137
ON04	1.13±0.52	1.77±0.87	-0.64±0.77	1.00	0.47	4229
FM05	1.83±0.54	2.06±0.74	-0.23±0.62	0.66	0.56	6100
ON05	1.20±0.45	1.65±0.90	-0.46±0.89	1.00	0.26	5331
FM06	1.93±0.54	2.06±0.74	-0.13±0.74	0.74	0.39	6119
ON06	1.24±0.58	1.55±0.72	-0.31±0.55	0.63	0.66	5534
MA07	1.89±0.49	2.02±0.61	-0.13±0.62	0.63	0.38	6169
ON07	0.74±0.41	2.09±0.94	-1.35±1.02	1.69	0.01	2244
FM08	1.55±0.47	1.86±0.58	-0.31±0.57	0.65	0.42	6376
ONs	1.10±0.49	1.73±0.81	-0.64±0.75	0.99	0.41	
FMs	1.76±0.50	1.97±0.67	-0.20±0.63	0.61	0.45	
All	1.43±0.50	1.85±0.74	-0.42±0.69	0.80	0.43	

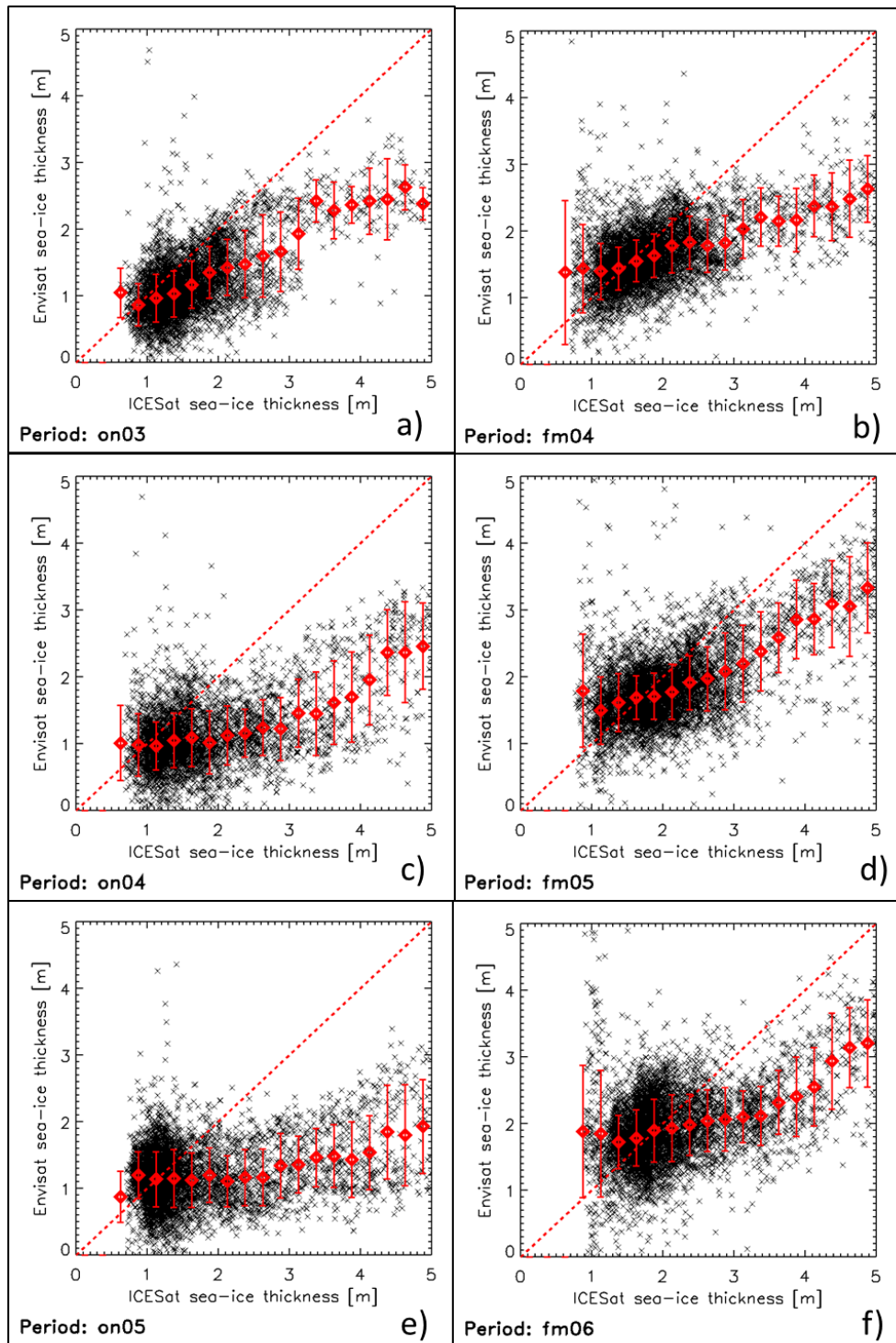


Figure 3-101: Scatterplot of individual data pairs SICCI-2 Envisat versus JPL ICESat SIT (black crosses) and mean Envisat SIT values derived for 0.2 m wide ICESat SIT bins starting with 0.0 m to 0.2 m (red diamonds). Error bars denote one standard deviation; the dashed red line denotes a 1-to-1 fit line. Like in Figure 3-89, the left (right) column is for ON (FM) periods for winters 2003/04 through 2005/06.

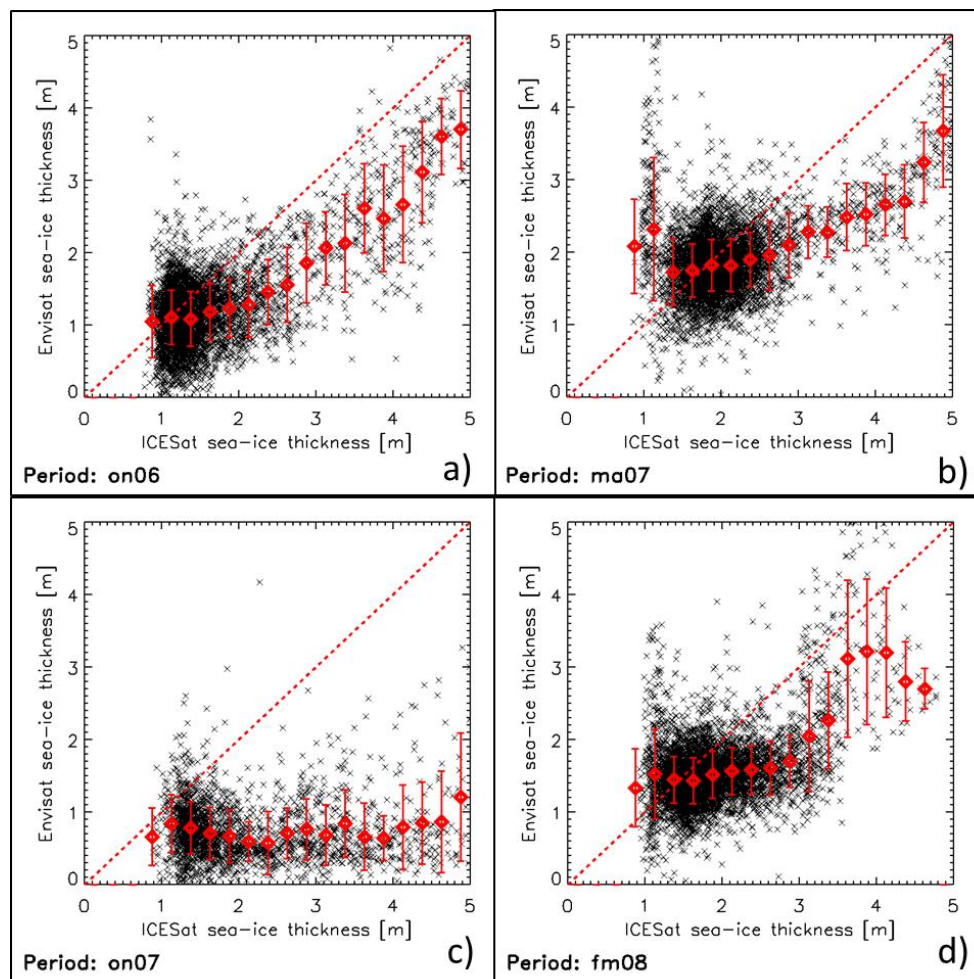


Figure 3-101 continued for winters 2006/07 and 2007/08.

The corresponding scatterplots (Figure 3-101) indicate – in agreement with the results obtained with the NSIDC ICESat SIT data set (see Figure 3-89) – that the histograms (Figure 3-100) suggest a much better agreement than is actually the case. For the majority of the data pairs we find that SICCI-2 Envisat SIT < JPL ICESat SIT. This underestimation increases with increasing SIT and it tends to be larger for ON- than FM-periods. Overall – in comparison to Figure 3-89 – one could state that the agreement between the two data sets is worse than for NSIDC ICESat SIT for thick sea ice, i.e. above 3 m or so. For ON-periods, we find best (worst) agreement for ON06 (ON07). We summarize the mean SIT values, differences and other parameters in Table 3-16 (compare Table 3-13).

The distribution of the differences shown in Figure 3-102 confirms the notion that SICCI-2 Envisat SIT is under-estimating JPL ICESat SIT more than NSIDC ICESat SIT (see Figure 3-96+Figure 3-97). We find the same hot-spots as in Figure 3-90. This applies to the widespread areas of negative SIT differences north of the Canadian Arctic Archipelago and northeast of Severnaya Zemlya, to the band of negative differences along the Eurasian shelf as well as to the areas of positive differences in the southern Laptev Sea and in the Chukchi Sea and north of it.

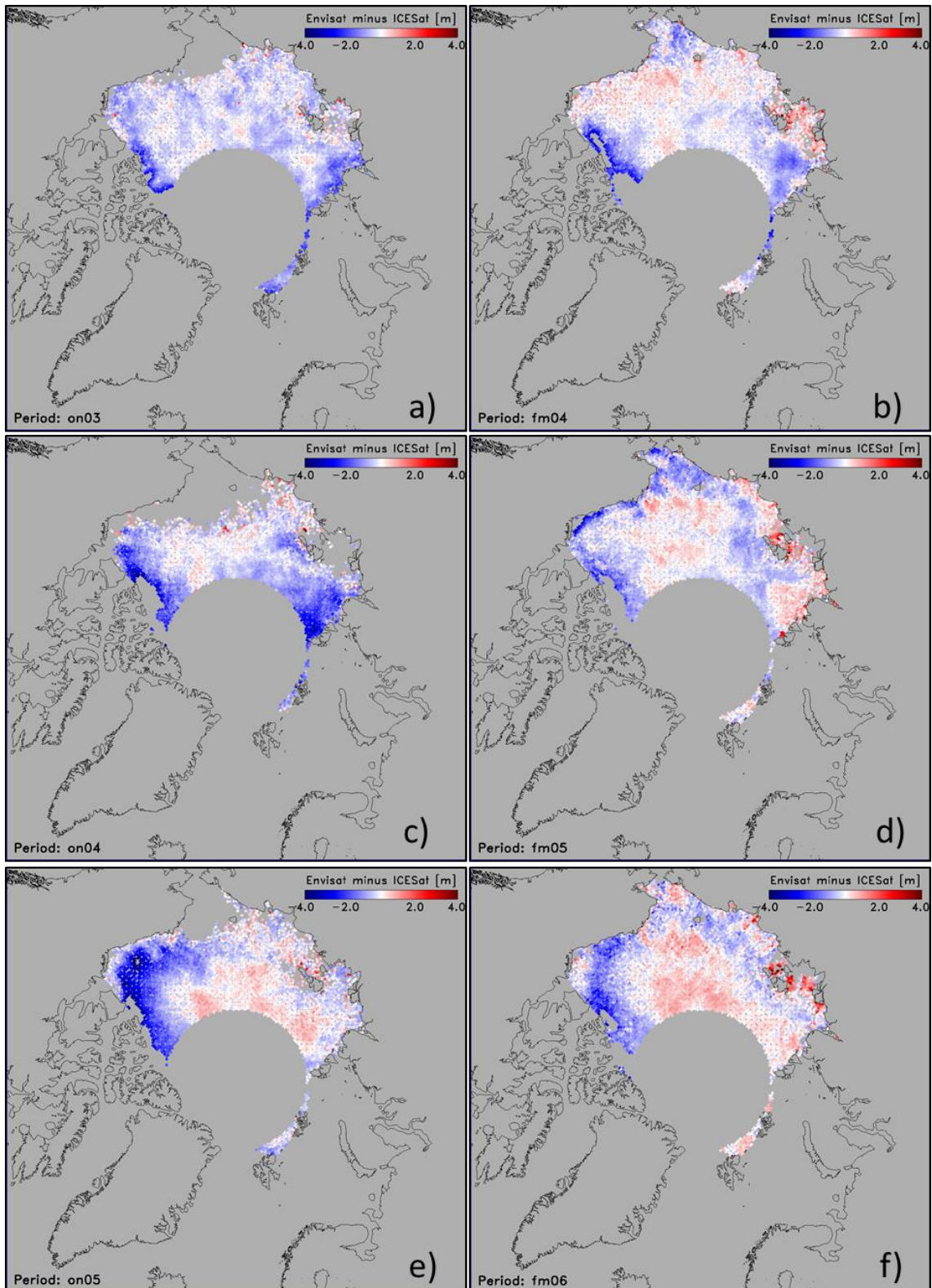


Figure 3-102: Distribution of the difference SICCI-2 Envisat minus JPL ICESat SIT for ON-periods (left) and FM-periods (right) for winters 2003/04 through 2005/06.

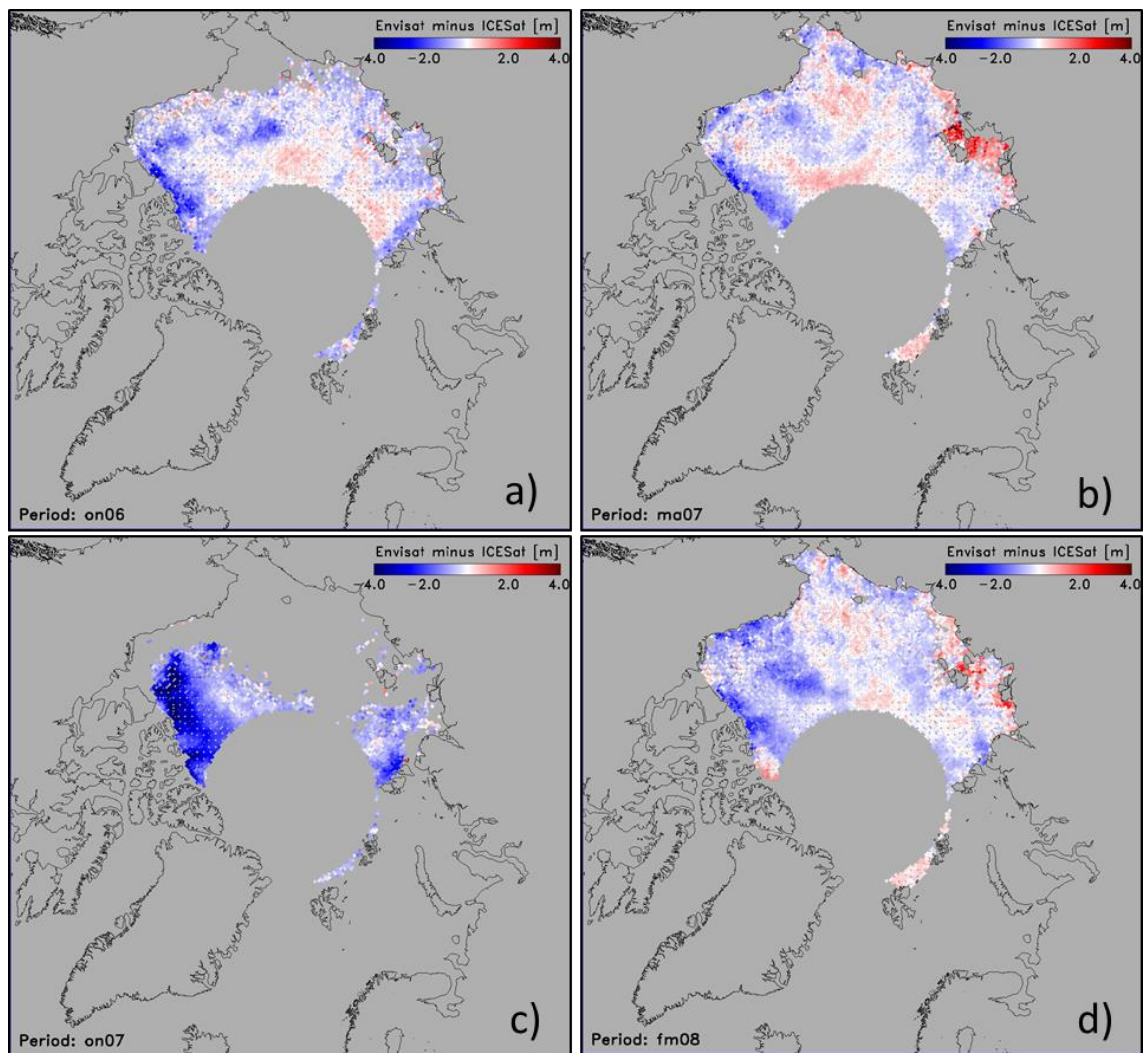


Figure 3-102 continued for winters 2006/07 and 2007/08.

Looking at Figure 3-102 continued c) it is not surprising, that the overall mean difference for period ON07 is -1.35 m, i.e. SICCI-2 Envisat underestimates JPL ICESat SIT on average by more than 1 meter. In general, as demonstrated in Table 3-16, differences for ON-periods are more negative than differences for FM-periods: -0.64 m and -0.20 m. If we compare Table 3-16 (JPL) and Table 3-13 (NSIDC) we find that the change in the overall mean difference from ON- to FM-periods is about the same: ~ 0.4 m; this lets us to conclude that the difference between the NSIDC and the JPL ICESat SIT data set can be regarded as an offset by ~ 0.4 m with JPL ICESat SIT being on average (entire Arctic Ocean, all ON- or all FM-periods) 0.4 m larger than NSIDC ICESat SIT.

Clearly, the comparison reveals much more variable results for the ON- than the FM-periods. The range in differences for ON-periods for JPL ICESat SIT is -0.31 m to -1.35 m while for FM-periods this range is just -0.13 m to -0.31 m. The same holds for NSIDC ICESat SIT with a range of $+0.13$ m to -0.69 m for ON-periods and of 0.08 m to 0.34 m for FM-periods.

We note that for FM-periods the correlation between SICCI-2 Envisat SIT and JPL ICESat SIT is a little smaller than for NSIDC ICESat SIT.

The values given in Table 3-16 are based on SIT < 5.0 m to allow direct comparison to the corresponding results involving the NSIDC ICESat SIT product (see Table 3-13). The JPL ICESat SIT product contains a considerable number of SIT values > 5.0 m however; if we increase the maximum SIT considered in the intercomparison to 8.0 m to incorporate these high SIT values as well, then, on average, ~100 (ON-periods) and ~170 (FM-periods) more valid data pairs can be used for the intercomparison, resulting in slightly larger absolute differences of -0.69 m for ON- and -0.24 m for FM-periods.

Like for the comparison with the NSIDC ICESat SIT product the distribution of positive and negative SIT differences suggests to conduct a comparison separately for FYI and MYI regions which results will be shown on the following pages. Note that we omit to show figures such as Figure 3-91 and Figure 3-92 but immediately show the scatterplots and tables.

For FYI, the scatterplots (Figure 3-103) reveal that the agreement between SICCI-2 Envisat SIT and JPL ICESat SIT is as worse as for NSIDC ICESat SIT. SICCI-2 Envisat SIT values tend not to increase with increasing JPL ICESat SIT in neither of the periods. Table 3-17 confirms this notion and also confirms that – with regard to FYI – the two ICESat SIT data sets are similar but offset by ~0.4 m. The overall increase in SIT between ON- and FM-periods is a little lower (~0.4 m instead of ~0.5 m) than for NSIDC ICESat SIT, however (compare with Table 3-14).

Table 3-17: Same as Table 3-16 but for > 85% FYI concentration.

Period	SIT _{ENV} ±1σ	SIT _{ICE} ±1σ	SIT _{DIFF} ±1σ	RMSD	Corr	N
ON03	0.97±0.39	1.30±0.32	-0.33±0.48	0.58	0.10	2563
FM04	1.48±0.40	1.55±0.41	-0.07±0.52	0.52	0.18	3634
ON04	0.96±0.50	1.25±0.33	-0.29±0.62	0.69	-0.09	1415
FM05	1.67±0.44	1.83±0.58	-0.16±0.66	0.68	0.20	3832
ON05	1.09±0.40	1.23±0.35	-0.13±0.57	0.58	-0.13	3394
FM06	1.78±0.52	1.83±0.52	-0.05±0.68	0.68	0.14	3917
ON06	1.07±0.40	1.37±0.38	-0.30±0.51	0.59	0.14	4030
MA07	1.80±0.45	1.88±0.37	-0.08±0.60	0.60	-0.05	4634
ON07	0.78±0.42	1.44±0.35	-0.66±0.57	0.87	-0.08	746
FM08	1.47±0.38	1.65±0.37	-0.17±0.51	0.54	0.07	4608
ONs	0.97±0.42	1.32±0.35	-0.34±0.55	0.66	-0.07	
FMs	1.64±0.44	1.75±0.45	-0.11±0.59	0.60	0.13	
All	1.31±0.43	1.53±0.40	-0.22±0.57	0.63	0.03	

The scatterplots (Figure 3-103) illustrate one potential shortcoming of the JPL ICESat SIT product – which kind of popped up already in the discussion of Table 3-16: JPL ICESat SIT products appear too thin over FYI during ON-periods. Evidence for this is given i) by the fact that in the SIT map shown in Figure 3-96 a) there is hardly any gradient in SIT from open water towards the pack ice – e.g. north of Bering Strait in the Chukchi Sea. Furthermore ii) it seems strange that both the histograms as well as the scatterplots do not show any JPL ICESat SIT values below about 0.5 m – not even for the ON-periods – when an applicable fraction of thin ice is present in the study area.

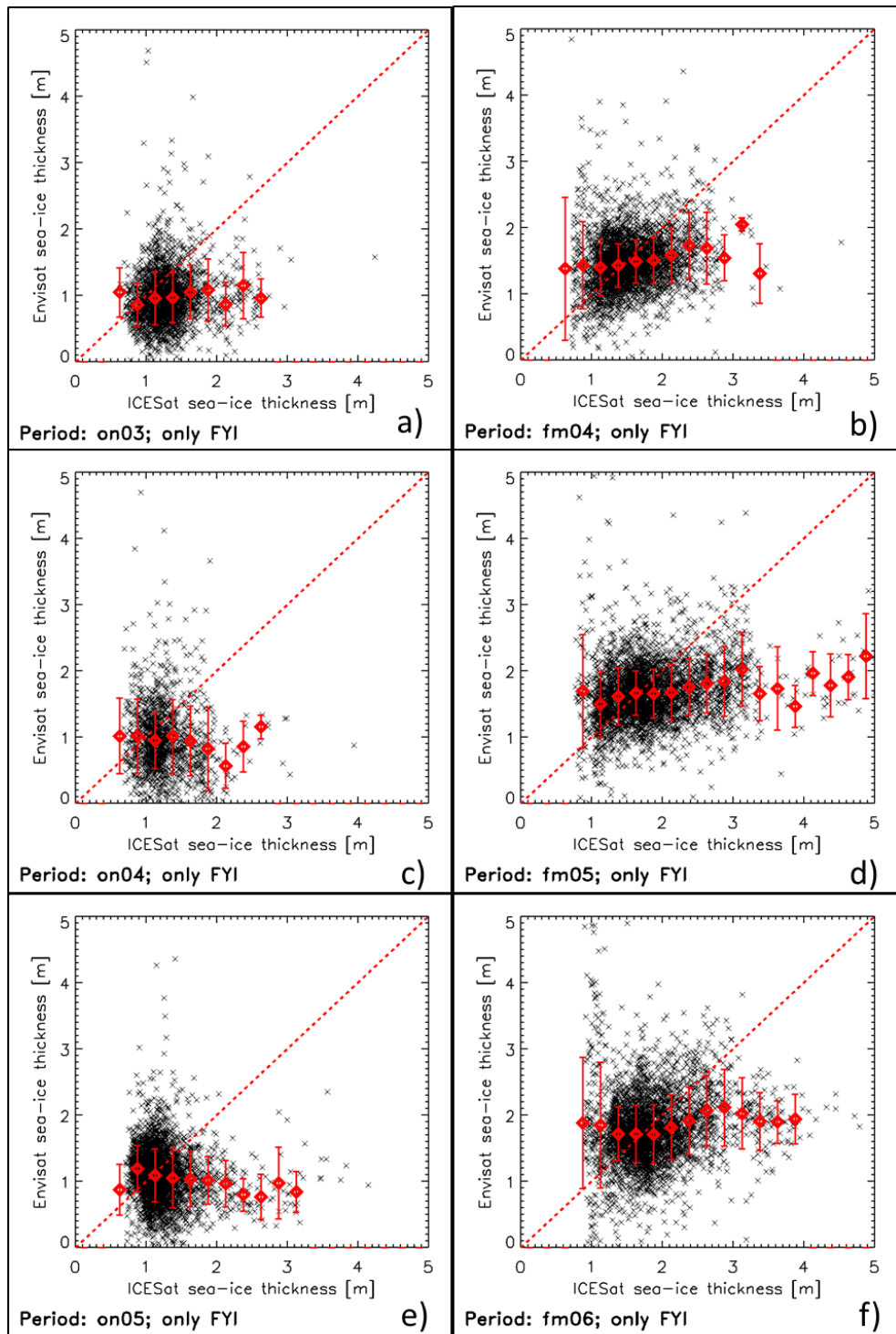


Figure 3-103: As Figure 3-101 but using only grid cells with > 85% FYI concentration.

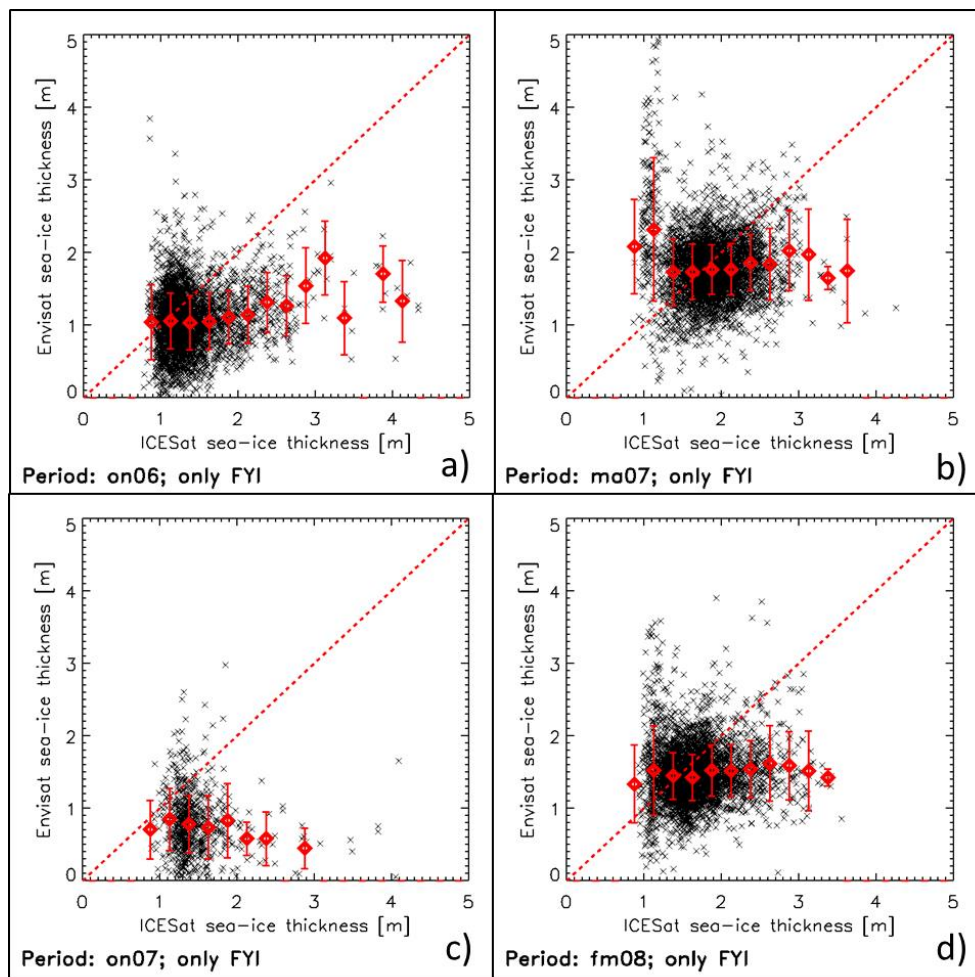


Figure 3-103, continued for winters 2006/07 and 2007/08.

For MYI regions (Figure 3-104) we find that the agreement between SICCI-2 Envisat SIT and JPL ICESat SIT is considerably worse than for NSIDC ICESat SIT (Figure 3-94). There is only a small SIT range within which the two SIT data sets are reasonably close to the 1-to-1 line. Common for all periods is a considerable underestimation – particularly for the ON-periods and particularly for the larger SIT values. This was to be expected from the SIT difference maps in Figure 3-102).

Table 3-18: Same as Table 3-16 but for > 85% MYI concentration.

Period	SIT _{ENV} ±1σ	SIT _{ICE} ±1σ	SIT _{DIFF} ±1σ	RMSD	Corr	N
ON03	1.87±0.42	2.28±0.64	-0.41±0.50	0.65	0.62	474
FM04	2.19±0.31	2.76±0.77	-0.57±0.71	0.91	0.38	558
ON04	1.73±0.62	2.88±1.03	-1.14±0.86	1.43	0.54	614
FM05	2.64±0.55	3.04±0.84	-0.40±0.52	0.65	0.80	660
ON05	1.56±0.53	2.34±1.04	-0.78±0.91	1.20	0.49	803
FM06	2.32±0.52	2.39±0.80	-0.07±0.61	0.61	0.65	749
ON06	2.23±0.83	2.74±1.19	-0.51±0.63	0.81	0.86	612
MA07	2.86±0.81	3.81±1.01	-0.95±0.58	1.11	0.82	197
ON07	0.80±0.60	2.66±0.93	-1.86±0.73	2.00	0.62	285
FM08	2.36±0.81	3.08±0.63	-0.73±0.67	0.99	0.59	447
ONs	1.64±0.60	2.58±0.97	-0.94±0.73	1.22	0.63	
FMs	2.47±0.60	3.02±0.81	-0.54±0.62	0.85	0.65	
All	2.06±0.60	2.80±0.89	-0.74±0.67	0.80	0.64	

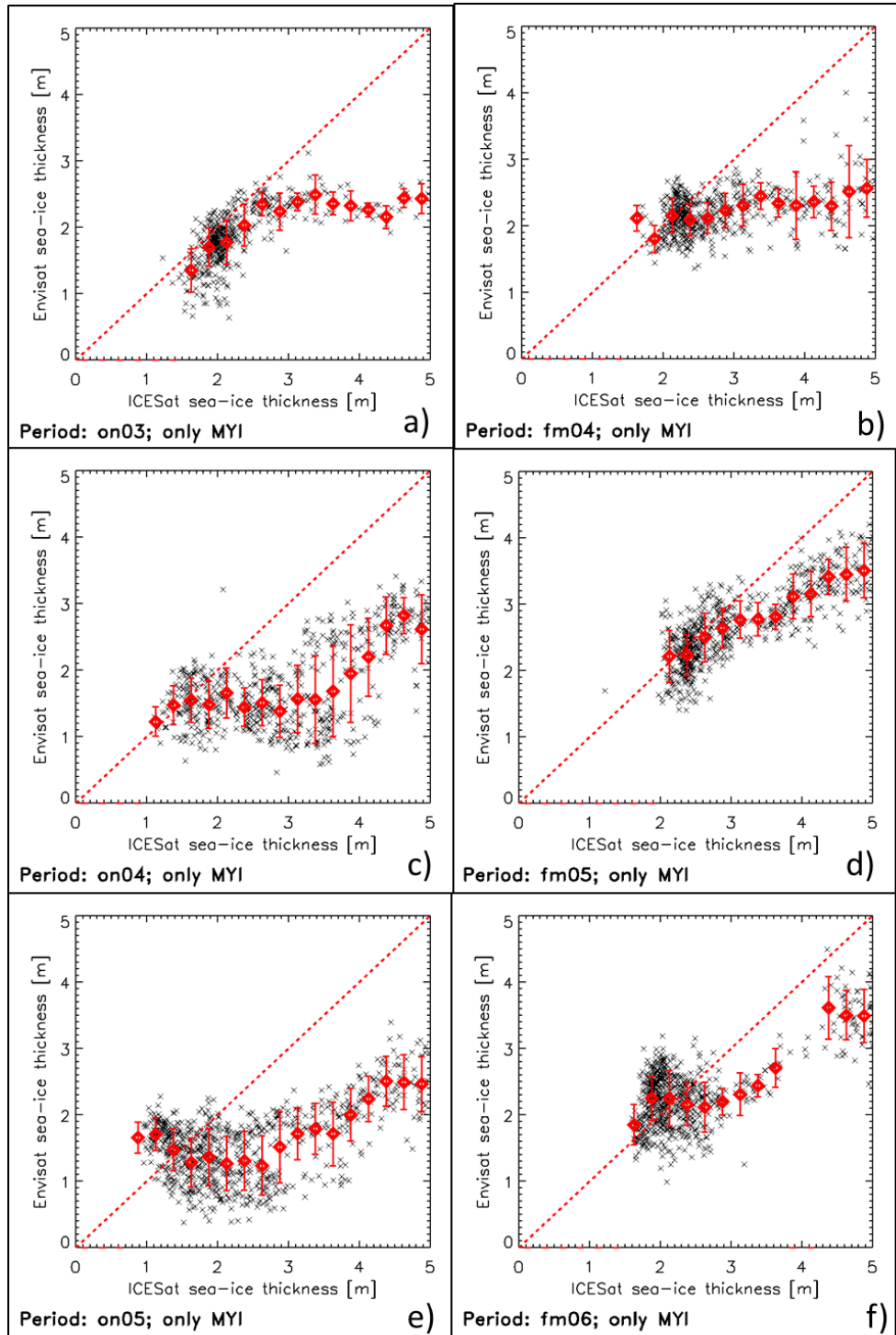


Figure 3-104: As Figure 3-103 but for > 85% MYI concentration

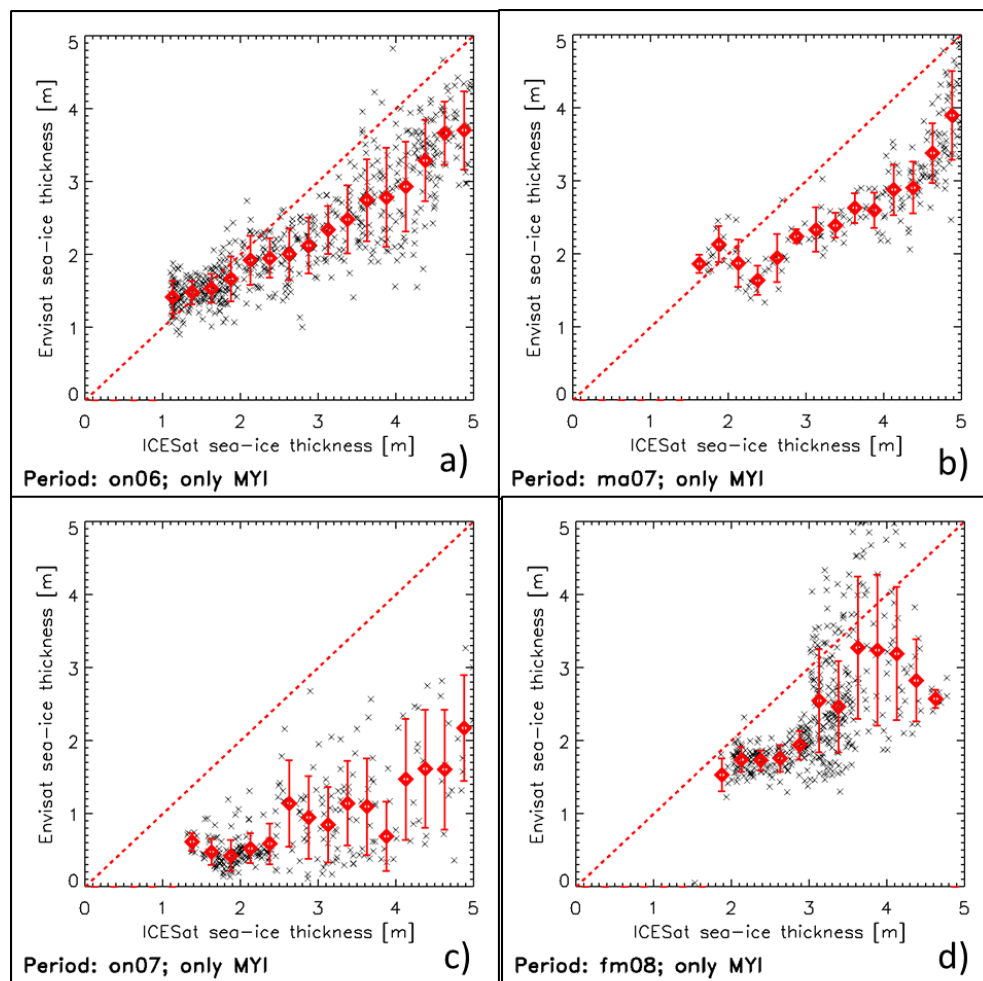


Figure 3-104 continued for winters 2006/07 and 2007/08.

The summary of the results for the comparison of SICCI-2 Envisat SIT and JPL ICESat SIT, constrained to FYI or MYI, compiled in Table 3-17 and Table 3-18, reveals:

- Poor correlation between the two data sets for FYI regions
- A more reasonable correlation between the two data sets for MYI regions but correlations vary over a large range: 0.38 to 0.86.
- An overall underestimation of JPL ICESat FYI SIT by the SICCI-2 Envisat data set by 0.64 m and 0.20 m for ON- and FM-periods, respectively.
- An overall, even larger underestimation of JPL ICESat MYI SIT by the SICCI-2 Envisat data set by 0.94 m and 0.54 m for ON- and FM-periods.
- For both ice types the change in the SIT difference between ON- and FM-periods is ~ 0.4 m.
- A similar ice growth between ON- and FM-periods for FYI and MYI (~ 0.4 m) for JPL ICESat SIT but an unrealistic magnitude in ice growth between ON- and FM-periods for MYI: ~ 0.8 m compared to ~ 0.7 m for FYI for SICCI-2 Envisat SIT (Table 3-17+Table 3-18).
- A small (moderate) range of SIT differences for FYI for FM-periods: -0.05 m to -0.17 m (ON-periods: -0.13 m to -0.66 m) (Table 3-17)
- A large range of SIT differences for MYI, particularly for the ON-periods: -1.86 m to -0.41 m for ON-periods and -0.95 m to -0.07 m for FM-periods (Table 3-18).

Summary

- Envisat tends to over-estimate thin ($< \sim 1$ m) sea ice and to under-estimate thicker ice compared to the ICESat products.
- Spatial distribution of regions with over- and underestimation of ICESat SIT by the SICCI-2 Envisat SIT are similar for both ICESat products. Highest underestimation is observed north of the Canadian Arctic Archipelago, northeast of Severnaya Zemlya, and in a band along the Eurasian shelf break. Highest overestimation is observed in the Chukchi Sea and north of it as well as in the Southern Laptev Sea.
- The overall average difference SICCI-2 Envisat minus ICESat SIT is zero for the NSIDC ICESat SIT data set and -0.4 m for the JPL ICESat SIT data set. This overall average difference is composed of an underestimation by ~ 0.2 m (NSIDC) and ~ 0.6 m (JPL) during ON-periods and an overestimation by ~ 0.2 m (NSIDC) and an underestimation (still) by ~ 0.2 m (JPL).
- JPL ICESat SIT is, on average, 0.4 m larger than NSIDC ICESat SIT.
- The overall average correlation between the two different SIT data sets is a bit larger for NSIDC (0.45) than JPL (0.43).
- There is almost no correlation between SICCI-2 Envisat SIT and ICESat SIT of both products over first-year ice (FYI) regions. NSIDC ICESat FYI SIT is overestimated by ~ 0.2 m while JPL ICESat FYI SIT is underestimated by ~ 0.2 m by SICCI-2 Envisat FYI SIT.
- There is a reasonable correlation (0.6 to 0.7 on average) between the two different SIT data sets over multiyear ice (MYI) regions. NSIDC ICESat MYI SIT is underestimated by ~ 0.15 m while JPL ICESat MYI SIT is underestimated by ~ 0.75 m by SICCI-2 Envisat MYI SIT.
- Particularly for MYI, results obtained for ON-periods are substantially more variable than those for FM-periods; this applies to the correlation as well as to the SIT differences. For ON-periods, MYI, the underestimation of ICESat SIT by SICCI-2 Envisat SIT is ~ 0.45 m for the NSIDC and ~ 0.95 for the JPL data set.
- For MYI, we find an unrealistically high (in general, in comparison to the two ICESat data sets and to FYI) increase in SIT between ON- and FM-periods of 0.8 m to 1.0 m compared to 0.7 m for FYI; the general ON-period to FM-period SIT increase is larger for SICCI-2 Envisat SIT than the two ICESat SIT data sets.

Comments

- The NSIDC ICESat SIT product used here employs a different parameterization of the Warren et al. ([RD-08]) snow depth climatology than is employed in the SICCI-2 Envisat SIT data set. The full snow depth is used for freeboard > 0.1 m (ON-periods) or freeboard > 0.4 m (FM-periods). Otherwise snow depth is multiplied by the ratio between the actually measured freeboard and the respective value of the two thresholds just given. Hence, in late winter, the multiplication factor for sea ice with 0.2 m freeboard would be 0.5 agreeing with the snow depth parameterization in the SICCI-2 Envisat SIT product for first-year ice. For freeboards < 0.2 m and between 0.2 and 0.4 m the multiplication factor would be smaller or larger than 0.5 , respectively, though. Note that snow depth is set to the freeboard in case it exceeds the freeboard. The most important difference of this snow-depth parameterization is perhaps its dependence on freeboard measurements; it does not involve an additional data set such as the multiyear ice concentration.
- The JPL ICESat SIT product used here employs a snow depth parameterization which is based on snow accumulation on drifting sea ice based on ECMWF re-analysis data. It can be expected that this

parameterization does not only result in a substantially different seasonal snow depth distribution as compared to the one used in the SICCI-2 Envisat SIT product and the NSIDC ICESat SIT product but it also allows to take into account inter-annual variation – a clear deficit of the other two mentioned products. I would recognize the snow depth parameterization used in the JPL product as the most reliable one of the three products inter-compared.

- Even though both ICESat SIT products are not necessarily representing the truth, this comparison gives an impression about whether and where both data sets differ by how much and how the differences are spatially and also temporally distributed. We believe, that the fact that the ICESat data set uses at least kind of a similar snow-depth parameterization and does not need to employ the snow depth twice for the SIT retrieval, makes it a valuable data set for this inter-comparison.
- This comparison revealed, however, at least one shortcoming of the JPL ICESat SIT product which needs to be kept in mind. It seems relatively clear that SIT is overestimated over FYI regions at the beginning of winter. The substantially lower modal and mean SIT values shown for ON-periods for the NSIDC ICESat SIT product might actually be more realistic than the corresponding values of the JPL ICESat SIT product used.

3.7 Comparison against ship-based sea-ice thickness estimates

Similar to the evaluation of the SICCI 2 SIC (see Section 3.5 of SICCI2-PVIR-SIC) ASPeCt and IceWatch/ASSIST ship-based observations of the sea-ice thickness are compared against SICCI-2 SIT product for both hemispheres. In addition to comparing SIT we also compare snow depth data, i.e. we compare the snow depth product included in the SICCI-2 SIT product with the ship-based observations of the snow depth.

For this exercise we first compute total sea-ice thickness and snow depth values from the ship-based observations. This is required because in a standard ship-based observation the sea-ice parameters of up to three of the most abundant sea-ice types encountered are observed. This means that ideally one has three sea-ice thickness and three snow-depth observations per ship-based observation, which come along with the area fractions of the three types involved.

The co-location between SICCI-2 SIT (and snow depth) and ship-based observations is carried out exactly the same way as is done for SIC (see SICCI2-PVIR-SIC) – except that the temporal scale is monthly instead of daily.

For data coverage in space and time we also refer to SICCI2-PVIR-SIC, section 3.5.

For the Northern Hemisphere we only used ship-based observations for months October through April; for this period only we have SICCI-2 SIT data anyways. For the Southern Hemisphere we use observations from the entire year. However, we carry out the intercomparison separately for summer (November through March) and winter (April through October). We note that this comparison covers SIT data from both Envisat and CS-2.

To compute a monthly mean value it is considered sufficient to have 3 SIT or snow depth observations in the respective search area around the SICCI-2 SIT data product grid cell center under collocation.

It needs to be kept in mind that the value of this evaluation might be relatively small because while the estimation of the SIC from aboard the ships' bridge has been proven to provide reasonable results it is known that ship-based sea-ice thickness (and snow depth) estimates under-estimate the actual thickness for various reasons. Therefore we give this part of the evaluation less weight. However, data coverage with in-situ or – like these – in-situ like observations is very sparse and it might make sense to exploit this data source despite the potential underestimation.

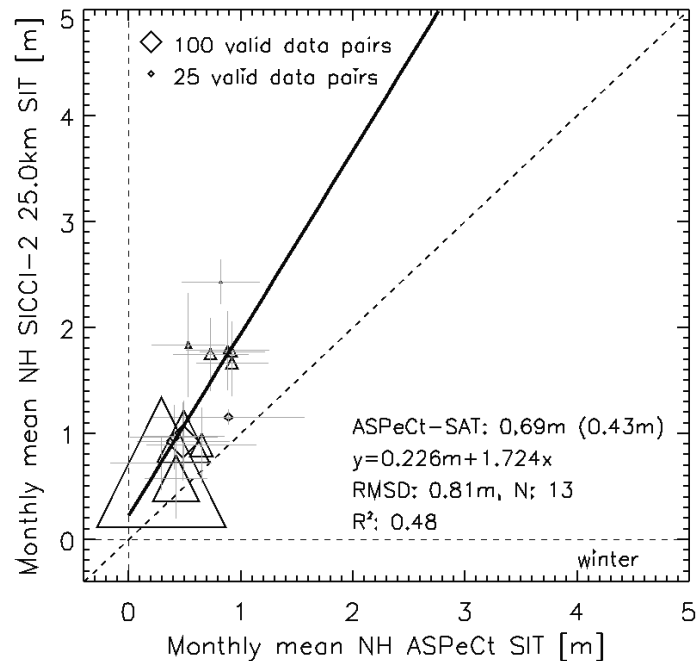
Sea-ice thickness

Figure 3-105: Monthly mean SICCI-2 SIT (also named "SAT") versus the monthly mean SIT based on ship-based observations (also named "ASPeCt") for the Northern Hemisphere. Error bars denote ± 1 standard deviation of the monthly mean. Size of the symbols denotes the number of valid co-located data pairs for the respective monthly mean value. Thick solid line is the linear regression line (not forced through zero). Given in the lower right corner is the mean difference and its standard deviation (in parenthesis), the equation of the linear regression, the root mean square difference (RMSD), the number of monthly data pairs N and the squared linear correlation coefficient R^2 . The diagonal dashed line denotes the line of 1-to-1 agreement.

All 13 pairs of monthly mean SIT values obtained for the comparison in the Northern Hemisphere are situated above the line of 1-to-1 agreement between SICCI-2 SIT and ship-based observed SIT (Figure 3-105). This suggests that SICCI-2 over-estimates the SIT observed from aboard ships. This is what one would expect because ships tend to navigate easy to navigate waters and "easy" ice conditions, following leads and openings and avoiding ridges. Data pairs are grouping relatively nicely – with a squared linear correlation coefficient of $R^2=0.48$ – along the linear regression line which suggests a positive bias (by SICCI-2) of ~ 0.2 m and which slope suggests that SICCI-2 SIT are 1.5 to 2 times larger than the corresponding ship-based observations. The mean difference is $0.69 \text{ m} \pm 0.43 \text{ m}$. We note that the maximum monthly SIT encountered during the cruises used is ~ 1 m in the ship-based observations and ~ 2 m in the SICCI-2 SIT product.

For the Southern Hemisphere, winter conditions, also all 19 data pairs of monthly mean SIT values obtained for the comparison are situated above the line of 1-to-1 agreement between SICCI-2 SIT and ship-based observed

SIT (Figure 3-106). These are, however, not aligned along the linear regression line ($R^2=0.19$) and albeit this line has a slope close to one (0.852) we suggest not to interpret this as a sign of good agreement.

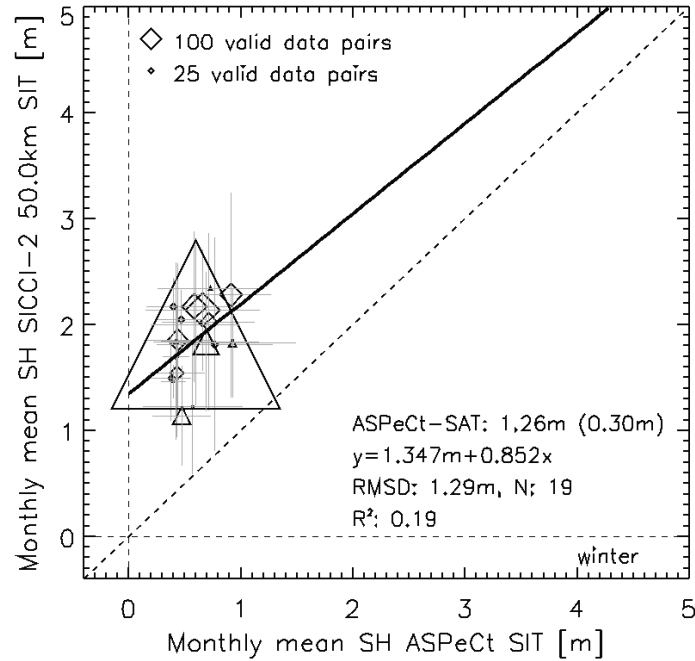


Figure 3-106: As Figure 3-105 but showing results for the Southern Hemisphere, winter months.

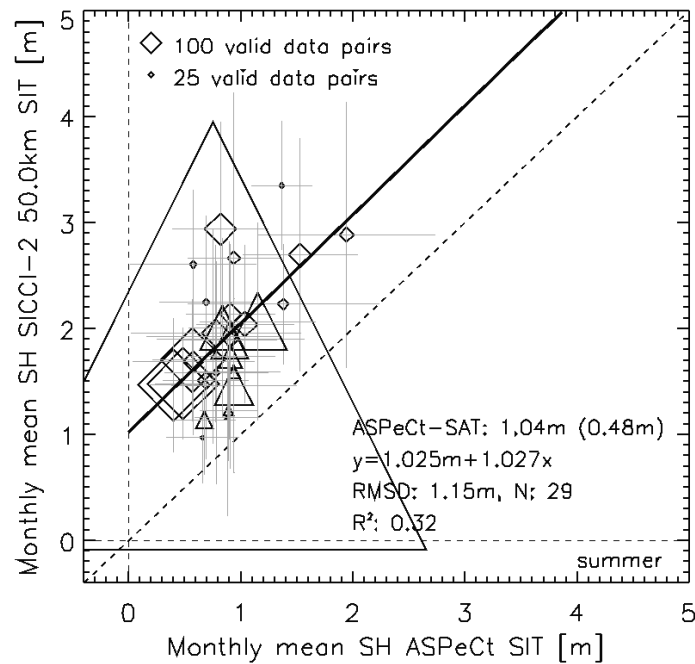


Figure 3-107: As Figure 3-105 but showing results of the Southern Hemisphere, summer months.

There is little to no improvement in the agreement when switching to summer conditions (Figure 3-107). We have considerably more data pairs to compare (29 instead of 19). ASPeCt SIT values range from 0.4 m to 2.0 m while SICCI-2 ones range from 1.0 m to 3.4 m. The squared linear correlation is 0.32 and hence better than for winter (Figure 3-106) but worse than for the Arctic (Figure 3-105). The linear regression suggests quite good agreement slope wise: 1.027, but the intercept and also the location of the regression line relative to the 1-to-1 line points to a positive bias of ~ 1 m for SICCI-2 SIT compared to ASPeCt SIT.

Snow depth

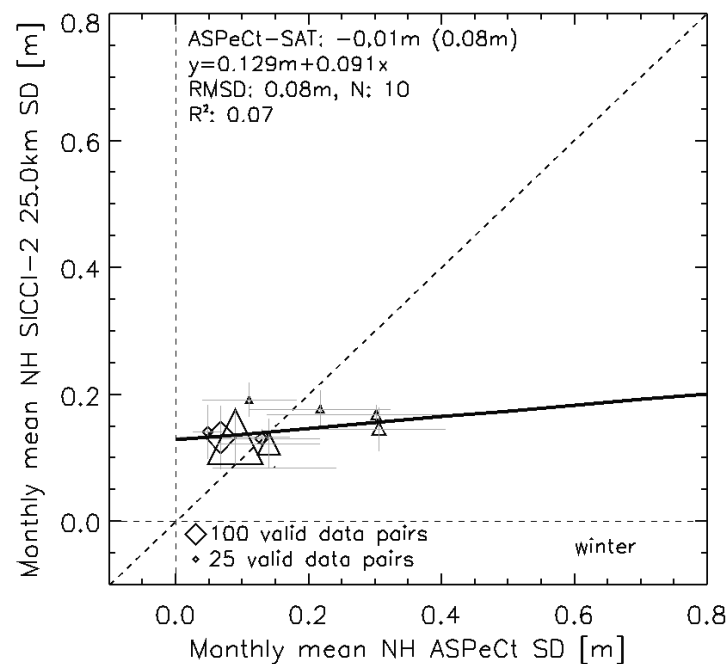


Figure 3-108: As Figure 3-105 but for the snow depth and with the statistical parameters grouped in the upper left instead of the bottom right corner. Note that N is smaller by one compared to Figure 3-105 because during one of the winter cruises no snow depth information was recorded.

The agreement between the snow depth used in the SICCI-2 SIT data product and the snow depths from the ship-based observations seems not to be too bad because most data pairs are within 10 cm to the 1-to-1 line (Figure 3-105). The data pairs basically cluster in the range 5 cm ... 20 cm. There is almost no correlation between the two data sets: $R^2=0.07$. The two data pairs outside that cluster (at ~ 30 cm ASPeCt snow depth) determine the obtained linear regression which slope is close to zero – suggesting that larger (observed) snow depths are possibly not very well represented by the snow depth data set used in the SICCI-2 SIT product; this data set is a modified version of the Warren et al. ([RD-08]) climatology. The very small mean difference of $1\text{ cm} \pm 8\text{ cm}$ and small RMSD of 8 cm illustrate in the context of the results just discussed, that these quantities are not a suitable quality measure.

In a way the observed relationship – though rooted poorly – is in line with the results shown in Figure 3-105 in that a too thin (compared to observations) snow layer would support a too thick (compared to observations) sea-ice thickness.

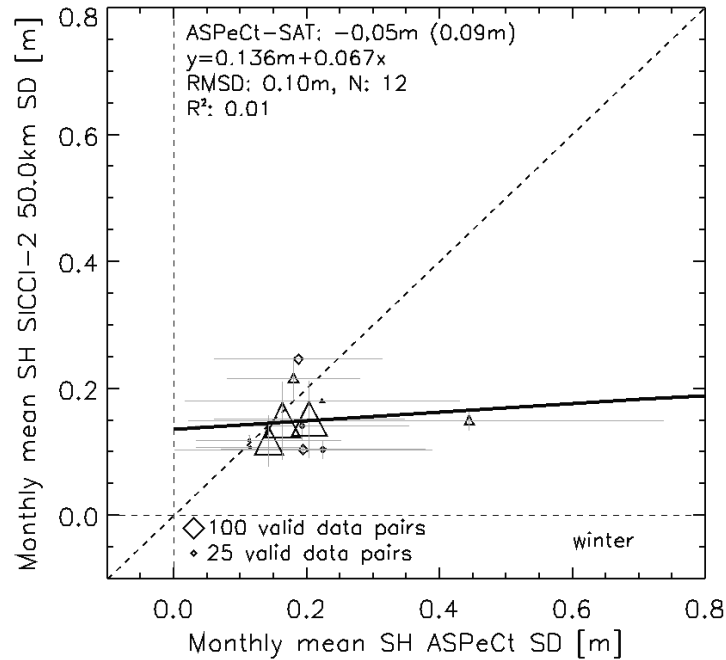


Figure 3-109: As Figure 3-108 but for the Southern Hemisphere, winter.

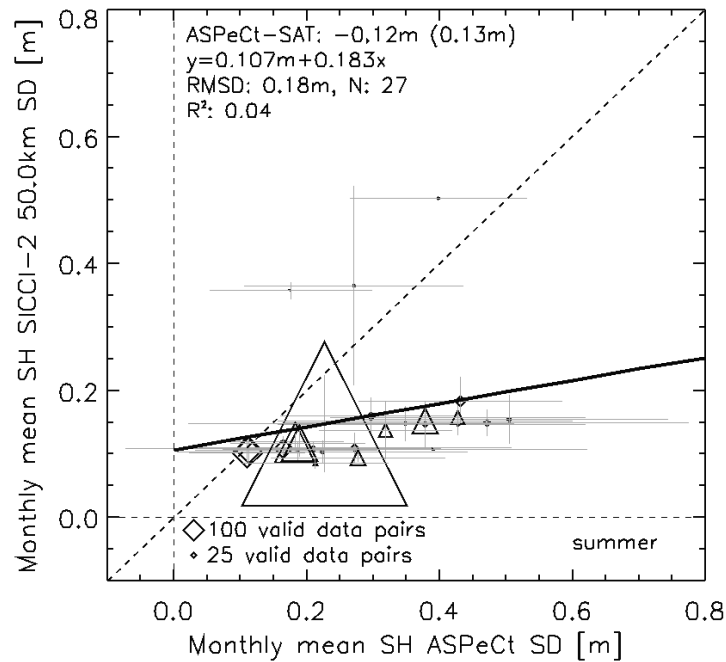


Figure 3-110: As Figure 3-108 but for the Southern Hemisphere, summer.

In the Southern Hemisphere, the snow depth data used in the SICCI-2 SIT product - a daily climatology based on satellite passive microwave retrieval - agree with ASPeCt snow depths as good (or as bad) as they do in the Northern Hemisphere (compare Figure 3-108 and Figure 3-109). All but one data pair cluster around the 1-to-1 line with a difference between 5 cm and 10 cm. The correlation is almost zero, the RMSD with 10 cm relatively small. The mean difference is, however, larger: $5 \text{ cm} \pm 9 \text{ cm}$, which is partly caused by one outlier which relates 0.13 cm snow depth in the SICCI-2 SIT product with 0.43 cm snow depth in the ASPeCt data set. This latter data pair also influences the linear regression having a slope even closer to zero than for the Northern Hemisphere. Still, if we exclude that outlier than the agreement of the snow depth data sets is not too bad.

This picture changes during summer conditions (Figure 3-110). The majority of the snow depth data pairs is located below the 1-to-1 line and only few of them are located within 10 cm to it. Most of the data pairs align along the linear regression line which again has a very low slope (compare Figure 3-108 and Figure 3-109). This suggests that the snow depth data set used in the SICCI-2 SIT product is under-estimating the actual snow depth considerably - the mean difference is already 12 cm.

We do not find these results very surprising because the algorithm used to compute the snow depth from the satellite passive microwave data cannot be used properly when the snow is wet and exhibits a known low bias. Consequently, our results show this under-estimation for summer months. Melt-refreeze processes can also result in an under-estimation of the snow depth. In addition to these caveats during summer it is known (and published) that this kind of snow-depth retrieval also under-estimates the actual snow depth over deformed sea ice. Therefore, in case of the Southern Hemisphere, two effects are acting against each other: One is the known under-estimation of actual snow depth in the ASPeCt data (x-axis of Figure 3-108 through Figure 3-110) due to preference of easy-to-navigate thin, less deformed sea ice. The second is the known under-estimation of actual snow depth in the passive microwave data based snow depths just discussed.

We are quite sure that the strong under-estimation of the observed snow depth in Figure 3-110 is due to the limitations of the snow-depth retrieval mentioned. If we assume that the actual snow depth was higher, then the retrieved SICCI-2 SIT values would be lower and would hence agree better with the ASPeCt observations (Figure 3-107) - provided that the freeboard retrieval is reliable under the melting conditions.

It is likely, that for the Southern Hemisphere, winter conditions (Figure 3-109), snow depths are also under-estimated for the reasons explained above and that elimination of the limiting factors would move the data pairs towards higher snow depths along the 1-to-1 line. The resulting higher snow depths would help reducing the too thick SICCI-2 SIT during winter (Figure 3-106) - but possibly not by the amount required to have reasonable agreement.

Summary

- When taking into account limitations of ship-based observations such as preference of thinner sea ice SICCI-2 SIT agrees reasonably well with these in the Northern Hemisphere, winter, and in the Southern Hemisphere, summer.

- The comparison with the ship-based snow depth observations confirms that snow depth on sea ice is potentially one of the largest sources for biases in SICCI-2 SIT.

3.8 SICCI-2 SIT evaluation with CryoSat-2 SIT data

Here we describe the results of the inter-comparison between the SICCI-2 SIT product (CryoSat-2 only) with two other SIT products derived from CryoSat-2 (CS-2). One is the "CryoSat-2 Level 4 Sea Ice Elevation, Freeboard, and Thickness, Version 1" data set from NSIDC under: <https://n5eil01u.ecs.nsidc.org/ICEBRIDGE/RDEFT4.001/> ([RD-29, RD-30]). This data set is available for the full CS-2 period with 25 km grid resolution (NSIDC polar-stereographic grid) and monthly temporal resolution. The other is the CS-2 SIT product from UCL-CPOM [RD-31]. Here we use the so-called "final precise data" which are available to fall (October/November) and spring (March/April) periods of years 2010/11 through 2016/17. This data set comes at 5 km grid resolution – as well on polar-stereographic grid projection.

As all data sets are based on CS-2 data we omit that extension when mentioning the respective data.

SICCI-2 SIT data and these two independent CS-2 SIT data sets are co-located as described in Section 3.6. Note that we do not average UCL SIT data – despite their finer grid resolution – because each 5 km grid cell value is computed as an average over a 50 km diameter disc centered at the respective grid cell. The UCL SIT product sets the temporal resolution (see above) which we also used for NSIDC SIT and SICCI-2 SIT; therefore we computed the fall (October/November) and spring (March/April) mean SIT for the NSIDC and the SICCI-2 SIT data sets.

Part I: Comparison to the NSIDC CS-2 SIT data set

Figure 3-111 and Figure 3-112 give – like Figure 3-86 and Figure 3-87 – an overview of the SIT distribution of both data sets for fall 2011 and spring 2012, respectively, together with a map of their difference, the SIT histograms and scatterplots. In fall 2011, the SIT distributions (Figure 3-111 a,b) are relatively similar with respect to the location of thicker (> 1.5 m) sea ice. We find, however, considerably more thinner (< 1.0 m) sea ice and also a larger SIT gradient and variability for SICCI-2 SIT. This is confirmed by the histograms (Figure 3-111 c): NSIDC SIT spans over a range of roughly one meter while SICCI-2 SIT spans over a range of almost two meters; almost no sea ice is thicker than 2 m. The modal SIT is larger: ~1.1 m for NSIDC than for SICCI-2: ~0.6 m. SICCI-2 SIT has the indication of a bi-modal distribution with a second mode at 1.2 m. The SIT difference map (Figure 3-111 d) shows wide-spread underestimation of the NSIDC SIT by the SICCI-2 SIT but the absolute value rarely exceeds 1 m. In a few areas SICCI-2 SIT overestimates NSIDC SIT. The point-to-point agreement between the two data sets is relatively good (Figure 3-111 e) but suggests an underestimation of about ~0.3 m (see Figure 3-111 c) by SICCI-2 SIT relative to NSIDC SIT.

The agreement in the spatial SIT distribution is much better for spring 2012 (Figure 3-112 a,b); areas with thinner sea ice (Eurasian side, belt across northern Beaufort and Chukchi Seas) and thicker sea ice (north of Greenland and the Canadian Arctic Archipelago) agree with each other and gradients agree as well. This is confirmed by the histograms (Figure 3-112

c) by means of a similar mode at ~ 1.6 m and a more or less similar tail towards thicker ice terminating at ~ 3.5 m; SICCI-2 SIT still exhibits more thin (< 1.0 m) sea ice than NSIDC SIT.

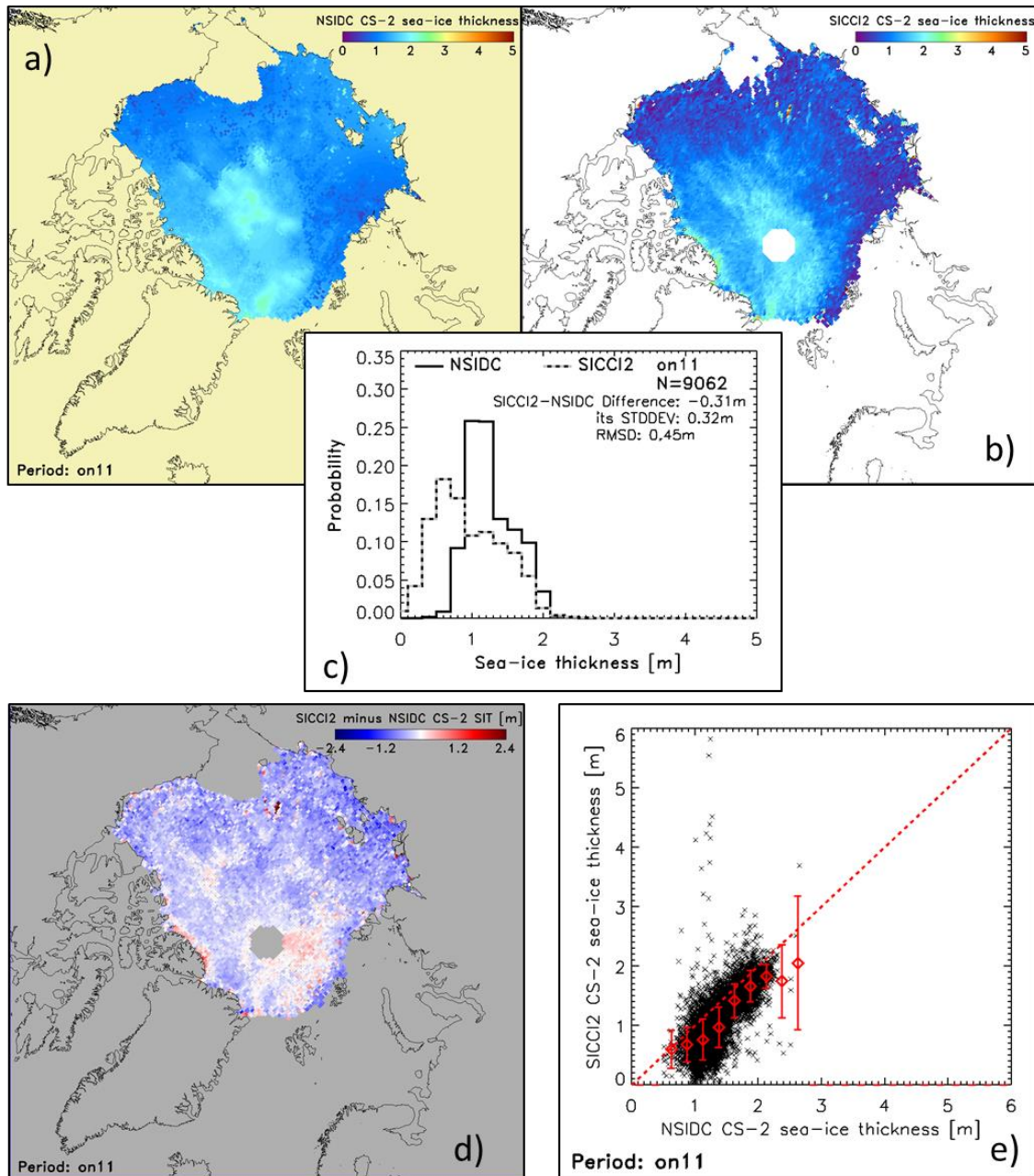


Figure 3-111: Inter-comparison of NSIDC versus SICCI-2 CS-2 sea-ice thickness (SIT) for fall 2011 (on11). a) NSIDC SIT, note that SIT values are interpolated over the polar data gap; b) SICCI-2 SIT, the white circular disk denotes the polar data gap; d) Difference SICCI-2 minus NSIDC SIT; c) histograms of the SIT from both data set for coinciding grid cells together with the count of data pairs "N", the root mean squared difference "RMSD" as well as the mean difference and its standard deviation; e) scatterplot of all co-located SIT values (black crosses) superposed by the mean SICCI-2 SIT value per 0.2 m NSIDC SIT bin. The error bars denote plus/minus one standard deviation. The red dashed line is the 1-to-1 fit line.

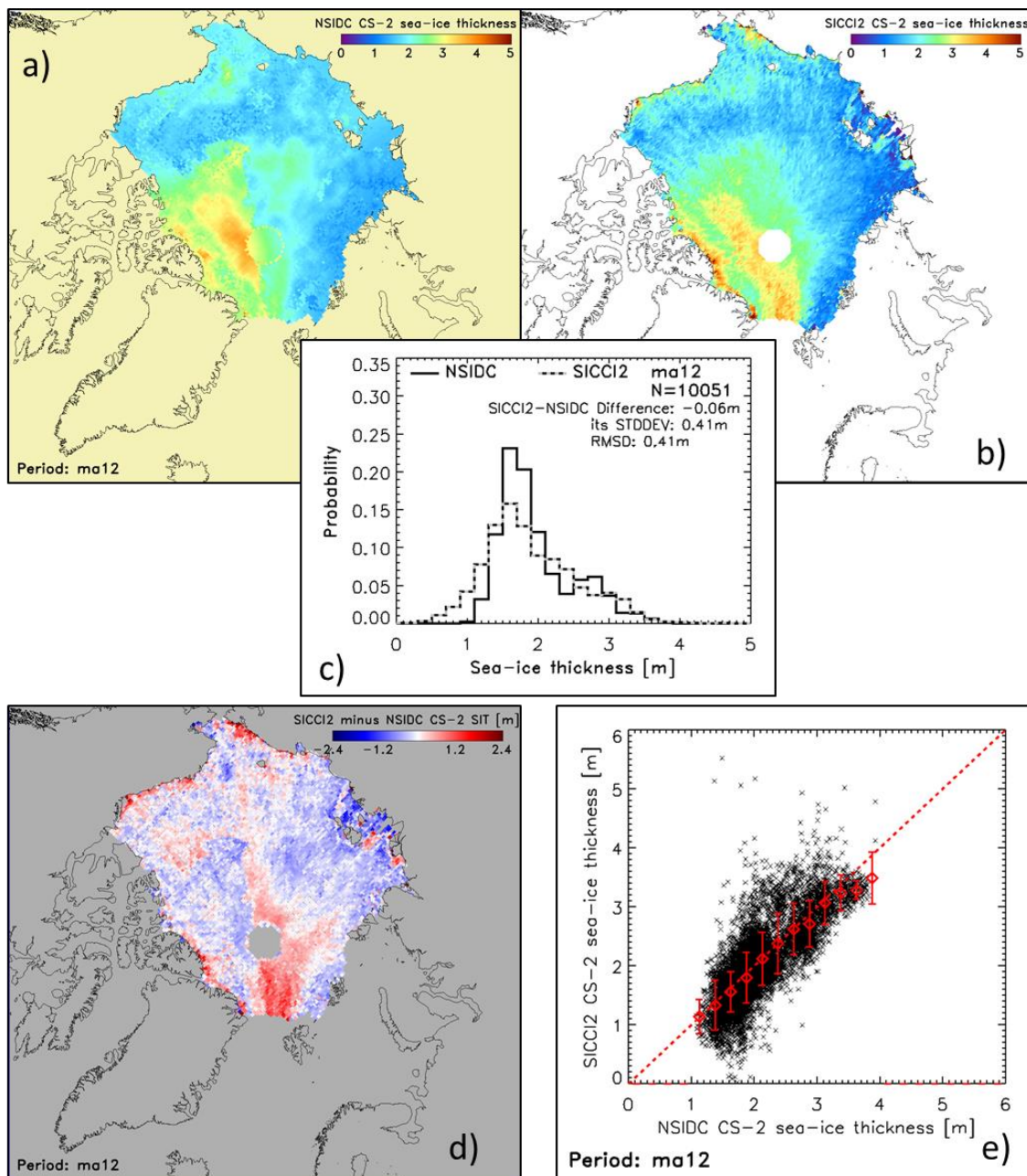


Figure 3-112: As Figure 3-111 but for spring 2012 (ma12).

Areas with negative differences (Figure 3-112 d) have reduced considerably compared to fall 2011 (Figure 3-111 d) and one can state that absolute SIT differences are < 0.5 m for the majority of the Arctic Ocean. Pronounced positive differences, i.e. SICCI-2 SIT $>$ NSIDC SIT, occur along the coasts of Greenland, Ellesmere Island, Canada, Alaska and Eastern Siberia, and, more interestingly, in a relatively confined region extending from the Fram Strait towards the central Arctic and beyond. In this region SICCI-2 SIT exceeds NSIDC SIC by 1 to 1.5 m. This region is known to be the gateway for advection of positive air-temperature and moisture anomalies even in the middle of winter. These events are possibly associated with elevated snow accumulation and/or freezing rain or at least enhance snow metamorphism due to the warm air advection. Elevated snow accumulation could result in a worse agreement between the modified Warren et al. [RD-08] snow depth

climatology used by both approaches and the actual snow depth. But if this would be the case it would have affected both retrievals and would not have caused the observed difference in SIT. In contrast, rain-on-snow events and/or enhanced snow metamorphism could have had an impact on the physical properties of the snow cover such as density or layering. The latter could impact the penetration depth of the radar altimeter signal in to the snow. Since the freeboard retrieval methods used differ between the NSIDC and the SICCI-2 product we hypothesize this as the likely cause for the observed SIT difference. More investigations are needed to figure out whether this hypothesis holds. To conclude the discussion of Figure 3-112 we note that the scatterplot (image e) shows a substantially better agreement between both SIT products compared to fall (Figure 3-111 e) with most per-0.2m-bin average SICCI-2 SIT values being located on the 1-to-1 line and with an overall difference SICCI-2 minus NSIDC SIT of -0.06 m for spring 2012.

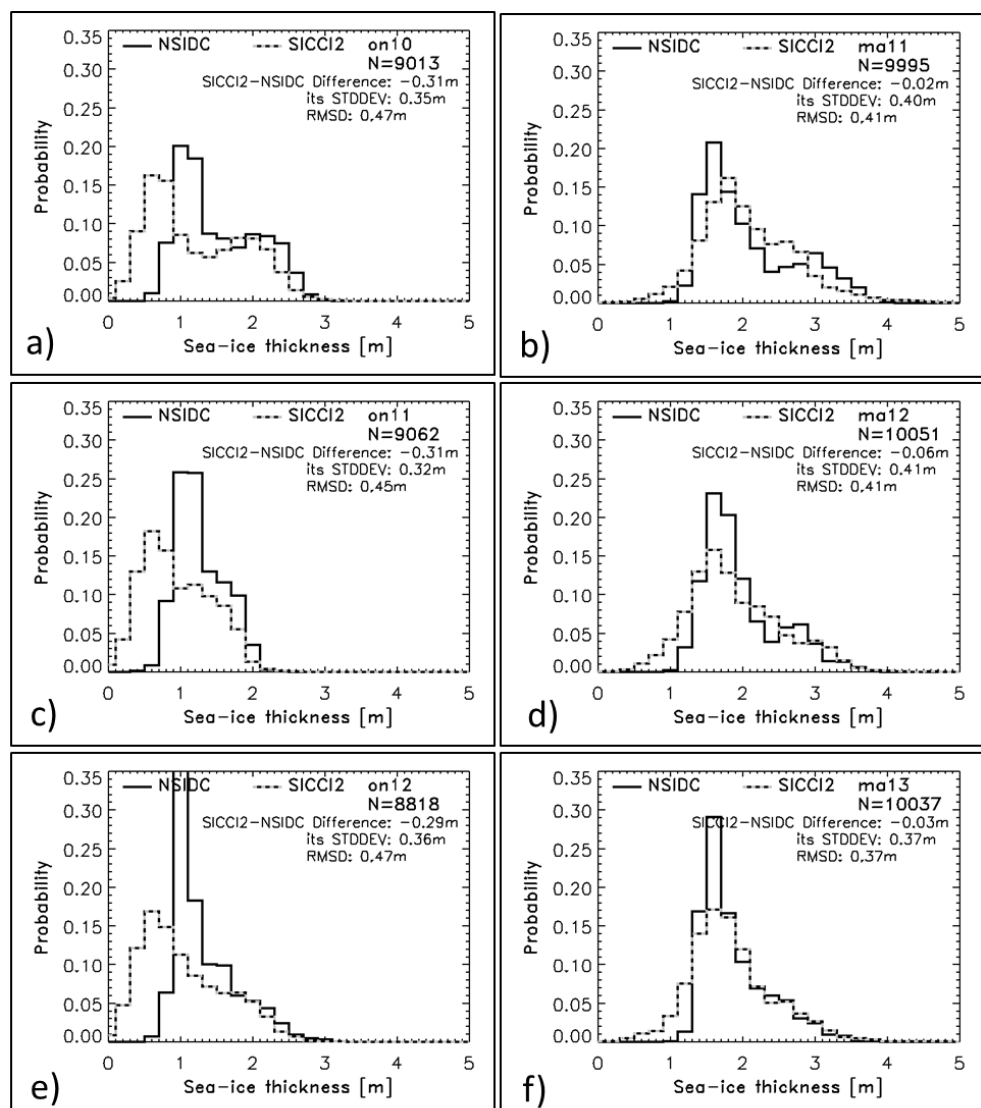


Figure 3-113: Histograms of NSIDC and SICCI-2 SIT for the Arctic Ocean for fall (ON periods, left column) and spring (MA periods, right column) for winters 2010/11 through 2012/13. In each image the number of valid data pairs, the mean difference SICCI-2 minus

NSIDC SIT and its standard deviation and the RMSD is given (see also Table 3-19).

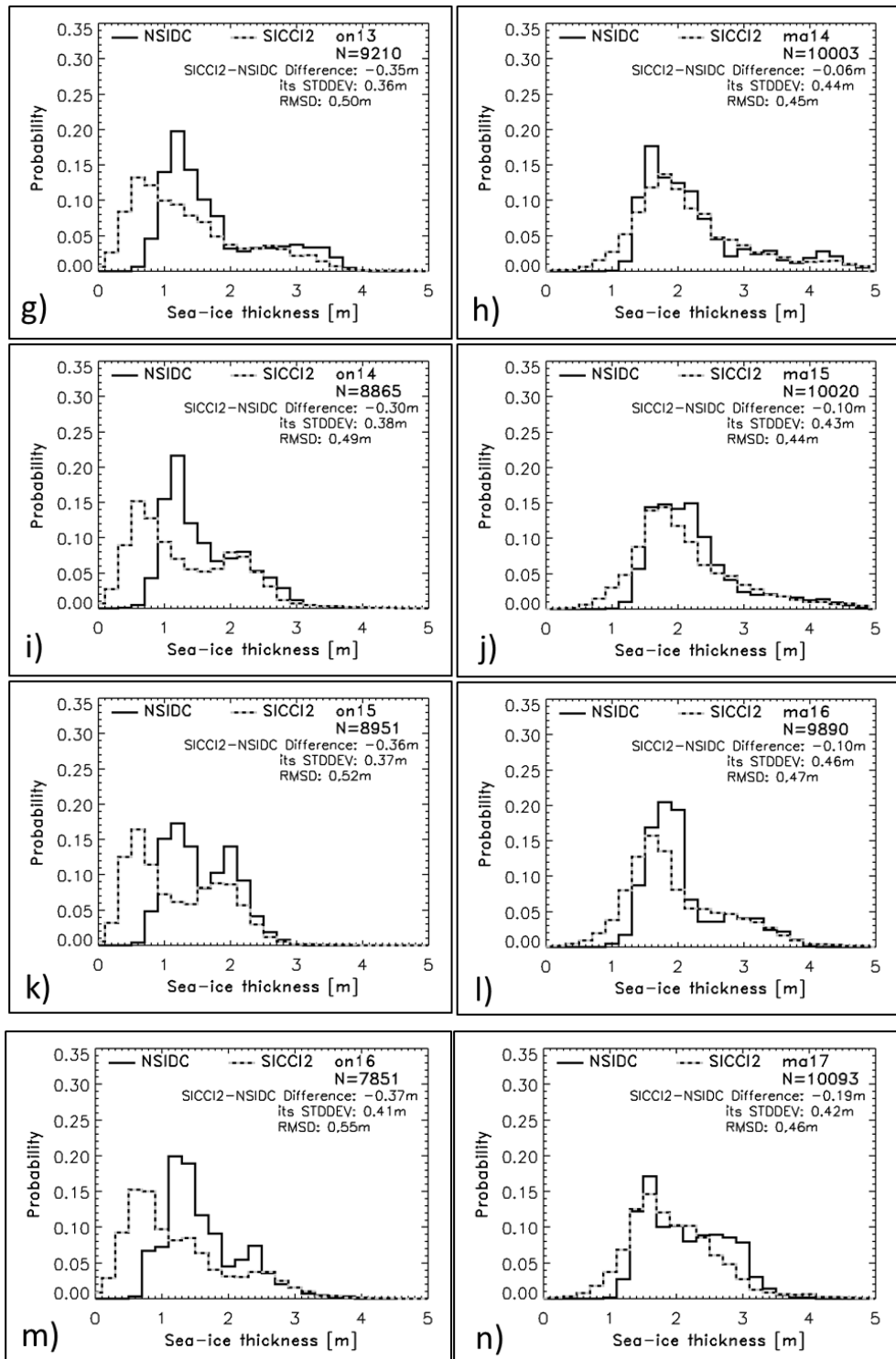


Figure 3-113 continued for winters 2013/14 through 2016/17.

Figure 3-113 illustrates that the histograms shown in Figure 3-111 and Figure 3-112 were kind of typical for the CS-2 period 2010/11 through 2016/17. For fall (on10 through on16, Figure 3-113 left column) we find

without exception that the modal value of the NSIDC SIT is at ~ 1.0 to 1.2 m while for SICCI-2 SIT the modal values is ~ 0.6 m. Accordingly, SICCI-2 SIT has considerable more thin (< 1.0 m) sea ice than NSIDC SIT in every fall. The tailing off towards thick (> 2.0 m) is more similar for both products. Both products agree in the number of modes for six of the seven fall periods with an uni-modal SIT distribution in 2011 and 2012, and a bi-modal SIT distribution in 2010, 2013, 2014, and 2015. In 2016, SICCI-2 offers three modes while NSIDC only has two modes. In case two modes are present NSIDC has a slightly (by ~ 0.2 m) larger modal SIT value. See Table 3-19 for a summary.

For spring (ma11 through ma17, Figure 3-113, right column) histograms agree better. In particular the modal values agree within 0.2 m. The tailing off towards thick (> 2.5 m) is remarkably similar for ma13 (Figure 3-113 f) and ma15 (Figure 3-113 j), not in too good agreement for ma11 and ma17 (Figure 3-113 b,n), but reasonably similar for the other years. Without exception, SICCI-2 has thinner (< 1.0 m) sea ice than NSIDC. Overall these results in a considerably smaller overall difference between both data sets for spring compared to fall (see Table 3-19).

Table 3-19: Per period (fall or spring) mean SICCI-2 SIT, NSIDC SIT, the difference SICCI-2 minus NSIDC, the RMSD, the linear correlation, and the count N of collocated data pairs. Bold numbers at the end provide the averages over all ON, all MA, and all ON and MA values. Standard deviations 1σ given at the end are the averages of the respective values of the previous rows.

Period	SIT _{SICCI2} $\pm 1\sigma$	SIT _{NSIDC} $\pm 1\sigma$	SIT _{DIFF} $\pm 1\sigma$	RMSD	Corr	N
ON10	1.32 ± 0.67	1.63 ± 0.55	-0.31 ± 0.35	0.47	0.85	9013
MA11	2.18 ± 0.67	2.20 ± 0.65	-0.02 ± 0.40	0.41	0.81	9995
ON11	1.06 ± 0.49	1.37 ± 0.33	-0.31 ± 0.32	0.45	0.76	9062
MA12	2.00 ± 0.65	2.06 ± 0.52	-0.06 ± 0.41	0.41	0.79	10051
ON12	1.15 ± 0.59	1.44 ± 0.45	-0.29 ± 0.36	0.47	0.79	8818
MA13	1.95 ± 0.60	1.98 ± 0.46	-0.03 ± 0.37	0.37	0.79	10037
ON13	1.48 ± 0.86	1.83 ± 0.77	-0.35 ± 0.36	0.50	0.91	9210
MA14	2.31 ± 0.91	2.37 ± 0.85	-0.06 ± 0.44	0.45	0.88	10003
ON14	1.41 ± 0.77	1.71 ± 0.60	-0.30 ± 0.38	0.49	0.88	8865
MA15	2.25 ± 0.86	2.36 ± 0.71	-0.10 ± 0.43	0.44	0.87	10020
ON15	1.30 ± 0.68	1.66 ± 0.48	-0.36 ± 0.37	0.52	0.85	8951
MA16	2.09 ± 0.78	2.19 ± 0.61	-0.10 ± 0.46	0.47	0.80	9890
ON16	1.36 ± 0.79	1.72 ± 0.58	-0.37 ± 0.41	0.55	0.86	7851
MA17	2.05 ± 0.67	2.24 ± 0.59	-0.19 ± 0.42	0.46	0.78	10093
ONs	1.30± 0.71	1.62± 0.64	-0.33± 0.36	0.49	0.84	
MAs	2.12± 0.73	2.20± 0.63	-0.08± 0.42	0.43	0.82	
All	1.71± 0.72	1.91± 0.63	-0.20± 0.39	0.46	0.83	

The scatterplots between SICCI-2 and NSIDC SIT shown in Figure 3-114 for all winters confirm the results from Figure 3-111 d) and Figure 3-112 d). We find a reasonable agreement for fall (ON-periods, left column) but we find a really good agreement for spring (MA-periods, right column), when the majority of the per- 0.2 m-bin SICCI-2 SIT values are located close to or on the 1-to-1 line; with a few exceptions the 1-to-1 line is included in the SIT range given by the standard deviation of the mean. For fall periods this is different, because of larger fraction of thin (< 1.0 m) sea ice in the SICCI-2 product. This causes a dip of the per- 0.2 m-bin SICCI-2 SIT values in every year which is located at NSIDC SIT values between 0.8 m and 1.5 m. For thicker (> 1.5 m) sea ice the 1-to-1 line is often within the range given by the standard deviation of the mean SIT; almost all these mean SIT values

are located below the 1-to-1 line. This is nicely summarized in Table 3-19 illustrating a mean SICCI-2 minus NSIDC SIT difference of -0.33 m for fall but only -0.08 m for spring; the overall (averaged over all winters and all periods) bias is -0.20 m, i.e. SICCI-2 SIT < NSIDC SIT. We note that the fall to spring increase in SIT is ~ 0.6 m for NSIDC and ~ 0.8 m for SICCI-2.

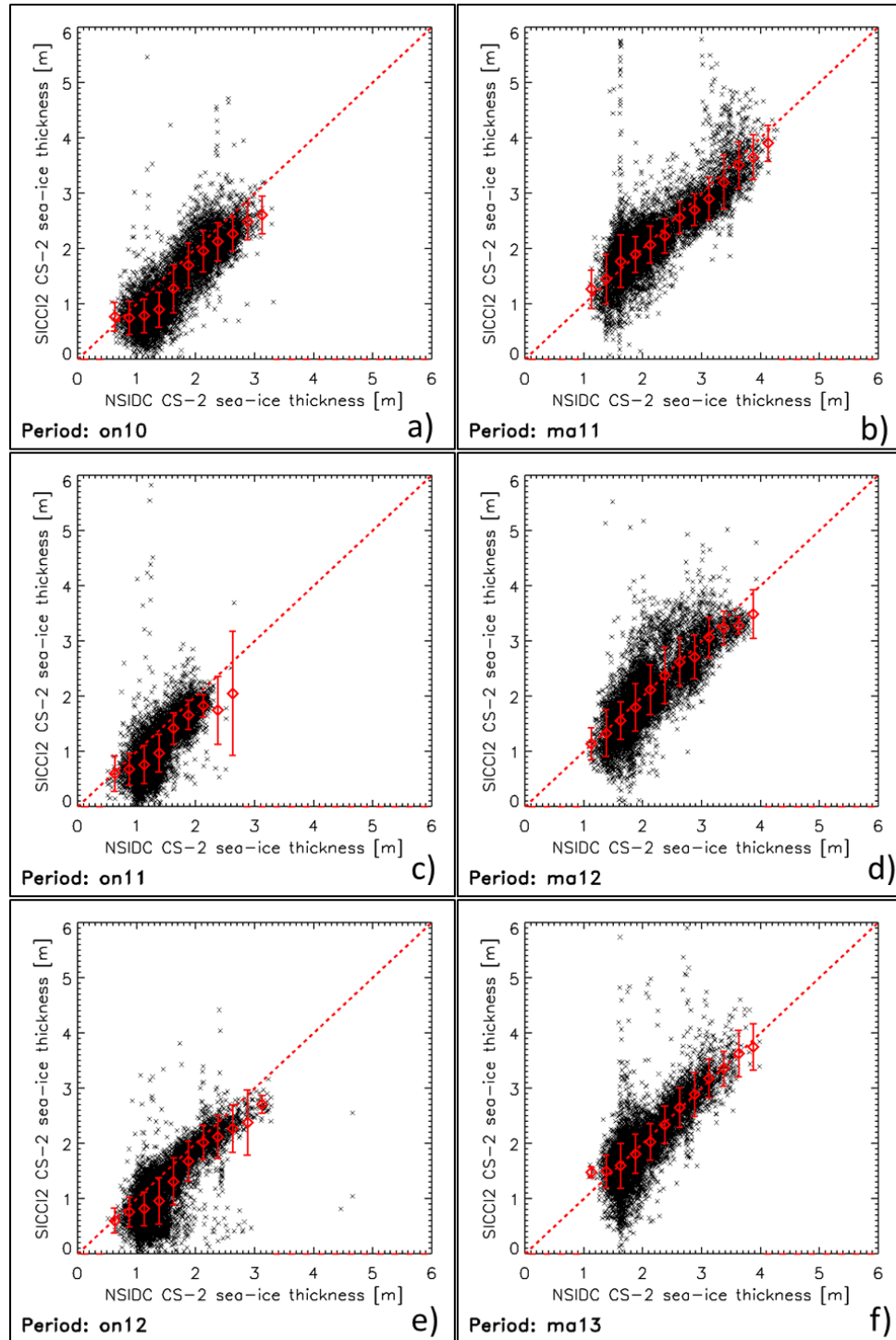


Figure 3-114: Scatterplot of individual data pairs SICCI-2 SIT versus NSIDC SIT (black crosses) and mean SICCI-2 SIT values derived for 0.2 m wide NSIDC SIT bins starting with 0.0 m to 0.2 m (red diamonds). Error bars denote one standard deviation; the dashed

red line denotes a 1-to-1 fit line. Like in Figure 3-113, the left (right) column is for ON (MA) periods for winters 2010/11 through 2012/13.

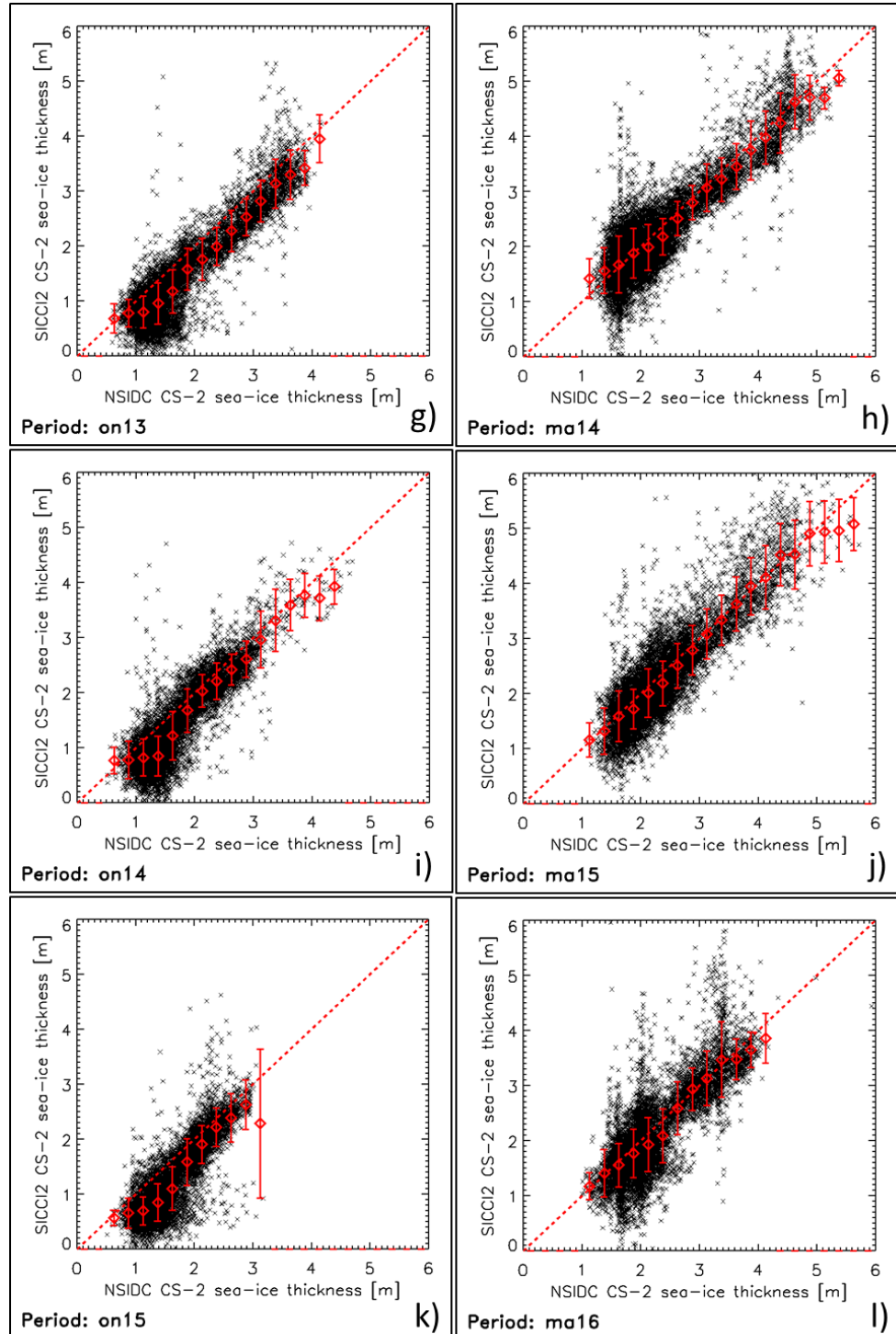


Figure 3-114 continued for winters 2013/14 through 2015/16.

With Figure 3-115 we try to answer the question how the observed differences between the two SIT products are distributed across the Arctic Ocean and where typically the largest and the smallest difference occur. In accordance with the results from Figure 3-113 and Figure 3-114 for fall periods, we find widespread negative (SICCI-2 SIT < NSIDC SIT) differences in at least 2/3 of the domain (Figure 3-115, left column). The differences are particularly large on the Eurasian side and in regions close to ice edge. We hypothesize that these occur predominantly over first-year ice (FYI).

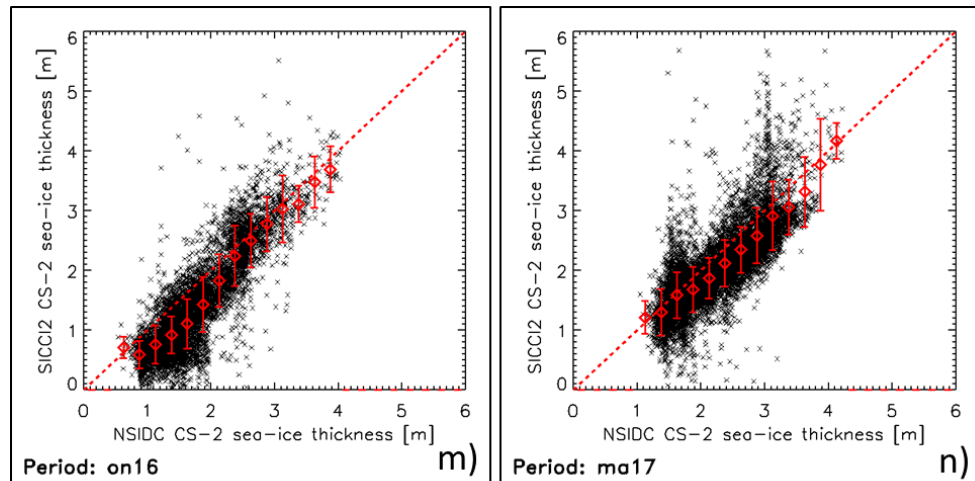


Figure 3-114 continued for winter 2016/17.

However, negative differences – albeit smaller in magnitude – also occur over regions known to be covered with multiyear ice (MYI), for example north of Greenland as in on11, on12, and on15 (Figure 3-115 c,e,k). It is fair to state that SIT differences are, on average, smallest over MYI regions for the fall periods.

For the spring periods (Figure 3-115, right column), we find a larger spatiotemporal variability of regions with negative and positive SIT differences. Often the transition between positive and negative SIT differences is quite abrupt as, for instance, in the central Arctic on the Pacific side of the observation data gap (Figure 3-115 d) or in the Beaufort Sea (Figure 3-115 l). Large (> 1.0 m) positive (SICCI-2 SIT > NSIDC SIT) occur predominantly north of the Canadian Arctic Archipelago and in isolated spots in the Laptev and East Siberian Seas. Some of the differences even look like speckle noise (see Figure 3-115 j) Lincoln Sea). The spring period with the smoothest distribution of SIT differences is ma13 (Figure 3-115 f). The large patch of positive SIT differences we reported about already in Figure 3-112 d) (see Figure 3-115 d) occurred several times within our period of interest. We find a similar pattern in periods ma14 through ma16 (Figure 3-115 h,j,l). Finally, important to note are, to our opinion, also the large regions of widespread negative (SICCI-2 SIT < NSIDC SIT) differences in the entire Laptev Sea (Figure 3-115 j), north of the Chukchi Sea (Figure 3-115 l), and a large part of the central Arctic (Figure 3-115 n).

Since both data sets use a modified version of the snow-depth climatology of Warren et al. [RD-08], modified in that extent that the snow depth is set to half the climatological value over FYI, we hypothesize that the observed difference can possibly not be explained by a difference in the snow depth products used. Remaining differences are i) the different freeboard retrieval and ii) the difference ice-type product used; NSIDC uses the OSI-403b sea-ice type product [RD-30] while SICCI-2 applies a MYI concentration product produced purely on SSM/I and SSMIS data using a NASA-Team algorithm

based approach [RD-32]. A comparison of these two MYI concentration data sets would be required to rule out a potential influence by the sea-ice type products used in the freeboard-to-thickness conversion.

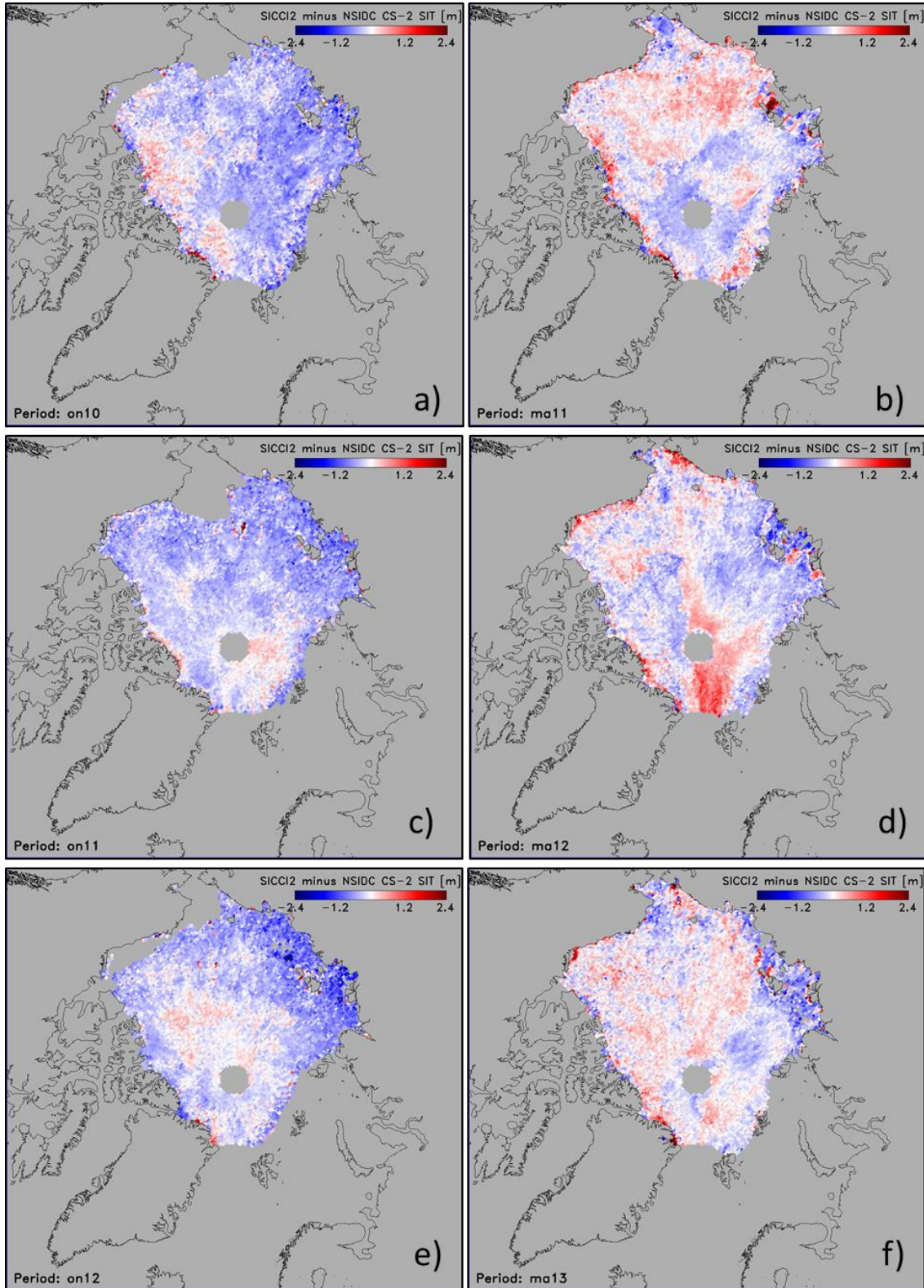


Figure 3-115: Distribution of the difference SICCI-2 SIT minus NSIDC SIT for fall (left column) and spring (right column) for winters 2010/11 through 2012/13.

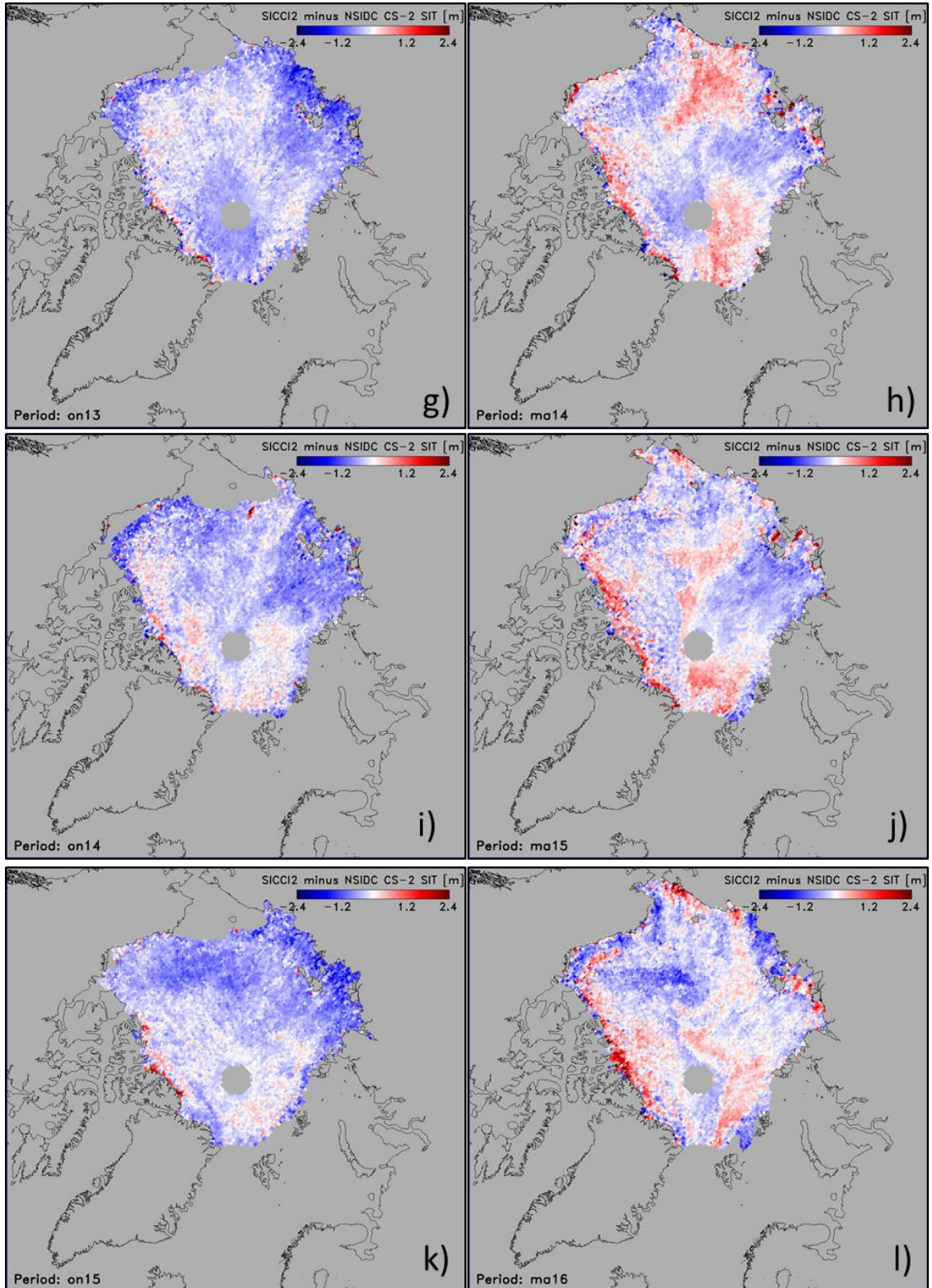


Figure 3-115 continued for winters 2013/14 through 2015/16.

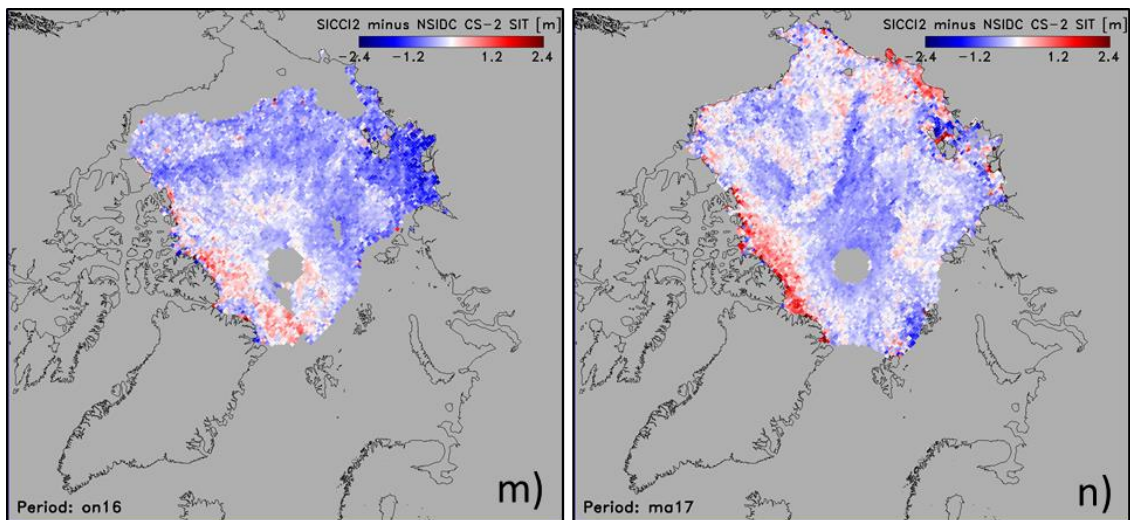


Figure 3-115 continued for winter 2016/17.

Before we take a look at some of the above-presented results separately for FYI and MYI we comment on Table 3-19. First, it is essential to note that the comparison based on CS-2 data provides substantially more data (compare Table 3-19 with Table 3-13) and hence is statistically more solid. Compared to the Section 3.6, where we carried out a comparison between SICCI-2 Envisat SIT and two different ICESat SIT data sets, we find substantially better correlation in this section. Here, correlations are > 0.8 while they were < 0.5 for the comparison presented in Section 3.6. As another notable difference to Section 3.6 we have much less variation in the SIT differences obtained for one season, i.e. fall or spring. For fall, differences range between -0.29 m and -0.37 m, and for spring differences range between -0.02 m and -0.19 m. See Table 3-13 and Table 3-16 and discussion of the results for comparison.

In the following, we repeat the analysis – similar to the approach used in section 3.6 – for grid cells with $> 85\%$ FYI and for grid cells with $> 85\%$ MYI to potentially arrive at a better understanding of the observed differences.

For fall 2011 (on11, Figure 3-116), we indeed find that most of the FYI area reveals considerable negative (SICCI-2 SIT $<$ NSIDC SIT) differences (Figure 3-116 a) which is confirmed by modal SIT values differing by 0.4 m (SICCI-2: 0.6 m, NSIDC: 1.0 m) (Figure 3-116 c). In contrast, over the area defined as MYI differences are substantially smaller which fits with the difference in modal SIT of only 0.2 m (SICCI-2: 1.4 m, NSIDC: 1.6 m) (Figure 3-116 b,d). The scatterplots (Figure 3-116 e,f) accordingly suggest an increasing amount of underestimation of NSIDC SIT by SICCI-2 SIT with a suggested linear regression slope of just ~ 0.5 for FYI. For MYI, the per- 0.2 m-bin mean SICCI-2 SIT values are considerably closer to the 1-to-1 line, suggesting slope close to 1. In agreement with that the mean difference is -0.45 m for FYI and -0.19 m for MYI.

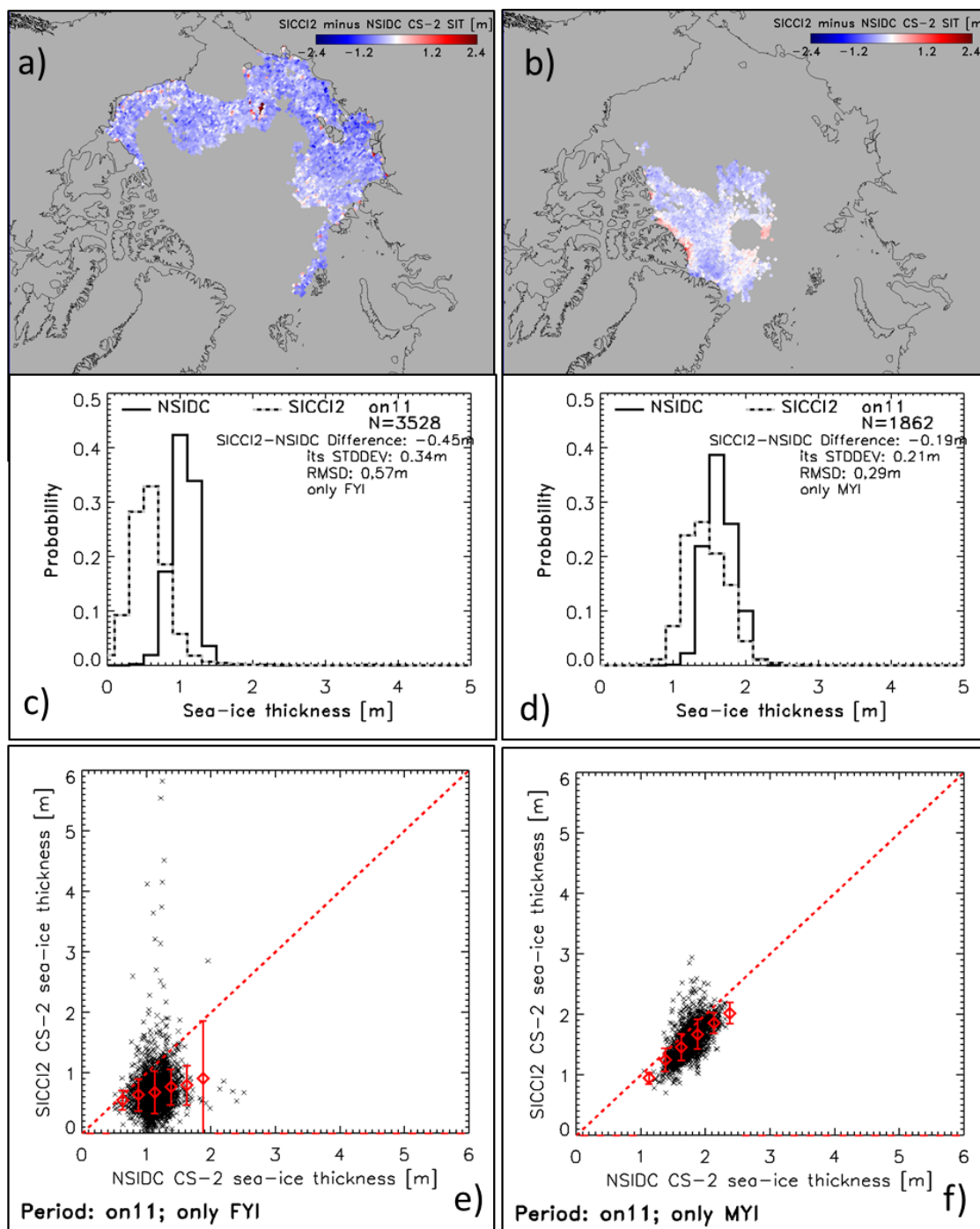


Figure 3-116: Comparison of SICCI-2 and NSIDC SIT for grid cells with FYI concentration > 85% (left column) and MYI concentration > 85% (right column) for fall 2011 (on11). Difference SICCI-2 SIT minus NSIDC SIT for a) > 85% FYI and b) > 85% MYI; histograms (c,d) and scatterplots (e,f) of the respective sub-sets of the data sets (compare Figure 3-111).

For spring 2012 (ma12, Figure 3-117), the agreement improves for both FYI and MYI. The difference maps reveal areas of both, positive and negative differences (Figure 3-117 a,b). The resulting histograms (Figure 3-117 c,d)

reveal agreement in modal SIT for FYI (1.6 m) and a difference in modal SIT of 0.2 m for MYI (SICCI-2: 2.6 m, NSIDC: 2.8 m). The reported larger fraction of thin (< 1.0 m) sea ice for spring periods (Figure 3-112 c), Figure 3-113, right column) shows up in the histogram for FYI but not for MYI. The tailing off to thin and thick sea ice agrees for MYI but overall the histogram is more narrow for NSIDC than for SICCI-2. The scatterplots (Figure 3-117 e,f) show favourable agreement between both SIT data sets for 75% of the per-0.2m-bin mean SICCI-2 SIT values. Accordingly, the mean SICCI-2 minus NSIDC SIT difference is -0.12 m for FYI and -0.08 m for MYI.

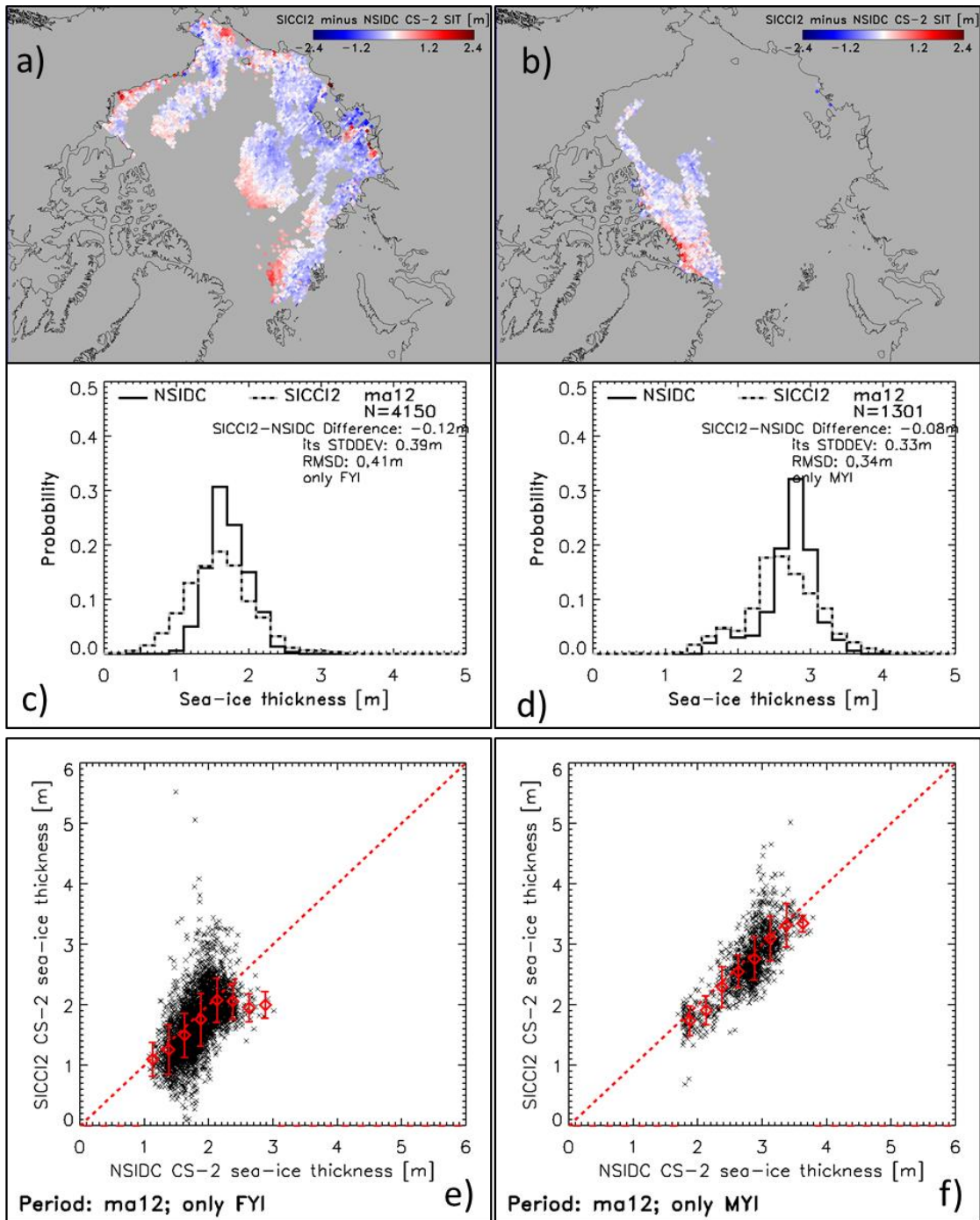


Figure 3-117: As Figure 3-116 but for spring 2012 (ma12).

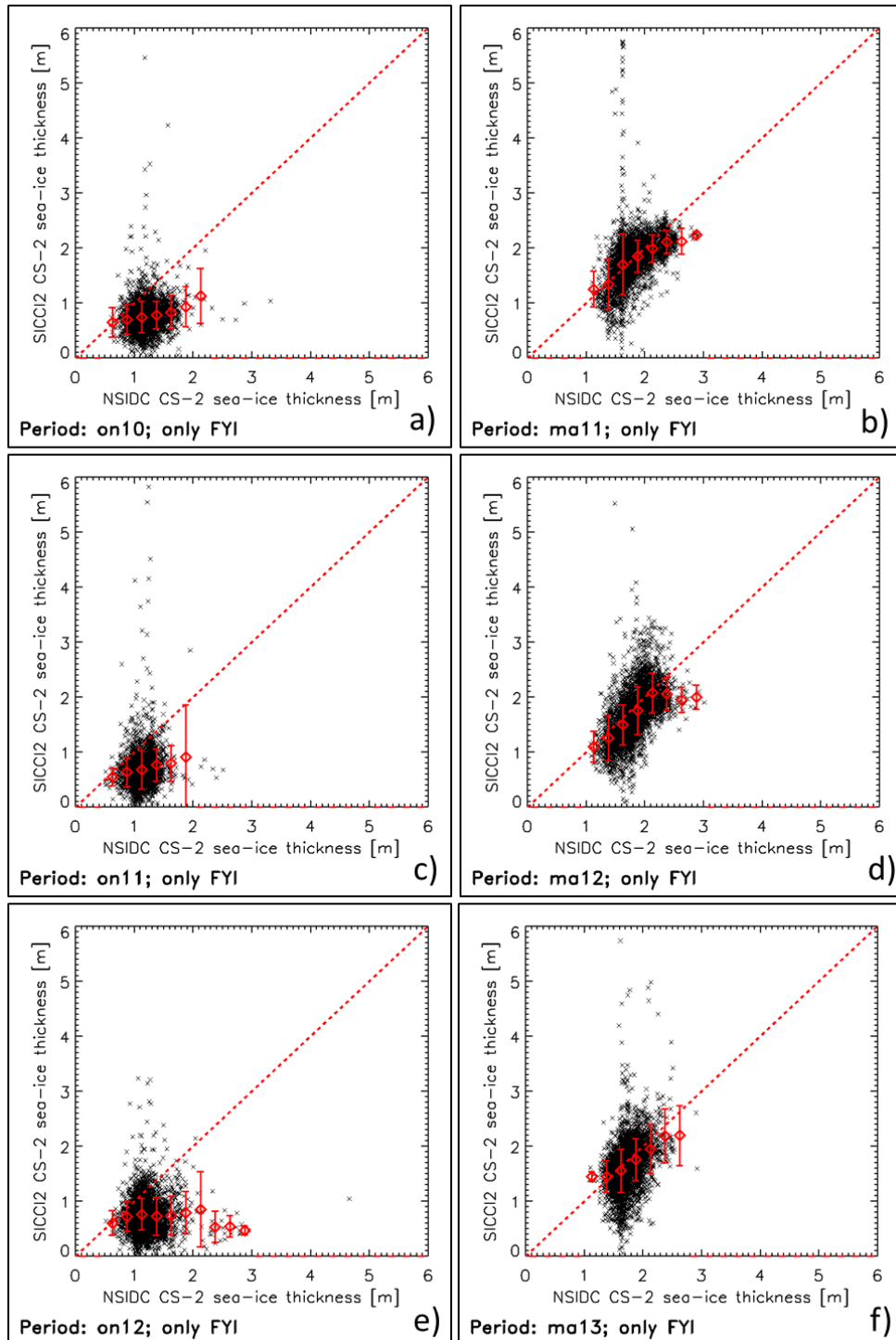


Figure 3-118: Scatterplot of individual data pairs SICCI-2 SIT versus NSIDC SIT (black crosses) and mean SICCI-2 SIT values derived for 0.2 m wide NSIDC SIT bins starting with 0.0 m to 0.2 m (red diamonds) for > 85% FYI concentration. Error bars denote one standard deviation; the dashed red line denotes a 1-to-1 fit line. Like

in Figure 3-114, the left (right) column is for ON (MA) periods for winters 2010/11 through 2012/13.

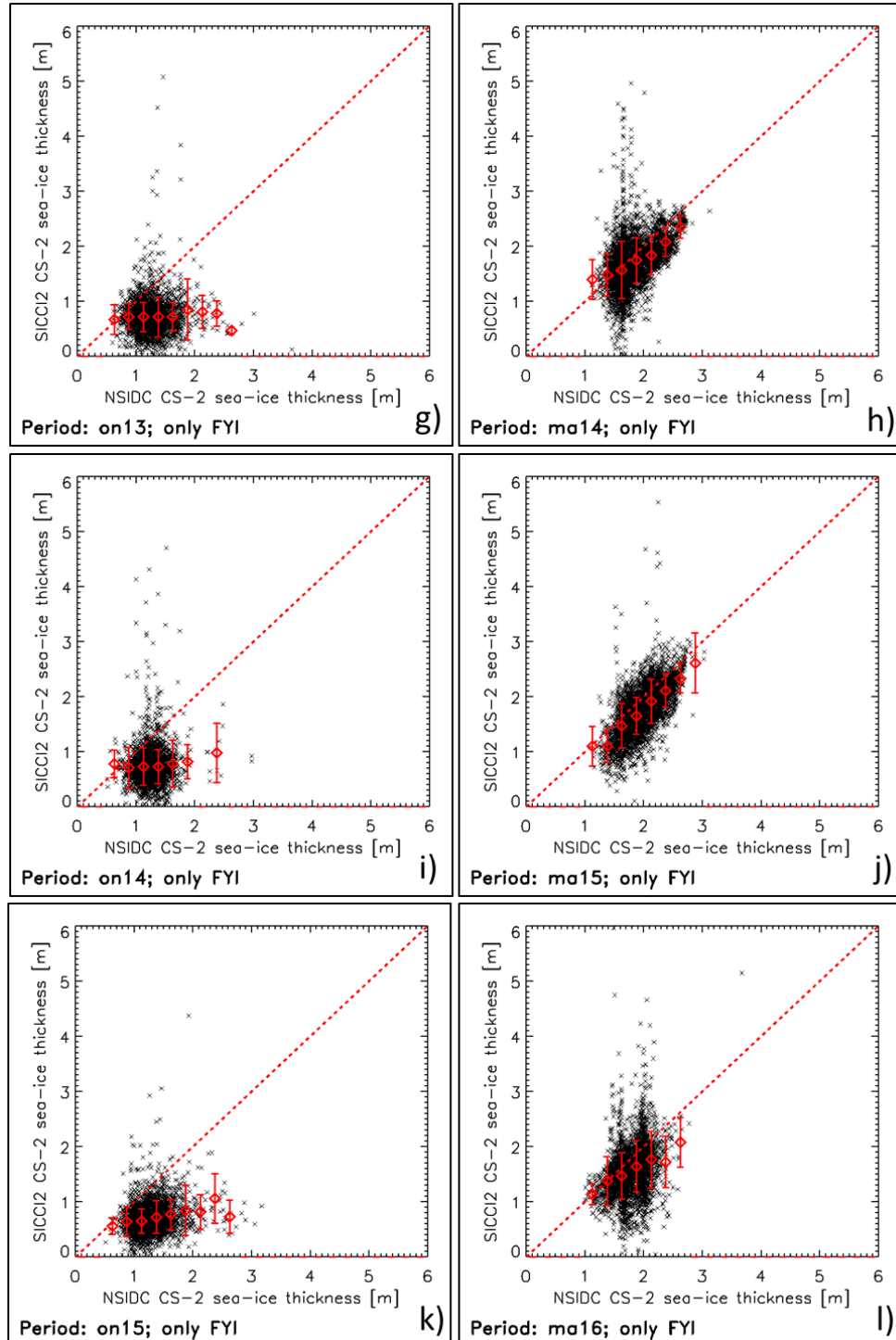


Figure 3-118 continued for winters 2013/14 through 2015/16.

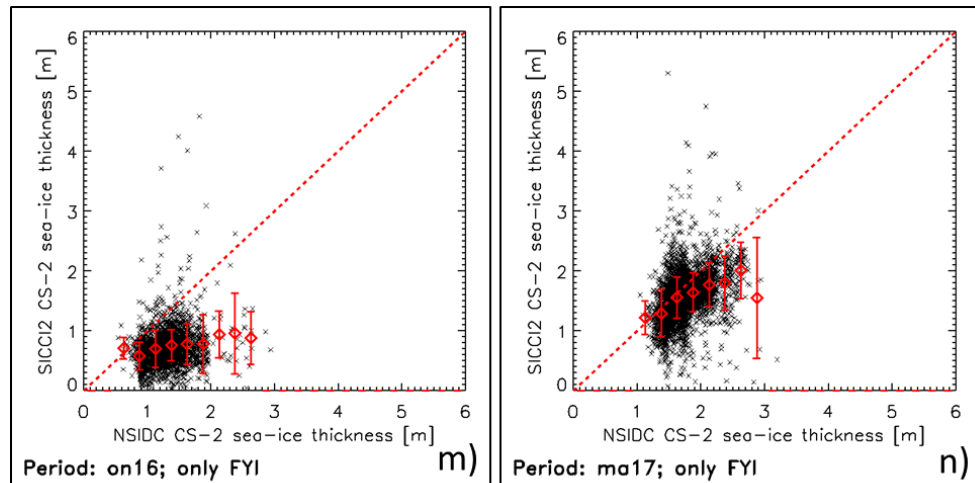


Figure 3-118 continued for winter 2016/17.

Focussing on FYI clearly reveals that the agreement between SICCI-2 SIT and NSIDC SIT is poor for fall (ON) periods (correlation: 0.12) but improves substantially for spring (MA) (Figure 3-118, left versus right column) periods (correlation: 0.45). Like we found in our comparison with ICESat SIT data (Section 3.6) there is little linear relationship between both SIT data sets for FYI in fall; a slope of a hypothetical linear regression through the per-0.2m-bin mean SICCI-2 SIT values would have a slope close to zero. In contrast, for spring, the majority of the per-0.2m-bin mean SICCI-2 SIT values are so close to the 1-to-1 line that the latter falls into the range given by the standard deviation of the mean. A fair linear relationship between the two SIT data sets is hence observed for FYI in spring; see also Table 3-20. We find that for FYI SICCI-2 SIT underestimates NSIDC SIT by ~ 0.5 m in fall and by ~ 0.15 m in spring. The fall-to-spring SIT increase for FYI is ~ 1.0 m for SICCI-2 but only ~ 0.6 m for NSIDC SIT.

Table 3-20: Per period (fall or spring) mean SICCI-2 SIT, NSIDC SIT, the difference SICCI-2 minus NSIDC, the RMSD, the linear correlation, and the count N of collocated data pairs for > 85% FYI concentration. Bold numbers at the end provide the averages over all ON, all MA, and all ON and MA values. Standard deviations 1σ given at the end are the averages of the respective values of the previous rows.

Period	SIT _{SICCI2} $\pm 1\sigma$	SIT _{NSIDC} $\pm 1\sigma$	SIT _{Diff} $\pm 1\sigma$	RMSD	Corr	N
ON10	0.75 ± 0.28	1.21 ± 0.21	-0.45 ± 0.32	0.55	0.15	3549
MA11	1.78 ± 0.47	1.81 ± 0.29	-0.03 ± 0.43	0.43	0.44	3621
ON11	0.69 ± 0.32	1.14 ± 0.17	-0.45 ± 0.34	0.57	0.16	3528
MA12	1.69 ± 0.47	1.81 ± 0.27	-0.12 ± 0.39	0.41	0.57	4150
ON12	0.75 ± 0.30	1.18 ± 0.21	-0.43 ± 0.36	0.56	0.01	4550
MA13	1.64 ± 0.42	1.72 ± 0.20	-0.08 ± 0.39	0.40	0.39	4757
ON13	0.72 ± 0.31	1.26 ± 0.26	-0.54 ± 0.40	0.67	0.03	2917
MA14	1.71 ± 0.48	1.83 ± 0.31	-0.12 ± 0.44	0.46	0.43	3768
ON14	0.73 ± 0.34	1.26 ± 0.21	-0.52 ± 0.39	0.65	0.06	2912
MA15	1.77 ± 0.46	2.00 ± 0.31	-0.22 ± 0.35	0.41	0.64	3730
ON15	0.69 ± 0.27	1.27 ± 0.28	-0.58 ± 0.35	0.68	0.20	3119
MA16	1.58 ± 0.48	1.79 ± 0.25	-0.21 ± 0.47	0.51	0.31	3234
ON16	0.72 ± 0.31	1.30 ± 0.29	-0.58 ± 0.38	0.70	0.21	2783
MA17	1.58 ± 0.39	1.75 ± 0.28	-0.18 ± 0.39	0.43	0.37	4185
ONs	0.72± 0.30	1.23± 0.23	-0.51± 0.36	0.63	0.12	

MAAs	1.68±0.45	1.82±0.27	-0.14±0.41	0.44	0.45	
All	1.20±0.38	1.52±0.25	-0.32±0.39	0.53	0.28	

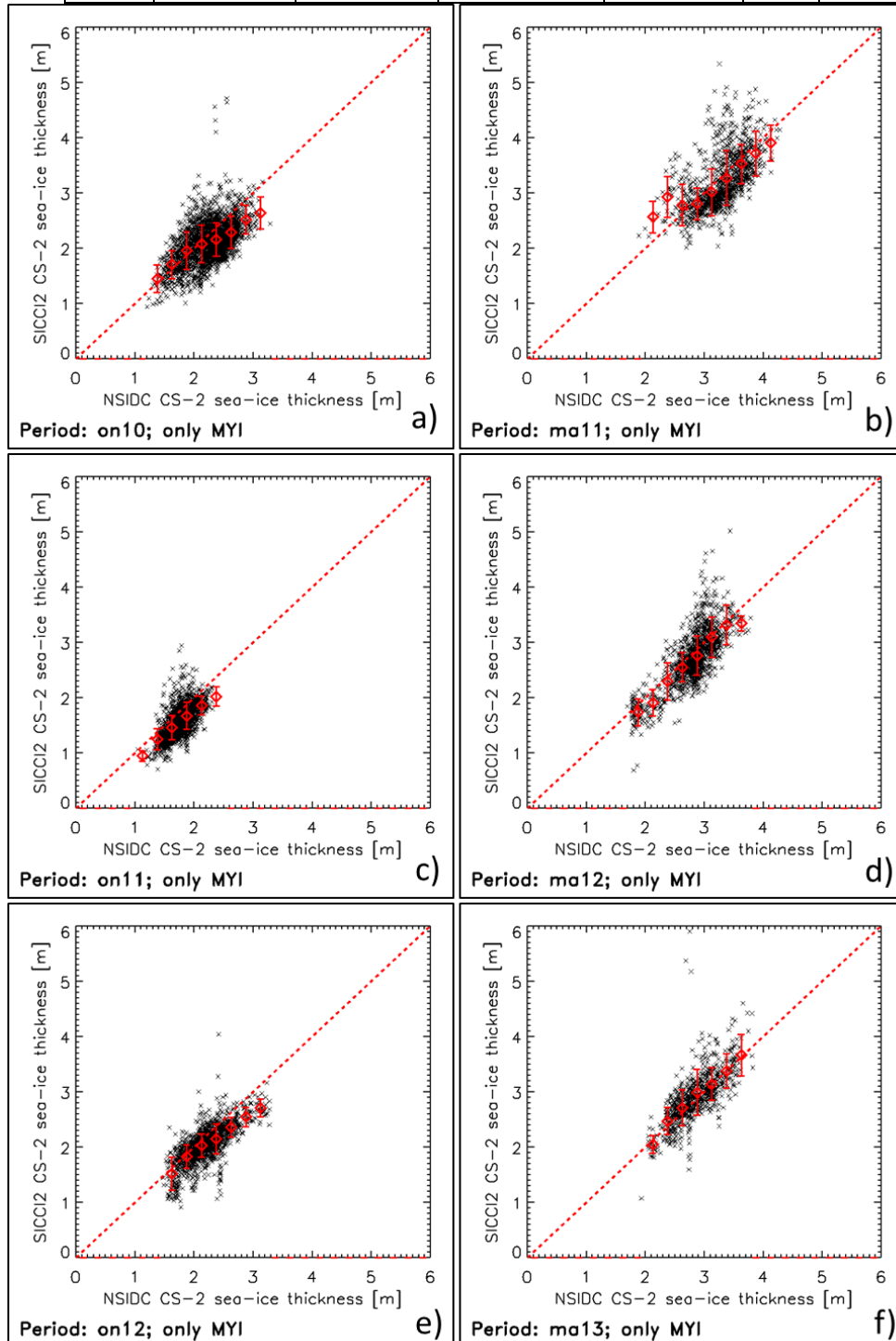


Figure 3-119: As Figure 3-118 but for > 85% MYI concentration.

For MYI (Figure 3-119) we find a considerable better agreement between the two SIT data sets. Many of the per-0.2m-bin mean SICCI-2 SIT values are located even on the 1-to-1 line and for the majority of these mean SIT values the 1-to-1 line falls within the range given by the standard deviation of the mean. In contrast to FYI, where we observed an underestimation for

almost all cases, here, for MYI, we have a good fraction of overestimation, i.e. per-0.2m-bin mean SICCI-2 SIT values above the 1-to-1 line (e.g. Figure 3-119 h,l).

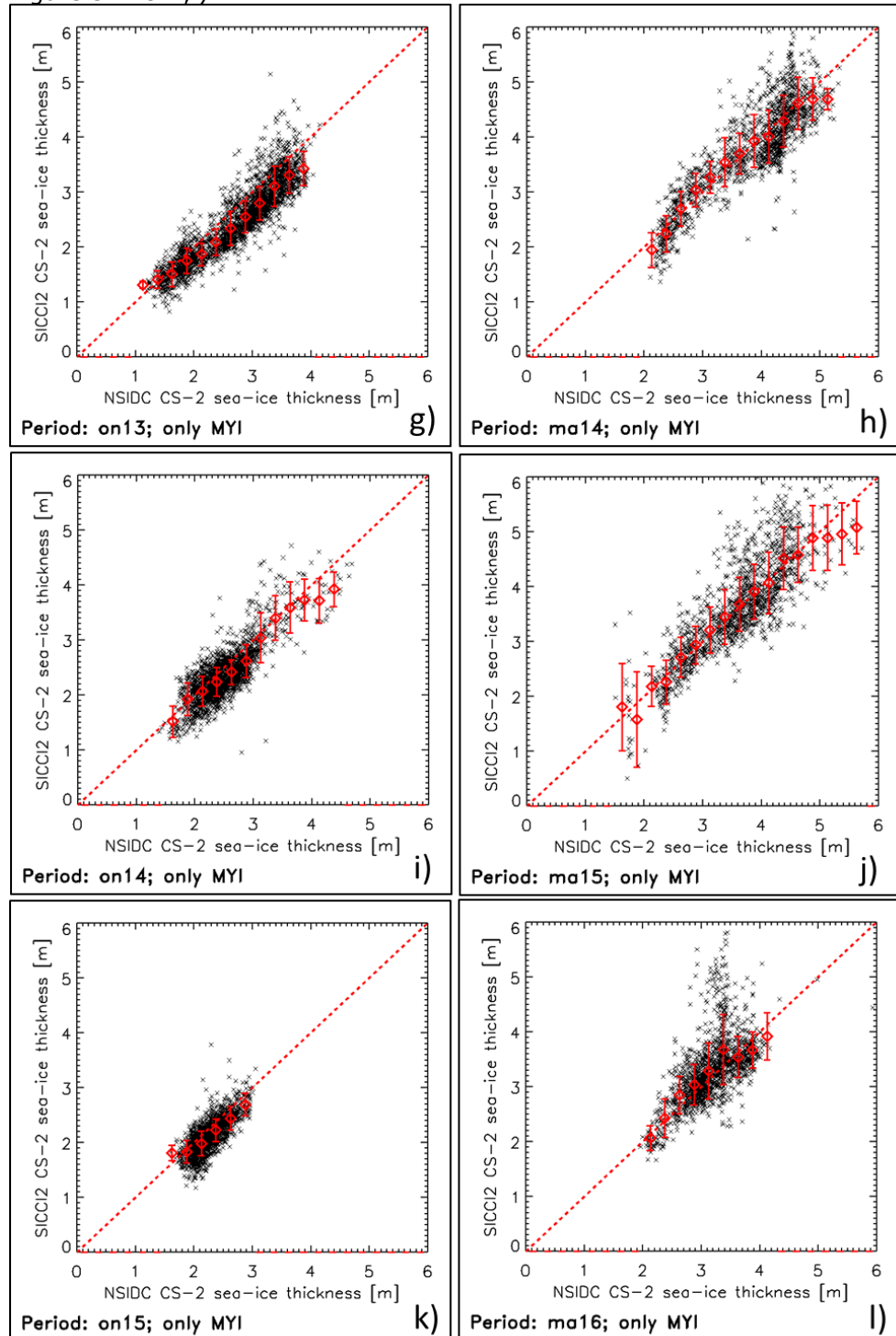


Figure 3-119 continued for winters 2013/14 through 2015/16.

These cases of SIT overestimation relative to the NSIDC SIT data sets occur mostly in spring, however. Table 3-21 summarizes the results and reveals in fact a few cases where for MYI SICCI-2 SIT > NSIDC SIT: MA16, MA15 and MA13. Overall, we find a negative difference, i.e. SICCI-2 SIT < NSIDC SIT, of -0.16 m for fall; for spring the difference is zero. The correlation between

the two data sets when constrained to MYI is ~ 0.7 and hence higher than for FYI but smaller than for the entire data set for which the correlation is > 0.8 (Table 3-19).

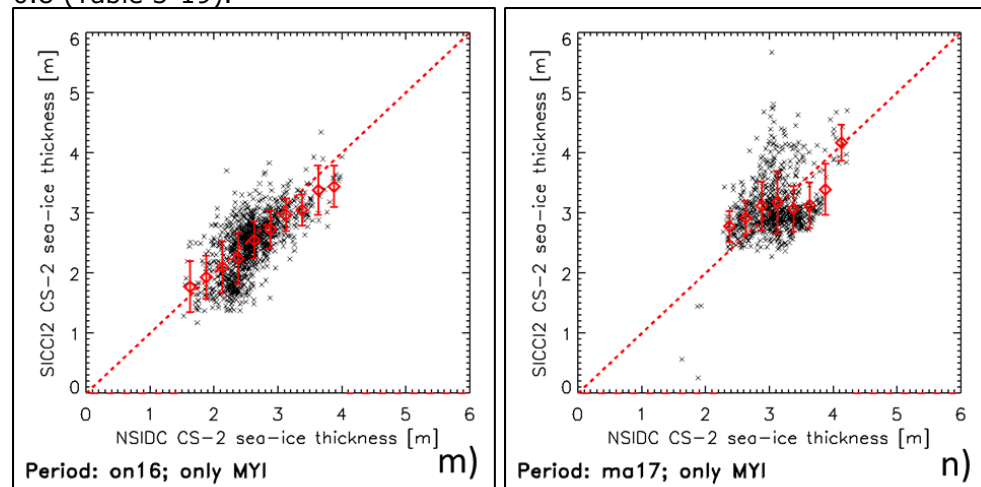


Figure 3-119 continued for winter 2016/17.

Table 3-21: Per period (fall or spring) mean SICCI-2 SIT, NSIDC SIT, the difference SICCI-2 minus NSIDC, the RMSD, the linear correlation, and the count N of collocated data pairs for $> 85\%$ MYI concentration. Bold numbers at the end provide the averages over all ON, all MA, and all ON and MA values. Standard deviations 1σ given at the end are the averages of the respective values of the previous rows.

Period	SIT _{SICCI2} $\pm 1\sigma$	SIT _{NSIDC} $\pm 1\sigma$	SIT _{DIFF} $\pm 1\sigma$	RMSD	Corr	N
ON10	2.11 ± 0.36	2.25 ± 0.34	-0.14 ± 0.34	0.37	0.53	2512
MA11	3.21 ± 0.51	3.29 ± 0.38	-0.07 ± 0.42	0.43	0.59	1085
ON11	1.56 ± 0.28	1.75 ± 0.20	-0.19 ± 0.21	0.29	0.66	1862
MA12	2.71 ± 0.52	2.80 ± 0.38	-0.08 ± 0.33	0.34	0.78	1301
ON12	2.05 ± 0.34	2.20 ± 0.32	-0.15 ± 0.24	0.29	0.73	1472
MA13	2.90 ± 0.48	2.84 ± 0.36	0.06 ± 0.33	0.33	0.73	772
ON13	2.48 ± 0.68	2.73 ± 0.69	-0.26 ± 0.30	0.39	0.91	2553
MA14	3.79 ± 0.86	3.82 ± 0.79	-0.03 ± 0.43	0.43	0.87	1394
ON14	2.37 ± 0.49	2.50 ± 0.44	-0.13 ± 0.29	0.32	0.81	2080
MA15	3.62 ± 0.88	3.59 ± 0.74	0.03 ± 0.49	0.49	0.83	1355
ON15	2.12 ± 0.31	2.26 ± 0.25	-0.13 ± 0.20	0.24	0.75	1896
MA16	3.27 ± 0.61	3.15 ± 0.43	0.13 ± 0.43	0.50	0.62	1522
ON16	2.46 ± 0.49	2.57 ± 0.39	-0.11 ± 0.36	0.38	0.68	1130
MA17	3.09 ± 0.48	3.09 ± 0.37	0.00 ± 0.50	0.48	0.33	816
ONs	2.16± 0.42	2.32± 0.38	-0.16± 0.28	0.33	0.72	
MAs	3.23± 0.62	3.23± 0.49	0.01± 0.43	0.43	0.68	
All	2.70± 0.52	2.77± 0.44	-0.07± 0.35	0.38	0.70	

We note that for the two years with the maximum mean SIT in spring (MA14 and MA15) the difference between the data sets is particularly small. We note further that the fall-to-spring SIT increase is ~ 0.95 m for SICCI-2 and ~ 0.9 m for NSIDC. In relation to the fall-to-spring SIT increase for FYI: ~ 1.0 m and ~ 0.6 m these increases do not look too reasonable – especially for the NSIDC SIT data set. It is unlikely that SIT growth over winter is larger for MYI than FYI as is the case for NSIDC: ~ 0.9 m versus ~ 0.6 m and SICCI-2: ~ 1.05 m versus ~ 0.95 m.

In conclusion and with an eye on the results of section 3.6 we note that for this comparison between two CS-2 SIT data sets better agreement is achieved for MYI (average bias 0.07 m) while over FYI the average bias is larger: 0.30 m; this is opposite to the results in section 3.6.

Part II: Comparison to the UCL CS-2 SIT data set

Figure 3-120 and Figure 3-121 give – like Figure 3-111 and Figure 3-112 – an overview of the SIT distribution of both data sets for fall 2011 and spring 2012, respectively, together with a map of their difference, the SIT histograms and scatterplots.

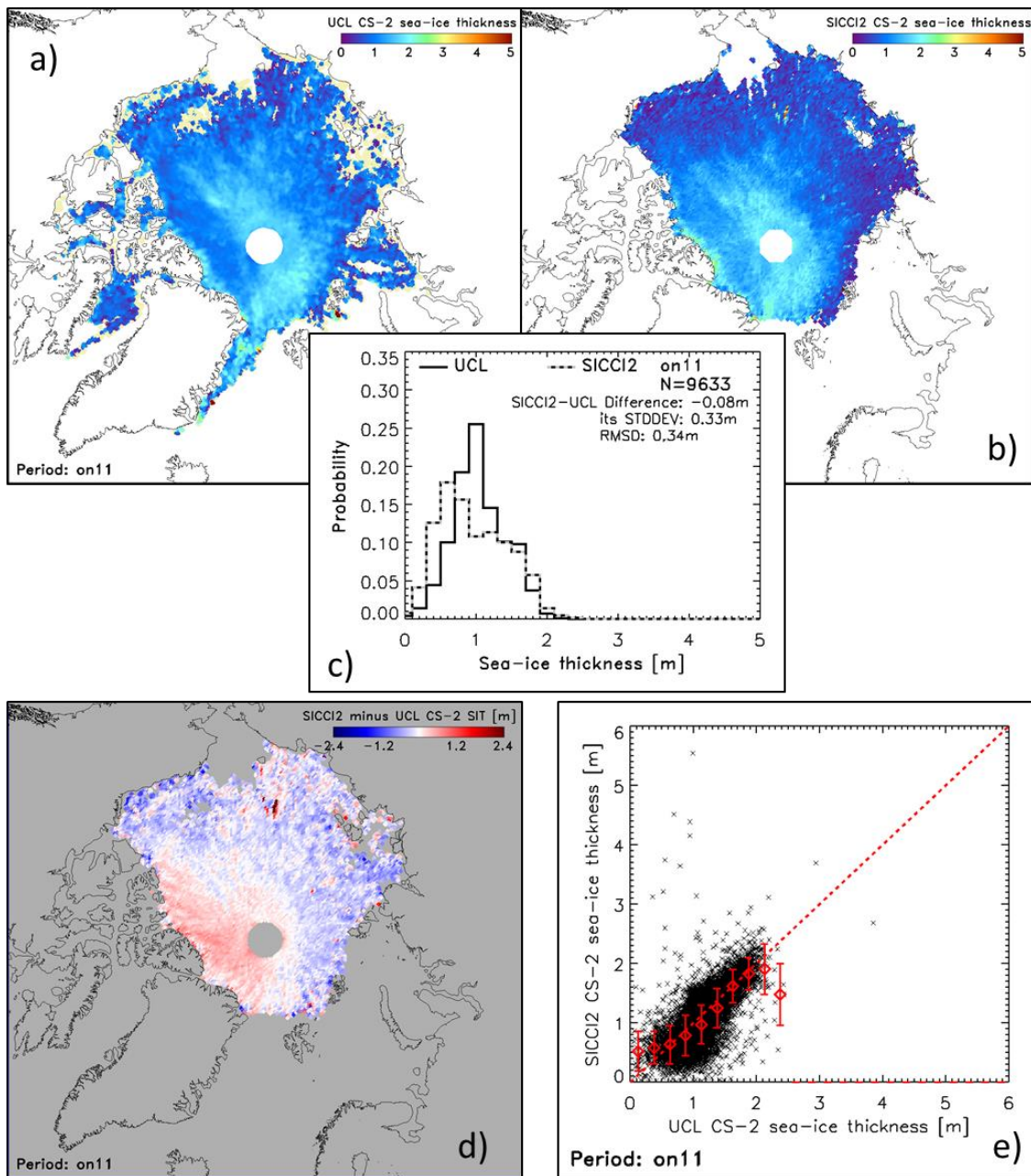


Figure 3-120: Inter-comparison of UCL versus SICCI-2 CS-2 sea-ice thickness (SIT) for fall 2011 (on11). a) UCL SIT, b) SICCI-2 SIT, the white circular disk denotes the polar data gap; d) Difference SICCI-2 minus UCL SIT; c) histograms of the SIT from both data set for coinciding grid cells together with the count of data pairs "N", the root mean squared difference "RMSD" as well as the mean difference and its standard deviation; e) scatterplot of all co-located SIT values (black crosses) superposed by the mean SICCI-2 SIT value per 0.2 m UCL SIT bin. The error bars denote plus/minus one standard deviation. The red dashed line is the 1-to-1 fit line.

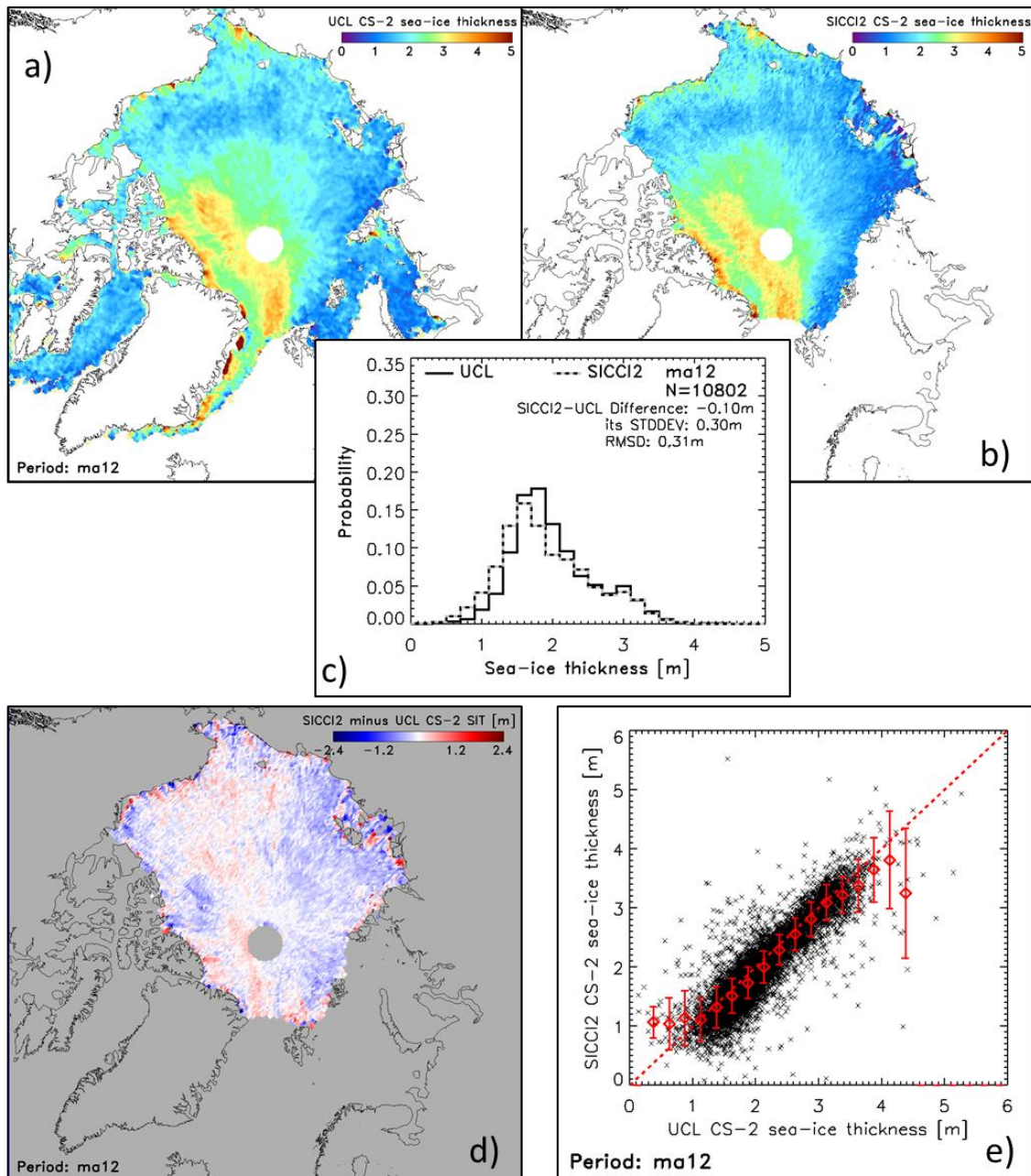


Figure 3-121: As Figure 3-120 but for spring 2012 (ma12).

The spatial distribution of these two SIT data is more similar than for the NSIDC SIT data set (see Figure 3-111 and Figure 3-112). For fall (Figure 3-120 a,b) this applies in particular to the regions of different SIT north of Greenland and Ellesmere Island where both data sets reveal relatively high SIT close to the coast followed by a broad area of reduced SIT before SIT again increases towards the central Arctic. We do also find considerably more thin (< 1.0 m) sea ice in the UCL SIT product than in the NSIDC SIT product. This is confirmed by the histograms (Figure 3-120 c). SICCI-2 SIT still has more of this thin sea ice, yes, but also UCL SIT has a substantial fraction of it. However, similar to NSIDC SIT the modal SIT value is 1.0 m for UCL SIT and 0.6 m for SICCI-2 SIT, the difference hence being the same as for NSIDC SIT. The tailing off towards thick (> 1.5 m) sea ice is similar in both data sets. The difference map (Figure 3-120 d) reveals a large fraction of grid cells with near zero SIT difference. Still we find one region of widespread positive differences (SICCI-2 SIT $>$ UCL SIT) north of Greenland and the Canadian Arctic Archipelago and a widespread coverage with negative differences (SICCI-2 SIT $<$ UCL SIT) towards the seas south of the central Arctic such as the Laptev Sea. However, the net overall difference is less than 0.1 m: -0.08 m and hence considerably smaller than for NSIDC Sit (Figure 3-111). Also the scatterplot (Figure 3-120 e) shows reasonable agreement between the two data sets. We note that some isolated several grid-cell size large large SIT differences (Laptev Sea and north of Wrangel Island) occurred also in the difference map for NSIDC SIT (Figure 3-111 d) and can possibly be attributed with a bias in the retrieved freeboard from SICCI-2.

Already Figure 3-120 a,b) suggests a greater degree of detail in the SICCI-2 SIT maps which is not present in the UCL SIT maps despite the fact that those data are on a 5 km grid. This is even more visible in Figure 3-121 a,b). This "smeared" appearance of the UCL SIT maps compared to the SICCI-2 SIT maps can possibly attributed to the 25 km search radius used to create a UCL SIT value – which is effectively a reduction of the grid resolution compared to SICCI-2 SIT.

The SIT distribution for spring 2012 (Figure 3-121 a,b) is even more similar. In contrast to the NSIDC SIT (Figure 3-112 a,b), also in the area north of the Fram Strait both SIT data sets are very similar – as is also visible in the SIT difference map (Figure 3-121 d). This difference map reveals that for basically the entire Arctic Ocean the SIT differences are $< |0.5|$ m; only in some coastal areas as in the southern Beaufort Sea and in the southern Laptev Sea differences are higher – but without a systematic over- or underestimation. This is nicely confirmed by the scatterplot (Figure 3-121 e) where per-0.2m-bin mean SICCI-2 SIT values are situated almost on the 1-to-1 line over the range 1.0 m through 3.5 m. At the high end, SICCI-2 SIT is too low while at the low end SICCI-2 SIT is too high. The corresponding histograms (Figure 3-121 c) hence also basically suggest an offset of the SIT distributions relative to each other by roughly one bin at the side of the histogram facing low thickness values. Modal values differ by 0.2 m: SICCI-2 has 1.6 m, UCL has 1.8 m. Tailing off towards thick (> 2.5 m) sea ice is very similar for both SIT products. Like for fall the overall difference is slightly negative: -0.10 m.

The interesting feature with the SIT difference map of spring 2012 is, that in the area north of Fram Strait, where SICCI-2 SIT and NSIDC SIT differed most (Figure 3-112 d), UCL SIT and SICCI-2 SIT agree with each other. This supports the hypothesis that the difference observed in that area in Figure 3-112 d) can be attributed to the different freeboard retrieval methods applied.

When looking at the SIT distributions in form of histograms (Figure 3-122) we find for fall (left column), that modal SIT values for SICCI-2 are ~ 0.6 m and with that between 0.2m and 0.4 m smaller than for UCL. For every fall

we find that SICCI-2 SIT has more thin (< 1.0 m) sea ice and more thick (> 1.5 m) sea ice than UCL SIT. If there is a bi-modal SIT distribution such as in on10, on14 and on15 (Figure 3-122 a,i,k) we find that the modal values are closer together for UCL than for SICCI-2 SIT. We hypothesize that these differences can primarily be attributed to the different averaging scales employed: 25 km (SICCI-2) versus 50 km (UCL, [RD-31]). A different treatment of the snow cover and usage of a different ice-type mask certainly play a role as well. For spring (right column), we find modal SICCI-2 SIT values which either equals or underestimates modal UCL SIT by up to 0.2 m. We find thinner (< 1.5 m) sea ice for SICCI-2 while the tailing off at thick (> 2.5 m) is quite similar in both products. The consequence for both seasons is that, on average, SICCI-2 SIT underestimates UCL SIT by between 0.05 m and 0.1 m (see Table 3-22).

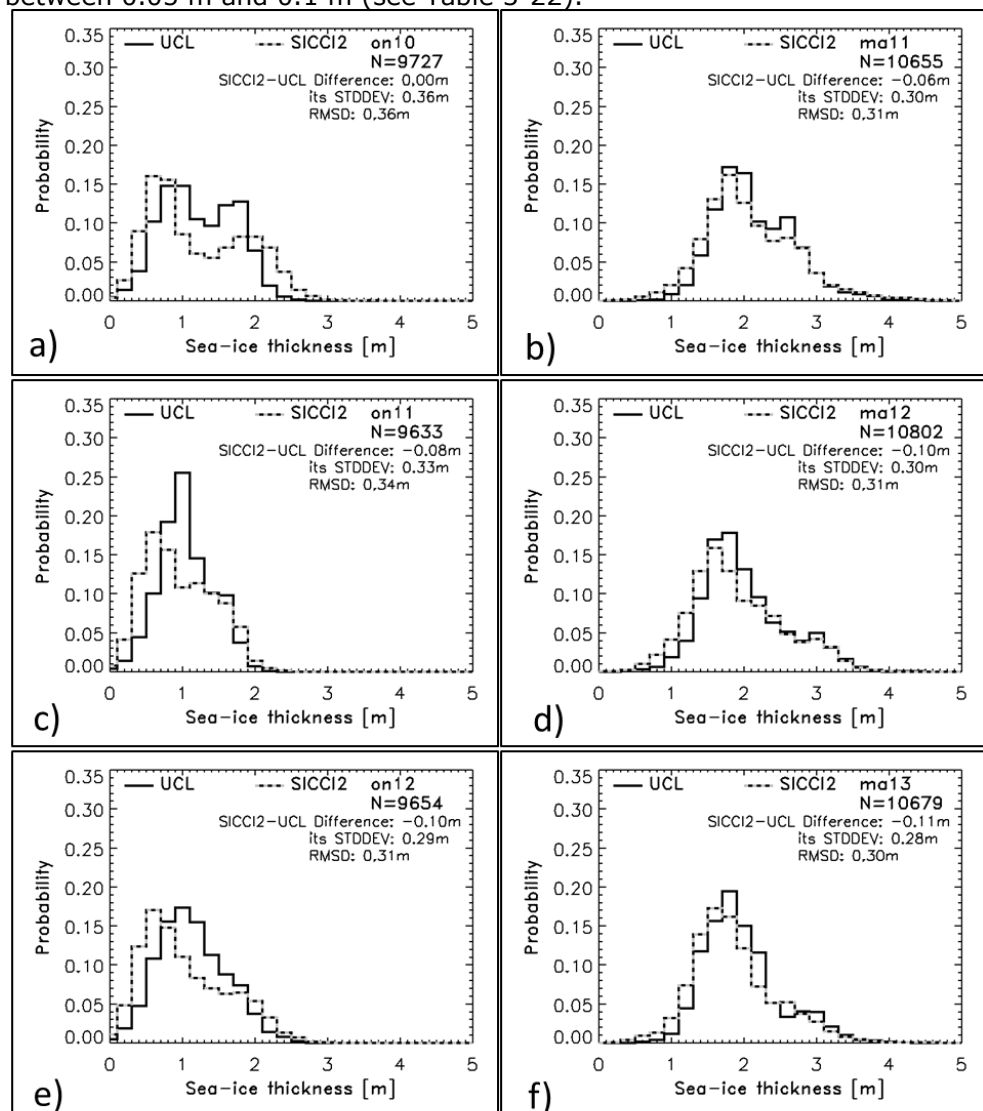


Figure 3-122: Histograms of UCL and SICCI-2 SIT for the Arctic Ocean for fall (ON periods, left column) and spring (MA periods, right column) for winters 2010/11 through 2012/13. In each image the number of valid data pairs, the mean difference SICCI-2 minus UCL SIT and its standard deviation and the RMSD is given (see also Table 3-22 and compare to Figure 3-113)

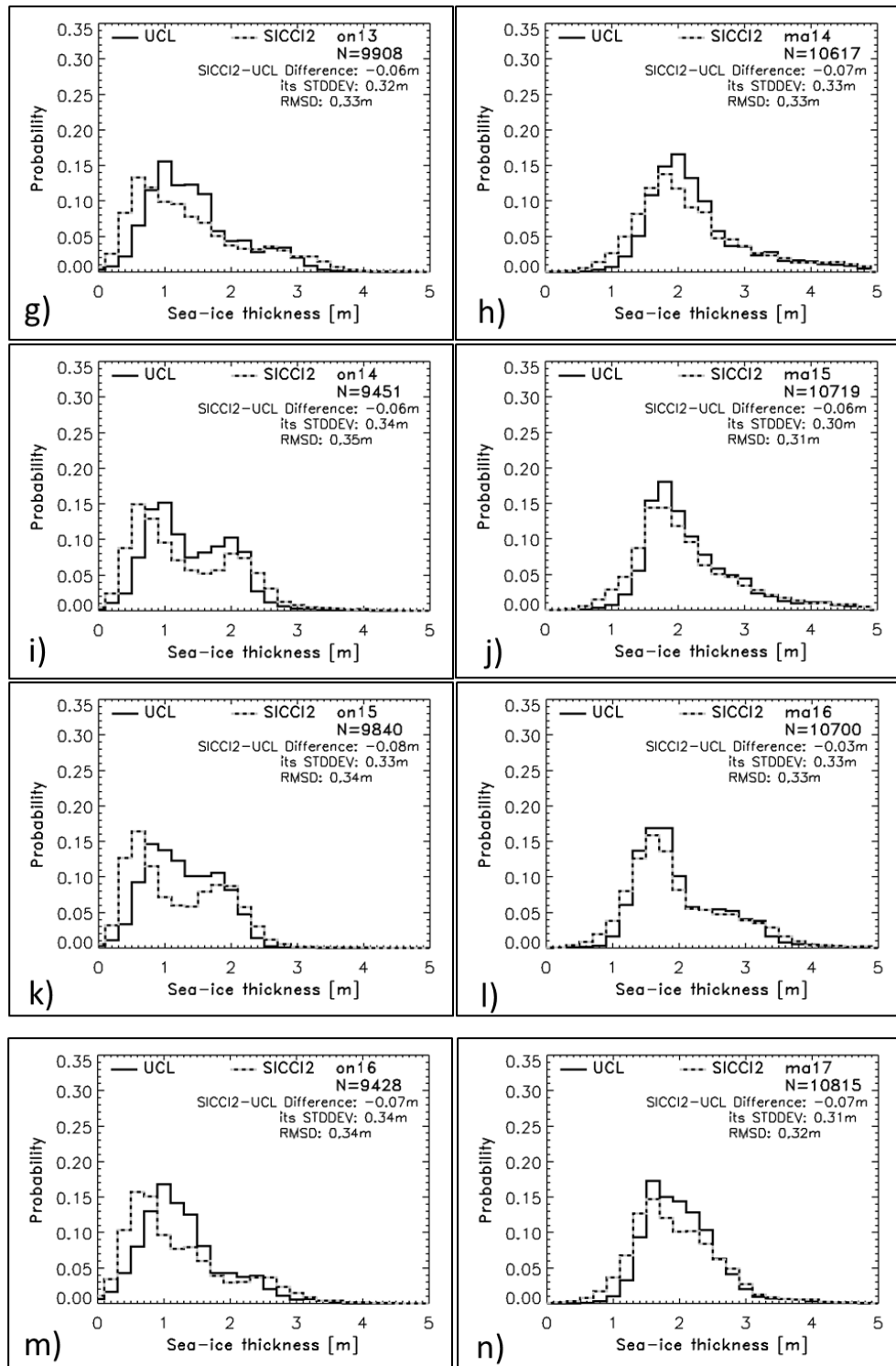


Figure 3-122 continued for winters 2013/14 through 2016/17.

The scatterplots (Figure 3-123) illustrate rather excellent agreement for spring (right column) with per-0.2m-bin mean SICCI-2 SIT values being located on or close to the 1-to-1 line over the SIT range from 1.0 m through 5.0 m. Below ~1.0 m and above ~5.0 m we find SICCI-2 SIT to overestimate and to underestimate UCL SIT, respectively; however, it is clear from Figure 3-123, right column, that these are just a few data pairs.

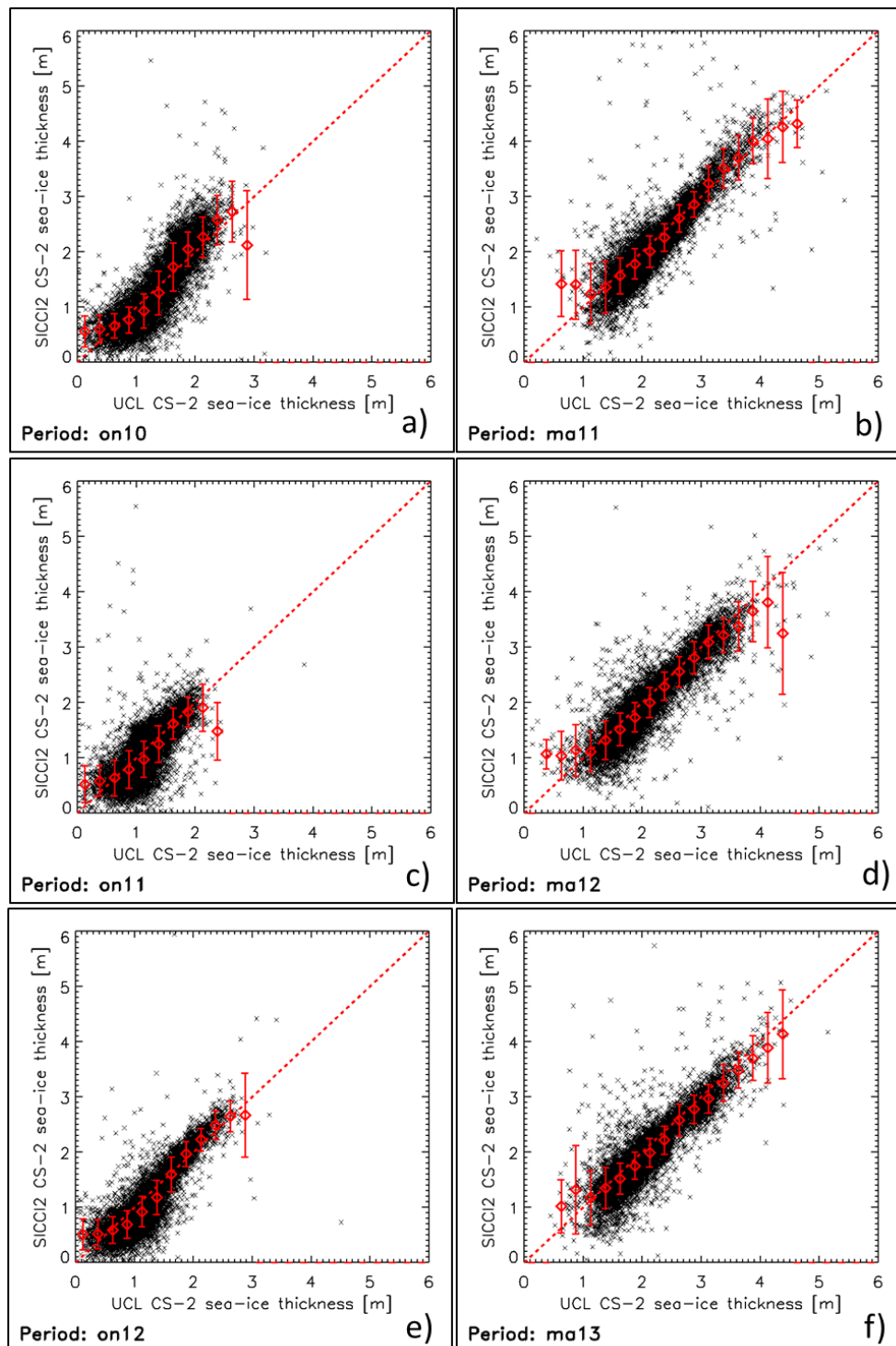


Figure 3-123: Scatterplot of individual data pairs SICCI-2 SIT versus UCL SIT (black crosses) and mean SICCI-2 SIT values derived for 0.2 m wide UCL SIT bins starting with 0.0 m to 0.2 m (red diamonds). Error bars denote one standard deviation; the dashed red line denotes a 1-to-1 fit line. Like in Figure 3-122, the left (right) column is for ON (MA) periods for winters 2010/11 through 2012/13 (compare Figure 3-114).

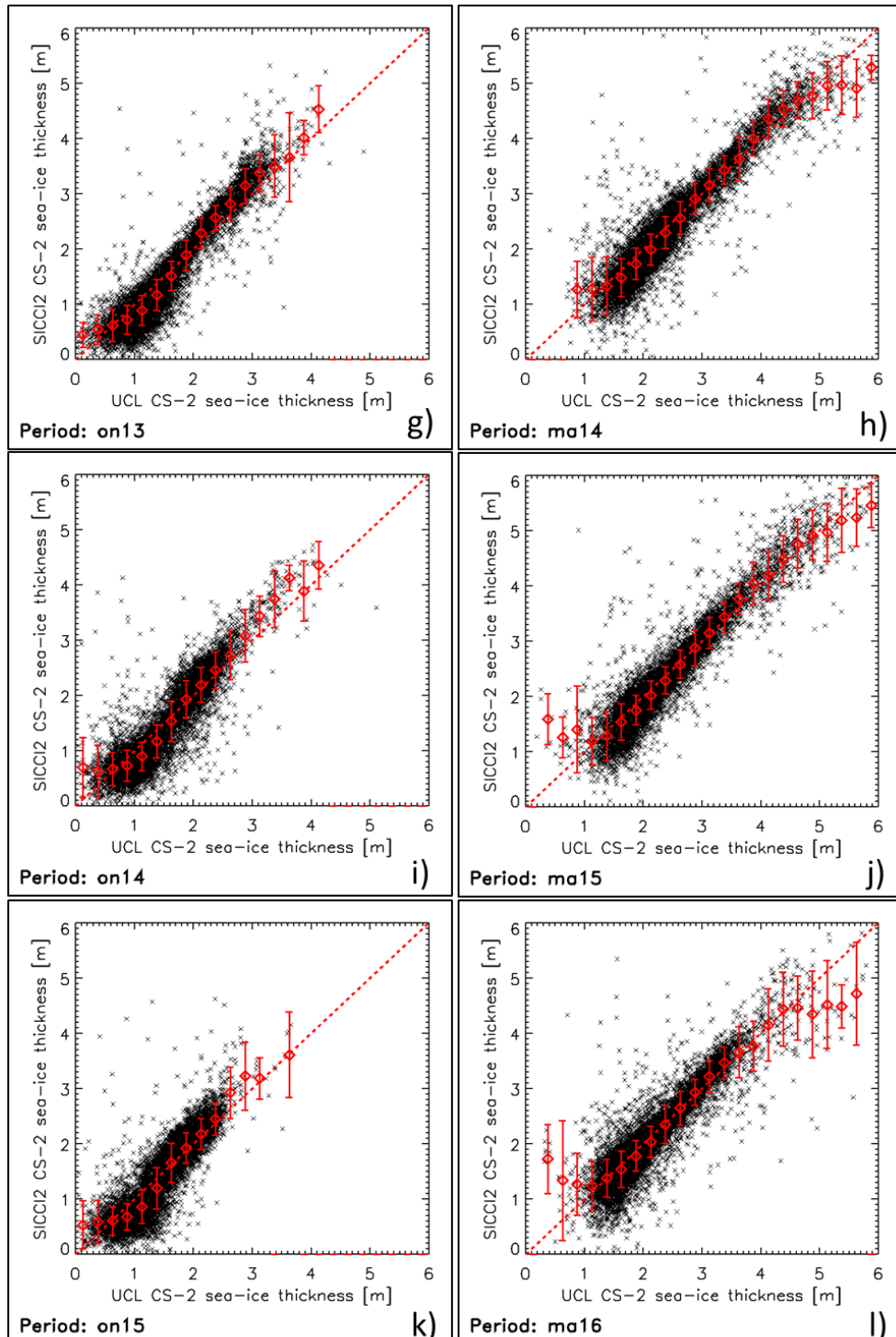


Figure 3-123 continued for winters 2013/14 through 2015/16.

The agreement for fall (Figure 3-123, left column) is less good but still almost all per-0.2m-bin mean SICCI-2 SIT values are within range of the 1-to-1 line given their standard deviation. We find an underestimation of UCL SIT at around 1.0 m to 1.2 m which is, however, smaller than for NSIDC SIT

(compare Figure 3-114, left column). In addition, we find an overestimation of UCL SIT for thicker (> 2.0 m to 2.5 m). Both these observations are in line with the histograms (Figure 3-122, left column) and have been discussed within their context.

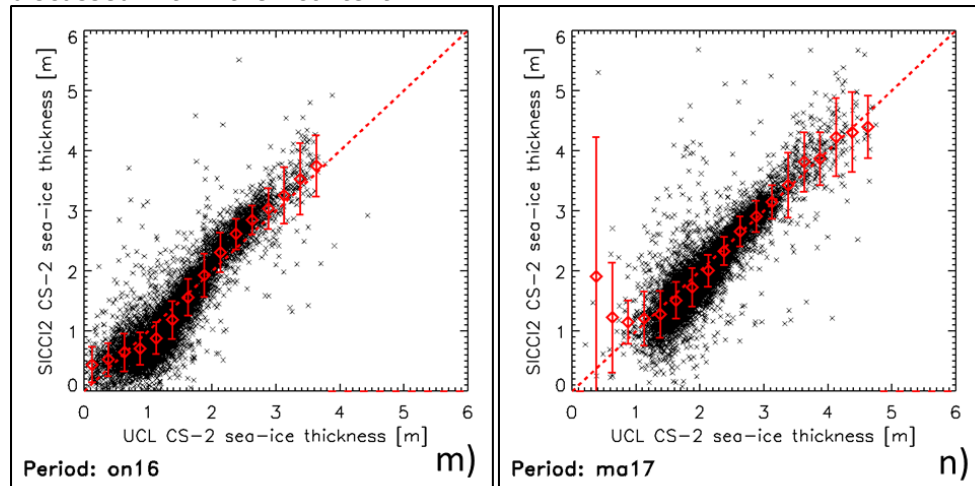


Figure 3-123 continued for winter 2016/17.

Table 3-22: Per period (fall or spring) mean SICCI-2 SIT, UCL SIT, the difference SICCI-2 minus UCL, the RMSD, the linear correlation, and the count N of collocated data pairs. Bold numbers at the end provide the averages over all ON, all MA, and all ON and MA values. Standard deviations 1σ given at the end are the averages of the respective values of the previous rows.

Period	SIT _{SICCI2} ±1σ	SIT _{UCL} ±1σ	SIT _{Diff} ±1σ	RMSD	Corr	N
ON10	1.33±0.67	1.33±0.50	0.00±0.36	0.36	0.86	9727
MA11	2.19±0.66	2.24±0.55	-0.06±0.30	0.31	0.89	10655
ON11	1.07±0.48	1.15±0.37	-0.08±0.33	0.33	0.74	9633
MA12	2.01±0.65	2.11±0.59	-0.10±0.29	0.31	0.89	10802
ON12	1.14±0.59	1.24±0.47	-0.10±0.29	0.31	0.87	9654
MA13	1.96±0.59	2.07±0.54	-0.11±0.28	0.30	0.88	10679
ON13	1.48±0.86	1.55±0.68	-0.06±0.32	0.33	0.94	9908
MA14	2.32±0.90	2.40±0.78	-0.07±0.33	0.33	0.93	10617
ON14	1.43±0.77	1.49±0.61	-0.06±0.34	0.35	0.90	9451
MA15	2.26±0.86	2.32±0.75	-0.06±0.30	0.31	0.94	10719
ON15	1.30±0.69	1.38±0.53	-0.08±0.33	0.34	0.89	9840
MA16	2.09±0.78	2.12±0.69	-0.03±0.33	0.33	0.91	10700
ON16	1.32±0.78	1.39±0.62	-0.07±0.34	0.34	0.91	9428
MA17	2.05±0.67	2.12±0.54	-0.07±0.31	0.32	0.89	10815
ONs	1.30±0.69	1.36±0.54	-0.06±0.33	0.34	0.87	
MAs	2.13±0.73	2.20±0.63	-0.07±0.31	0.32	0.90	
All	1.71±0.71	1.78±0.59	-0.07±0.32	0.33	0.89	

The summary given in Table 3-22 underlines the excellent agreement of SICCI-2 SIT with UCL SIT by, e.g. an overall difference of 0.07 m (SICCI-2 SIT < UCL SIT), an overall linear correlation of ~ 0.9 with peak seasons reaching 0.94 (ON13, MA15), a RMSD as low as 0.33 m compared to 0.46 m for the comparison with NSIDC SIT (Table 3-19) and 0.80 m compared to the comparison between SICCI-2 Envisat SIT and NSIDC or JPL ICESat SIT (section 3.6), and, finally, almost similar fall-to-spring growth rates: 0.83 m for SICCI-2 and 0.84 m for UCL (this was 0.82 m and 0.58 m for SICCI-2 and NSIDC, respectively, Table 3-19).

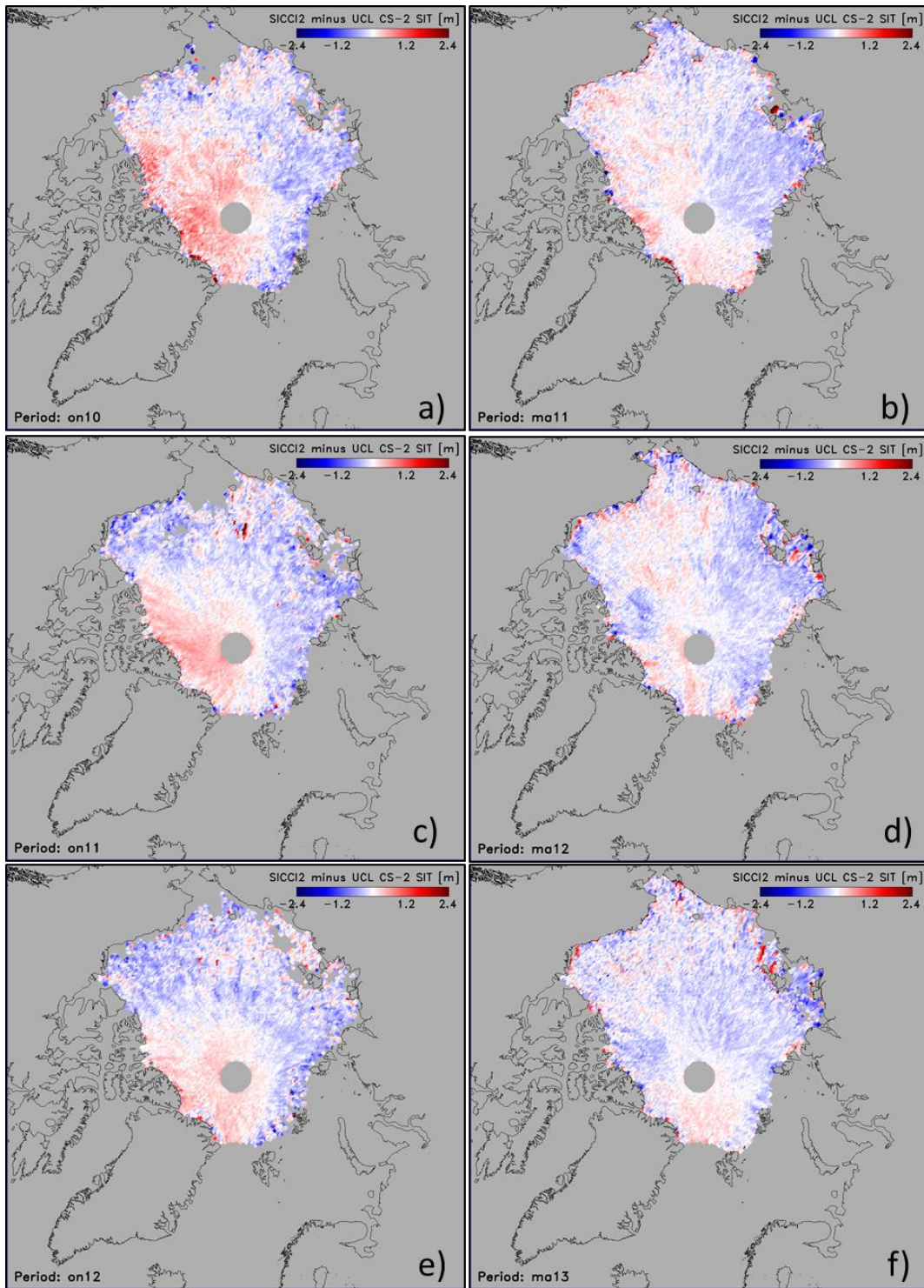


Figure 3-124: Distribution of the difference SICCI-2 SIT minus UCL SIT for fall (left column) and spring (right column) for winters 2010/11 through 2012/13.

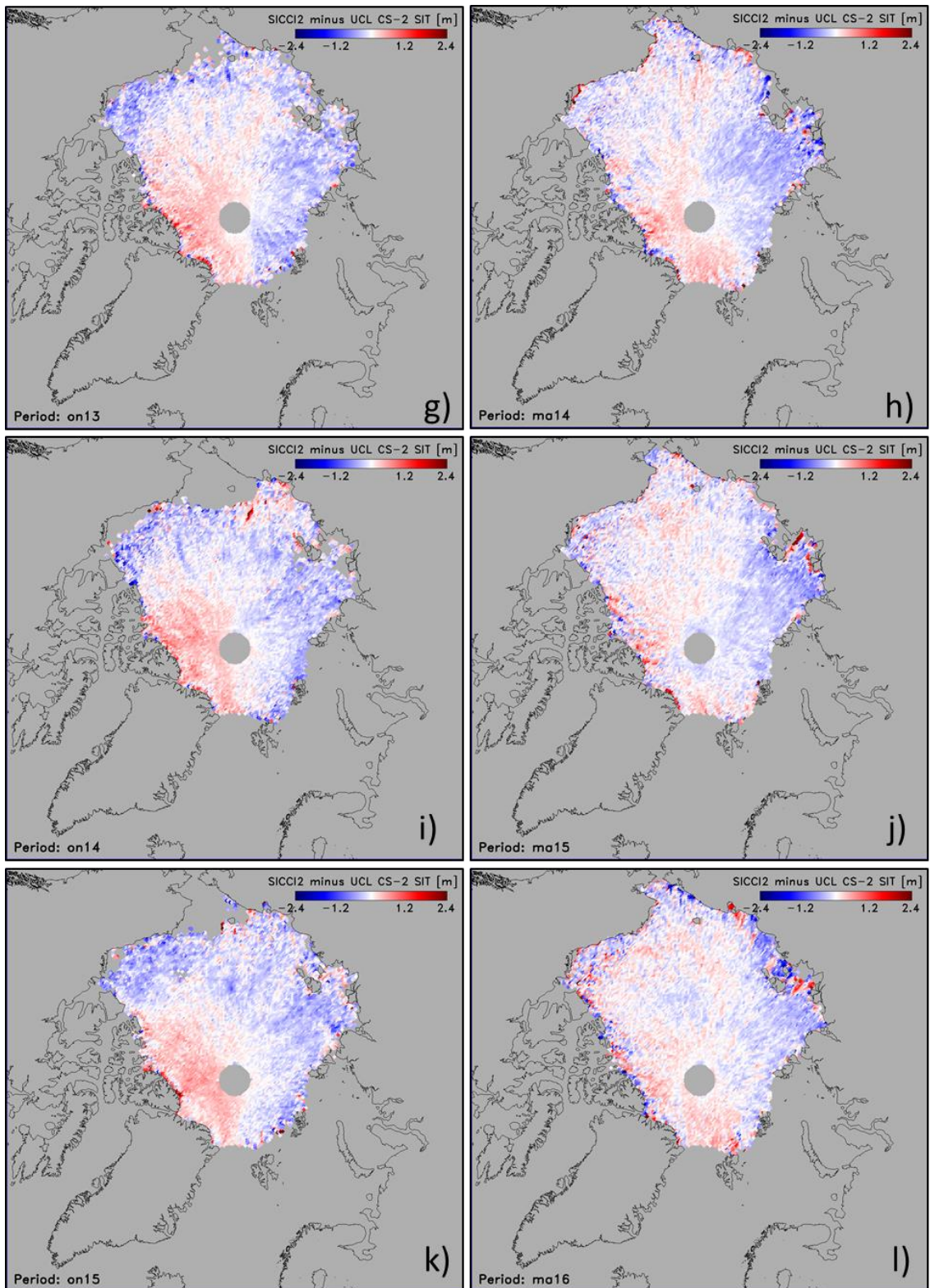


Figure 3-124 continued for winters 2013/14 through 2015/16.

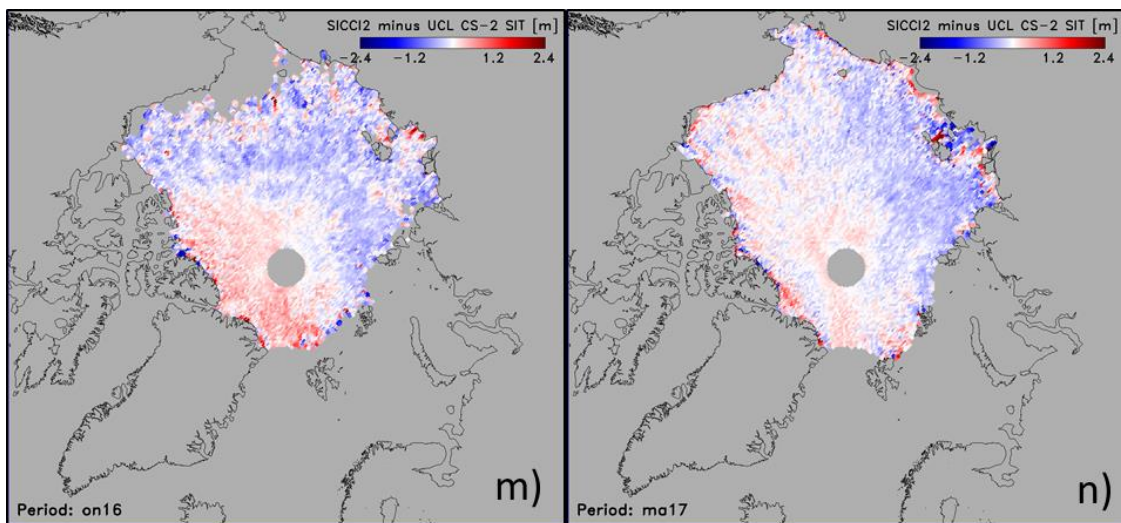


Figure 3-124 continued for winter 2016/17.

In Figure 3-124 we want to answer the question where we observe the largest differences. For fall (Figure 3-124, left column) we find wide-spread positive differences (SICCI-2 SIT > UCL SIT) over the “classic” MYI regions north of Greenland and the Canadian Arctic Archipelago, extending into the central Arctic Ocean. These differences rarely exceed 1.0 m and occur consistently in every winter. Isolated spots of positive differences also occur in other regions of the Arctic – predominantly close to coasts. Most of the other areas exhibit either small differences (< |0.5| m) or negative differences (SICCI-2 SIT < UCL SIT). Actually, one can say that there is a gradient from close to zero to increasingly negative differences from the central Arctic Ocean towards the coasts of Canada, Alaska, and Eurasia.

For spring (Figure 3-124, right column) we find a less regular pattern of differences. Positive differences tend to occur in a band stretching from the Fram Strait northwards across the central Arctic Ocean towards the Beaufort / Chukchi Seas but this band is interspersed with negative differences as well. While these large-scale positive differences are small, we find isolated spots of positive differences > 1.0 m almost everywhere along the coasts. Such isolated spots also occur in form of negative differences < -1.0 m, also predominantly along the coasts. Further, we find widespread negative differences on the Eurasian side of the Arctic Ocean, namely in the Laptev Sea but also in the East Siberian Sea. Most of these differences are < 1.0 m though.

In the following we are again limiting the comparison to FYI regions, identified by > 85% FYI concentration, and to MYI regions, identified by > 85% MYI concentration. Figure 3-125 (a,b) illustrates nicely that negative differences (SICCI-2 SIT < UCL SIT) dominate for FYI while positive differences (SICCI-2 SIT > UCL SIT) dominate for MYI. This is confirmed in the histograms (Figure 3-125 c,d) where SICCI-2 SIT is 0.6 m for FYI and 1.4 m for MYI while it is 0.8 m for FYI (and hence larger) and 1.0 m for MYI (and hence smaller) for UCL SIT. This is also illustrated by the overall difference which is -0.20 m for FYI but +0.20 m for MYI, completely opposite. Accordingly, the respective scatterplots (Figure 3-125 e,f) show per-0.2m-bin mean SICCI-2 SIT values which are predominantly below the 1-to-1 line for FYI but above the 1-to-1 line for MYI. It should be noted, however, that the data pairs scatter much less for MYI which might have to do with the absence of the many spuriously large, noise-like differences that are visible in the FYI SIT difference map (Figure 3-125 a) but do not appear in the MYI SIT difference map (Figure 3-125 b).

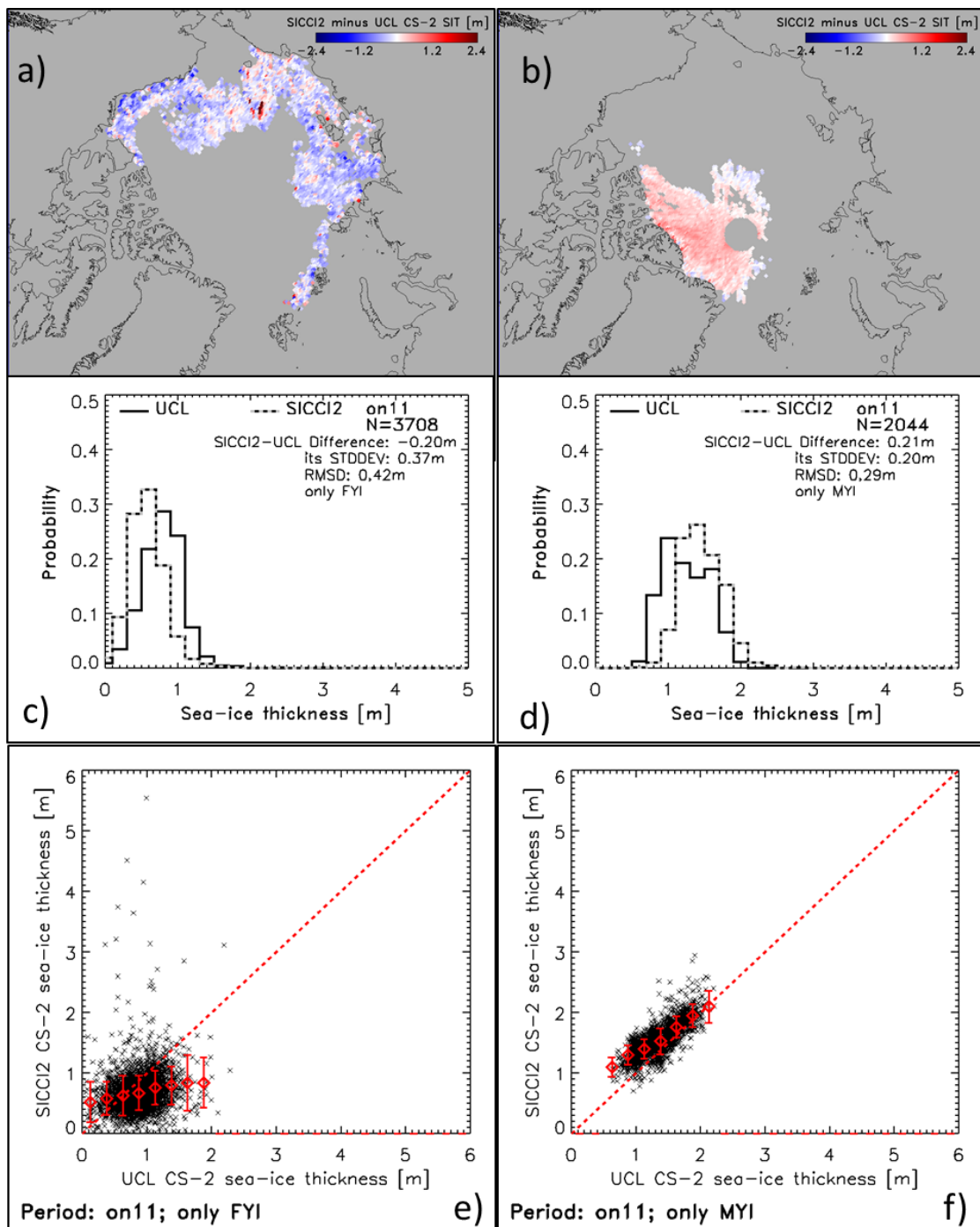


Figure 3-125: Comparison of SICCI-2 and UCL SIT for grid cells with FYI concentration > 85% (left column) and MYI concentration > 85% (right column) for fall 2011 (on11). Difference SICCI-2 SIT minus UCL SIT for a) > 85% FYI and b) > 85% MYI; histograms (c,d) and scatterplots (e,f) of the respective sub-sets of the data sets (compare Figure 3-120).

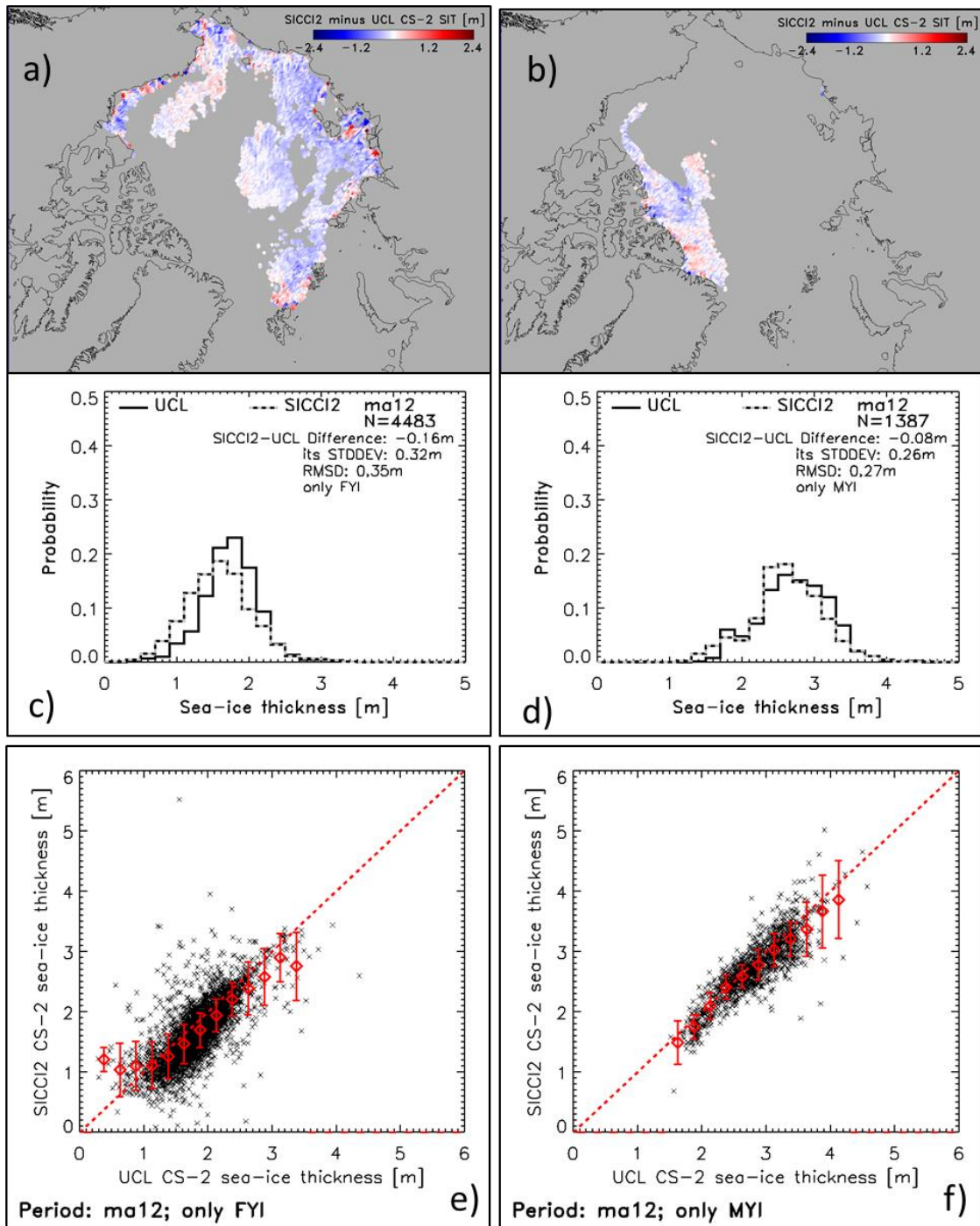


Figure 3-126: As Figure 3-125 but for spring 2012 (ma12).

The clear picture given by Figure 3-125 for fall changes a bit for spring 2012 (Figure 3-126). While for FYI still negative differences dominate (Figure 3-126 a) – except the already discussed isolated areas of large positive differences along the coasts – for MYI we find positive and negative SIT differences (Figure 3-126 b). For MYI, the modal SIT values agree at 2.6 m while for FYI modal SIT values are 1.6 m for SICCI-2 and 1.8 m for UCL (Figure 3-126 c,d). It is evident that UCL has more thick ice (> 1.5 m for FYI and > 2.5 m for MYI) than SICCI-2. In turn, it is evident that SICCI-2

has more thin ice (< 1.5 m for FYI and < 2.5 m for MYI) than UCL. This is visible in the scatterplots partly as well (Figure 3-126 e,f).

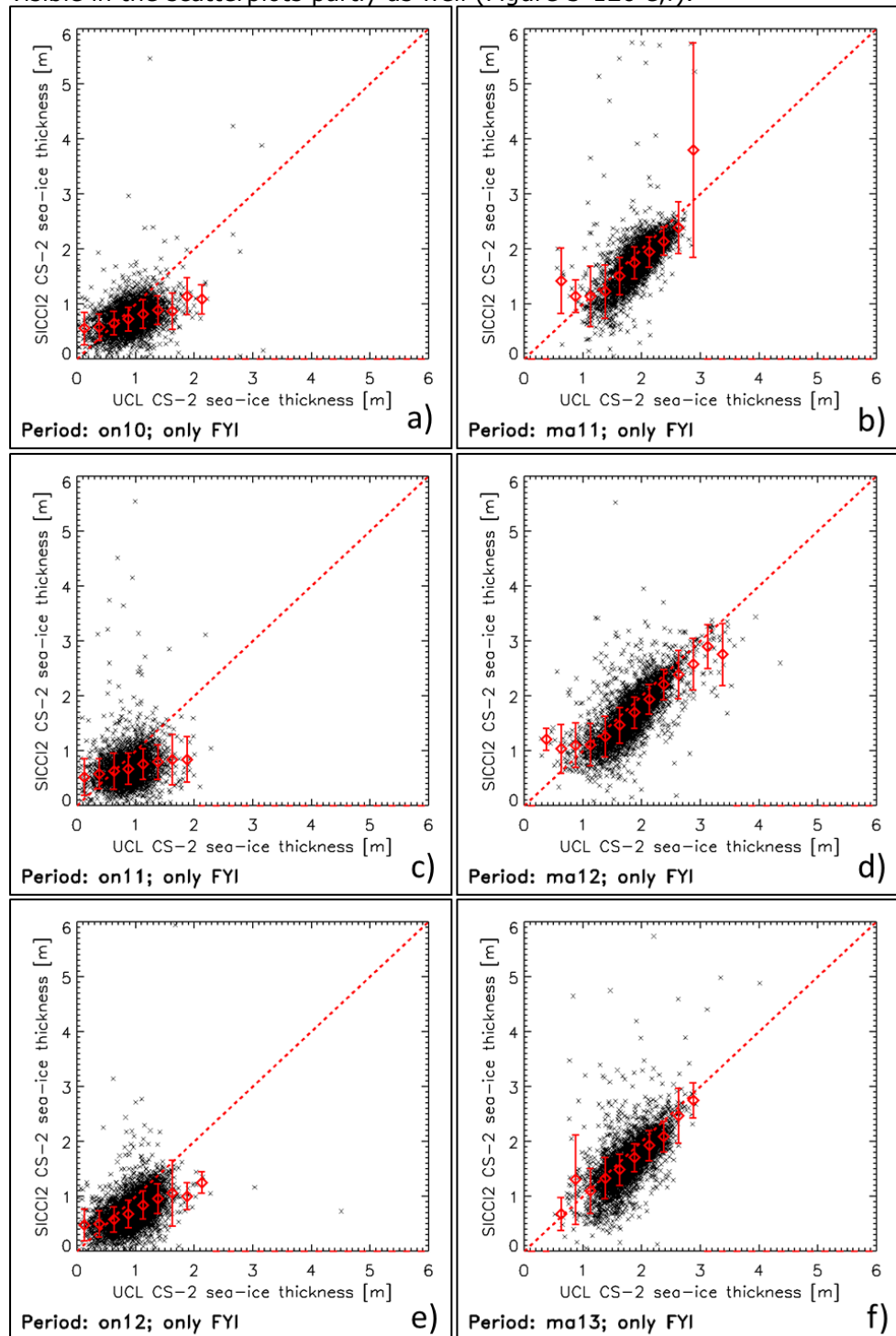


Figure 3-127: Scatterplot of individual data pairs SICCI-2 SIT versus UCL SIT (black crosses) and mean SICCI-2 SIT values derived for 0.2 m wide UCL SIT bins starting with 0.0 m to 0.2 m (red diamonds) for > 85% FYI concentration. Error bars denote one standard deviation; the dashed red line denotes a 1-to-1 fit line. Like in Figure 3-123, the left (right) column is for ON (MA) periods for winters 2010/11 through 2012/13.

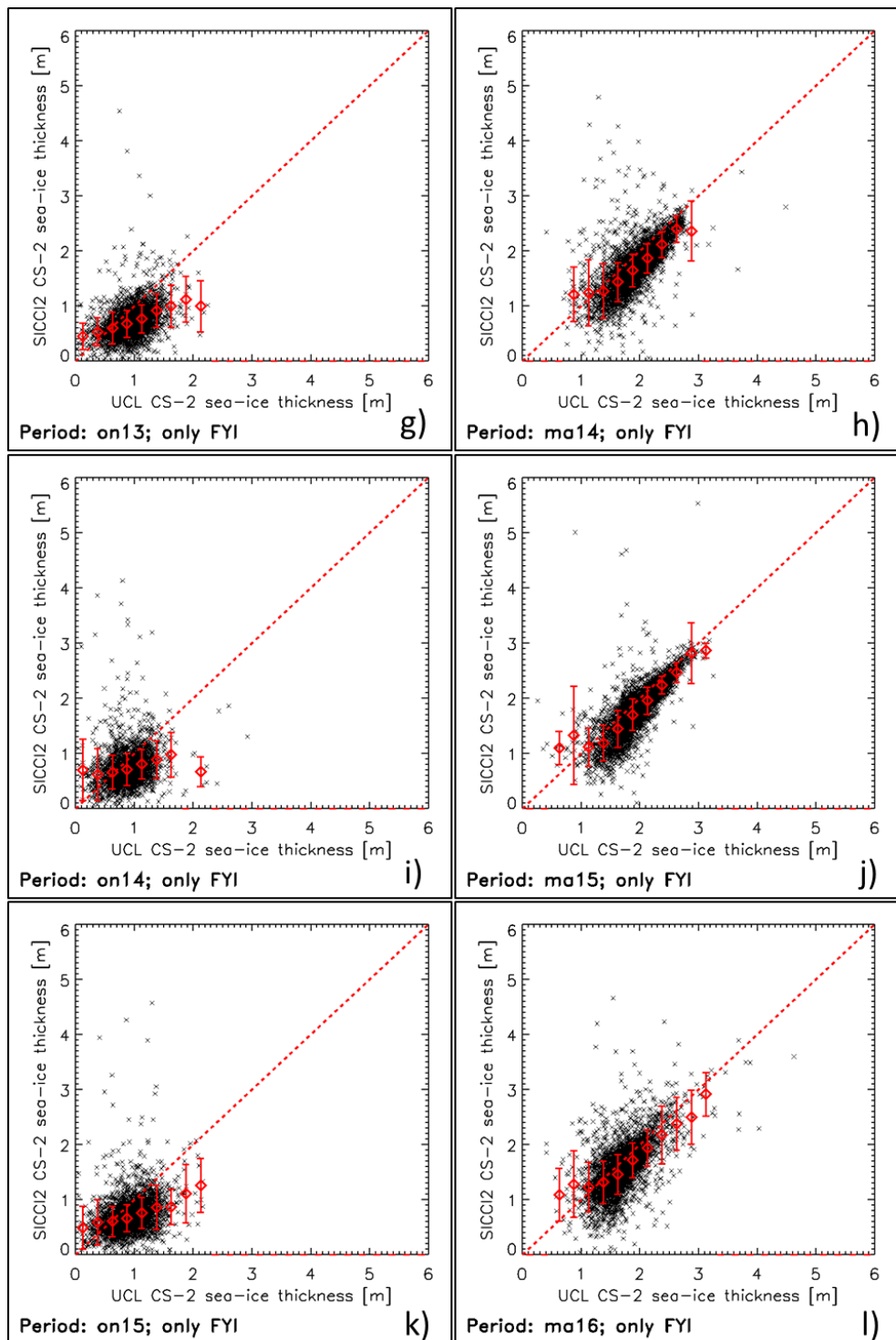


Figure 3-127 continued for winters 2013/14 through 2015/16.

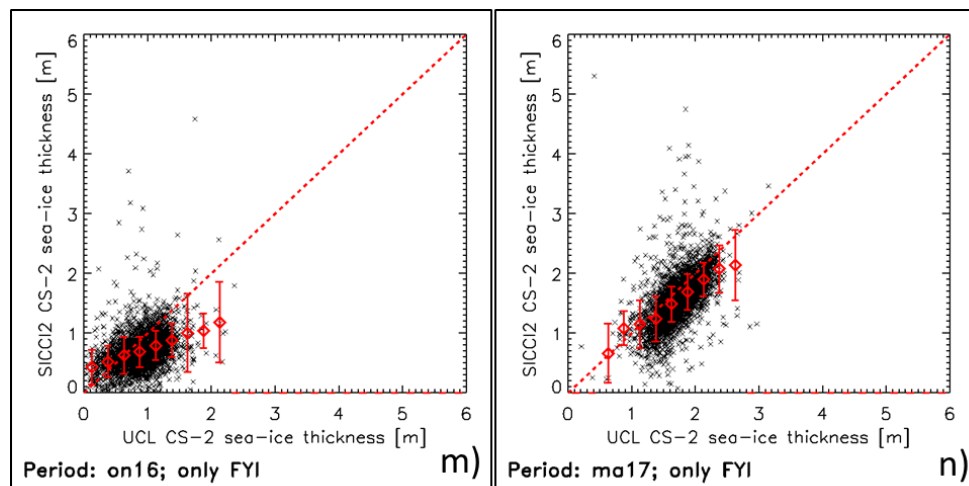


Figure 3-127 continued for winter 2016/17.

The underestimation we found for fall for FYI in Figure 3-125 a, c, e) is typical for the entire period of investigation. The scatterplots shown in Figure 3-127, left column, illustrate that for FYI SICCI-2 underestimates SIT relative to UCL. Most of the per-0.2m-bin mean SICCI-2 SIT values are located below the 1-to-1 line; a hypothetical linear regression line would have a slope ~ 0.5 . We can hence state that a large fraction of the negative differences found in Figure 3-124, left column, can be attributed to SIT underestimation over FYI – as was kind of expected from the spatial distribution of the differences.

The agreement is much better for spring (Figure 3-127, right column), when most per-0.2m-bin mean SICCI-2 SIT values are within range of the 1-to-1 line by means of their standard deviation, but again situated mostly below it, hence pointing to a negative (SICCI-2 SIT < UCL SIT) difference (see Table 3-23).

Table 3-23: Per period (fall or spring) mean SICCI-2 SIT, UCL SIT, the difference SICCI-2 minus UCL, the RMSD, the linear correlation, and the count N of collocated data pairs for > 85% FYI concentration. Bold numbers at the end provide the averages over all ON, all MA, and all ON and MA values. Standard deviations 1σ given at the end are the averages of the respective values of the previous rows.

Period	SIT _{SICCI2} $\pm 1\sigma$	SIT _{UCL} $\pm 1\sigma$	SIT _{DIFF} $\pm 1\sigma$	RMSD	Corr	N
ON10	0.75 ± 0.27	0.92 ± 0.30	-0.17 ± 0.31	0.36	0.39	3855
MA11	1.77 ± 0.43	1.92 ± 0.31	-0.15 ± 0.32	0.36	0.66	3816
ON11	0.69 ± 0.31	0.89 ± 0.28	-0.20 ± 0.37	0.42	0.22	3708
MA12	1.69 ± 0.46	1.85 ± 0.39	-0.16 ± 0.32	0.35	0.74	4483
ON12	0.74 ± 0.30	0.94 ± 0.30	-0.20 ± 0.30	0.36	0.49	5104
MA13	1.64 ± 0.41	1.79 ± 0.33	-0.15 ± 0.31	0.34	0.67	5098
ON13	0.72 ± 0.29	0.96 ± 0.28	-0.24 ± 0.31	0.40	0.39	3147
MA14	1.72 ± 0.45	1.92 ± 0.36	-0.21 ± 0.33	0.39	0.68	3924
ON14	0.74 ± 0.32	0.91 ± 0.26	-0.17 ± 0.36	0.40	0.22	3012
MA15	1.78 ± 0.46	1.94 ± 0.36	-0.16 ± 0.28	0.32	0.79	4047
ON15	0.70 ± 0.30	0.93 ± 0.28	-0.23 ± 0.35	0.42	0.30	3496
MA16	1.58 ± 0.47	1.70 ± 0.35	-0.12 ± 0.38	0.40	0.60	3510
ON16	0.71 ± 0.30	0.91 ± 0.30	-0.19 ± 0.33	0.38	0.39	3725
MA17	1.58 ± 0.39	1.74 ± 0.27	-0.16 ± 0.32	0.36	0.58	4511
ONs	0.72± 0.30	0.92± 0.29	-0.20± 0.33	0.39	0.34	

MAAs	1.68±0.44	1.84±0.34	-0.16±0.34	0.36	0.67	
All	1.20±0.37	1.38±0.31	-0.18±0.33	0.38	0.50	

We note that these results are considerably better than for NSIDC SIT (compare with Figure 3-118 and Table 3-20 with Table 3-23). The overall SIT difference for FYI is -0.18 m (SICCI-2 SIT < UCL SIT), with little change between fall and spring: 0.04 m (was 0.37 m for NSIDC SIT). The correlation is 0.50 and the RMSD is 0.39 m (was 0.28 and 0.53 m, respectively, for SICCI-2 vs. NSIDC SIT).

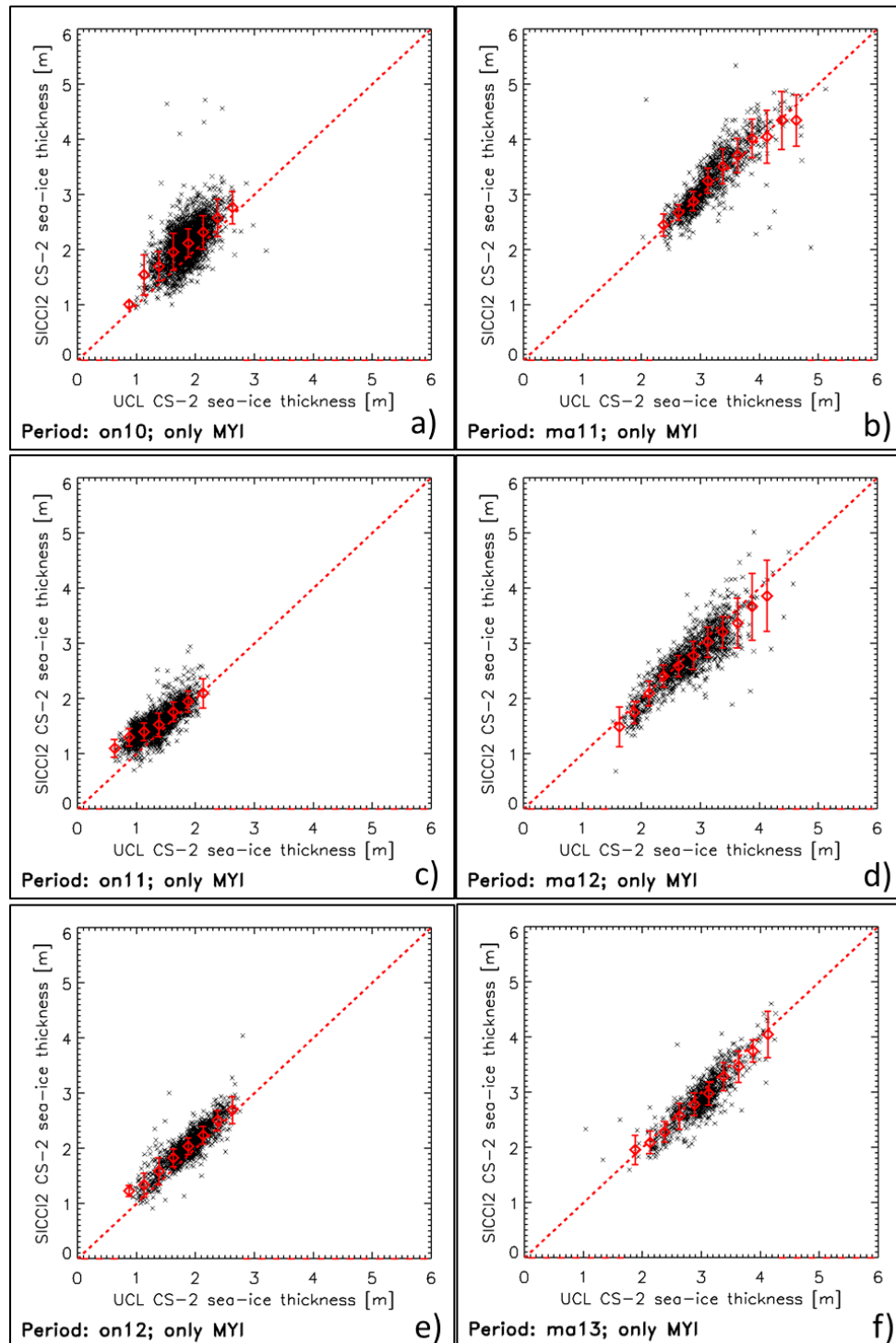


Figure 3-128: As Figure 3-127 but for > 85% MYI concentration.

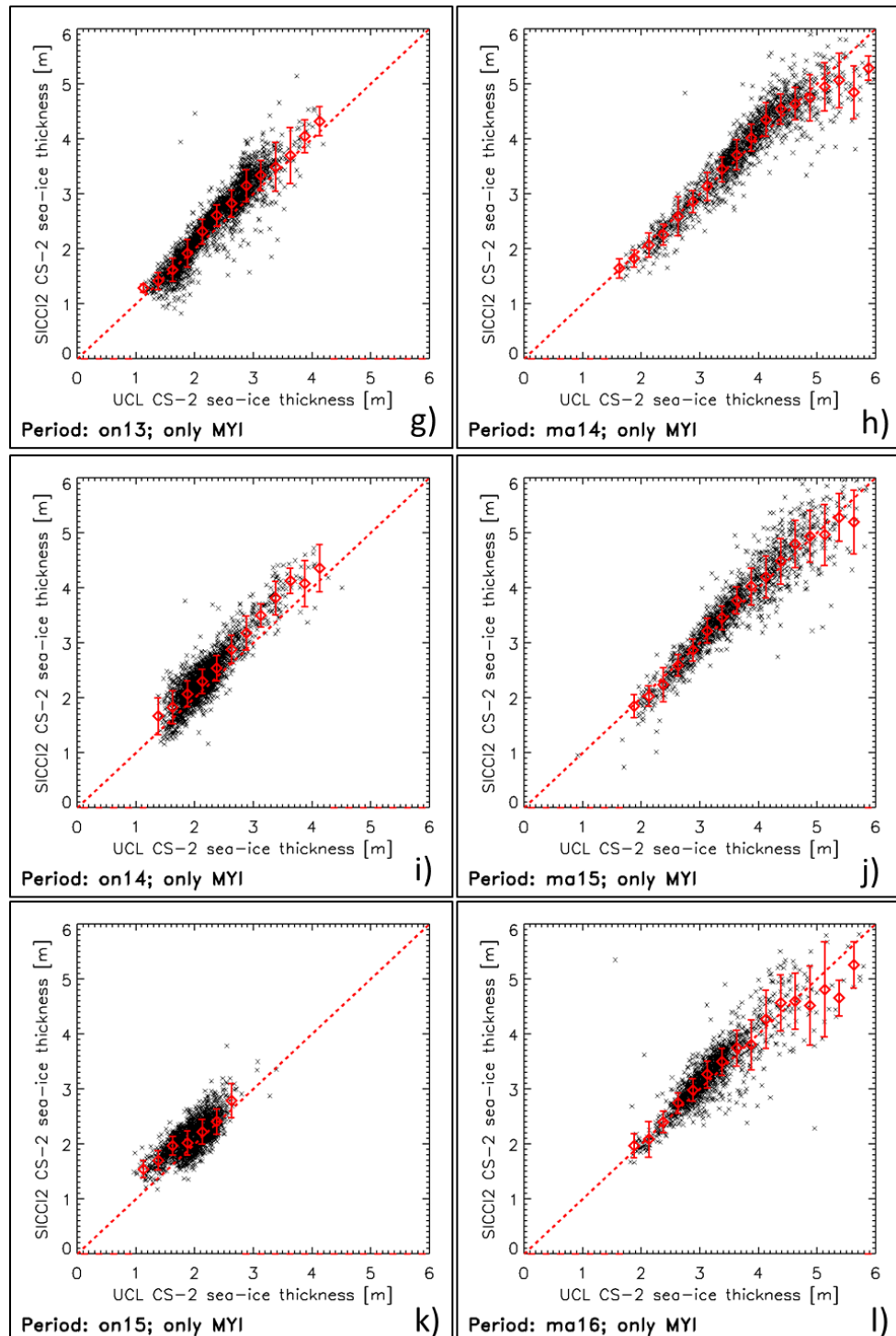


Figure 3-128 continued for winters 2013/14 through 2015/16.

The overestimation we found for fall for MYI in Figure 3-125 b,d,f) is typical for the entire period of investigation. The scatterplots shown in Figure 3-128, left column, illustrate that for MYI SICCI-2 overestimates SIT relative to UCL. Most of the per-0.2m-bin mean SICCI-2 SIT values are located

above the 1-to-1 line but still within the range given by one standard deviation. In contrast to FYI (Figure 3-127, left column) a hypothetical linear regression line would still have slope close to 1. Possibly a large fraction of the positive differences found in Figure 3-124, left column, can be attributed to SIT overestimation over MYI – as was kind of expected from the spatial distribution of the differences.

For spring (Figure 3-128, right column) the agreement again looks better. The majority of the per-0.2m-bin mean SICCI-2 SIT values is located on or close to the 1-to-1 line; we find these values to be located both, above and below the 1-to-1 line in all winters, leading us to conclude that the distribution of positive and negative SIT differences shown in Figure 3-126 b) is typical.

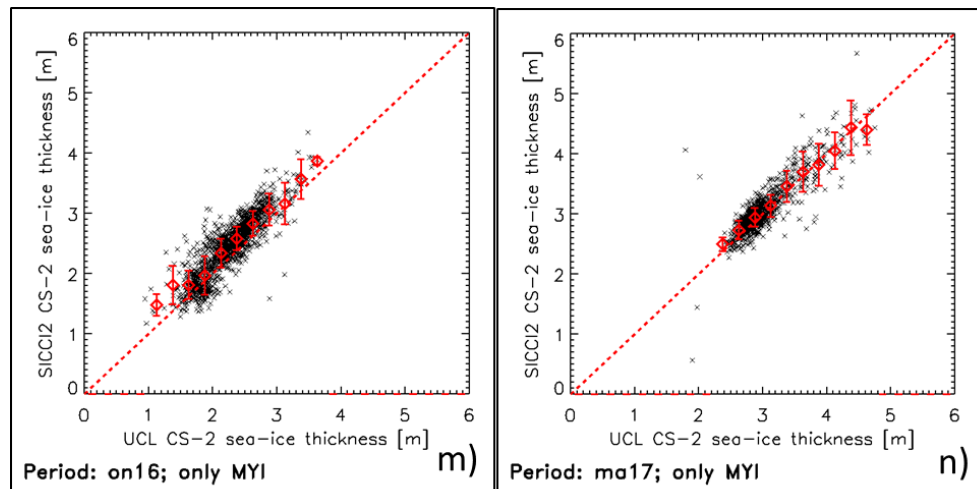


Figure 3-128 continued for winter 2016/17.

Table 3-24: Per period (fall or spring) mean SICCI-2 SIT, UCL SIT, the difference SICCI-2 minus UCL, the RMSD, the linear correlation, and the count N of collocated data pairs for > 85% MYI concentration. Bold numbers at the end provide the averages over all ON, all MA, and all ON and MA values. Standard deviations 1σ given at the end are the averages of the respective values of the previous rows.

Period	SIT _{SICCI2} ±1σ	SIT _{UCL} ±1σ	SIT _{DIFF} ±1σ	RMSD	Corr	N
ON10	2.12±0.36	1.86±0.26	0.26±0.29	0.39	0.60	2755
MA11	3.21±0.51	3.14±0.42	0.08±0.27	0.28	0.84	1168
ON11	1.56±0.28	1.35±0.31	0.21±0.20	0.29	0.78	2044
MA12	2.73±0.51	2.81±0.48	0.08±0.26	0.27	0.86	1387
ON12	2.05±0.33	1.89±0.31	0.16±0.16	0.23	0.88	1623
MA13	2.90±0.45	3.01±0.41	-0.10±0.23	0.25	0.86	816
ON13	2.48±0.67	2.32±0.55	0.16±0.26	0.30	0.93	2762
MA14	3.80±0.85	3.75±0.80	0.05±0.31	0.32	0.93	1486
ON14	2.38±0.50	2.18±0.40	0.20±0.24	0.31	0.88	2273
MA15	3.65±0.87	3.59±0.78	0.06±0.31	0.32	0.93	1436
ON15	2.12±0.31	1.96±0.30	0.16±0.23	0.28	0.72	2096
MA16	3.29±0.60	3.19±0.55	0.10±0.30	0.32	0.87	1656
ON16	2.45±0.48	2.27±0.40	0.19±0.24	0.30	0.87	1346
MA17	3.09±0.45	3.03±0.43	0.06±0.22	0.23	0.88	894
ONs	2.17±0.42	1.98±0.36	0.19±0.23	0.30	0.81	
MAs	3.24±0.61	3.22±0.55	0.02±0.27	0.28	0.88	
All	2.70±0.51	2.60±0.45	0.10±0.25	0.29	0.84	

The summary of the results for MYI (Table 3-24) reveals an overall SIT difference of 0.10 m (SICCI-2 SIT > UCL SIT) which, in contrast to FYI (Table 3-23), results from an overestimation of ~0.20 m for fall and a difference close to zero in spring. This is interesting to see in comparison to the comparison for MYI with NSIDC SIT; there we also found a close to zero difference for spring but an underestimation of ~0.15 m for fall. In other words the average NSIDC SIT for FYI is about 0.35 m larger than UCL SIT while both "external" CS-2 data based SIT data sets agree fairly well for MYI in spring. Table 3-24 further reveals a considerably higher linear correlation: 0.84, compared to NSIDC: 0.70 (Table 3-21), and a considerably smaller RMSD: 0.29 m compared to 0.38 m for NSIDC (Table 3-21). So, overall, we could state that the intercomparison between SICCI-2 SIT and independent CS-2 SIT data sets reveals better results for UCL than for NSIDC. The only concern visible from Table 3-23 and Table 3-24 is the fall-to-spring change in SIT. For FYI this is 0.96 m and 0.92 m for SICCI-2 and UCL, respectively. For MYI this is 1.07 m and 1.24 m for SICCI-2 and UCL, respectively. As expressed already earlier in this section as well as in section 3.6, it is unrealistic to have more ice growth for MYI than FYI during winter – at least when we consider pure thermodynamic growth. This casts some doubt on the results and a further discussion of this issue should be carried out in the future.

Summary

- The SICCI-2 CS-2 SIT product is closer to the UCL CS-2 SIT product [RD-31] than the NSIDC CS-2 SIT product [RD-30]. The overall bias relative to NSIDC SIT is -0.20 m, the one to UCL SIT is -0.07 m; this bias does not depend on season for UCL SIT.
- The two "external" SIT products differ particularly in fall (October/November), when NSIDC SIT is 0.26 m thicker than UCL SIT. This applies also when analyzing FYI and MYI regions separately: for FYI NSIDC SIT is 0.31 m thicker than UCL SIT; for MYI NSIDC SIT is 0.34 m thicker than UCL SIT.
- Correlations between SICCI-2 SIT and UCL SIT are 0.89 (all), 0.50 (FYI), and 0.84 (MYI) and hence considerably larger than for NSIDC SIT: 0.83 (all), 0.28 (FYI), and 0.70 (MYI).
- Root mean square differences (RMSD) are considerably smaller when pairing SICCI-2 and UCL SIT: 0.33 m (all), 0.38 m (FYI), and 0.29 m (MYI) compared to pairing SICCI-2 and NSIDC SIT: 0.46 m (all), 0.53 m (FYI), and 0.38 m (MYI).
- The distribution of SIT differences is less "erratic" for UCL SIT than for NSIDC SIT; this applies especially to the spring periods. Moreover, we find a convincing separation between areas of negative differences (SICCI-2 SIT < UCL SIT) and a positive differences (SICCI-2 SIT > UCL SIT) which could be attributed to the typical distributions of FYI and MYI.
- There is an indication that a certain fraction of the differences observed between SICCI-2 SIT and UCL SIT could be caused by the different averaging scales used (25 km versus 50 km).
- We hypothesize that large-scale positive differences found for spring periods for NSIDC SIT for a region extending from the Fram Strait over the Central Arctic towards the Beaufort/Chukchi Seas are related to differences in freeboard retrieval and not to differences in data sets such as snow depth or ice type or spatial resolution.
- We voice concerns about the fall-to-spring SIT change which is found to be larger for MYI than FYI for all three CS-2 SIT data sets. This could only be explained with substantially more deformation

affecting MYI regions than it has affected FYI regions because thermodynamic growth should on average be larger for FYI than MYI. Another possibility could be a much thinner snow cover on MYI than FYI which we consider unlikely to have occurred.

4 Summary

An intra-product consistency analysis has been carried out for the gridded values of the SICCI-2 SIT product v2.0 in which the focus was on comparing Envisat RA-2 and CryoSat-2 SIT and SIT uncertainty as well as sea-ice freeboard and its uncertainty estimates. The results of this analysis can be summarized as follows:

- On hemispheric scale, the agreement between Envisat RA-2 and CryoSat-2 SIT is similar for both hemispheres. The overall, wintertime SIT difference CryoSat-2 minus Envisat RA-2 is $< |\sim 0.1\text{m}|$. Compare to CryoSat-2, we find that Envisat RA-2 overestimates SIT in the Northern Hemisphere and underestimates SIT in the Southern Hemisphere.
- At regional scale (6 selected regions of 250 km x 250 km size), we find that the agreement between Envisat RA-2 and CryoSat-2 is better in the Northern than in the Southern Hemisphere. In the Northern Hemisphere, the wintertime average SIT difference CryoSat-2 minus Envisat RA-2 ranges between -0.26 m for a first-year ice (FYI) region and +0.20 m for a multiyear ice (MYI) region. In the Southern Hemisphere, this differences ranges between -0.64 m for a FYI dominated region and +0.40 m for a MYI dominated region.
- Values obtained for the sea-ice freeboard are similar, except that differences are about 1/10 of those we find for SIT.
- The retrieval uncertainties of sea-ice freeboard don't while those of SIT do exhibit some seasonal variation; they are relatively similar between the regions of one hemisphere and we did not find any inter-annual variation or trend. There is a substantial reduction in sea-ice freeboard and SIT uncertainty from Envisat to CS-2. As a ball-park number one can state that the uncertainty for CS-2 is just 2/3 of the uncertainty for Envisat. In values for freeboard uncertainty this means ~ 0.1 m for CS-2 but ~ 0.15 m for Envisat.
- The transition between Envisat RA-2 and CryoSat-2 period may cause jumps in the obtained sea-ice freeboard and sea-ice thickness values in some regions of the Southern Hemisphere, where also the SIT at the beginning of the freezing season seems to be high. This transition is much smoother in the Northern Hemisphere.

The level 2P sea-ice freeboard (SIF) was compared to Operation Ice Bridge (OIB) sea-ice freeboard computed as the difference OIB total freeboard minus OIB snow depth. Note that in OIB snow depth products thin snow (< 0.05 m) is usually underrepresented as is thick snow over deformed sea ice.

- Envisat and CS-2 sea-ice freeboard agree well with each other for the overlap period at OIB locations: RMSD = 0.07 m, linear correlation coefficient: 0.80 and linear regression: $y = 0.801x + 0.03$ m; for this overlap modal and mean SIF values agree within 0.04 m and 0.02 m, respectively.
- Comparison between OIB and Envisat SIF for their overlap (2009-2012) results in a RMSD = 0.14 m and poor linear correlation: 0.32. Modal and mean SIF agree with 0.03 m and 0.02 m, though.

- Comparison between OIB and CS-2 SIF for their overlap (2011-2016) results a RMSD = 0.13 m and moderate linear correlation: 0.55. Modal and mean SIF values suggest overestimation of OIB SIF by CS-2 SIF by 0.05 and 0.08 m, respectively.

The gridded SIT values of the SICCI-2 SIT product v2.0 have been compared to various airborne, moored, ground-based, and space-borne independent SIT and sea-ice draft observations. The main results of these inter-comparisons are as follows:

- Total (sea ice + snow) thickness from airborne electromagnetic sounding (AEM) agrees better with the CryoSat-2 SIT (RMSD: 0.73 m, $SICCI2_SIT = 0.88 * AEM_SIT + 0.03$ m) than the Envisat RA-2 SIT (RMSD: 0.90 m, $SICCI2_SIT = 0.26 * AEM_SIT + 1.45$ m); the agreement is less good for the Southern Hemisphere.
- Wintertime sea-ice draft or sea-ice thickness observations from moored ULS are mostly in reasonable agreement with SICCI-2 SIT products. SICCI-2 SIT from both sensors share a similar seasonal cycle for the BGEP moorings; BGEP sea-ice draft is under-estimated by 0.17 m by Envisat RA-2 and overestimated by 0.15 m by CryoSat-2. SICCI-2 SIT fall into the same SIT range as the NPI mooring observations in the Fram Strait for Envisat RA-2 with an RMSD: 0.69 m, $SICCI2_SIT = 0.96 * NPI_SIT + 0.24$ m for the modal SIT. SICCI-2 SIT fall into the same SIT range as the AWI mooring observations in the Weddell Sea for Envisat RA-2 for MYI dominated cases: RMSD: 1.08 m, $SICCI2_SIT = 0.52 * AWI_SIT + 1.53$ m. The quality of all these ULS data sets differs, however, and results have to be interpreted carefully.
- Results of our inter-comparison with in-situ (NorthPole drift stations) and ship-based observations (ASPeCt / ASSIST) of SIT and snow depth seem inconclusive. However, mostly these results tend to confirm the role inaccurate snow-depth data sets have for the freeboard-to-thickness conversion, in the sense that an under-estimation of the actual snow depth can cause an over-estimation of the actual SIT.
- For the Northern Hemisphere, we compared Envisat RA-2 SIT with ICESat SIT from two products: NSIDC and JPL. These two products seem to be offset – on average – by ~0.4 m thanks to slight differences in total freeboard retrieval and considerable differences in the snow depth treatment which seem to lead to shortcomings in both data sets used. For the spatiotemporal distribution we find that agreement between Envisat RA-2 and ICESat SIT is better for MYI regions: correlation > 0.6 than for FYI regions: correlation < 0.1; in scatterplots of both data sets for FYI there is almost no agreement – caused by Envisat RA-2 SIT not varying with ICESat SIT. On average, absolute differences between Envisat RA-2 and ICESat SIT tend to be smaller during February/March than during October/November. Overall, the difference between Envisat RA-2 and ICESat SIT is smaller for the NSIDC than the JPL product. Table 4-1 summarizes these differences.

Table 4-1: Overall difference (SIT DIFF) Envisat RA-2 minus ICESat SIT for the NSIDC and the JPL ICESat SIT products using all data (top), only FYI data (< 15% MYI concentration from SICCI2 product) (middle), and only MYI data (> 85% MYI concentration from SICCI2 product) (bottom) together with the root-mean squared difference (RMSD) and the linear correlation coefficient R. SIT DIFF and RMSD are given in meters. In bold we mark the "better" results

		Oct./Nov.			Feb./Mar.		
		SIT DIFF	RMSD	R	SIT DIFF	RMSD	R
All	NSIDC	-0.22	0.92	0.40	+0.23	0.67	0.51
	JPL	-0.64	0.99	0.41	-0.20	0.61	0.45
FYI	NSIDC	+0.12	0.80	-0.02	+0.29	0.68	0.09
	JPL	-0.34	0.66	-0.07	-0.11	0.60	0.13
MYI	NSIDC	-0.44	0.91	0.60	+0.14	0.68	0.68
	JPL	-0.94	1.22	0.63	-0.54	0.85	0.65

- Also for the Northern Hemisphere, we compared the SICCI-2 CryoSat-2 (CS-2) SIT product with two independent data sets: the NSIDC CS-2 SIT data set and the UCL CS-2 SIT data set. Also these two products seem to be offset by ~0.3 m but only during fall (October/November); they agree fairly well for spring (March/April). We find a substantially better agreement between these all CS-2 data based SIT data sets (as illustrated in Table 4-2) and would state that the better agreement is obtained with the UCL SIT product with a seasonally independent bias < 0.1 m and a correlation close to 0.9. We find SICCI-2 to have thinner (< 1.0 m) sea ice than the other two products, particularly during fall. We could identify that this agrees with FYI regions, especially when compared to UCL SIT and for fall. We suggest that a considerable part of the differences between SICCI-2 and UCL is driven by the different averaging scale: 25 km versus 50 km. We hypothesize that particularly large positive differences (SICCI-2 SIT > NSIDC SIT) extending from the Fram Strait across the Arctic can be attributed to a difference in the freeboard retrieval.

Table 4-2: Overall difference (SIT DIFF) SICCI-2 CS-2 minus CS-2 SIT for the NSIDC and the UCL products using all data (top), only FYI data (< 15% MYI concentration from SICCI2 product) (middle), and only MYI data (> 85% MYI concentration from SICCI2 product) (bottom) together with the root-mean squared difference (RMSD) and the linear correlation coefficient R. SIT DIFF and RMSD are given in meters. In bold we mark the "better" results

		Oct./Nov.			Mar./Apr.		
		SIT DIFF	RMSD	R	SIT DIFF	RMSD	R
All	NSIDC	-0.33	0.49	0.84	-0.08	0.43	0.82
	UCL	-0.06	0.34	0.87	-0.07	0.32	0.90
FYI	NSIDC	-0.51	0.63	0.12	-0.14	0.44	0.45
	UCL	-0.20	0.36	0.34	-0.16	0.36	0.67
MYI	NSIDC	-0.16	0.33	0.72	+0.01	0.43	0.68
	UCL	+0.19	0.30	0.81	+0.02	0.28	0.88

5 Open issues / Outlook

- Results of the inter-comparison between freeboard from air-borne measurement campaigns such as CryoVEx are not part of this report and need to be included later. CryoVEx data were just released shortly before the deadline of this report
- It is certainly worth to still extend parts of the inter-comparison to the I2p product – simply to investigate the influence of the monthly gridding and interpolation in comparison to the daily, along-orbit SIT data.
- Still missing is an inter-comparison to ICESat SIT estimates of the Southern Hemisphere. Since the uncertainties and potential biases in data sets of the Southern Hemisphere are larger and hence results of any intercomparison more uncertain, we did not give priority to this comparison.
- The inter-comparison of the snow depth products used for the freeboard-to-thickness conversion should be extended in the future.
- Missing is an evaluation of the validity of the sea-ice freeboard and sea-ice thickness uncertainties provided with the product. Strategies to do so need to be developed first.
- Also missing is information about the sea-ice thickness and sea-ice thickness uncertainty correlation scales.

< End of Document >